

**HYPERSPECTRAL REMOTE SENSING FOR
DETECTING VEGETATION AFFECTED BY
HYDROCARBONS IN THE AMAZON FOREST**

Thesis submitted for the degree of
Doctor of Philosophy
at the University of Leicester

by

Paul-Nelson Arellano Mora

College of Science and Engineering

Department of Geography

June, 2014

Dedication



*I dedicate this thesis to my lovely wife Tume.
And to my mom Mariana in the sky*

Abstract

This thesis seeks to understand the effects of hydrocarbons on the vegetation of tropical forests. It explores hyperspectral methods to detect changes in biophysical and biochemical parameters of vegetation affected by hydrocarbons in the Amazon rainforest of Ecuador. The literature review revealed that experiments in the laboratory, showed that in specific species hydrocarbons caused a reduced level of chlorophyll content, which is an indicator of stress. However, it was unclear whether the same effect would be observed in tropical forests. Fieldwork was conducted in several sites of the Amazon forest of Ecuador to establish whether this was the case. Foliage samples were collected in sites located within oil spills and also from pristine forest in the Yasuni National Park. More than 1,100 leaves from three different levels of the vertical canopy profile (upper, medium and understory) were analysed for biophysical, biochemical and spectral properties. A second-order polynomial chlorophyll content model was estimated based on several published calibrations models which use a portable chlorophyll meter. Modelled chlorophyll content showed high correlations with methods using reflectance indices (0.76) and the inversion process of the PROSPECT radiative transfer model (0.71). The analysis of biophysical and biochemical parameters at the three canopy levels of vegetation growing near hydrocarbons leakages showed decreasing levels of foliar chlorophyll content which suggest a reduced photosynthetic activity, higher levels of water content, which may explain the thicker leaves in the upper canopy, and thinner leaves in the understory. Based on these results, hyperspectral Hyperion and CHRIS-Proba satellite images were used to explore the potential of several vegetation indices to detect the symptoms of vegetation affected by hydrocarbons. The results indicated that a combination of an index sensitive to chlorophyll content at canopy level (Sum Green) with the NDVI index (Normalized Difference Vegetation Index) are suitable to detect vegetation affected by hydrocarbons. Those indices accurately identified vegetation growing near sites polluted by the petroleum industry and also when applied to an area affected by hydrocarbons from natural macro-seepages, and areas where hydrocarbons may be near the surface. Two new vegetation indices are proposed to identify vegetation affected by hydrocarbon pollution. Those indices showed sensitivity to differentiate secondary forest polluted and non-polluted. Chlorophyll content maps were computed based on an approach which uses the MTCI (MERIS Terrestrial Chlorophyll Index) at leaf level and scaled up to canopy level. The results of this research contribute to knowledge of regarding forest degradation. The approach could be used to detect hydrocarbon seepages as indicators of petroleum reservoirs, as well as significant pollution from oil spills in forest ecosystems. Moreover, the parameters for hydrocarbon stressed

vegetation could be employed in a carbon cycle model to explore the impacts of hydrocarbon pollution on the carbon dioxide and water fluxes from tropical forests which are crucial for the carbon and water cycles.

Acknowledgements

I would like to thank my supervisors Dr Kevin Tansey and Prof Heiko Balzter for their support and advise during my PhD project. This research has been self-funded and partially supported by the Ecuadorian government through the National Secretariat for Science and Technology of Ecuador (SENESCYT). There are many other people and institutions to thank, firstly the Ministry of Non-Renewable Resources (Secretariat of Hydrocarbons) and the Environmental Ministry of Ecuador for the permissions granted for my fieldwork campaign in the Amazon region. In addition, I would like to thank Andes Petroleum Ecuador Ltd., for the logistics and support provided during my field campaign, and especially to Dr Zhang Xing, Douglas Good and Mauricio Avila who believed in the potential of this research. During data collection in the Amazon forest, many people supported the intensive and exhausting work. Collecting leaves from the vertical profile of every tree was always a challenging task, in which I was aided by my fieldwork assistances: Ivan Becerra, Angel Donoso and Elias. In the scientific research station at Yasuni National Park I had the great support of Dr Renato Valencia, Dr Hugo Romero, David Lasso, Carlos Padilla, Milton Pavon, Pablo Alvia and Milton Zambrano. I appreciate the assistance of the biologist Tatiana Avila for the vegetation species identification and their description.

I would also like to thank Prof Stéphane Jacquemoud and his team at the University of Paris Diderot; Dr Jean-Baptiste Féret from Carnegie Institution for Science and Prof Jean Philippe Gastellu-Etchegorry and his team at the Centre d'Etudes Spatiales de la Biosphère (CESBIO) for their support during the leaf and canopy vegetation modelling.

I wish to thank Dr Jörg Kaduk for his valuable computer programming guidance and advice during this research. He was/is always willing to provide support to students in spite of his busy schedule. I also extend my thanks to Dr Arnoud Boom for his great knowledge about the Amazon forest and his valuable advice during this research, and to Dr Javier Medina for his contribution and ideas.

Thanks to my friends Javier, Caroline, Alberto, Juan Carlos and Natalia for the memorable moments together. I acknowledge the friendship and great time given to me by my PhD friends and colleagues: Hao, Am, Claire, Andrea, Dimitris, Ramesh, Bashir, Firdos, Zamzam, Ajoke, Yahaya, Prem, Valentin, Peshawa, Alex, Azad, Mustafa, Idris and many others I have not mentioned.

And of course, the greatest support I have enjoyed from my lovely wife, Tume. Thanks for your love, support, encouragement and patience.

Table of contents

| | |
|--|-------|
| Dedication..... | i |
| Abstract..... | ii |
| Acknowledgements..... | iv |
| Table of contents..... | v |
| List of figures..... | ix |
| List of tables..... | xviii |
| List of abbreviations | xxi |
| Chapter 1. Introduction..... | 1 |
| 1.1 The importance of tropical forests | 1 |
| 1.2 Hydrocarbons and tropical forests | 3 |
| 1.3 The Amazon region of Ecuador | 5 |
| 1.4 Research questions and objectives | 8 |
| 1.5 Thesis structure | 10 |
| Chapter 2. Literature Review | 12 |
| 2.1 Introduction | 12 |
| 2.2 Vegetation optical properties | 12 |
| 2.2.1 Plant pigments..... | 12 |
| 2.2.2 Radiative transfer theory..... | 15 |
| 2.2.3 Leaf reflectance models | 16 |
| 2.2.4 Canopy reflectance models..... | 19 |
| 2.2.5 Coupling Models..... | 24 |
| 2.3 Hydrocarbons | 24 |
| 2.3.1 Hydrocarbon migration – seepages..... | 29 |
| 2.3.2 Hydrocarbon seepages in the study area..... | 31 |
| 2.3.3 Oil spills..... | 33 |
| 2.4 Hydrocarbons and environment interactions | 35 |
| 2.4.1 Hydrocarbon and atmospheric interactions | 36 |
| 2.4.2 Hydrocarbons and soil interactions..... | 39 |
| 2.4.3 Hydrocarbons and vegetation interactions..... | 40 |
| 2.5 Remote sensing for detection of vegetation stress caused by hydrocarbons..... | 42 |

| | | |
|------------|--|----|
| 2.5.1 | Vegetation anomalies in areas influenced by hydrocarbon seepages | 42 |
| 2.5.2 | Vegetation stress caused by natural gas..... | 44 |
| 2.6 | Summary | 49 |
| Chapter 3. | Chlorophyll Estimation in the Amazon Rainforest..... | 52 |
| 3.1 | Introduction | 52 |
| 3.1.1 | Chlorophyll meter SPAD-502 | 54 |
| 3.1.2 | Reflectance indices | 56 |
| 3.1.3 | PROSPECT model..... | 57 |
| 3.1.4 | MTCI index..... | 57 |
| 3.1.5 | The Red Edge Position (REP) | 58 |
| 3.2 | Materials and methods | 59 |
| 3.2.1 | Study area and sites..... | 59 |
| 3.2.2 | Sampling process | 66 |
| 3.2.3 | Chlorophyll meter readings | 68 |
| 3.2.4 | Spectroradiometer measurements | 70 |
| 3.2.5 | Chlorophyll indices based on SPAD-502 readings (transmittance) | 71 |
| 3.2.6 | Chlorophyll index based on reflectance indices. | 74 |
| 3.2.7 | PROSPECT model..... | 75 |
| 3.2.8 | MTCI Index | 79 |
| 3.2.9 | REP (first derivative method)..... | 79 |
| 3.3 | Results | 79 |
| 3.3.1 | Chlorophyll content based on SPAD-indices | 79 |
| 3.3.2 | Chlorophyll content based on reflectance indices | 80 |
| 3.3.3 | Comparison between the three methods for chlorophyll estimation | 81 |
| 3.4 | Discussion | 84 |
| 3.5 | Conclusion..... | 88 |
| Chapter 4. | Evidence of Vegetation Stress Caused by Hydrocarbons..... | 90 |
| 4.1 | Introduction | 90 |
| 4.1.1 | Foliar biophysical and biochemical parameters..... | 90 |
| 4.1.2 | Vertical profile of tropical forest | 93 |
| 4.2 | Materials and Methods | 94 |

| | | |
|---|---|-----|
| 4.2.1 | Study area and sites..... | 94 |
| 4.2.2 | Soil samples | 94 |
| 4.2.3 | Foliar sampling | 96 |
| 4.2.4 | Foliar biophysical and biochemical measurements | 96 |
| 4.3 | Results | 99 |
| 4.3.1 | Results per site | 99 |
| 4.3.2 | Results per site and vertical profile of the forest | 101 |
| 4.4 | Discussion | 105 |
| 4.4.1 | Leaf traits analysis per site..... | 105 |
| 4.4.2 | Leaf parameters analysis per site and vertical profile..... | 106 |
| 4.5 | Conclusions | 108 |
| Chapter 5. Response of Vegetation Indices from Hyperion to Petroleum | | |
| Pollution in the Amazon Rainforest..... | | 110 |
| 5.1 | Introduction | 110 |
| 5.1.1 | Vegetation indices for vegetation stress caused by hydrocarbons..... | 111 |
| 5.2 | Materials and Methods | 113 |
| 5.2.1 | Study sites | 113 |
| 5.2.2 | Satellite images | 117 |
| 5.2.3 | Hyperion image pre-processing | 125 |
| 5.2.4 | CHRIS-Proba image pre-processing..... | 144 |
| 5.2.5 | Vegetation indices..... | 145 |
| 5.2.6 | Exploring new vegetation indices for detecting hydrocarbon pollution in the tropical rainforest..... | 150 |
| 5.3 | Results | 151 |
| 5.3.1 | Broad-band Indices | 151 |
| 5.3.2 | Narrow-band-greenness/chlorophyll | 153 |
| 5.3.3 | Other pigments indices | 157 |
| 5.3.4 | Water indices | 158 |
| 5.3.5 | Vegetation indices suitable to detect hydrocarbon pollution..... | 159 |
| 5.3.6 | Mapping vegetation stress | 163 |
| 5.3.7 | Exploring new vegetation indices for vegetation affected by petroleum pollution..... | 171 |

| | | |
|--------------|---|-----|
| 5.3.8 | Mapping chlorophyll content..... | 177 |
| 5.4 | Discussion | 183 |
| 5.4.1 | Vegetation indices suitable to detect hydrocarbon pollution..... | 183 |
| 5.4.2 | Mapping vegetation stress | 186 |
| 5.4.3 | Exploring new vegetation indices for vegetation affected by petroleum pollution..... | 188 |
| 5.4.4 | Mapping chlorophyll content..... | 190 |
| 5.5 | Conclusions | 192 |
| Chapter 6. | Conclusions, Limitations and Further Research | 197 |
| 6.1 | Conclusions | 197 |
| 6.1.1 | Conclusions for Research Question 1 | 197 |
| 6.1.2 | Conclusions for Research Question 2..... | 199 |
| 6.1.3 | Conclusions for Research Question 3..... | 201 |
| 6.2 | Contribution to knowledge..... | 204 |
| 6.3 | Limitations | 205 |
| 6.4 | Further research..... | 206 |
| ANNEXES | | 209 |
| Bibliography | | 241 |

List of figures

| | |
|--|----|
| FIGURE 1.1 NORTH-EAST AMAZON REGION OF ECUADOR. PETROLEUM SPILLS AND OPEN PITS HAVE BEEN A SOURCE OF PETROLEUM POLLUTION. A HYDROCARBON SEEPAGE LOCATED IN PUNGARAYACU PETROLEUM FIELD IS IDENTIFIED IN THE STUDY AREA. SOURCE: ENVIRONMENTAL MINISTRY OF ECUADOR AND BACKGROUND IS A LANDSAT IMAGE..... | 6 |
| FIGURE 1.2. OIL SPILL IN THE STUDY AREA | 7 |
| FIGURE 1.3 OPEN PITS OF PETROLEUM INDUSTRY | 7 |
| FIGURE 1.4. A SECTION OF THE HYDROCARBON MACROSEEPAGE IN THE STUDY AREA (PUNGARAYACU OIL FIELD). THE DARK AREAS ARE CRUDE OIL EXPOSED TO THE SURFACE | 8 |
| FIGURE 2.1. ABSORPTION SPECTRAL OF THE MAJOR PLANTS PIGMENTS (BLACKBURN 2007) | 13 |
| FIGURE 2.2. RED EDGE POSITION IN THE REFLECTANCE SPECTRUM OF A TYPICAL GREEN LEAF (BLACKBURN 2007)..... | 14 |
| FIGURE 2.3. INFLECTION POINTS (REP) SHIFT BETWEEN TWO CHLOROPHYLL CONTENT VALUES (DEMAREZ&GASTELLU-ETCHEGORRY 2000)..... | 15 |
| FIGURE 2.4 A) SCHEMATIC CROSS-SECTION OF A LEAF ILLUSTRATING THE PATHS OF THE RADIATION INTERACTION. B) ILLUSTRATION OF LEAF MODEL FOR REPRESENTING RADIATION INTERACTION IN A LEAF (JONES & VAUGHAM, 2010)..... | 17 |
| FIGURE 2.5. SCHEMATIC OF THE LIGHT INTERACTIONS IN A CANOPY MODEL REPRESENTATION..... | 20 |
| FIGURE 2.6. REPRESENTATION OF A CONIFEROUS FOREST AS USED BY FLIGHT MODEL. FROM: RADIATION TRANSFER MODEL INTERCOMPARISON (RAMI) PROJECT WEBSITE AT: HTTP://RAMI-BENCHMARK.JRC.EC.EUROPA.EU/HTML/RAMI3/MODELS/FLIGHT/FLIGHT.PHP | 22 |
| FIGURE 2.7. DART COMPUTER SCENE REPRESENTATION (LEFT) AND EXAMPLE OF SIMULATION (RIGHT). FROM: RADIATION TRANSFER MODEL | |

| | |
|--|----|
| INTERCOMPARISON (RAMI) PROJECT WEBPAGE AT: HTTP://RAMI-BENCHMARK.JRC.EC.EUROPA.EU/HTML/RAMI2/MODELS/DART/ | 23 |
| FIGURE 2.8 TROPICAL RAINFOREST AND SEDIMENTARY BASINS IN SOUTH AMERICA. | |
| A) TROPICAL FOREST DISTRIBUTION; B) SEDIMENTARY BASINS (U.S DEPARTMENT OF ENERGY OPEN COPYRIGHT POLICY) | 32 |
| FIGURE 2.9 A) PETROLEUM RESERVOIRS IN THE AMAZON REGION OF ECUADOR (BLACK AREAS). PUNGARAYACU OIL FIELD WHERE HYDROCARBON MACRO-SEEPAGES HAVE BEEN IDENTIFIED. ITT OIL FIELD INSIDE OF YASUNI NATIONAL PARK. B) PHOTOGRAPHY OF MACRO-SEEPAGES IN PUNGARAYACU OIL FIELD WHERE GEOLOGICAL UPLIFT HAS EXPOSED CRUDE OIL TO THE SURFACE..... | 33 |
| FIGURE 2.10. DISTRIBUTION OF THE SEDIMENTARY BASINS IN THE WORLD (KVENVOLDEN&ROGERS 2005). | 37 |
| FIGURE 2.11. GLOBAL DISTRIBUTION OF OFFSHORE AND ONSHORE OIL SEEPAGES. NUMBERS INDICATE THE COUNT OF SEEPS. FROM (KVENVOLDEN&ROGERS 2005) | 38 |
| FIGURE 2.12. A GENERALISED MODEL OF HYDROCARBON MICROSEEPAGE AND ITS SURFACE EXPRESSIONS. (YANG 1999) | 40 |
| FIGURE 2.13. REFLECTANCE RESPONSE OF CONTROL GRASS PLOTS (SMITH;STEVEN & COLLS 2004)..... | 45 |
| FIGURE 2.14. REFLECTANCE RESPONSE GASSED. EACH LINE REPRESENTS A DISTANCE ALONG THE TRANSECT (SMITH;STEVEN & COLLS 2004) | 46 |
| FIGURE 2.15. VISIBLE SYMPTOMS OF OILSEED RAPE LEAVES (SMITH;STEVEN & COLLS 2005)..... | 47 |
| FIGURE 2.16. CHLOROPHYLL CONTENT OF PLANTS EXPOSED TO STRESS COMPARED TO CONTROL PLANTS. (SMITH;STEVEN & COLLS 2005) | 48 |
| FIGURE 3.1 MAP OF THE STUDY AREA-NORTH-EAST AMAZON REGION OF ECUADOR. SITE 1 AND SITE 2 ARE LOCATED IN SUCUMBIOS PROVINCE AND SITE 3 IS LOCATED IN ORELLANA PROVINCE. BACKGROUND IS A LANDSAT IMAGE. SOURCE OF ZOOM-IN MAP: COLOUR SHADED RELIEF IMAGE, WORLDSAT INTERNATIONAL, INC. | 60 |

| | |
|--|----|
| FIGURE 3.2 SITE 1 AFFECTED BY OIL SPILL. A) FOREST CANOPY; B) OIL SPILL; C) VEGETATION GROWING ON THE CRUDE OIL | 62 |
| FIGURE 3.3 SECONDARY FOREST NOT AFFECTED BY OIL POLLUTION. A) SITE 2A B) SITE 2B | 64 |
| FIGURE 3.4 LOCATION OF SAMPLED AREAS. BLACK POLYGONS = POLLUTED SITE; RED POLYGONS = NON POLLUTED SECONDARY FOREST. IKONOS IMAGE AS BACKGROUND | 64 |
| FIGURE 3.5 PRISTINE FOREST IN YASUNI NATIONAL PARK | 65 |
| FIGURE 3.6. MAP OF THE SAMPLED PARCELS OF THE YASUNI PLOT. | 66 |
| FIGURE 3.7 PHOTOGRAPHS OF LEAF SAMPLING PROCESS. A) COLLECTING LEAVES USING THE TELESCOPIC PRUNER B) CLIMBING TREES C) TELESCOPIC PRUNER NINE METERS LONG D) CLIMBING TREES TECHNIQUES E) CANOPY TOWERS IN THE STUDY AREA..... | 67 |
| FIGURE 3.8 LEAF SAMPLES AND CLIPPED DISKS FROM PLANTS OF DIFFERENT SPECIES AND HEALTH STATUS. THE LAST PHOTO SHOWS THE SPAD-502 METER | 68 |
| FIGURE 3.9 HISTOGRAM AND BOXPLOT OF THE SPAD-502 CHLOROPHYLL METER. TOTAL SAMPLES COLLECT IN BOTH SITES OF THE AMAZON FOREST IN ECUADOR | 69 |
| FIGURE 3.10. A) ASD HANDHELD 2 SPECTROPHOTOMETER, B) PLANT PROBE + LEAF CLIP..... | 70 |
| FIGURE 3.11 MEASURED AND ESTIMATED REFLECTANCE OF SOME REPRESENTATIVE SAMPLES OF THE FOLIAR DATASET | 78 |
| FIGURE 3.12. PROCESS TO ESTIMATE CHLOROPHYLL CONTENT ($\mu\text{G CM}^{-2}$) APPLYING THE INVERSION PROCESS OF PROSPECT LEAF REFLECTANCE MODEL..... | 78 |
| FIGURE 3.13. ESTIMATED CHLOROPHYLL CONTENT FOR EACH SPAD-502 CALIBRATION MODEL APPLIED TO THE TOTAL SAMPLES OF OUR DATASET. THE BLACK LINE REPRESENTS THE AVERAGE VALUE ACROSS MODELS AND ITS CONFIDENTIAL INTERVAL OF 95% FOR THE BINNED SPAD-502 READINGS..... | 80 |
| FIGURE 3.14 AVERAGE CHLOROPHYLL CONTENT ESTIMATES FROM FIVE REFLECTANCE MODELS (ERRORS BARS AT 1.96 STANDARD DEVIATIONS) COMPARED TO ESTIMATED GROUND TRUTH CHLOROPHYLL CONTENT BASED ON | |

| | |
|---|-----|
| SPAD-502 CHLOROPHYLL METER READINGS (ERROR BARS AT 1.96 STANDARD DEVIATIONS)..... | 81 |
| FIGURE 3.15 COMPARISON OF AVERAGE CHLOROPHYLL CONTENT ESTIMATES FROM THE SPAD-502 CHLOROPHYLL METER INDEX AND THE AVERAGES OF ALL SPECTRORADIOMETER-BASED CHLOROPHYLL ESTIMATES (ERROR BARS AT 1.96 STANDARD DEVIATIONS). | 82 |
| FIGURE 3.16 BOXPLOTS OF THE THREE ESTIMATION OF CHLOROPHYLL CONTENT (OUTLIERS NOT INCLUDED) | 83 |
| FIGURE 3.17 SCATTER PLOTS, HISTOGRAMS AND PEARSON CORRELATION BETWEEN THREE CHLOROPHYLL ESTIMATIONS (SPAD, REFLECTANCE AND PROSPECT) AND MTCI INDEX AND REP | 83 |
| FIGURE 3.18 COMPARISON OF THREE GENERALIZED MODELS DERIVED FROM SPAD-502 READINGS. THE SECOND ORDER POLYNOMIAL MODEL PROPOSED IN THIS STUDY (BLACK LINE), THE HOMOGRAPHIC MODEL PROPOSED BY CEROVIC ET AL. (2012) (DOTTED LINE) AND THE HOMOGRAPHIC MODEL PROPOSED BY COSTE ET AL. (2012) FOR A TREES FROM THE AMAZON FOREST..... | 85 |
| FIGURE 4.1 HISTOGRAM OF THE SPAD-502 CHLOROPHYLL METER READINGS AND BOXPLOT SHOWING THE OUTLIERS. TOTAL SAMPLES COLLECTED IN THE STUDY SITES. | 97 |
| FIGURE 4.2 LEAF PARAMETER IN THE VERTICAL PROFILE FOR THE THREE STUDY SITES | 102 |
| FIGURE 4.3 PLOTS OF MEAN WEIGHT GAIN FOR EACH LEVEL OF THE TWO FACTORS. THE HORIZONTAL LINE REPRESENTS THE MEAN VALUE FOR EACH TRAIT AND THE VERTICAL LINES THE LOCATION OF THE MEAN FOR THE CORRESPONDING FACTOR (SITE AND CANOPY HIGH) | 105 |
| FIGURE 5.1 LOCATION OF SAMPLED SITES IN THE AMAZON REGION OF ECUADOR WHICH CORRESPOND TO THE THREE SAMPLED SITES DESCRIBED IN CHAPTER 3 | 114 |
| FIGURE 5.2 STUDY AREA AND SAMPLED SITES IN THE PETROLEUM PRODUCTIVE REGION IN THE AMAZON REGION OF ECUADOR. BACKGROUND AN IKONOS | |

| | |
|---|-----|
| IMAGE ACCESSED FROM GOOGLE EARTH. THE YELLOW SQUARE IS ZOOMED IN THE NEXT FIGURE. | 115 |
| FIGURE 5.3 SAMPLED FIELDWORK SITES IN SECONDARY FOREST OF PETROLEUM PRODUCTIVE REGION. POLLUTED SITE (PINK AREAS) AND NON-POLLUTED SITES (GREEN CIRCLES). SQUARES REPRESENT AREAS OF INTEREST FROM WHERE STATISTICS AND VEGETATION INDICES ARE DERIVED. | 115 |
| FIGURE 5.4 PUNGARAYACU HYDROCARBON SEEPAGE LOCATED IN NAPO PROVINCE IN THE AMAZON REGION OF ECUADOR A) CRUDE OIL ON THE SURFACE B) CRUDE OIL LEAKING FROM ROCKS | 116 |
| FIGURE 5.5 SCHEMATIC REPRESENTATION OF THE SATELLITE ORBIT AND SENSORS FOOTPRINT OF THE INSTRUMENTS: HYPERION, (ADVANCED LANDSAT IMAGER). FROM EO-1/HYPERION SCIENCE DATA USER’S GUIDE (BARRY 2001)..... | 118 |
| FIGURE 5.6 RADIANCE SIGNAL FROM A CLOUD PIXEL OF HYPERION IMAGE. SPECTRAL ABSORPTION FEATURES SHOW VERY LOW VALUES. NO CALIBRATED BANDS ARE SET TO ZERO. | 121 |
| FIGURE 5.7 SIGNAL TO NOISE RATIO (SNR) MEASURED IN THE STUDY AREA..... | 123 |
| FIGURE 5.8. LOCATION OF THE CHRIS-PROBA IMAGE IN THE HYDROCARBON SEEPAGE AREA (READ RECTANGLE). PETROLEUM BLOCK 20 IS OPERATED BY IVANHOE ENERGY COMPANY. DATA SOURCE: HTTP://FOOTPRINTSOFEQUADOR.WEEBLY.COM/ ACCESSED ON: 14 TH APRIL 2014. | 124 |
| FIGURE 5.9 PROCESS FOR PRE-PROCESSING HYPERION IMAGES DEVELOPED IN THIS STUDY..... | 125 |
| FIGURE 5.10 SPECTRA REFLECTANCE RESULTS FROM FLAASH. THE BLUE OVAL HIGHLIGHTS TWO PEAKS DISCONNECTED IN THE RANGE OF 950-1300 NANOMETRES. THIS UNUSUAL RESULT IS SHOWN WHEN WAVELENGTH RECALIBRATION OPTION IS ENABLED. | 131 |
| FIGURE 5.11 SUBSET OF HYPERION IMAGE (BAND 16) IN THE STUDY AREA. COLOUR REPRESENTATION IS ARBITRARY TO HIGHLIGHT THE ABNORMAL PIXEL-COLUMN (ARROW). A) BEFORE CORRECTION AND B) AFTER CORRECTION. | 133 |

| | |
|--|-----|
| FIGURE 5.12 O ₂ ABSORPTION CURVE AT DIFFERENT COLUMNS ACROSS THE IMAGE. NOTE THE CHANGES IN THE ANGLES OF THE SLOPE IN THE SHOULDERS OF THE ABSORPTION FEATURE..... | 135 |
| FIGURE 5.13 A) DERIVATIVE IMAGE ESTIMATED IN THE O ₂ ABSORPTION FEATURE AROUND 760. B) SECTION ACROSS COLUMNS (HORIZONTAL PROFILE) OF THE DERIVATIVE IMAGE WHERE THE SMILE EFFECT IS CLEARLY IDENTIFIED. | 136 |
| FIGURE 5.14 MINIMUM NOISE FRACTION (MNF) PROCEDURE IN ENVI® SOFTWARE. | 137 |
| FIGURE 5.15 MINIMUM NOISE FRACTION TRANSFORMATION OF THE HYPERION IMAGE. A) MNF BAND 1 SHOWS A SPECTRA GRADIENT ON THE RIGHT SIDE OF THE IMAGE. B) SECTION ACROSS COLUMNS (HORIZONTAL PROFILE) OF THE MNF BAND 1 WHERE THE SMILE EFFECT IS DETECTED. | 138 |
| FIGURE 5.16 RESULTS OF THE DE-STRIPPING METHOD FOR BANDS A) 8, B) 9 C) 10 AND D) 37. THE FIRST THREE ARE BANDS STRONGLY AFFECTED BY STRIPES. RESULTS SHOW ARTEFACTS INTRODUCED BY THE METHOD ALONG COLUMNS AFFECTED BY CLOUDS..... | 140 |
| FIGURE 5.17 BAND 8A AND 9A BEFORE DE-STRIPPING. BAND 8B AND 9B AFTER DE- STRIPPING. SELECTION OF COLOURS ARE ARBITRARY TO DEMONSTRATE THE EFFECTS OF THE DE-STRIPPING PROCESS..... | 141 |
| FIGURE 5.18 A) DERIVATIVE IMAGE ESTIMATED IN THE O ₂ ABSORPTION FEATURE (BANDS 42 AND 43 OF HYPERION) AFTER THE DE-STRIPPING CORRECTION. B) HORIZONTAL PROFILE OF THE DERIVATIVE IMAGE WHERE THE SMILE EFFECT HAS BEEN REMOVED..... | 141 |
| FIGURE 5.19 EIGENVALUES FOR THE MNF TRANSFORMATION OF THE HYPERION IMAGE..... | 143 |
| FIGURE 5.20 MNF TRANSFORMATION RESULTS OF HYPERION IMAGE. A) MNF-1, B) MNF-2, C) MNF-10 AND D) MNF-15..... | 143 |
| FIGURE 5.21 A) REFLECTANCE SIGNAL BEFORE THE INVERSE MNF PROCESS TO REMOVE NOISE; B) REFLECTANCE SIGNAL AFTER REMOVE NOISE (SAME PIXEL FOR BOTH FIGURES)..... | 144 |

| | |
|---|-----|
| FIGURE 5.22. BOX PLOTS OF THE CALCULATED BROAD-BAND VEGETATION INDICES | 153 |
| | |
| FIGURE 5.23. BOX PLOTS OF THE CALCULATED NARROW-BAND VEGETATION INDICES: GREENNESS / CHLOROPHYLL | 156 |
| FIGURE 5.24. BOX PLOTS OF THE CALCULATED NARROW-BAND VEGETATION INDICES: OTHER PIGMENTS | 158 |
| FIGURE 5.25. BOX PLOTS OF THE CALCULATED NARROW-BAND VEGETATION INDICES: WATER INDICES | 159 |
| FIGURE 5.26. BOXPLOTS OF SELECTED VEGETATION INDICES HIGHLIGHTING THE THRESHOLD (YELLOW AREA) DEFINED BY THE MEDIAN AND THE MIN/MAX VALUES OF THE OIL-SPILL SITE. | 165 |
| FIGURE 5.27. AREAS IDENTIFIED AS VEGETATION STRESS BASED ON THE ELEVEN VEGETATION INDICES (ORANGE) | 166 |
| FIGURE 5.28. DISCRIMINANT FUNCTION ANALYSIS RESULTS APPLIED TO THE THREE STUDY SITES BASED ON THE SELECTED VEGETATION INDICES. | 167 |
| FIGURE 5.29. AREAS IDENTIFIED AS VEGETATION STRESS BASED ON THE SG, NDVI AND NDVI_705 INDICES WHICH TOGETHER CONTRIBUTE TO 83% OF THE SITE SEPARABILITY | 169 |
| FIGURE 5.30 RESULTS OF VEGETATION STRESS DETECTION IN PUNGARAYACU SITE USING A CHRIS-PROBA IMAGE. THE RED AREAS CORRESPOND TO PIXELS DETECTED AS VEGETATION STRESS BASED ON THE PROPOSED APPROACH | 170 |
| FIGURE 5.31 COEFFICIENT OF DETERMINATION (R^2) FOR EACH WAVELENGTH COMBINATION BETWEEN RSI AND FOLIAR PARAMETERS: A) CHLOROPHYLL CONTENT FROM SPAD-502 READINGS, B) CHLOROPHYLL CONTENT FROM PROSPECT MODEL, C) WATER CONTENT AND D) ORGANIC MATTER CONTENT. | 171 |
| | |
| FIGURE 5.32 COEFFICIENT OF DETERMINATION (R^2) FOR EACH WAVELENGTH COMBINATION BETWEEN NDSI AND FOLIAR PARAMETERS: A) CHLOROPHYLL CONTENT FROM SPAD-502 READINGS, B) CHLOROPHYLL CONTENT FROM PROSPECT MODEL, C) WATER CONTENT AND D) ORGANIC MATTER CONTENT. | 172 |
| | |

| | |
|---|-----|
| FIGURE 5.33 RSI BAND COMBINATION. SMOOTH BLUE REGION REPRESENTS A SCATTER PLOT OF BAND 36 (712 NM) AND BAND 55 (905 NM) OF HYPERION IMAGE (RED DOTS = POLLUTED SITE; GREEN DOTS = NON-POLLUTED SITE) ... | 174 |
| FIGURE 5.34 NDSI BAND COMBINATION. SMOOTH BLUE REGION REPRESENTS A SCATTER PLOT OF BAND 37 (721 NM) AND BAND 45 (803 NM) OF HYPERION IMAGE (RED DOTS = POLLUTED SITE; GREEN DOTS = NON-POLLUTED SITE) ... | 174 |
| FIGURE 5.35 CORRELATION BETWEEN BAND COMBINATIONS APPLIED TO HYPERION IMAGES BANDS IN THE STUDY AREA FOR: A) RSI BAND COMBINATION B) NDSI BAND COMBINATION | 175 |
| FIGURE 5.36 IDENTIFICATION OF TROPICAL RAINFOREST HEALTH BASED ON THE VEGETATION INDICES PROPOSED IN THIS STUDY AND MTCI. A) RSI vs MTCI B) NSDI vs MTCI | 177 |
| FIGURE 5.37 MTCI BANDS COMPARING WITH MTCI APPLIED TO HYPERION IMAGE | 178 |
| FIGURE 5.38 REGRESSION MODEL MTCI AND CHLOROPHYLL CONTENT AT FOLIAR LEVEL FOR SAMPLES AT THE UPPER CANOPY. A) INCLUDING OUTLIERS AND B) EXCLUDING OUTLIERS | 179 |
| FIGURE 5.39. MAPS OF THE ESTIMATIONS OF CHLOROPHYLL CONTENT AT CANOPY LEVEL BEFORE OUTLIER REMOVAL A) PETROLEUM PRODUCTIVE AREA B) PRISTINE FOREST (YASUNI) | 180 |
| FIGURE 5.40 MAPS OF THE ESTIMATIONS OF CHLOROPHYLL CONTENT AT CANOPY LEVEL AFTER OUTLIER REMOVAL A) PETROLEUM PRODUCTIVE AREA B) PRISTINE FOREST (YASUNI) | 181 |
| FIGURE 5.41 DIAGRAM OF THE PROCESS FOLLOWED TO ESTIMATE CHLOROPHYLL CONTENT FROM LEAF TO CANOPY LEVEL..... | 182 |
| FIGURE 5.42 CHLOROPHYLL CONTENT LEVELS FOR THE THREE STUDY SITES BASED ON THE MTCI INDEX APPLIED FROM LEAF TO CANOPY LEVEL. A) ALL LEAF SAMPLES AND B) SAMPLES EXCLUDING OUTLIERS | 183 |
| FIGURE 5.43. AREAS IDENTIFIED AS VEGETATION STRESS BY A) ELEVEN SELECTED INDICES AND B) THREE SELECTED INDICES REPRESENTING 83% OF THE SITE SEPARABILITY. THE EIGHT YELLOW AREAS REPRESENT SAMPLED SITES DURING | |

| | |
|--|-----|
| FIELDWORK AND BLACK SQUARES THE SAMPLED AREAS TO ESTIMATE VEGETATION INDICES..... | 187 |
| FIGURE 5.44 SCATTER PLOT OF HYPERION NSDI INDEX BAND COMBINATION (BLUE SMOOTHED). SECONDARY FOREST DETECTED AS POLLUTED BY THE THREE VEGETATION INDICES (SG-NDVI-NDVI ₇₀₅) IN RED; VEGETATION NON- POLLUTED IN GREEN..... | 190 |

List of tables

| | |
|---|----|
| TABLE 2.1. ELEMENTAL COMPOSITION OF PETROLEUM..... | 25 |
| TABLE 2.2. THE PHYSICAL PROPERTIES OF THE NORMAL ALKANES UNTIL C ₄₀ H ₈₂ ... | 26 |
| TABLE 2.3. CHEMICAL COMPOSITION OF NATURAL GAS..... | 26 |
| TABLE 2.4 HYDROCARBONS BIODEGRADABILITY..... | 28 |
| TABLE 2.5. ESTIMATIONS OF METHANE EMISSION FROM GEOLOGICAL SOURCES Tg(CH ₄) YR ⁻¹ | 37 |
| TABLE 2.6. ESTIMATIONS OF METHANE EMISSION FROM GEOLOGICAL SOURCES Tg(CH ₄) YR ⁻¹ | 38 |
| TABLE 3.1 TRADITIONAL METHODS FOR CHLOROPHYLL ESTIMATION | 53 |
| TABLE 3.2 DESCRIPTION OF THE SITES IN THE STUDY AREA | 61 |
| TABLE 3.3 NUMBER OF FOLIAR SAMPLES AND DESCRIPTIVE STATISTICS OF THE SPAD-502 CHLOROPHYLL METER READINGS FROM TWO SITES OF THE STUDY AREA..... | 69 |
| TABLE 3.4 INDICES OF CHLOROPHYLL CONTENT ESTIMATION BASED ON SPAD-502 CHLOROPHYLL METER MODELS APPLIED IN THIS STUDY..... | 73 |
| TABLE 3.5 CHLOROPHYLL CONTENT INDICES BASED ON REFLECTANCE DERIVED FROM SPECTRORADIOMETER DATA. | 75 |
| TABLE 3.6 DESCRIPTIVE STATISTICS OF LEAF CHLOROPHYLL CONTENT (μG CM ⁻²) BASED ON SEVEN PUBLISHED SPAD-502 CHLOROPHYLL METER MODELS..... | 79 |
| TABLE 3.7 DESCRIPTIVE STATISTICS OF CHLOROPHYLL CONCENTRATION (μG CM ⁻²) FROM THE REFLECTANCE MODELS BASED ON THE SPECTRORADIOMETER DATA. | 81 |
| TABLE 3.8 DESCRIPTIVE STATISTICS OF AVERAGE CHLOROPHYLL CONTENT ESTIMATES (μG CM ⁻²) FROM ALL SPAD-502 MODELS AND SPECTRORADIOMETER REFLECTANCE MODELS..... | 82 |
| TABLE 3.9 ANOVA AND PAIRWISE COMPARISON BETWEEN THE THREE CHLOROPHYLL METHODS FOR CHLOROPHYLL ESTIMATION BASED ON THE BINNED SPAD-502 INDEX | 87 |

| | |
|---|-----|
| TABLE 4.1 RESULTS OF LABORATORY ANALYSIS OF SOILS FOR THE THREE STUDY SITES | 95 |
| TABLE 4.2 NUMBER OF SAMPLES ACCORDING TO THE THREE SAMPLES SITES AND VERTICAL PROFILE OF THE FOREST..... | 96 |
| TABLE 4.3 DESCRIPTIVE STATISTICS OF FOLIAR PARAMETERS FOR THE THREE STUDY SITES..... | 99 |
| TABLE 4.4 ANOVA I TEST FOR THE SEVEN LEAF TRAITS..... | 100 |
| TABLE 4.5 PAIRWISE COMPARISON OF <i>P</i> -VALUES WITH HOLM ADJUSTMENT METHOD | 100 |
| TABLE 4.6 PAIRWISE COMPARISON OF <i>P</i> -VALUES BY THE ADJUSTMENT METHOD OF HOLMS FOR EACH SITE AND THE VERTICAL PROFILE OF THE FOREST | 103 |
| TABLE 5.1 HYPERION IMAGES CALIBRATED AND UN-CALIBRATED BANDS..... | 119 |
| TABLE 5.2 HYPERION BANDS AFFECTED BY ATMOSPHERIC ABSORPTION FEATURES | 120 |
| TABLE 5.3 SIGNAL TO NOISE RATIO OF HYPERION IMAGES | 122 |
| TABLE 5.4 UNUSABLE AND USABLE HYPERION BANDS | 127 |
| TABLE 5.5 FLAASH PARAMETERS FOR ATMOSPHERIC CORRECTIONS..... | 129 |
| TABLE 5.6 IDENTIFICATION OF PRE-LAUNCH AND REMAINING ABNORMAL PIXELS (COLUMNS) IN L1-R HYPERION IMAGES..... | 132 |
| TABLE 5.7 VEGETATION INDICES APPLIED TO HYPERION IMAGES IN THE STUDY AREA..... | 146 |
| TABLE 5.8 DESCRIPTION OF THE VEGETATION INDICES APPLIED IN THIS STUDY.... | 148 |
| TABLE 5.9 ANOVA COMPARISON OF MEANS AND SIGNIFICANCE..... | 160 |
| TABLE 5.10 ANALYSIS OF VARIANCE AND PAIRWISE COMPARISON OF MEANS USING HOLM ADJUSTMENT METHOD FOR THE STUDY SITES (OIL POLLUTION, SECONDARY FOREST AND PRISTINE FOREST) | 162 |
| TABLE 5.11. THRESHOLD VALUES DEFINED FOR SELECTED VEGETATION INDICES IN THE AREA AFFECTED BY HYDROCARBON POLLUTION | 165 |
| TABLE 5.12. RESULTS OF DISCRIMINATION FUNCTION ANALYSIS..... | 168 |

| | |
|---|-----|
| TABLE 5.13 MAXIMUM R^2 AND SPECTRAL BANDS FOR RSI AND NDSI INDICES FOR FOLIAR BIOPHYSICAL AND BIOCHEMICAL PARAMETERS OF TROPICAL FOREST. | 173 |
| TABLE 5.14. AVERAGE CHLOROPHYLL ($\mu\text{G CM}^{-2}$) CONTENT ESTIMATIONS FOR THE THREE STUDY SITES..... | 191 |

List of abbreviations

| | |
|-----------------|---|
| ANOVA | ANalysis Of VAriance |
| AOT | Aerosol Optical Thickness |
| APAR | Absorbed Photosynthetic Active Radiation |
| C_{ab} | Chlorophyll a and Chlorophyll b |
| CESBIO | Centre d'Etudes Spatiales de la BIOsphère of France |
| CHRIS-PROBA | Compact High Resolution Imaging Spectrometer-Project for On Board Autonomy |
| C_m | Foliar Organic Matter content |
| CO ₂ | Carbon dioxide |
| C_w | Foliar Water Content |
| CWV | Column Water Vapour |
| DART | Discrete Anisotropic Radiative Transfer model |
| DBH | Diameter at Breast Height |
| DEM | Digital Elevation Model |
| DN | Digital Number |
| EO-1 | Earth Observation 1 Mission of NASA |
| ESA | European Space Agency |
| FLAASH | Fast Line-of-sight Atmospheric Analysis of Spectral Hypercubes |
| FLIGHT | Forest LIGHT model |
| fPAR | Fraction of Photosynthetically Active Radiation |
| FOV | Field-of-View |
| FWHM | Full-Width Half Maximum |
| GPP | Gross Primary Production |
| HAP | Hydrocarbons Aromatic Polycyclic |
| ITT | Ishpingo Tambococha Tiputuni petroleum field |
| IPCC | Intergovernmental Panel of Climate Change |
| LAI | Leaf Area Index |
| LIBERTY | Leaf Incorporating Biochemistry Exhibiting Reflectance and Transmittance Yields model |
| LDMC | Leaf Dry Matter Content expressed in mass basis (%) |
| LiDAR | Light detection and ranging |

| | |
|----------|--|
| LOWTRAN | LOW resolution atmospheric TRANsmission |
| Lt | Leaf thickness |
| LWC | Leaf Water Content expressed in mass basis (%) |
| MERIS | Medium Resolution Imaging Spectrometer |
| MODTRAN | MODerate resolution atmospheric TRANsmission |
| MTCI | MERIS Terrestrial Chlorophyll Index |
| NIR | Near Infrared |
| NASA | The National Aeronautics and Space Administration |
| NDVI | Normalized Difference Vegetation Index |
| NPP | Net Primary Production |
| PAR | Photosynthetically Active Radiation |
| PROSPECT | Leaf Optical PROPERTIES SPECTra |
| RAMI | Radiation Transfer Model Inter-comparison |
| REDD | Reducing Emissions from Deforestation and Degradation |
| REP | Red Edge Position |
| RTM | Radiative Transfer Models |
| SENESCYT | National Secretariat for Science and Technology of Ecuador |
| SLA | Specific Leaf Area |
| SNR | Signal to Noise Ratio |
| SWIR | Short Wave Infrared |
| TIR | Thermal Infrared |
| TOA | Top of Atmosphere |
| TPH | Total Petroleum Hydrocarbons |
| UAV | Unmanned Aerial Vehicles |
| UNFCCC | United Nations Framework Convention on Climate Change |
| USGS | United States of America Geological Survey |
| VNIR | Visible and Near Infrared |
| VIs | Vegetation indices |

Chapter 1. Introduction

This chapter describes the importance of the tropical forest in ecological, climate and biogeochemical processes at regional and global level and describes some of the issues that face tropical forests, one of them related to the pollution events caused by petroleum in the Amazon region of Ecuador. The research questions and objectives of this thesis are presented later and finally the thesis structure is described.

1.1 The importance of tropical forests

The Amazon rainforest holds half of the tropical forested area of the world and accounts for 30% of global biomass productivity and 25% of global biodiversity (Malhi et al. 2006). Evaporation and condensation in tropical forests play a pivotal role in the regional and global atmospheric circulation (Malhi et al. 2008) and their rivers systems produce about 20% of the world's fresh water discharge (Davidson et al. 2012). Photosynthesis and respiration process more than twice the carbon of the annual rate of anthropogenic fossil fuel emissions (Phillips et al. 2009). Tropical forests store large amounts of carbon in high diversity ecosystems and play an important role in the global carbon cycle due to its Net Primary Production (NPP). According to the estimates of Houghton, et al. (2001 cited in Asner, et al., 2004, p. 6039), Amazon forests contain 70-80 billion metric tonnes (Pg or 10^{15} g) of carbon in plant biomass and assimilate 4-6 Pg of carbon each year in NPP. Despite its importance, a better understanding is needed of the interactions between the tropical forest and global processes, such as climate change.

During the last decades the Amazon forest has been threatened by deforestation, selective logging, hunting, fire and global and regional climate variations (Malhi et al. 2008, Davidson et al. 2012, Asner et al. 2004). Furthermore, the Amazon region consists of sedimentary basins in which vast petroleum reservoirs have been found (Kvenvolden&Rogers 2005), some of which have been exploited

during the previous decades (Finer et al. 2008). Little or no attention has been given to the impacts of the petroleum and hydrocarbons on the Amazonian forests, and their effects in tropical vegetation still remain poorly understood.

Tropical forest deforestation and degradation has raised international concerns since they contribute approximately 20% to the Global Greenhouse Gases (GHGs) emissions (UNFCCC 2007). Reducing Emissions from Deforestation and Forest Degradation (REDD) is a United Nations Framework Convention on Climate Change (UNFCCC) initiative that developed a financial framework and mechanisms to reduce forest losses and the associated GHGs emissions aiming to prevent further deforestation and consequently mitigate climate change.

Deforestation is defined as the ‘permanent’ conversion of a forest type to another land cover. ‘Forest degradation’ is a reduction of biomass density within a forest cover. The relative contribution of deforestation and degradation to the net emissions of carbon are not readily distinguished (Houghton 2012). Research has aimed to quantify global deforestation from satellite and census data, but there is an ongoing debate on the uncertainties of the estimates (Hoscilo 2009). On the other hand forest degradation has been more difficult to measure with remote sensing and there are no estimates for the entire tropics (Houghton 2012).

The Amazon rainforest plays an essential role in ecological, climate and biogeochemical processes on Earth. In this highly diverse environment, complex interactions between plant communities and their surrounding environment need to be better understood. Remote sensing can provide a better understanding of the interactions between hydrocarbons and vegetation in the tropical forest due its ability to evaluate leaf and canopy chemical properties which are the principal determinants of plant physiology and biochemical processes in terrestrial ecosystems. Due to its high spectral resolution, hyperspectral remote sensing has proven to be a promising tool to assess forest degradation through the investigation of biophysical and biochemical parameters such as chlorophyll and other pigment concentrations at leaf and canopy level. (Yang, 1999; van der Meer

et al., 2006; Noomen *et al.*, 2007; Smith *et al.*, 2004; Smith *et al.*, 2005, Blackburn, 2007).

This study focuses on tropical forest degradation caused by hydrocarbons impacts on the biophysical and biochemical composition of tropical rainforest in the Amazon region of Ecuador.

1.2 Hydrocarbons and tropical forests

The global demand for fossil energy and the high prices of crude oil are triggering oil exploration and production projects all around the Amazon basin, even very remote areas have already been leased out or are being negotiated for petroleum and gas exploration and production (Finer *et al.* 2008). In Ecuador, petroleum productive areas located in the Amazon region have been exploited for oil and gas since 1967 (Bernal 2011). During the first decades of production a considerable number of oil spills from pipeline networks and leakages from unlined open pits were recurrent (Bernal 2011, Hurtig&San-Sebastián 2005). Some polluted areas have been identified and cleaned-up, however others are still hidden and covered by tropical vegetation. Those polluted areas need to be detected and cleaned-up. Nowadays, these polluted areas from the early stages of the petroleum industry are the focus of international legal actions between local residents against international oil companies.

Petroleum production and its environmental and social interactions are in the centre of debate in Ecuador. Yasuni National Park is one of the most bio-diverse hot spots in the world (Tedersoo *et al.* 2010, Bass *et al.* 2010) and lies in an area where vast petroleum reservoirs have been discovered, one of them, Ishpingo-Tambocoha-Tiputini (ITT), accounts for 20% of the total proven reserves of the country. In 2007, the Ecuadorian government launched an innovative initiative called Yasuni-ITT which proposed a global responsibility to prevent petroleum production and keep the petroleum permanently underground in order to protect the area and avoid forest degradation and global carbon emissions in exchange for

donations from the international community that covers a fraction of the profits that the country will not receive from the petroleum market (Marx 2010, Martin 2011). A United National trust fund was created to receive the international contributions which will be invested in conservation and sustainability projects in the region.

As the aforementioned initiative did not reach the expected support from the international community, the Ecuadorian government decided, on 13th August 2013, to terminate the trust fund, return the funds to the contributors and exploit the petroleum reserves located within the protected area. This decision was backed by the Ecuadorian Parliament based on intense debates and the commitment to minimise the environmental impact caused by drilling and petroleum production. In this context, the author of this thesis based on the outcomes of this research, prepared a proposal for social and environmental monitoring using multi-level and multi-sensor remote sensing techniques which was submitted to the Ecuadorian Parliament where it was analysed and used as a framework for the new national resolution for petroleum projects in social and environmentally sensitive areas of the Amazon region in Ecuador. The new resolution is called “National interest statement for exploitation of petroleum Blocks 31 and 43 in Yasuni National Park” and was promulgated on 4th October 2013.

At global level, the demand of oil and gas has been continuously increasing and alternative sources for obtaining crude oil and gas have been proposed (Jaspal&Nerlich 2014). One example entails gas production using hydraulic fracturing techniques, also known as fracking, which is a process to extract natural gas by drilling and injecting fluid into the ground at a high pressure in order to fracture shale rocks and release natural gas (principally methane) to flow into the well. However, it is difficult to determine the amount of natural gas that escapes to the surface. Concerns have been raised about potential environmental impacts

and health risks (Boudet et al. 2014). More research is needed in these areas in order to understand the effects of this technique.

In addition to human hydrocarbons extraction, petroleum-hydrocarbons may reach the surface through a natural process where hydrocarbons leak vertically or near-vertical from the geological reservoirs to the surface. Once on the surface, hydrocarbons interact with the environment and vegetation of the tropical forest. This process is known as 'hydrocarbon seepage' (Horvitz 1982, Abrams 1996, van der Meer; Yang & Kroonenberg 2006). Contributions of hydrocarbon seepages to global atmospheric methane have been included in the last IPCC report (Solomon et al. 2007) but more research is needed to understand the contribution of the on-shore seepages in sedimentary basins to the global methane balance.

Using satellite images to monitor vegetation health in petroleum productive areas can contribute to increase the environmental control of industrial activities. On the other hand, detecting vegetation affected by gases from hydrocarbon seepages can significantly contribute to exploration projects during the search of potential oil/gas reservoirs in remote areas. In this context, the rationale behind this research is to assess the biophysical and biochemical parameters of tropical vegetation in order to detect vegetation stress in areas affected by hydrocarbons using hyperspectral remote sensing information.

1.3 The Amazon region of Ecuador

During the last five decades, private and public companies have been expanding petroleum exploration and production in this region. Several oil spills occurred in the past and open pits containing crude oil have been a permanent source of environmental pollution. Natural hydrocarbon seepages are located in this region which also may contribute to the environmental pollution, but their effects have been not investigated yet. New routes and infrastructure used by local settlers for colonisation have caused deforestation through small-scale agriculture,

commercial logging and cattle ranching. Nowadays the areas near to the petroleum facilities and infrastructure are used by local people for agriculture and livestock farming (Finer et al. 2008).

The environmental Ministry of Ecuador has been working to detect oil spills that occurred decades ago (see Figure 1.1).

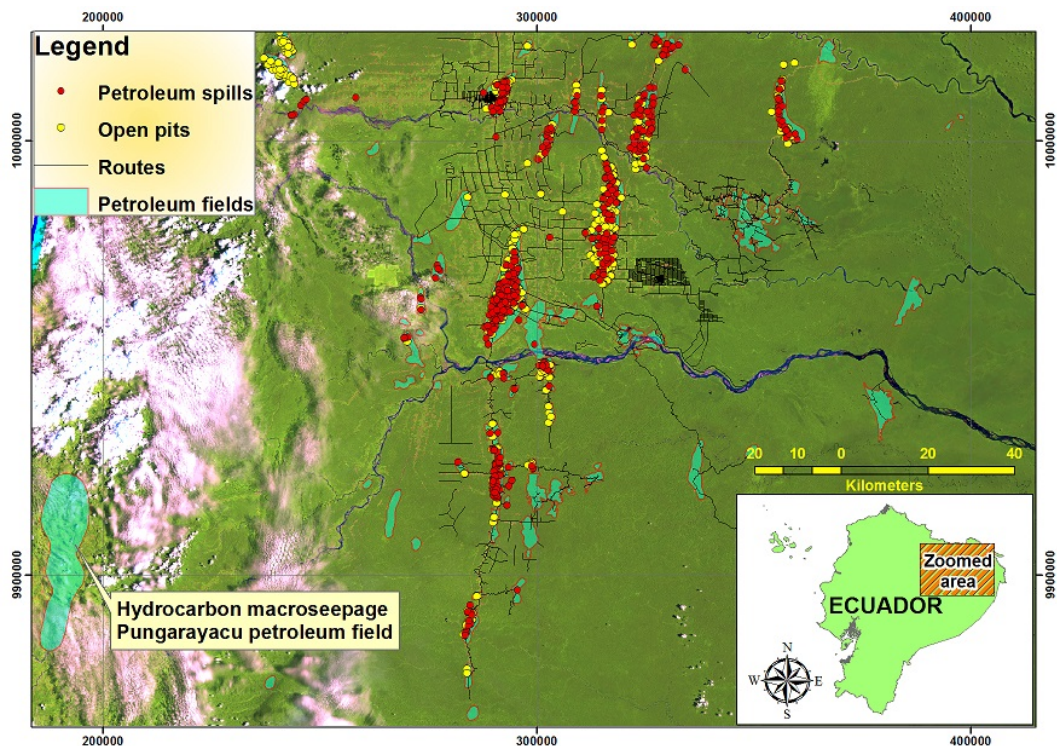


Figure 1.1 North-east Amazon region of Ecuador. Petroleum spills and open pits have been a source of petroleum pollution. A hydrocarbon seepage located in Pungarayacu petroleum field is identified in the study area. Source: Environmental Ministry of Ecuador and background is a LandSat image.

Several oil spills have been detected but many others still need to be identified and remain covered by tropical vegetation. Figure 1.2 illustrate an oil spill in the Amazon region of Ecuador.



Figure 1.2. Oil spill in the study area

Open pits from the early decades of petroleum production are still a source of pollution in the study area. They contain crude oil that has been discharging to the environment or leaching out as the pits degrade or overflow from rainwater (Figure 1.3).



Figure 1.3 Open pits of petroleum industry

A hydrocarbon macroseepage is located in the Western part of the study area known as the Pungarayacu oil field (Figure 1.4) which is part of a geological structure known as the Napo uplift. This is an extensive deformation zone along the Andean range as a result of tectonic stress of the Nazca and Continental plates

Annex 13 illustrates the structural profile of the Oriente sedimentary basin where Pungarayacu hydrocarbon seepages I located. Hydrocarbons have been exposed at the surface permanently. The environmental effects of seepages have not yet been studied.



Figure 1.4. A section of the hydrocarbon macroseepage in the study area (Pungarayacu oil field). The dark areas are crude oil exposed to the surface

The region of interest for this thesis covers some areas where hydrocarbons have been interacting with the environment, and specifically with vegetation of the tropical forest. However, the region also holds vast areas of intact and highly biodiverse primary forests located in protected and still inaccessible areas of the Amazon region (Figure 1.1 presents a map where oil spills and hydrocarbon seepages are located in the Amazon region of Ecuador).

1.4 Research questions and objectives

The aim of this research is to understand the effects of hydrocarbon pollution in vegetation of tropical forest and develop a method to detect vegetation stress through the evaluation of biophysical and biochemical parameters measured at

leaf level and then scaling-up to canopy level using hyperspectral remote sensing data. Specifically, this research work has the following research questions and objectives:

Research Question 1: As knowledge and in-situ observations about chlorophyll levels in tropical forests are limited, what alternative method based on non-destructive and portable instruments can provide rapid and accurate estimations of chlorophyll content in diverse tropical rainforest environments?

Objective 1: Assess the estimates of chlorophyll content in vegetation of the Amazon forest from the portable chlorophyll meter SPAD-502 Konica-Minolta and evaluate its results through comparison with other non-destructive methods: reflectance indices from spectro-radiometer and radiative transfer modelling using the inversion of PROSPECT model.

Research Question 2: Are biophysical and biochemical foliar parameters across the vertical profile of the tropical rainforest affected by hydrocarbon pollution?

Objective 2: Determine how the vegetation of the tropical forest may be affected by hydrocarbon pollution and which biophysical and biochemical foliar parameters change along the vertical profile of the forest between polluted and non-polluted sites of the Amazon forest.

Research Question 3: What is the potential of hyperspectral satellite images for detecting changes of biophysical and biochemical parameters of the tropical rainforest affected by hydrocarbon from oil spills or hydrocarbon seepages?. In this context, this research question can be split in the following parts:

- Which vegetation indices can best identify vegetation stress caused by hydrocarbon pollution?
- Can new vegetation indices sensitive to detecting tropical rainforest affected by hydrocarbon pollution be derived?

- Can chlorophyll content maps be derived from hyperspectral satellite images and can they highlight vegetation stress caused by hydrocarbons?

Objective 3: Investigate vegetation indices allowing the detection of changes of biophysical and biochemical parameters of the tropical forest caused by hydrocarbon pollution and develop an approach to map chlorophyll content at canopy level based on chlorophyll measured at leaf level.

1.5 Thesis structure

This thesis is composed of six chapters each of them describing a particular aspect that contributes to answering the main questions of this research.

Chapter 2. Literature Review. This chapter justifies the research questions and presents a review of hydrocarbon composition and how they interact with the environment. Subsequently, optical properties of vegetation, and their relationship with biophysical and biochemical parameters of plants are discussed. Remote sensing and radiative transfer methods are assessed vegetation parameters. Finally, remote sensing approaches to detect vegetation stress in areas affected by hydrocarbon pollution are reviewed.

Chapter 3. Chlorophyll Estimations in the Amazon Rainforest. It focuses on the analysis of different optical approaches to estimate chlorophyll content in the tropical rainforests. Transmittance, reflectance and a radiative transfer models are applied to estimate chlorophyll content for a collection of more than 1,100 leaves sampled in pristine and secondary tropical forests of the Amazon region.

Chapter 4. Evidence of Vegetation Stress Caused by Hydrocarbons. It investigates the effects of hydrocarbon pollution on the biophysical and biochemical parameters of tropical rainforests. Those effects are assessed in the vertical profile of the tropical rainforest.

In *Chapter 5. Response of Vegetation Indices from Hyperion to Petroleum Pollution in the Amazon Rainforest.* In this chapter several vegetation indices

derived from hyperspectral satellite images are computed in order to assess vegetation stress based on changes of biophysical and biochemical parameters identified in the previous chapter. New vegetation indices are explored to identify vegetation stress caused by hydrocarbon pollution. Vegetation stress is mapped and provides evidence of hydrocarbon pollution. Finally a method to estimate canopy chlorophyll content from leaf chlorophyll concentrations is discussed.

Chapter 6. Conclusions, Limitations and Further Research. It summarises the key findings of this research. The answers to the research questions are presented together with their contributions for knowledge. To conclude, some limitations and suggestions for further work are presented.

Chapter 2. Literature Review

2.1 Introduction

This chapter compiles information on the interactions between hydrocarbons and the surrounding environment. It is divided into five sections covering the main research objectives. The first section focuses on plant pigments, vegetation optical properties and the different approaches used in this research. The second section analyses the interactions between hydrocarbons and atmosphere, soils and vegetation. The third section discusses hydrocarbon composition and how hydrocarbons reach the Earth's surface. Section four will compile experiences from around the globe to detect vegetation anomalies caused by hydrocarbon influence by using remote sensing techniques. Finally the last section summarizes the relevant aspects found in the literature.

2.2 Vegetation optical properties

2.2.1 Plant pigments

Leaf optical properties are influenced by the concentration of plant pigments and other biochemicals, water content and leaf structure. The main plant pigments are chlorophyll *a* and *b*, α -carotene, β -carotene, anthocyanins and xanthophylls. The distribution is variable between plant species but a general distribution is chlorophylls -65%, xanthophylls-29%, carotenes-6% (Kumar;Schmidt & Dury 2006). The most important plant pigments are the chlorophylls since they are essential for photosynthesis. They absorb violet-blue light for photosynthesis and green light is not absorbed for photosynthesis. Chlorophyll absorption in the visible range of the electromagnetic spectrum is located at 0.43 μm (Chl_a), 0.46 μm (Chl_b), 0.64 μm (Chl_b) and 0.66 (Chl_a), and it generally decreases under stress conditions (Jones&Vaughan 2010). As a group, leaf pigments interact with the visible portion of the spectrum electromagnetic (400 nm to 700 nm), although the effects vary depending upon the type of pigment. Figure 2.1 shows the absorption spectra of plant pigments (Blackburn 2007).

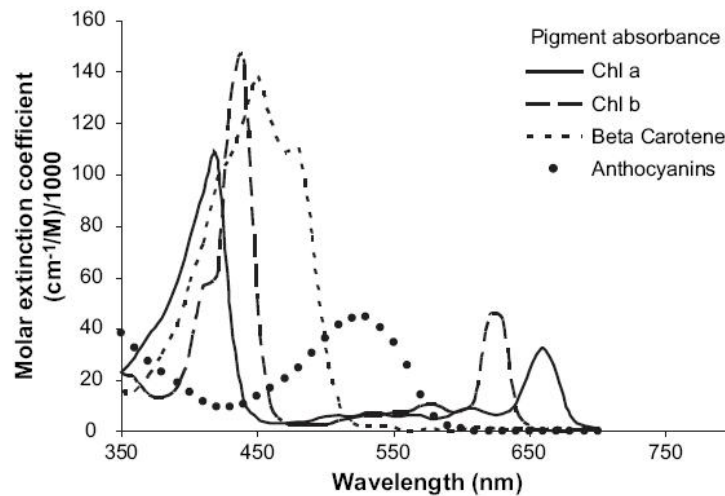


Figure 2.1. Absorption spectral of the major plants pigments (Blackburn 2007)

A characteristic feature of green vegetation spectra response is the sharp increase of reflectance between the RED and near infrared (NIR) known as red-edge position (REP), or red-edge shoulder. It takes into account the low red chlorophyll reflectance (around 680 nm) related to the high reflectance, around 800 nm, which is associated with leaf internal structure and water content of the plant. To estimate the REP, the red-edge inflection point is used. This is the point of maximum slope in the red-infrared curve (Kumar;Schmidt & Dury 2006). Figure 2.2 describes the red edge position in the reflectance spectrum of a typical green leaf (Blackburn 2007).

There is considerable evidence that hydrocarbon gases in the soil are a source of vegetation stress (Gustafson 1944, Gustafson 1950, Horvitz 1972, Lang;Aldman & Sabins 1985, Lang;Curtis & Kavacs 1985, Melo et al. 1996). Spectral reflectance of stressed vegetation has shown an increased value in visible wavelengths due to the chlorophyll content reduction, and a decreased reflectance in the NIR due to the structural damage of the plants.

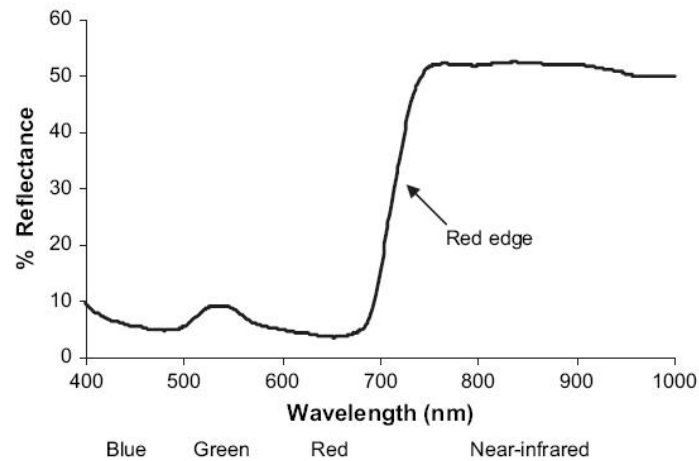


Figure 2.2. Red edge position in the reflectance spectrum of a typical green leaf (Blackburn 2007)

Changes in chlorophyll concentration of the plants produce a spectral shift of the absorption edge near 700 nm. The REP, defined as the point of the maximum slope on the reflectance spectrum of vegetation between red and near-infrared wavelengths, shifts towards the blue part of the spectrum with loss of chlorophyll and shifts towards the red part of the spectrum with increase of chlorophyll (van der Meer;de Jong & Bakker 2006). The results are:

- A decrease in the height of the infrared shoulder due to structural damage.
- An increase in the reflectance of maximum chlorophyll absorption due to detecting of leaf chlorophyll.
- A shift in the position of the red edge towards shorter wavelengths which is illustrated in Figure 2.3 (Demarez&Gastellu-Etchegorry 2000).

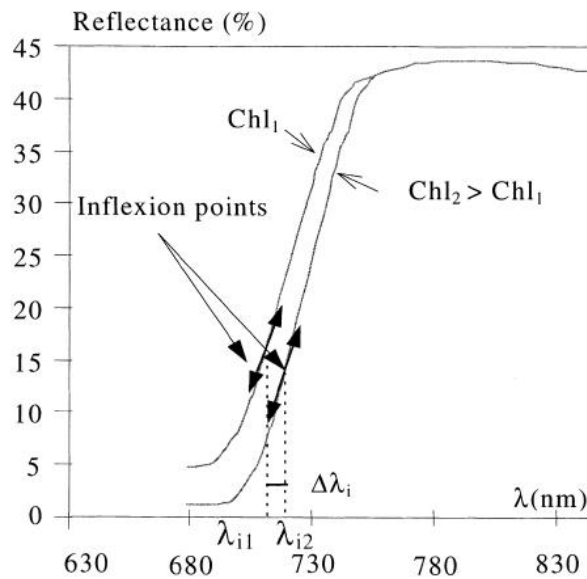


Figure 2.3. Inflexion points (REP) shift between two chlorophyll content values (Demarez&Gastellu-Etchegorry 2000)

2.2.2 Radiative transfer theory

The radiative transfer theory for a turbid medium was originally evolved in astrophysics (Chandrasekhar 1950) and has been modified to describe the main features of radiation in horizontally homogeneous well-developed stands (France 1990).

Radiative transfer theory treats a canopy structure as a turbid medium where the leaves scatter the radiation. According to Ross, J. (1975), the radiation regime in stands is determined by the following factors:

- Conditions of incident radiation including two components: direct solar radiation reaching the canopy directly from the sun; and diffuse solar radiation reaching the stand from all directions due to the atmospheric scattering.
- Optical properties of the canopy. Solar radiation hitting the leaf surface is reflected, absorbed or transmitted. The amounts of reflection, absorption or

transmission depend on the wavelength, angle of incidence, surface roughness and the optical properties and biochemical contents of the leaves.

- The interaction radiation-leaf produces three effects: thermal, photosynthetic and photomorphogenic. Over 70% of the solar radiation absorbed by plants is converted into heat (thermal) for transpiration. Up to 28% of the absorbed energy is used during the Photosynthetic Active Radiation (PAR) for photosynthesis. The region of photomorphogenically active radiation begins in the ultraviolet region, extends over the whole visible range and ends in the near-infrared near 750 nm. The optical properties of leaves in the PAR region depend on conditions of radiation, species, leaf thickness, leaf surface, structure, chlorophyll, carotenoid content, dry matter content per leaf unit area, leaf internal structure and water content.
- Optical properties of the ground surface. The ground below the canopy reflectance response (albedo). It depends on the vegetation density, LAI and the surface composition.
- Canopy architecture. It can have an important influence on reflectance according to the distribution of plants on the ground surface, leaves within a plant volume, leaf size and orientation, and other factors.

2.2.3 Leaf reflectance models

Solar radiation is the principal source of energy used by plant leaves and it can be reflected, absorbed or transmitted. Photosynthetically active radiation (PAR) is used during photosynthesis process and for conversion of high-energy organic compounds. The optical properties of the leaves depend on conditions of radiation, species, leaf thickness, leaf surface structure, chlorophyll and carotenoid content, dry matter and leaf internal structure (Kumar;Schmidt & Dury 2006). Figure 2.4 shows the incident energy interaction with the internal structure

of a leaf. Figure 2.4a is a schematic representation of a typical dicotyledonous leaf (cotton) illustrating the diversity of paths of radiation interaction with the leaf. A substantial proportion of visible radiation is absorbed by chloroplasts but a large fraction of the infrared is reflected or scattered either at the surface or specially at the interfaces between cells and intercellular spaces. Figure 2.4b illustrate a “plate” model for representing radiation interaction in a leaf. In this approximation, the leaf is comprises a number (n) of individual homogeneous chlorophyll-containing abserver plates separated by an airspace, with refelction/diffeaction acurring at the air/cell interfaces (Jones&Vaughan 2010).

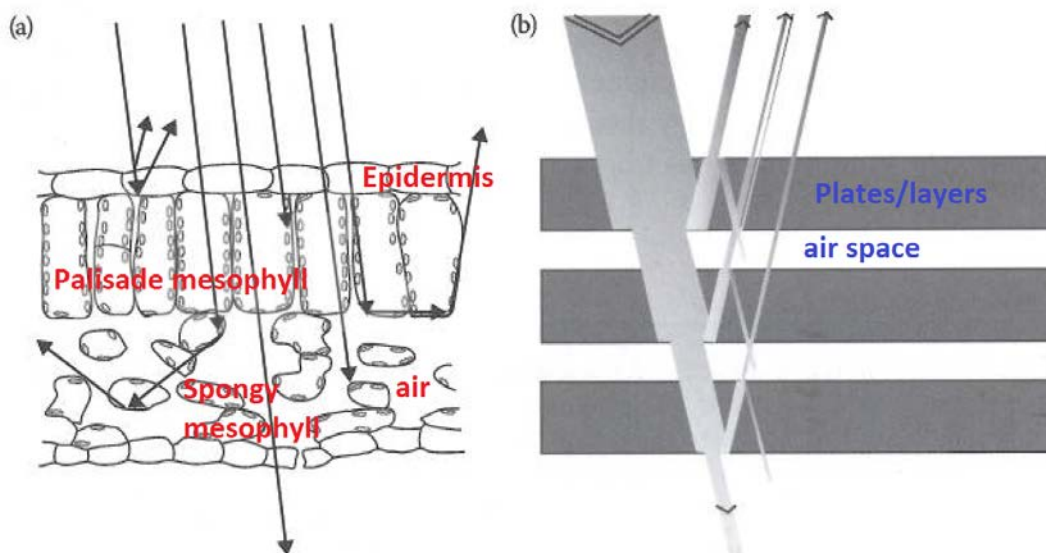


Figure 2.4 a) Schematic cross-section of a leaf illustrating the paths of the radiation interaction. **b)** Illustration of leaf model for representing radiation interaction in a leaf (Jones & Vaugham, 2010)

In the near infrared region, the primary contribution of reflectance comes from water absorption features. In the shortwave infrared region, reflectance is a result of water, nitrogen and various forms of carbon (Asner 1998).

Based on the relationship between reflectance and the biochemical and biophysical properties of the leaves, reflectance models have been created in order

to simulate the interaction of the light with the plant leaves through the radiative transfer theory.

The **Leaf Optical Properties Spectra (PROSPECT)** model describes radiative transfer within a broadleaf with a plate model. Plate models treat internal leaf structure as sheets or plates (as shown in Figure 2.4b) and calculate multiple reflections of diffuse radiation between these interfaces (Kumar;Schmidt & Dury 2006). PROSPECT is based on the representation of the leaf as one or several absorbing plates with a rough surface giving rise to isotropic scattering. The model estimates the directional-hemispherical reflectance and transmittance of leaves across the solar spectrum from 400 nm to 2500 nm (Jacquemoud 2009). A leaf structure parameter of the model is represented by N which is the number of compact layers specifying the average number of air/cell wall interfaces within the mesophyll. The leaf biophysical parameters of the model are represented by chlorophyll a+b content (C_{ab}) and equivalent water thickness (C_w). The latest versions of the model include the parameters dry matter content (C_m) and brown pigments content (C_{bp}).

The inversion process of the model is performed numerically with an interactive optimisation method. The forward model can be applied directly at each interaction, although lookup tables might be a better option if performance of the model is critical (Kempeneers et al. 2008) as biophysical and biochemical parameters of the leaf can be estimated.

Inversion of PROSPECT revealed a good agreement between measured and predicted leaf chlorophyll concentrations (Kumar;Schmidt & Dury 2006, Jacquemoud 2009, Feret 2008). Moreover, Feret(2008) extended the model capabilities by improving the chlorophyll estimation and including the retrieval of carotenoid pigments.

Other models have been developed for the estimation of reflectance and transmittance of the leaves. **Leaf Incorporating Biochemistry Exhibiting**

Reflectance and Transmittance Yields (LIBERTY) is a model that is a radiative transfer leaf model for conifer (particularly pine) needles (Dawson;Curran & Plummer 1998).

2.2.4 Canopy reflectance models

Following the same principle of leaf reflectance models, canopy reflectance models provide the logical connection between optical and structural features of the canopy, the geometry of the radiometric interaction and the resulting alteration to the reflected radiance. According to Goel(1988), the resulting reflectance value from a canopy is a function of the following general subsystems Figure 2.5:

- The source of the radiation (usually the sun) is defined by a set $\{A_i\}$ of properties: spectral intensity, $I(\lambda)$ and location (θ_s, ψ_s) , where λ is the wavelength and θ_s and ψ_s are the source zenith and azimuth angles, respectively.
- Atmosphere is characterised by a set $\{B_i\}$ of properties: spatial dependent constraints, λ -dependent absorption and scattering properties of aerosol particles, water vapour and ozone.
- Vegetation canopy is characterised by a set $\{C_i\}$ properties: optical parameters (reflectance and transmittance), structural parameters (geometry shapes and positions) of vegetation components, (leaves, stalks, stems, etc.), and other parameters like temperature, relative humidity, wind speed, and precipitation.
- Ground or Soil, defined by a set $\{D_i\}$ of properties such as reflectance and absorption, surface roughness and texture, bulk density and moisture profile.
- Sensor, characterized by a set $\{E_i\}$ of properties which defines its spectral sensitivity, aperture, calibration and position (view zenith angle θ_o and view azimuth angle ψ_o) .

Canopy models predict reflectance $\{R_i\}$ by the function f that invokes the radiative transfer model:

$$R_i = f(A_i, B_i, C_i, D_i, E_i) \quad (1)$$

Inverting the model in order to predict optical and structural parameters $\{C_i\}$ at canopy level involves defining or deriving a function, relation, or an algorithm g from the reflectance measured at canopy level $\{R_i\}$:

$$C_i = g(A_i, B_i, R_i, D_i, E_i) \quad (2)$$

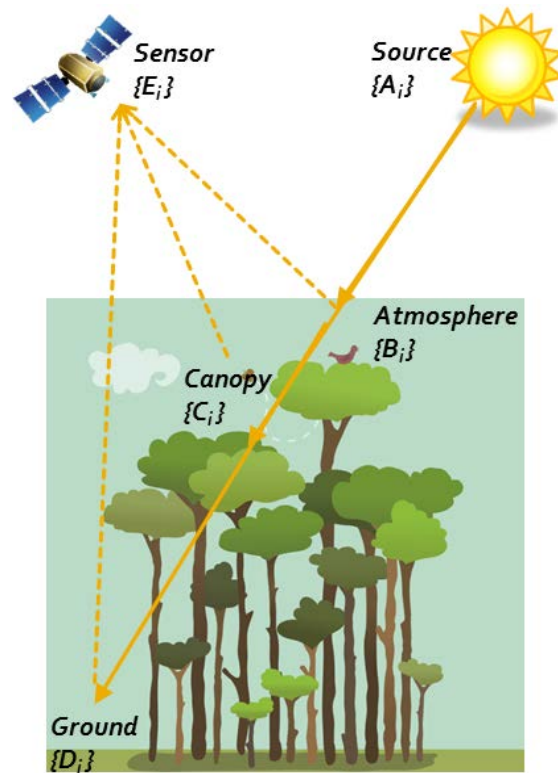


Figure 2.5. Schematic of the light interactions in a canopy model representation **SAIL (Scattering by Arbitrarily Inclined Leaves)** is a turbid-medium canopy model developed by Verhoef(1984) for homogeneous cultural crops and grassland canopies based on the radiative transfer theory. Turbid-medium models are suitable to apply to dense horizontal uniform canopies, assuming canopies of a

plane-parallel, infinite medium which is made up of one or more horizontal layers of vegetation where the lower layer is the soil substrate. The optical and structural properties of the vegetation elements in each layer are assumed to be constant and the canopy structure is usually defined by LAI (Leaf Area Index) and LAD (Leaf Angle Distribution) values (France 1990). Since SAIL was developed, new capabilities and complexity have been added to the model and incorporated into new versions of the model (SAILH, GeoSAIL, 4SAIL2 among others). According to Jacquemoud(2009), the SAIL model demonstrates intrinsic limitations in simulating reflectance in heterogeneous canopies showing clumping at several scales. The results, under these circumstances, are comparable to those of empirical relationships with vegetation index.

Forest LIGHT (FLIGHT) is a canopy model hybrid 3-D radiative transfer/geometric optical model developed by North(1996). The model adapts the Monte Carlo technique to simulate *i*) multiple scattering within crowns and *ii*) multiple scattering between discrete-crowns and trunk elements and the ground surface. Multiple scattering is accurate when simulated in the canopy, taking into account interactions within and between crowns, trunks and the ground surface. Figure 2.6 shows a representation of a coniferous forest as used by this model and available at the Radiation transfer Model Intercomparison (RAMI) project webpage at <http://rami-benchmark.jrc.ec.europa.eu/HTML/RAMI3/MODELS/FLIGHT/FLIGHT.php>.

Validation measurements have shown a better agreement of predicted and measured directional reflectance in the visible and near-infrared regions than the use of non-3-D approximation like plane-parallel models.



Figure 2.6. Representation of a coniferous forest as used by FLIGHT model.
From: Radiation transfer Model Intercomparison (RAMI) project webpage at:
<http://rami-benchmark.jrc.ec.europa.eu/HTML/RAMI3/MODELS/FLIGHT/FLIGHT.php>

Three-Dimensional models have a better approximation of the forest structure compared with radiative transfer models. An accurate scale-up simulation of photosynthesis from leaf to canopy level within three-dimensional, heterogeneous tree canopies was performed using an expanded version of the FLIGHT model. The simulation calculates accurately the leaf irradiance at different heights within the canopy (Alton et al. 2005).

An important component of the tropical rainforest structure is the understory vegetation and its contribution to the total canopy reflectance. The influence of the understory reflectance in the estimation of chlorophyll and other forest parameters and pigments was demonstrated by Demarez and Gastellu-Etchegorry (2000) and Gastellu-Etchegorry(1999). Additionally, the cited authors inferred that a major limitation of the turbid medium models is that they do not account for certain canopy structure variables such as tree crown closure, tree density, tree heights, shapes and dimensions of crowns, which may lead to incorrect estimation of forest reflectance. **Discrete Anisotropic Radiative Transfer (DART)** model created by Gastellu-Etchegorry et al. (1996), simulates radiative transfer in

complex 3-D scenes which are represented as realistic 3-D cell matrices, including any distribution of grass, water, soil, trees and topography. Its approach combines the ray tracing (Monte Carlo approximation) and the discrete ordinate methods. DART simulates any landscape as a 3-D matrix of cells that contain turbid material and triangles. Turbid material is used for simulating vegetation (e.g., tree crowns, grass, and agricultural crops) and the atmosphere. Triangles are used for simulating translucent and opaque surfaces that make up topography, urban elements and 3-D vegetation. Figure 2.7 shows a computer representation of a scene modelled by DART available at the Radiation transfer Model Intercomparison (RAMI) project webpage at: <http://rami-benchmark.jrc.ec.europa.eu/HTML/RAMI2/MODELS/DART/DART.php>. DART can use structural and spectral databases (atmosphere, vegetation, soil). The model uses a specific module for simulation of reflectance at leaf level which relies on the PROSPECT model.

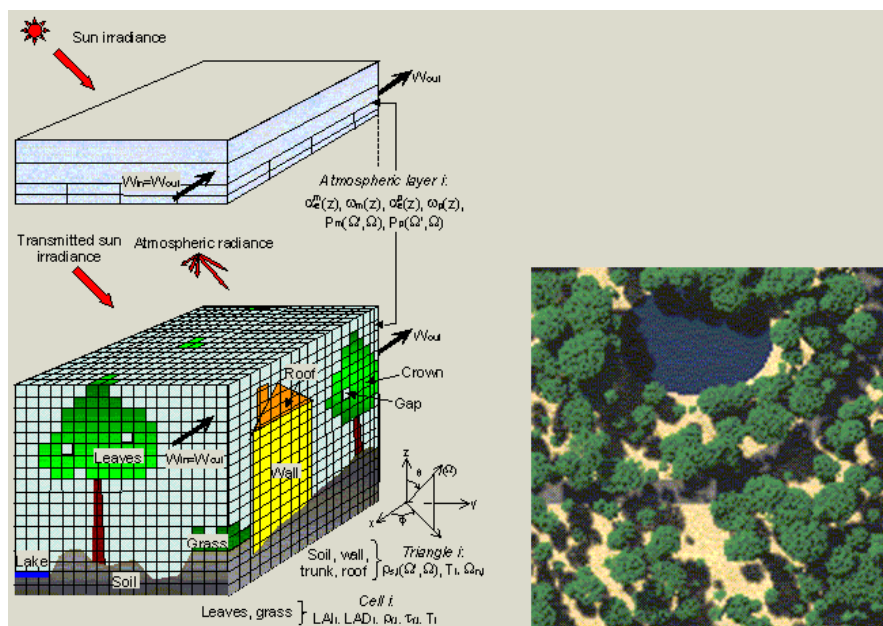


Figure 2.7. DART computer scene representation (left) and example of simulation (right). From: Radiation transfer Model Intercomparison (RAMI) project webpage at: <http://rami-benchmark.jrc.ec.europa.eu/HTML/RAMI2/MODELS/DART/>

2.2.5 Coupling Models

Linking leaf models and canopy models has allowed description of both the spectral and directional variation of canopy reflectance as a function of leaf biochemistry - mainly chlorophyll, water, and dry matter contents –and canopy architecture - primarily leaf area index, leaf angle distribution, and relative leaf size (Jacquemoud 2009). The coupling of leaf and canopy models has shown good results in estimating forest biophysical and biochemical parameters, some of which are listed below:

- PROSPECT leaf model + different versions of SAIL canopy model (Jacquemoud 2009, Casa&Jones 2004, Verhoef 2007, Colombo et al. 2008, Panigada et al. 2010).
- PROSPECT leaf model + FLIGHT canopy model (Kempeneers et al. 2008, Prieto-Blanco et al. 2009).
- LIBERTY leaf model + FLIGHT canopy model (Dawson et al. 1999, Dawson et al. 2003).
- PROSPECT leaf model + DART canopy model (Demarez&Gastellu-Etchegorry 2000).

2.3 Hydrocarbons

Crude oil is a very complex mixture of many thousands of different hydrocarbons which predominantly contain carbon and hydrogen in the form of alkanes (saturated hydrocarbons), alkenes and alkynes (unsaturated), and aromatic hydrocarbons. Sulphur, nitrogen and oxygen represent less than 3% of most petroleum. Heavy metal traces, such as vanadium and nickel, are also present. Table 2.1 shows the elemental composition of petroleum. In its natural reservoir, petroleum exists in gaseous or liquid state: *Natural gas*, which does not condense at standard temperature and pressure; *condensate*, which is gaseous in the ground but liquid on the surface and *crude oil*, the liquid component (Hunt 1996).

The lightest molecule in petroleum is methane (molecular weight 16) and the heaviest molecules are the asphaltenes (molecular weight in the tens of thousands). Between these two extremes there are thousands of compounds which range from simple to very complex structures. According to the type of molecular variation, petroleum contains the following classes of hydrocarbons:

- *Alkanes (paraffins, 30%)* are open-chain molecules with single bonds between the carbon atoms.
- *Cycloalkanes (naphthenes or cycloparaffins, 49%)* are alkane rings.
- *Alkenes (olefins)* contain one or more double bonds between the carbon atoms.
- *Arenes (aromatics, 15%)* are hydrocarbons with one or more benzene rings (Hunt 1996, McAuliffe 1982).

Table 2.1. Elemental composition of petroleum

| ELEMENT | CRUDE OILS (% by weight) |
|----------------------|---------------------------------|
| Carbon | 84 – 87 |
| Hydrogen | 11 – 14 |
| Sulphur | < 0.1 – 8 |
| Nitrogen | < 0.1 – 1.8 |
| Oxygen | < 0.1 – 1.8 |
| Metals (Ni, V, etc.) | Trace – 1000 ppm |

Source: (Lyons&Plisga 2005)

Hydrocarbon components comprise a range of saturated alkanes from methane (CH₄), ethane (C₂H₆) and propane (C₃H₈) through straight and branched chains to n-Hexaheptacontane (C₇₆H₁₅₄). Other constituents of petroleum deposits are the aromatic hydrocarbons and organic components containing nitrogen and sulphur. The hydrocarbons derived from petroleum tend to form the main group of organic macro-pollutants in soils (Alloway 2000). The physical properties of the normal alkanes are shown in Table 2.2.

Table 2.2. The physical properties of the normal alkanes until C₄₀H₈₂

| Name | Molecular | State | Name | Molecular | State |
|--------------------|---------------------------------|--------|------------------------|---------------------------------|--------|
| Methane | CH ₄ | Gas | <i>n</i> -Dodecane | C ₁₂ H ₂₆ | Liquid |
| Ethane | C ₂ H ₆ | Gas | <i>n</i> -Tridecane | C ₁₃ H ₂₈ | Liquid |
| Propane | C ₃ H ₈ | Gas | <i>n</i> -Tetradecane | C ₁₄ H ₃₀ | Liquid |
| <i>n</i> -Butane | C ₄ H ₁₀ | Gas | <i>n</i> -Pentadecane | C ₁₅ H ₃₂ | Liquid |
| <i>n</i> -Pentane | C ₅ H ₁₂ | Liquid | <i>n</i> -Hexadecane | C ₁₆ H ₃₄ | Liquid |
| <i>n</i> -Hexane | C ₆ H ₁₄ | Liquid | <i>n</i> -Heptadecane | C ₁₇ H ₃₆ | Liquid |
| <i>n</i> -Heptane | C ₇ H ₁₆ | Liquid | <i>n</i> -Octadecane | C ₁₈ H ₃₈ | Solid |
| <i>n</i> -Octane | C ₈ H ₁₈ | Liquid | <i>n</i> -Nonadecane | C ₁₉ H ₄₀ | Solid |
| <i>n</i> -Nonane | C ₉ H ₂₀ | Liquid | <i>n</i> -Eicosane | C ₂₀ H ₄₂ | Solid |
| <i>n</i> -Decane | C ₁₀ H ₂₂ | Liquid | <i>n</i> -Triacontane | C ₃₀ H ₆₂ | Solid |
| <i>n</i> -Undecane | C ₁₁ H ₂₄ | Liquid | <i>n</i> -Tetracontane | C ₄₀ H ₈₂ | Solid |

Source: (Lyons&Plisga 2005)

Depending on the hydrocarbon reservoir characteristics, natural gas and petroleum liquid are largely composed of methane. However it also contains quantities of ethane, propane, butane, pentane, hexane, heptane and small concentrations of other components such as nitrogen, carbon dioxide, hydrogen sulphide, and occasionally helium (Marquez-Riquelme et al. 2010). Table 2.3 shows the composition of a typical natural gas.

Table 2.3. Chemical composition of natural gas

| | Natural Gas | Gas from well |
|-------------------|--------------|---------------|
| Methane | 70 – 98% | 45 – 92% |
| Ethane | 1 – 10% | 4 – 21% |
| Propane | trace – 5% | 1 – 15% |
| Butanes | trace – 2% | 0.5 – 7% |
| Pentanes | trace – 1% | trace – 3% |
| Hexanes | trace – 0.5% | trace – 2% |
| Heptanes | trace – 0.5% | none – 1.5% |
| Non-hydrocarbon | | |
| Nitrogen | trace – 15% | trace – 10% |
| Carbon dioxide | trace – 5% | trace – 4% |
| Hydrogen sulphide | trace – 3% | trace – 6% |
| Helium | trace - 5% | none |

Source: (Lyons&Plisga 2005)

Total Petroleum Hydrocarbons (TPH) is a useful indicator of petroleum contamination. It is a measurement of the total amount of petroleum-based

hydrocarbons in a sample without the identification of its constituents. There are several hundred individual hydrocarbon chemicals defined as petroleum-based, with more than 250 individual petroleum components that are known as petroleum hydrocarbons (ATSDR&EPA 1999).

Hydrocarbons Aromatic Polycyclic (HAPs) are the toxic environmental pollutants group, some of them are potent carcinogens (benzofluoranthenes, benzo[a]anthracenes, dibenzo[ah]anthracene and indenol[1,2,3-cd]pyrene). The persistence of HAPs in the environment depends on their physical and chemical characteristics but may degrade by photo oxidation, chemical oxidation and biological transformation. In natural environments, microbial-mediate biological transformation is probably the most prevailing route of HAPs degradation (Doble&Kumar 2005) .

TPH and HAPs are indicators of petroleum pollution, and laboratory analysis of soils in this study took into account these parameters.

Once the crude oil enters in contact with the environment, hydrocarbons migrate in two ways: one part is infiltrated into the soil and other parts are dissolved in air or water. Many factors affect this migration: soil texture, soil moisture, vegetation, slope, climate, amount of discharge and oil viscosity. The remaining crude oil that does not migrate and remains *in situ* is known as “residual saturation” which may act as a permanent source of pollution (ATSDR&EPA 1999).

Hydrocarbons in the environment migrate to the air as a vapour through a **volatility** process. This is a function of air and soil temperature, humidity, wind speed, soil type, moisture content, oil composition, solar radiation and thickness of the oil layer. Lighter hydrocarbons (<C₁₈) are subject to volatilisation which means that the gaseous and liquid components are subject to an early volatilisation.

Numerous microorganisms including eubacteria, fungi and possible archaea (an ancient genus of bacteria also known as archaeobacteria) which have evolved metabolic pathways to consume saturated and aromatic hydrocarbons degrade the organic compounds of petroleum and use them as source of energy. This process is known as *microbial degradation or biodegradation* which can be aerobic or anaerobic. The aerobic biodegradation is a respiration (oxidation) process where the final products are CO₂, water and microbial biomass. Anaerobic organisms use various inorganic compounds as terminal electron acceptors, such as nitrate, sulphate and ferric ions (ATSDR&EPA 1999). Table 2.4 shows the susceptibility of the hydrocarbons to biodegradation.

Table 2.4 Hydrocarbons Biodegradability

| <i>n</i> -alkanes, <i>n</i> -alkyl aromatics and the aromatics | Biodegradability |
|--|---|
| Smaller <i>n</i> -alkanes in the range C ₁ -C ₄ | Biodegradables only by very specialized hydrocarbon degraders. Toxic to many micro organisms |
| <i>n</i> -alkanes in the range range C ₅ -C ₉ | Biodegradables but usually they are evaporated before the action of microbes. Toxic to many micro organisms |
| Long-chain <i>n</i> -alkanes in the range C ₁₀ -C ₂₄ | Most easily biodegradables |
| Normal <i>n</i> -alkanes in the range > C ₂₄ | More difficult to transport across cell membranes then degradation is limited |

Source: (ATSDR&EPA 1999)

Another key factor during the migration of hydrocarbons in the environment is the **solubility** which determines the propensity of the crude components to dissolve into water. Most hydrocarbons, however, are nearly insoluble in water but microorganisms existing in water have evolved several mechanisms to access hydrocarbons. Some microbes excrete biosurfactants that emulsify hydrocarbons which can then be transported across cellular membranes. Enzymes that react with hydrocarbons and biopolymers may also be excreted, converting them into water-

soluble compounds which then diffuse into the organism. Some bacteria appear to be able to utilise hydrocarbons directly by existing at the oil-water interface (Peters;Walters & Moldowan 2005).

Environmental factors such as oxygen and soil moisture content, pH, temperature and nutrient concentration affect the rate of biodegradation. Oxygen is a key agent during the respiration process of the microbe's activity but also anaerobic decomposition is possible with very low rates of degradation. Experiments in the laboratory have shown that aerobic degradation tends to be ten times faster than the anaerobic degradation rate. The ideal pH range to promote biodegradation is close to neutral, between 6 and 8. Soil moisture content between 50-70% favours biodegradation and biological activity is closely related to temperature. A range between 18⁰C to 30⁰C is optimal for the biodegradation of hydrocarbons, but microbial degradation may occur in reservoir depths at temperatures of 60-80⁰C. The presence of macro and micro soil nutrients, in the right amounts, powers bacteria activity: nitrogen, phosphorus, potassium, sodium, sulphur, calcium, manganese, iron, manganese, zinc and copper where the principal are nitrogen and phosphorus (ATSDR&EPA 1999, Peters;Walters & Moldowan 2005).

Biodegradation rates are affected by the ***concentration*** of crude oil in the soil. When oil reaches saturation conditions in the soil (i.e., 30-50% oil) biodegradation will virtually cease.

2.3.1 Hydrocarbon migration – seepages

Under 'normal' conditions, petroleum accumulations are located in geological reservoirs far below the surface. However, as oil and gas are mobile fluids they seep into the rock which is generally permeable, and then rise to the surface. Migrations of the hydrocarbons from the reservoirs to the surface have been used by geology exploration as an indicator of the presence of petroleum reservoirs. In contrast, human activities related to production, transportation and

industrialisation of petroleum have led to oil spillages which are an important source of petroleum leaks at surface level.

The occurrence of hydrocarbon seepages at the surface suggests that an oil or gas reservoir leaks even though it acts as a trap for hydrocarbons. Macroseepages are the visible presence of oil and gas seeping to the surface. Microseepages are the invisible trace quantities of hydrocarbon (natural gas) seeping vertically or near-vertically from the reservoir to the surface (Yang 1999, Horvitz 1982, Abrams 1996, van der Meer; Yang & Kroonenberg 2006, McAuliffe 1982, Yang et al. 1999). Light hydrocarbon gases measured in soil gases and soils above petroleum deposits are an evidence of petroleum reservoirs used by geochemists for petroleum exploration. Historically, most of the major oil and gas reservoirs around the world were first brought to attention by the visible presence of oil and gas seepages.

Hydrocarbon seepages may have an important contribution to the total atmospheric methane. Etiope (2002) estimated that onshore and offshore hydrocarbon seepage (thermogenic methane) emissions range from 42 to 67 Tg(CH₄) yr⁻¹, which corresponds to 5 – 13% of the total methane budget in the atmosphere as indicated by the Intergovernmental Panel on Climate Change-IPCC (Solomon et al. 2007) (more details in Section 2.4.1, page 36).

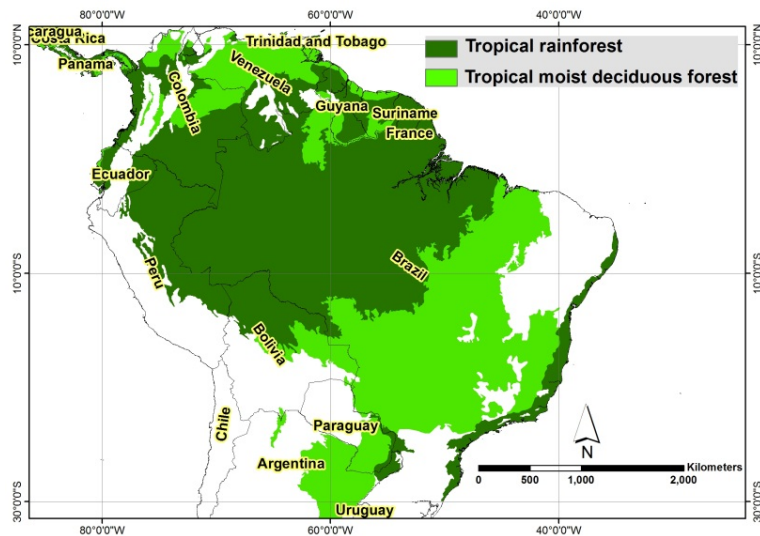
Hunt (1996) compiled a classification of the seepages according to their geological origins:

- Young sedimentary rocks in regional and local tectonically active areas host the most seepages (Tertarina basins-California).
- Seepages are common in earthquake prone areas along the edges of crustal plates where the continents collide. Worldwide there is a correlation between seepages and earthquake activity, for example along the Pacific coast of South America (Ecuador, Peru and Chile), Trinidad, southern California, southern Alaska, the Philippines, Indonesia and Burma.

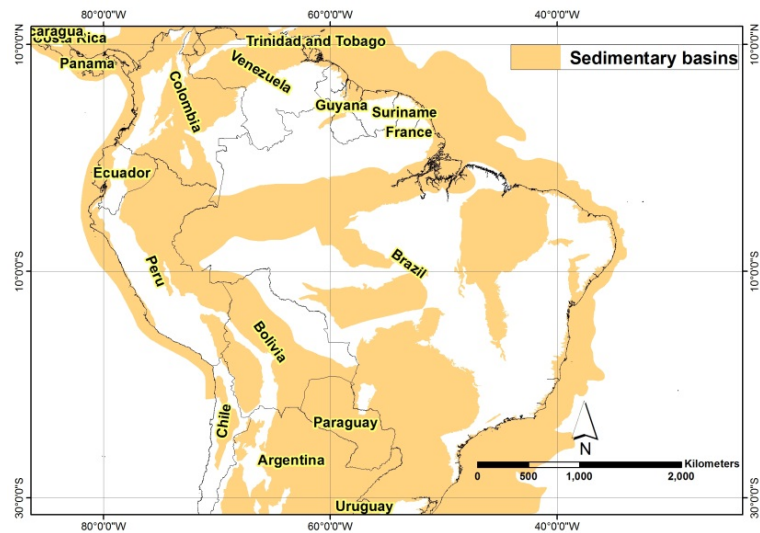
- Small inter-montane basins (Indonesia and Magdalena Valley in Colombia).
- There are many hydrocarbon seepages from the mobile sides of basins, such as in the Mesopotamian geosyncline, the Managas Basin of eastern Venezuela, and the eastern foothills of the Andes mountain chain along South America.
- Along normal faults (Gebel Zeit in Egypt) and along thrust faults (Infantas field in Colombia).
- Associated with intrusions e.g. mud volcanoes (Caspian Sea) and salt domes (U.S. Gulf Coast).
- Along edges of a basin where unconformities and oil-producing formations reach the surface (North-eastern and Southern Oklahoma USA, the lake Maracaibo-Venezuela, along the flanks of the Venezuela Andes and the Perijia Mountains).

2.3.2 Hydrocarbon seepages in the study area

Figure 2.8 illustrates the overlapped area between tropical rainforest and sedimentary basins in South America.



a) Source: Global ecofloristic zones. Creative Commons Licenses-CC (FAO 2000)



b) Source: (Hall 2013)

Figure 2.8 Tropical rainforest and sedimentary basins in South America. a) Tropical forest distribution; b) Sedimentary basins (U.S Department of Energy open copyright policy)

Figure 2.9a shows the petroleum reservoirs in the Amazon region of Ecuador where ITT oil fields and Pungarayacu oil fields are identified. The photography displayed in Figure 2.9b corresponds to the hydrocarbon macro-seepages located in the Pungarayacu oil field where hydrocarbons have been exposed to the surface.

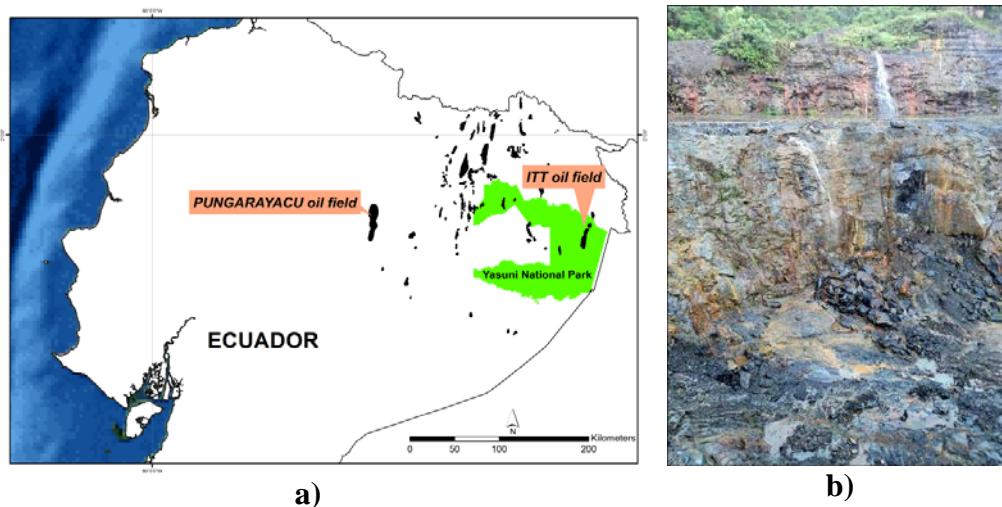


Figure 2.9 a) Petroleum reservoirs in the Amazon region of Ecuador (black areas). Pungarayacu oil field where hydrocarbon macro-seepages have been identified. ITT oil field inside of Yasuni National Park. b) Photography of macro-seepages in Pungarayacu oil field where geological uplift has exposed crude oil to the surface.

Tropical vegetation located in areas affected by hydrocarbon pollution has been exposed over long periods of time to gaseous, liquid and solid hydrocarbon components. This reduced environment affects the vegetation which produces different levels of stress that changes the biophysical and biochemical composition at both leaf and canopy level. An important indicator of vegetation stress is the reduction of chlorophyll content levels.

The relationship between hydrocarbon seepages and vegetation of the tropical forest has not been studied in the past. The objective is to determine how the vegetation of the tropical forest may be affected by hydrocarbon pollution and which biophysical and biochemical foliar parameters experience changes in the vertical profile of the forest in polluted and non-polluted sites of the Amazon forest.

2.3.3 Oil spills

During the last few decades, petroleum production has been an important cause of man-made pollution in some areas of the Amazon tropical rainforest. The early

stages of petroleum production did not consider environmental regulations which caused several oil spills from pipeline leaks and unlined open pits which have seeping hydrocarbons and other pollutants into the natural environment.

A mixture of crude oil and 'water formation' is extracted together during petroleum production from wells. The mixture then is separated following a chemical process. Crude oil then is transported by pipelines to storage and distribution centres. Due to the potential toxic nature of the water formation, a common practice of the petroleum industry is to re-inject it into its original geological formation.

In Ecuador, petroleum productive areas have been exploited since 1967. The majority of these areas are located in the Amazon rain forest region. During the first decades of petroleum production, billions of gallons of toxic water formation were disposed into unlined open pits without treatment and monitoring. Over the years, the toxic waste has seeped into the natural environment causing pollution of the water, soils and vegetation. In contrast, accidental oil spills from the pipeline networks have resulted in approximately 16.8 million gallons of crude oil being leaked into the environment. To put it into perspective, the Exxon Valdez disaster in Alaska spilled 10.9 million gallons of oil (Bernal 2011, Hurtig&San-Sebastián 2005).

In 2007, the Ecuadorian government proposed the Yasuni-ITT initiative to the global community which aims to keep the oil permanently underground in exchange for international compensation that would be administered in a United Nations trust fund. This initiative has generated an intense debate in conservation and climate change forums because its support may serve as a model for preserving intact biodiversity in other oil-rich portions of the western Amazon. At present, the initiative did not reach the expected contributions from the international community and petroleum production projects are expected to start soon in highly diverse areas of the Amazon region. An intensive social and environmental monitoring campaign is required in order to minimise the impacts

of hydrocarbons in this sensitive environment (as discussed in Section 1.2, page 3).

2.4 Hydrocarbons and environment interactions

When hydrocarbons leak to the surface they undergo a series of changes that considerably alter their physical and chemical composition. The following points explain the changes of hydrocarbons when are exposed to the environment (Hunt 1996).

- **Evaporation of the more volatile hydrocarbons.** In the first two weeks after oil reaches the surface it loses its hydrocarbons molecules up to C₁₅. In following months, additional hydrocarbons are lost, up to C₂₄.
- **Leaching of water soluble constituents.** The most soluble nitrogen, sulphur, and oxygen compounds, along with some lighter aromatic hydrocarbons, may be leached out by groundwater.
- **Microbial degradation.** Microorganisms utilise hydrocarbon as a source of energy. Paraffins, naphtenes and aromatics, including gases, liquids and solids are susceptible to microbial decomposition. More than 30 genera and 100 species of bacteria, fungi and yeast metabolise one or more kinds of hydrocarbons. Hydrocarbons are oxidised into alcohols, ketones and acids. Generally, the lightest molecules up to C₂₀ are consumed before the heaviest and after fourteen days most of the n-paraffins have disappeared. Further details are included in the next section.
- **Polymerisation.** This is the combination of some of the intermediate to large molecules to form very large complex structures after the elimination of water, carbon dioxide and hydrogen.
- **Auto-oxidation.** Many constituents of petroleum absorb sunlight and oxygen which convert the oil to asphalt high in oxygen.
- **Gelation.** The formation of a rigid gel structure may develop.

All these reactions lead to thickening or solidification of the original oil. The crude is gradually converted from liquid oil to an asphaltite and eventually into a substance physically close to a pyrobitumen. Consequently, unless a seepage is supplied by a continuous flow of fresh oil, it hardens into a black bitumen or pyrobitumen. The term pyrobitumen is most often used to indicate a late stage of thermal maturation.

2.4.1 Hydrocarbon and atmospheric interactions

Methane contributions from geological sources to the global budget are only available since the IPCC report of 2007 showing a contribution of $14 \text{ Tg}(\text{CH}_4) \text{ yr}^{-1}$. The considered geological sources of methane are natural gas seepage in sedimentary basins and geothermal/volcanic (Solomon et al. 2007).

Hydrocarbons from macro and micro seeps appear to have an important contribution to the natural and total methane budget in the atmosphere. Several studies suggest that significant amounts of methane, produced within the Earth's crust (mainly by bacterial and thermogenic processes), are released into the atmosphere through faults and fractured rocks, mud volcanoes on land and the seafloor, submarine gas seepage, microseepage over dry lands and geothermal seeps (Kvenvolden&Rogers 2005, Etiope&Klusman 2002, Etiope 2004). Emissions from these sources are estimated to be as large as $40 \text{ to } 70 \text{ Tg}(\text{CH}_4) \text{ yr}^{-1}$.

Etiope & Klusman (2002) argues that the production of methane in sedimentary basins can be due to biogenic and thermogenic processes. Figure 2.10 shows the distribution of the sedimentary basins in the world. Biogenic methane is produced by the bacteria breakdown of organic material in sediments, while at great depths thermogenic methane is produced by the thermal breakdown of organic matter or heavier hydrocarbons. Hydrocarbons trapped in sedimentary basins produce thermogenically derived methane and others light alkenes gases that seep to the surface. The interaction of the gases produces an anaerobic or aerobic bacteria oxidation, also called methanotropic oxidation.

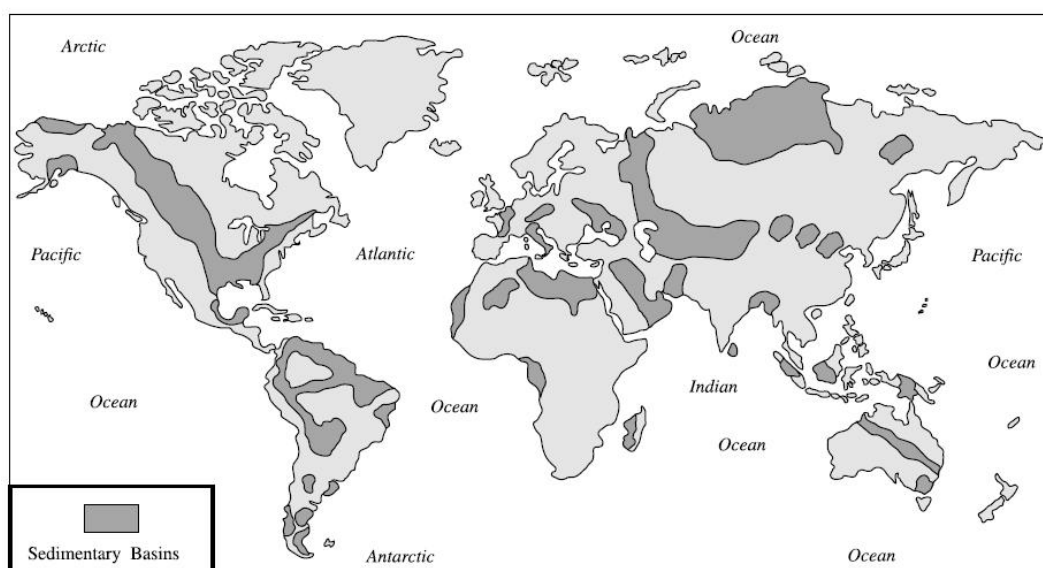


Figure 2.10. Distribution of the sedimentary basins in the World (Kvenvolden&Rogers 2005).

Etiopie (2004) provided an additional estimation of the methane geological sources. Methane contribution from seeps in sedimentary basins is estimated based on the mean of fluxes determined in several studies around the world. The study suggests that by adding the geological sources of methane (40-70 Tg y⁻¹) to the atmospheric methane global budget, the imbalance between total source and sink, as shown in the Second and Third Assessment reports of the IPCC, could be strongly reduced (Solomon et al. 2007, Houghton et al. 1996). Table 2.5 shows the estimated values of methane from geological sources defined in the cited study.

Table 2.5. Estimations of Methane Emission from Geological Sources
Tg(CH₄) yr⁻¹

| Source of Methane | Average | Min | Max |
|---|-------------|-------------|-------------|
| Hydrocarbon seepages from sedimentary basins ¹ | 21 | 14 | 28 |
| Hydrocarbon seepages from submarine basins | 20 | 20 | 20 |
| Mud volcanoes | 9 | 5 | 13 |
| Geothermal | 4.4 | 2.5 | 6.3 |
| TOTAL | 54.4 | 41.5 | 67.3 |

¹Based on fluxes estimations from several studies in USA, former Soviet Union, Romania, Italy and USGS data

Another study (Kvenvolden&Rogers 2005) indicates that an important contribution of methane produced by geological natural sources has been omitted from the assessments of the global methane budget summarised for the IPCC reports. These natural sources include macroseeps and mud volcanoes from terrestrial and marine environments and microseeps located in sedimentary basins (Figure 2.11 and Table 2.6).

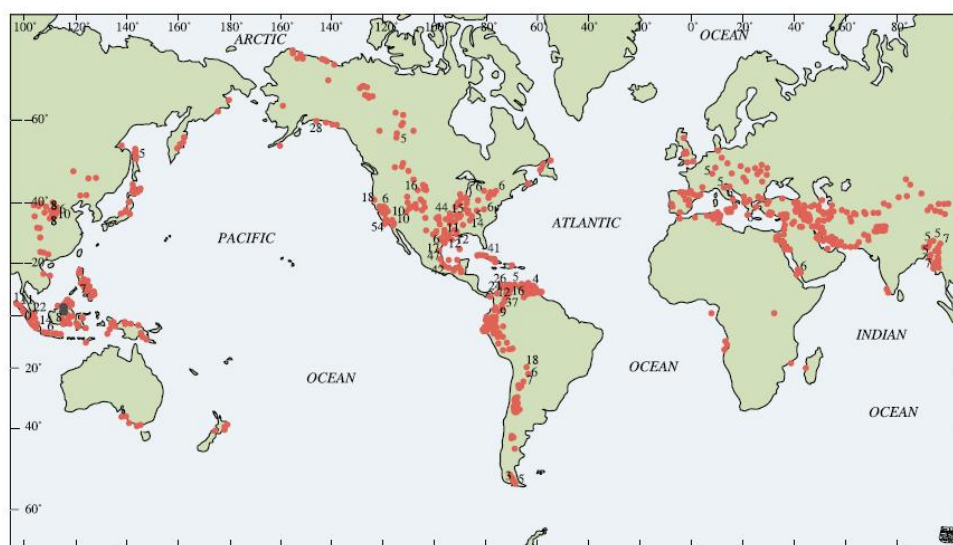


Figure 2.11. Global distribution of offshore and onshore oil seepages. Numbers indicate the count of seeps. From (Kvenvolden&Rogers 2005)

Table 2.6. Estimations of Methane Emission from Geological Sources
 $T_g(\text{CH}_4) \text{ yr}^{-1}$

| Geological source of methane | Average |
|------------------------------|-----------|
| Macro and microseepage | 32 |
| Mud and magmatic volcanoes | 9 |
| Gas hydrate | 4 |
| Geothermal areas | 3 |
| TOTAL | 48 |

The estimations of methane from geological sources are based on data fluxes from a limited number of locations followed by methane fluxes extrapolations to the

global scale, therefore further research to detect macro and micro hydrocarbon seepages will contribute considerably to the estimations.

The contribution of methane to the total budget from macroseepages in sedimentary basins has not been considered in the estimations and their contribution is probably high due to huge areas influenced by oil sands, also known as tar. Vast areas of oil sands are located in Canada, Venezuela, Russia and the USA. The oil reserves of these areas are probably equal to conventional reserves of oil around the world. Further research needs to be done in this area.

According to the cited studies, the Amazon region of Ecuador located in sedimentary basins is an active source of hydrocarbon seepages. This is the area where this research is focussed.

2.4.2 Hydrocarbons and soil interactions

Bacteria and other microbes found in the soils play an important role in the oxidation of hydrocarbons. Oxidation is the loss of electrons or an increase in oxidation state by a molecule, atom or ion. Reduction is the gain of electrons or a decrease in oxidation state by a molecule, atom, or ion. Microbial hydrocarbon oxidation consumes oxygen via one of the two main metabolic pathways. First, aerobic bacteria oxidise hydrocarbons to form carbon dioxide or bicarbonate that eventually precipitates as carbonate. Second, once oxygen is depleted within the sediments or pore fluid, other bacteria reduce sulphate to produce hydrogen sulphide. These changes can significantly alter the oxidation-reduction potential (Eh) and affect the pH of the surrounding environment. Such Eh/pH changes can result in new mineral stability fields in which some minerals become unstable and are dissolved and mobilised, while others are precipitated from solutions. The resulting alterations include the formation of calcite, pyrite, uraninite, elemental sulphur, and certain magnetic iron oxides and iron sulphides; bleaching of red beds, clay mineral alteration, electrochemical changes, geomorphic anomaly, the edge anomaly of adsorbed or occluded hydrocarbon in soil and Delta C (ferrous carbonate); biogeochemical and geobotanical anomalies (Shumacher 1996). The

environmental changes will affect the root structure of vegetation, vigour and therefore its spectral response (Smith;Steven & Colls 2005, van der Meer;Yang & Kroonenberg 2006, Kumar;Schmidt & Dury 2006, Smith;Colls & Steven 2005). Figure 2.12 shows a generalised model of hydrocarbon microseepage and its surface expression from Yang (1999).

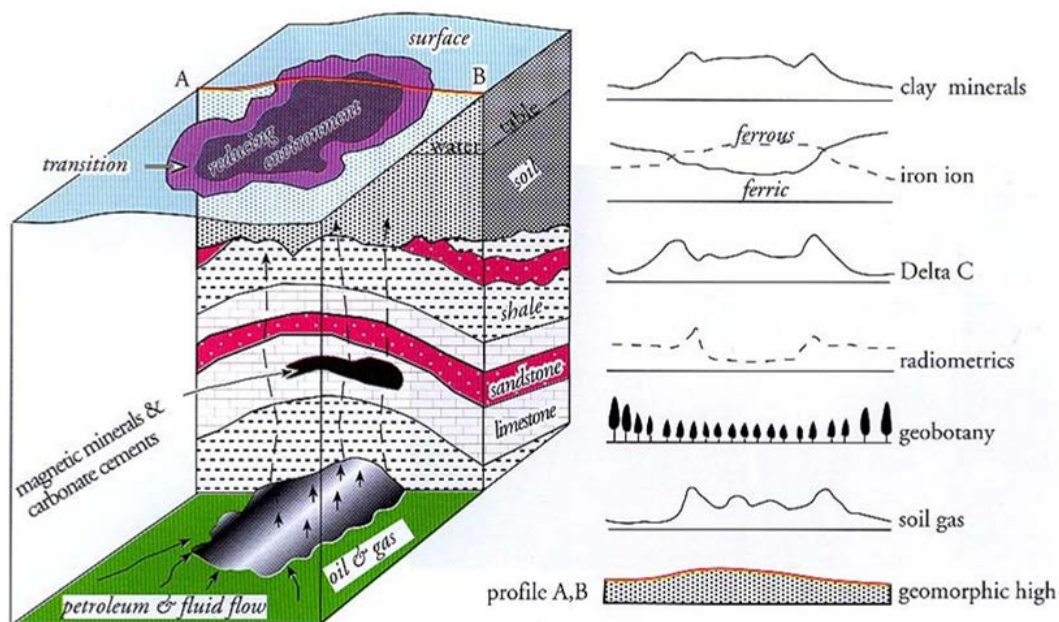


Figure 2.12. A generalised model of hydrocarbon microseepage and its surface expressions. (Yang 1999)

2.4.3 Hydrocarbons and vegetation interactions

This research focuses on the impact of hydrocarbons on the plants which suggest changes in biophysical and biochemical parameters of vegetation. Several definitions of vegetation stress have been developed based on the research of the last decades. Lichtenthaler (1996) defined vegetation stress as any unfavourable condition or substance that affects or blocks a plant's metabolism, growth or development. Larcher (2003) defined plant stress as 'a state in which increasing demands made upon a plant lead to an initial destabilization of functions, followed by a state of normalization and ultimately leading to improved

resistance. If the limits of tolerance are exceeded and the adaptive capacity is overtaxed, permanent damage or even death may result'.

Vegetation responds to stress conditions by long-term metabolic and morphological changes: these included changes in the rate of photosynthesis, changes in the absolute and relative concentration of the photosynthetic pigment (chlorophyll a and b, carotenoids) and changes in leaf size, thickness and structure (Davids&Tyler 2003).

Despite the capacity of vegetation for fast acclimation and certain stress tolerance mechanisms, vegetation is always exposed to sudden short-term or long-term stress events which reduce cell activity and keep plant growth to a minimum or even death. There exist many natural or anthropogenic stress factors which, depending on their intensity and duration, can cause damage to plants. These stresses can also be characterised as abiotic or biotic stress (Lichtenthaler 1996).

Different plant species respond differently to a particular stressor. Furthermore, the nature, intensity and length to exposure are factors that define the stress level on the vegetation. Baker (1970) summarised several pieces of research related to the effects of crude-oil on plants and showed that the toxicity of petroleum oil depends on the concentration of unsaturated, aromatics and acids compounds: the higher their concentration, the more toxic the oil is for plants. Molecules of crude-oil can penetrate the plant through its leaf tissue, stomata, and roots. The rate of penetration depends on the oil type, the contact part (leaves, roots), time of exposure, thickness of the cuticle and the density of the stomata. After penetrating into the plant, the oil may travel into the intercellular space and possibly also into the vascular system. Cell membranes are damaged by the penetration of hydrocarbon molecules leading to the leakage of cell contents, and the possible entrance of oil into the cells.

Plant transpiration, respiration and photosynthetic rates are affected by hydrocarbon pollution (Baker 1970). The effects of hydrocarbons in plants reduce

plant transpiration rates. On the other hand, plant respiration may either decrease or increase depending on the plant species or the oil type. Hydrocarbons reduce the rate of photosynthesis, and the amount of reduction varies with the type and amount of oil and with the species of plant. Cell injury may be the principal cause of photosynthesis inhibition because hydrocarbons tend to accumulate in the chloroplasts, which explains the reduced levels of chlorophyll content in vegetation affected by hydrocarbons.

2.5 Remote sensing for detection of vegetation stress caused by hydrocarbons

This section discusses previous experiences using remote sensing for the detection of vegetation affected by hydrocarbons from seepages and gas leakage.

2.5.1 Vegetation anomalies in areas influenced by hydrocarbon seepages

Direct and indirect geochemical methods were applied during the period 1979-1982 in Patrick Draw, Wyoming-USA in order to detect hydrocarbon microseepage anomalies. Soil analysis and geochemical surveys showed that the area was affected by microseepage alterations. Chemical and anatomical analysis, species distribution, species diversity and vegetation cover analysis were carried out. The results revealed a tonal anomaly recognised in the interpretation of NS-001 Thematic Mapper Simulator images which corresponded to the location at the approximate centre of the underlying gas cap of the reservoir and areas of high soil hydrocarbon gas, high soil helium gas, high soil pH, and high elemental concentration. Laboratory anatomical evaluation demonstrates that stunting has been chronic in the area for 95 years. The anatomical and morphological characteristics of the stunted sage are symptomatic of a zinc nutrients deficiency. The deficiency may be the result of local high soil pH which can effectively block zinc uptake. The study concludes that the seasonal influence in the vegetation is a variable to be considered (Lang;Aldman & Sabins 1985).

A similar study was developed by Lang et al. (1985) in the Lost River gas field in West Virginia-USA. In this case a densely covered vegetation area was considered. The conclusions show anomalous manganese concentrations in the soil. Vegetation analysis reveals subtle vegetation distributional anomalies over the field in the form of concentration of weed trees (maples) at sites where the more typical oak-hickory climax vegetation is expected. Assuming that methane concentrations in the soil affect the trees' roots, samples of these roots (in-field and off-field) were collected for laboratory analysis. In addition, a laboratory experiment was conducted by applying air and methane (commercial natural gas) directly into the pots in which plants of Chestnut Oak were growing. The results suggest differences in fungal diversity and fungal vigour. Such differences may influence both the distribution and vigour of host plants in the area. In vitro data indicate that small amounts of methane in soil will neither inhibit the growth of Oak seedlings nor the formation of mycorrhizal associations between the oak root and fungus.

Geochemical, microbiological, and remote sensing investigative techniques were used to reduce exploration risk in the Juruá gas accumulation in the Solimões Basin in the Amazon tropical rainforest in Brazil. The results indicated an anomalous concentration of hydrocarbons and hydrocarbon-consuming bacteria detected in the soil that are concordantly aligned with the trace of a major reverse fault. Landsat MSS images showed an anomalous spectral response of vegetation over the geochemical anomalies which may represent the response of plants to long-term anaerobic conditions due to the gas leakage from the subsurface reservoir (Melo et al. 1996).

Yang (1997) implemented a study to detect botanical anomalies using Landsat TM data in hydrocarbon microseepage areas in China. The results point out that the reflectivity of leaves above oil-gas accumulations increases in the range of visible light with a shift of 10-20 nm toward blue light and increasing reflectance

values between 670 nm and 1300 nm. Four vegetation species were assessed in the study: bamboo, camphor tree, *Cyathea spinulosa* and cypress.

Another author, Yang (1999), implemented a set of experiments to measure the spectral response relationship between Red Edge Position (REP) and Leaf Area Index (LAI). The results showed that measures of reflectance, and consequently the REP estimations, are influenced by the background (ground) independently of the brightness of the background. This suggests that if the LAI remains relatively constant, the REP shift is only related to chlorophyll content, which may be significant in detecting hydrocarbon microseepage in vegetated area. This can be an important assumption in the case of tropical rainforests where the LAI remains relatively constant.

Furthermore, the above mentioned research estimated the REP in a monocultural area of wheat in China where there was a proven presence of hydrocarbon microseepages. Modular Airborne Imaging Spectrometer (MAIS) sensor data was used which provided hyperspectral images of the study area. The results showed high correlation between ethane concentrations and REP of wheat which has been shifted 7 nm to a longer wavelength (red) with respect to wheat samples located outside of the oil field.

The previously cited studies, Yang B. (1997) and Yang H. (1999), reach different conclusions about the spectral response of the vegetation affected. The first one concludes that the peaks of chlorophyll absorption shift to the blue side of the spectrum and the second one infers a shift to the red side of the spectrum.

2.5.2 Vegetation stress caused by natural gas

From 2002 until 2005, experiments were developed to test the influence of natural gas on the plants through the observance of their spectral response. In one of these (Smith;Steven & Colls 2004) grass, wheat and bean plants were stressed by elevated concentrations of natural gas in the soil. The spectral reflectance showed an increased reflectance in the visible wavelengths and decreased reflectance in

the NIR. The effects of the stress on the plants were detected by spectral analysis even though it was not directly detectable by the eye.

The effects of the gas on the grass showed chlorosis (yellow colour due to reduction of chlorophyll content) on leaves and reduction in growth in a circle of 50 cm diameter. The visible symptoms appeared 44 and 32 days after the injection of gas. The effects on bean and wheat showed a reduction in growth and discoloured leaves. No visible symptoms were observed when the gas was applied to wheat and bean plants with full canopies. All three plant species showed peaks at 725 nm and 702 nm in the first derivative analysis. This result was seen in all three plant species when the soil gas concentration was raised shortly after germination.

The decrease in ratio was not observed in wheat and bean when soil gas concentration was raised after full canopy cover had been established. Figure 2.13 and Figure 2.14 show the spectral response of the control plots and the gassed plots.

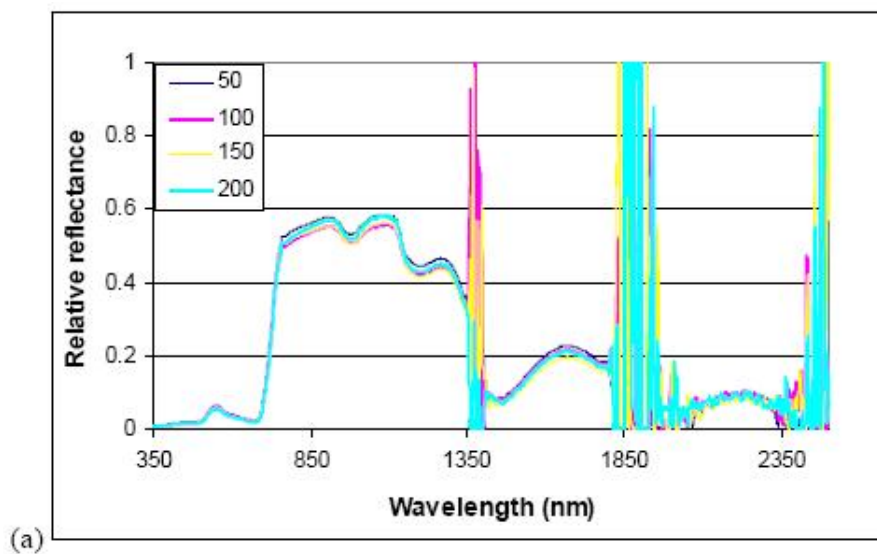


Figure 2.13. Reflectance response of control grass plots (Smith;Steven & Colls 2004)

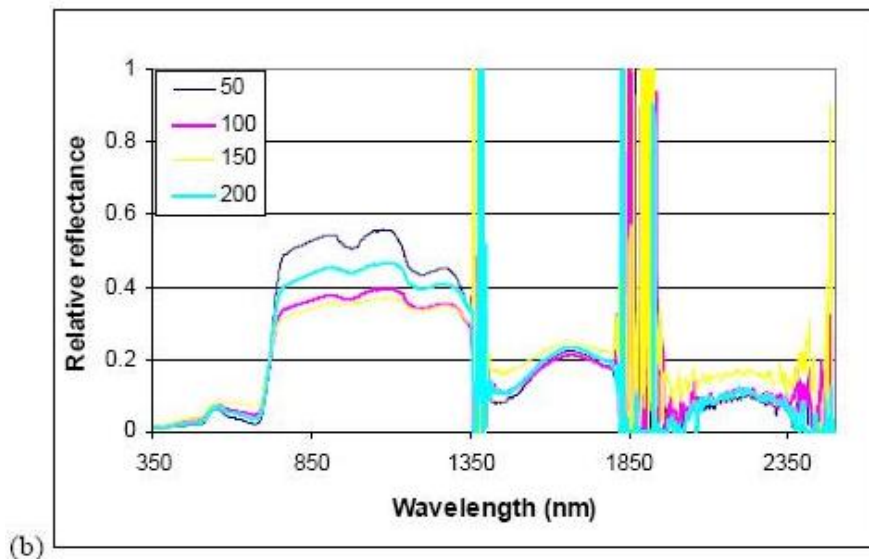


Figure 2.14. Reflectance response gassed. Each line represents a distance along the transect (Smith;Steven & Colls 2004)

In a further experiment developed by Smith (2005), different sources of stress were applied to plants of oilseed rape (*Brassica napus*): natural gas, herbicide and extreme shade.

Visible effects of natural gas treatment showed that leaves turned purple in a circle of 50 cm diameter after eight days of gas application. In extreme shade conditions the leaves became pale green in colour. These changes started on the sixth day of the experiment. After 21 days the leaves were wilted and yellow. The herbicide effect on the leaves began to produce mottled yellow patches that progressed with time, eventually covering the whole leaf. Later, the leaves exhibited yellow, orange or red colours. Figure 2.15 shows the visible symptoms of the leaves after five weeks of stress.

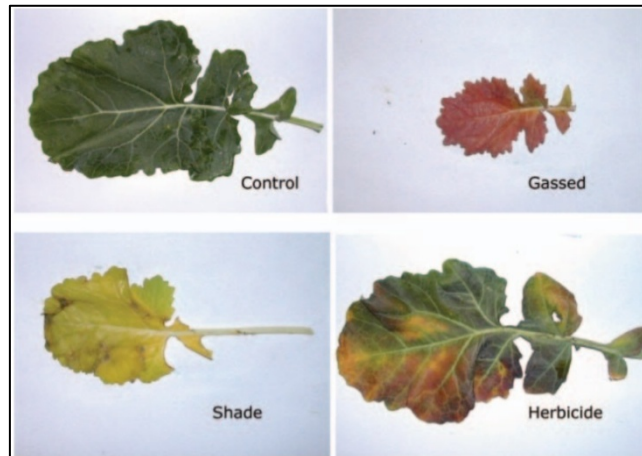


Figure 2.15. Visible symptoms of oilseed rape leaves (Smith;Steven & Colls 2005)

For the three stress sources, plants showed a higher reflectance in the visible range. In addition, all of them showed a decrease in reflectance in the NIR. This suggests that changes in reflectance are a generic response to stress-induced changes in chlorophyll concentration. An important difference of spectral reflectance pattern is observed for plants stressed by extreme shade whilst plants stressed by natural gas and herbicide showed similar patterns. The primary red edge peak is displaced towards shorter wavelengths in all three stress treatments, and this effect was most pronounced in the shaded stress treatment.

In addition, the chlorophyll content was measured in all plants. The results suggest similar values for the plants exposed to gas and to herbicide. The plants exposed to shade revealed low chlorophyll content compared with other experimental plants. Figure 2.16 shows the results of chlorophyll content for the experiment.

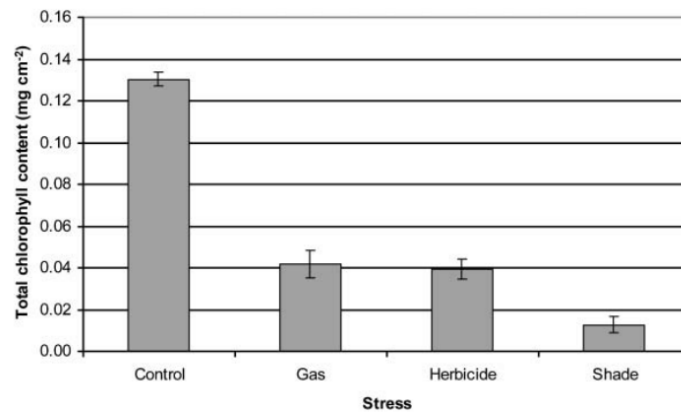


Figure 2.16. Chlorophyll content of plants exposed to stress compared to control plants. (Smith;Steven & Colls 2005)

It was assumed that natural gas displaces the soil air and that oxygen shortage is the cause of changes in vegetation growth and reflectance. However it was not known whether the hydrocarbon gases have an additional effect on the vegetation. Therefore Noomen (2007) undertook two experiments to compare the effects of small gas leaks: one of them without oxygen shortage and the other with large gas leaks with oxygen shortage on maize and wheat plants' growth and reflectance. Whereas in several studies a decrease in vegetation chlorophyll was one of the main indicators of large gas leaks, this study showed that leaf area is a better indicator of natural gas pollution. Moreover, it was shown that when the ethane concentration in the soil reaches 0.75%, plant growth is not only affected by oxygen shortage but also by the gas itself.

Since hydrocarbon gases in the soil are often accompanied by elevated carbon dioxide concentrations due to bacterial methane oxidation, an additional experiment was performed to study the effects on vegetation reflectance of CO₂ gas in concentrations ranging from 2% to 50%. The REP in combination with a new index named the "yellow edge position" showed that an increasing CO₂ concentration corresponded to decreasing leaf chlorophyll. Two water absorption features at 1400 and 1900 nm indicated that a concentration of 50% CO₂ decreased leaf water content.

Finally, the results of the simulated gas leak were tested in a hydrocarbon microseepage area located in Upper Ojai Valley, Ventura Basin-USA. A Probe-1 hyperspectral image was used. Even though the image dated from several years earlier, the patterns observed in the field were also observed in the image using the indices applied in the cited study. This supports the conclusion that the selected indices are not season dependent and can be used at any moment in time. Moreover, using vegetation indices that are related to biomass makes the method generally applicable.

2.6 Summary

The review of the literature has highlighted the following points:

Plant pigments play an important role in the photosynthetic activity of vegetation therefore, the study of plant pigments may contribute to understand and assess plant health under stress conditions. It has been established a close relationship between optical properties of vegetation in the visible range of the electromagnetic spectrum and chlorophyll content levels. Moreover, alterations in plants' biophysical and biochemical parameters imposed by environmental stressors are reflected in changes of leaf cellular structure, water content, pigment concentrations and biochemical composition. Optical properties of leaves and canopies are sensitive to those changes and can be detected by remote sensing instruments and techniques. Due the lack of knowledge and in-situ observations about chlorophyll levels in tropical rainforests, *Research Question 1* will address optical approaches to assess chlorophyll content in areas of the tropical forest where laboratory facilities are not available (Chapter 3).

The review of the literature has shown that the interaction of hydrocarbons and the soils reduces the amount of oxygen and increases the CO₂ concentration, soils turn acidic and minerals are mobilised. These changes affect the vegetation health. Furthermore, hydrocarbons reaching the Earth's surface by anthropogenic or natural processes can penetrate vegetation through leaves, stomata and roots

which affect plant transpiration, respiration and photosynthetic rates. Controlled experiments in the laboratory have demonstrated reduced levels of chlorophyll content in plants affected by hydrocarbons. The relationship between hydrocarbons and changes in biophysical and biochemical parameters has been studied under controlled experiments with most of them being applied to crops. It is not clear how hydrocarbons influence changes in biophysical and biochemical parameters of vegetation growing in natural environments. There are no references that investigated the effects of hydrocarbons in vegetation of tropical forest from the Amazon region. The effects of hydrocarbons in the biophysical and biochemical parameters of tropical rainforest will be addressed by answering Research Question 2 in Chapter 4.

Migration of hydrocarbons from underground reservoirs to the surface is a natural process widely spread in sedimentary basins. Hydrocarbons from macro and micro seeps appear to have an important contribution to the natural and total methane budget in the atmosphere. Estimations of gas emissions from these sources are based on the distribution of global sedimentary basins. Moreover, contributions of on-shore macro seepages are yet to be considered. A more accurate identification of hydrocarbon seepages will contribute considerable to understand the global methane balance but also the potential of commercial petroleum/gas reservoirs. On the other hand, oil spills have been a source of pollution in the tropical rainforest of Ecuador in the past, and new petroleum projects are planned in environment and social sensitive areas

Remote sensing techniques are useful tools in detecting vegetation stress in areas affected by hydrocarbons, most of them researched in temperate forests, agricultural fields and grass. No previous research has been conducted in rainforest ecosystems which are characterised by a high diversity plant species, high LAI, and a particular vertical structure and forest layering. Detecting areas affected by petroleum pollution and identification of hydrocarbon seepages based

on hyperspectral satellite images will be addressed by answering *Research Question 3* in Chapter 5.

Applying and developing efficient techniques based on remote sensing to detect vegetation stress caused by hydrocarbons in natural environments can contribute in the discussion about:

- Detect vegetation affected by hydrocarbon pollution caused by oil spills and invisible gas leakage from the petroleum industry and infrastructure: platforms, pipelines and open pits.
- Exploration petroleum projects in search of new oil/gas reservoirs face extremely difficult conditions and high costs when need to carry out 2-D and 3-D seismic projects in inaccessible forested areas. Using alternative exploratory techniques which apply remote sensing to detect vegetation stress that suggest the presence of hydrocarbon seepages can contribute to identify commercial productive petroleum reservoirs.
- Identify hydrocarbon macro and micro seepages in remote areas that can contribute to the general discussion about methane atmospheric budgets.

Chapter 3. Chlorophyll Estimation in the Amazon Rainforest

This chapter focuses on the analysis of different optical approaches to estimate chlorophyll content in the tropical forest. Transmittance, reflectance and a radiative transfer models are applied to estimate chlorophyll content for a collection of more than 1,100 leaves sampled in pristine and secondary tropical forests of the Amazon region.

3.1 Introduction

Photosynthesis is probably the most important biochemical process on earth. It allows plants to absorb certain wavelengths of the incoming radiation from the sun and transform its energy into organic compounds. Photosynthetically active radiation (PAR) is the amount of sunlight in the 400 to 700 nm wavelength range that is available for photosynthesis. Its agents are the photosynthetic pigments in the chloroplasts of which chlorophyll is the most important.

Plant eco-physiology studies the response of vegetation to environmental changes. Alterations in plant biophysical and biochemical parameters imposed by environmental stressors are reflected in changes of leaf cellular structure, water content, pigments concentrations, biochemical composition (cellulose, lignin, starch, proteins, sugars) (Rosso et al. 2005, Lambers;Chapin III & Pons 2008). Those alterations produce changes in the radiance reflected by leaves and canopies that can be detected using remote sensing instruments and techniques

The leaf chlorophyll content is closely related to the plant's health and physiology. This characteristic has been considered to assess vegetation stress in agricultural areas and forest plantations (Kumar;Schmidt & Dury 2006, Jones&Vaughan 2010, Smith;Colls & Steven 2005, Clevers et al. 2002) but studies of chlorophyll content in tropical rainforest environments, and specifically in the Amazon rainforest, are rare (Cao&Booth 2001, Coste et al. 2010). A better knowledge of leaf chlorophyll content in the tropical rainforest is required to

contribute to detecting and modelling vegetation stress during drought or pollution events by using satellite data and in this way to better understand the potential of photosynthetic capacity and its implications in regional and global carbon cycle and climate models.

Traditional methods for estimating pigment content in vegetation need to be performed in a well-equipped laboratory. They require the extraction of plant pigments from the leaves by applying organic solvents such as dimethyl sulphoxide (DSMO), methanol, ethanol, acetone or ether. Depending on the solvent being used, the position of the maximum absorption of plant pigments varies due to the differences in polarity and the loss of pigment-protein interaction (Ustin et al. 2009). The extracted foliar solution is analysed by a spectrophotometer in specific absorption wavelength ranges. Finally, absorbance is converted to chlorophyll concentration by applying equations described in the literature (Arnon 1949, Hiscox&Israelstam 1979, Lichtenthaler 1987, Porra;Thompson & Kriedemann 1989). Table 3.1 shows the traditional methods for chlorophyll estimation.

Table 3.1 Traditional methods for chlorophyll estimation

| Method | Solvent | Absorption features | Equations | Reference |
|-----------------------------|--|---------------------------------------|--|--|
| Porra et al., 1989 | Acetone | 646.6, 663.6 and 750.0 nm | | (Marwell;Osterman & Mitchell 1995); (Gitelson et al. 2005), (Ciganda;Gitelson & Schepers 2009) |
| Lichtenthaler, 1987 | Acetone, ethanol, methanol, diethyl ether | Various depending on the solvent used | Various depending on the solvent used | (Gitelson&Merzlyak 1994) |
| Hiscox and Israelstam, 1979 | Dimethyl sulphoxide, DSMO, acetone, methanol | 647 nm and 664 nm | Chla (mg ml ⁻¹) = 22 DO664 – 9.1 DO647 Chlb(mg ml ⁻¹) = 29.5 DO647 – 10.2 DO664 | (Richardson;Duigan & Berlyn 2002); (Coste et al. 2010); (Torres-Netto et al. 2002); (Torres-Netto et al. 2005); (Hawkins;Gardiner & Comer 2009); (Sánchez-Azofeifa et al. 2009); (Gitelson;Gritz & Merzlyak 2003); (Monje&Bugbee 1992) |
| Arnon, 1949 | Acetone | 645 nm and 663 nm | | (Marenco;Antezana-Vera & Nascimento 2009); (Ruiz-Espinoza et al. 2010b); (Terashima&Saeki 1983) |

These traditional chemical methods are widely applied in studies related to foliar chlorophyll content but they require laboratory conditions are time-consuming. The leaves also need to be analysed as soon as possible after collection from the field in order to preserve their biophysical and biochemical integrity. In addition, the leaf samples have to be destroyed during this process preventing any further analysis of changes over time using the same samples.

Alternative, non-destructive methods for chlorophyll estimation are available from spectral methods for plant pigment estimation. These methods are based on measuring light reflectance and transmittance properties of the vegetation using field spectroradiometers that can be carried in a rucksack or by hand. They provide indirect estimations of relative pigment content expressed as an index, which needs to be converted to foliar pigment content through often a linear, a polynomial or an exponential model. Several indices have been created and tested based on the reflectance properties in the visible and near-infrared range of the vegetation. These indices are classified into red/NIR ratios, green, red edge and derivative indices. A useful description of chlorophyll indices can be found in (Jones&Vaughan 2010, Ustin et al. 2009) and carotenoid indices (Gitelson;Gritz & Merzlyak 2003, Gitelson;Keydan & Merzlyak 2006, Féret et al. 2011).

3.1.1 Chlorophyll meter SPAD-502

Chlorophyll meters based on transmittance have been produced and are available commercially. They offer an inexpensive, easy, rapid and portable approach for an indirect estimation of chlorophyll content. One of these is the SPAD-502 chlorophyll meter (SPAD-502, Konica-Minolta, Osaka, Japan) which bases its measurements on the light that is transmitted by the leaf in two wavelength regions: the first is located in the red region at 650 nm which corresponds to the chlorophyll absorption peak unaffected by carotene and the second is located in the infrared region at 940 nm where chlorophyll absorption is extremely low. The light emitted by the instrument and transmitted by the leaf is measured by the receptor and converted into electrical signals. Finally, a chlorophyll index is

calculated by using the ratio of the intensity of the transmitted light (Konica Minolta 2009). Chlorophyll meters have been used extensively in agriculture to estimate chlorophyll and nitrogen in different species (Marwell;Osterman & Mitchell 1995, Torres-Netto et al. 2002, Torres-Netto et al. 2005, Hawkins;Gardiner & Comer 2009, Monje&Bugbee 1992) and also in forest studies (Coste et al. 2010, Richardson;Duigan & Berlyn 2002, Marengo;Antezana-Vera & Nascimento 2009, Richardson 2002, Castro-Esau et al. 2006, Cerovic et al. 2012). Furthermore, chlorophyll meters have been used in the indirect assessment of foliar nitrogen (Torres-Netto et al. 2002, Torres-Netto et al. 2005, Hoel 1998), and carotenoid content (Torres-Netto et al. 2002, Poorter et al. 2000).

Despite the advantages of chlorophyll meters, their principal drawback is to find an optimal model that transforms the recorded SPAD-502 index into foliar chlorophyll content. It has been shown that the chlorophyll index can vary with plant species, physiology, growth state, morphology, water content and dry matter content (Richardson;Duigan & Berlyn 2002, Torres-Netto et al. 2005, Hawkins;Gardiner & Comer 2009, Ruiz-Espinoza et al. 2010a). Nevertheless, other studies have found that the same calibration functions can apply to very different species. Marwell et al. (1995) found that a single calibration equation can be applied to soybean (a C3 plant) and maize (a C4 plant) plants even though these two species have a different leaf anatomy derived from their photosynthetic metabolic pathway.

According to the technical specifications of the Konica-Minolta SPAD-502, the accuracy of the instrument is within 1 SPAD-502 unit until 50 units. Values greater than 50 may be less accurate (Richardson;Duigan & Berlyn 2002, Monje&Bugbee 1992, Konica Minolta 2009). It is not clear how the accuracy of the instrument varies in values greater than 50. An explanation of the reduced accuracy of the instrument in high chlorophyll readings may be attributed to the sieve effect which results from a less homogeneous distribution of the photosynthetic pigments in plants with high chlorophyll levels (Terashima&Saeki

1983). In leaves with high chlorophyll concentrations, the chloroplasts may contain an increased density of chlorophyll rather than an increased density of chloroplasts. This effect may explain the reduced accuracy of the SPAD-502 readings in high chlorophyll plants (Richardson; Duigan & Berlyn 2002, Hawkins; Gardiner & Comer 2009, Monje & Bugbee 1992).

3.1.2 Reflectance indices

Another spectral method for chlorophyll content estimation is based on reflectance measurements to create pigment indices. Such indices take into account between two and four spectral bands and have shown high accuracy. Despite the literature offering many options for pigment indices, the majority of them have been tested for a specific plant species or vegetation type. As a result, they have become plant or vegetation specific. Estimations of chlorophyll content based on reflectance indices has been widely used (Gitelson et al. 2005, Ciganda; Gitelson & Schepers 2009, Richardson; Duigan & Berlyn 2002, Gitelson; Gritz & Merzlyak 2003, Gitelson; Keydan & Merzlyak 2006, Féret et al. 2011, Datt 1999, Gitelson; Chivkunova & Merzlyak 2009).

Chlorophyll indices are increasingly being used in crops and forest assessments and several calibration models have been described in the literature, most of which, however, have been calibrated and validated in few or closely related plant species with a limited number of samples. Under these conditions, most of the models can only be applied to specific species and environmental conditions. There is no scientific consensus as to whether a universal model can be found that can be applied for species-rich forest stands in different latitudes, phenological stages and leaf structures (Ustin et al. 2009). Feret et al. (2011) noted this limitation of the spectral indices and proposed new indices for chlorophyll and carotenoid estimation. They were based on a vegetation dataset collected in various ecosystems around the world including a wide variety of plant physiology and leaf structure.

3.1.3 PROSPECT model

Based on the relationship between reflectance and the biochemical and biophysical properties of the leaves and canopies, models have been created in order to simulate the interaction of the light with the plant leaves through the radiative transfer theory. The Leaf Optical Properties Spectra (PROSPECT) model describes radiative transfer within a broadleaf with a plate model. Plate models treat internal leaf structure as sheets or plates and calculate multiple reflections of diffuse radiation between these interfaces (Kumar;Schmidt & Dury 2006). PROSPECT is based on the representation of the leaf as one or several absorbing plates with a rough surface giving rise to isotropic scattering. The model estimates the directional-hemispherical reflectance and transmittance of leaves across the solar spectrum from 400 nm to 2500 nm (Jacquemoud 2009).

A leaf structure parameter of the model is represented by N which is the number of compact layers specifying the average number of air/cell wall interfaces within the mesophyll. The leaf biophysical parameters of the model are represented by chlorophyll a+b content (C_{ab}) and equivalent water thickness (C_w). The latest versions of the model include the parameters dry matter content (C_m) and brown pigments content (C_{bp}). Inversion of PROSPECT revealed good agreement between measured and predicted leaf chlorophyll concentrations (Kumar;Schmidt & Dury 2006, Jacquemoud 2009, Feret 2008).

3.1.4 MTCI index

The Medium Resolution Imaging Spectrometer (MERIS) Terrestrial Chlorophyll Index (MTCI) is a standard product of the European Space Agency (ESA) which provides estimations of chlorophyll content of vegetation (amount of chlorophyll per unit area of ground) at global level. MTCI index is simple to calculate, sensitive to high values of chlorophyll content (Dash&Curran 2004, España-Boquera et al. 2006) and estimations are independent to soil and atmospheric conditions, spatial resolution and illumination and observation geometry (Curran&Dash 2005). Validation of MTCI index and ground chlorophyll content

across a range of crop types and environmental conditions resulted in a strong relationship of $R^2=0.8$ and (Root Mean Square Error) RMSE=192 g per MERIS pixel (Dash et al. 2010). Moreover, the strong relationship of MTCI and canopy chlorophyll content has been used to estimate Gross Primary Production (GPP) across a range of ecosystems. Boyd et al. (2012) applied MTCI index, together with radiation information (photosynthetically active radiation-PAR and fraction of photosynthetically active radiation-fPAR), into models which extended the accuracy of GPP estimated.

MTCI is computed by the ratio of the difference in reflectance between band 10 and band 9 and the difference in reflectance between band 9 and band 8 of the MERIS standard band setting:

$$MTCI = \frac{R_{Band10} - R_{Band9}}{R_{Band9} - R_{Band8}} = \frac{R_{753.75} - R_{708.75}}{R_{708.75} - R_{681.25}}$$

Where $R_{753.75}$, $R_{708.75}$ and $R_{681.25}$ are the MERIS reflectance at wavelength 753.75 nm, 708.75 nm and 681.25 nm respectively.

3.1.5 The Red Edge Position (REP)

The red-edge position is a unique feature of green plants related to leaf chlorophyll content and to LAI. REP is defined as the inflection point (or sharp change) of the low red reflectance caused by chlorophyll absorption near 680 nm and high infrared reflectance governed by the internal structure of leaves near 750 nm (Clevers&Jongschaap 2006). REP has been used as an indicator of chlorophyll content in vegetation, as increasing chlorophyll content implies an enlargement of the chlorophyll absorption peak: this moves the red-edge to longer wavelengths while a decrease in chlorophyll shifts the red-edge towards shorter wavelengths (Jones&Vaughan 2010). However the REP has been reported not to be an accurate indicator of chlorophyll content in vegetated areas showing high chlorophyll content values because of the asymptotic relationship between REP

and chlorophyll content (Jago;Cutler & Curran 1999, Munden;Curran & Catt 1994).

Several methods have been proposed to estimate REP. Dawson & Curran (1998) developed a three-point Lagrangian interpolation technique, but this method has shown some problems when the reflectance spectrum exhibits more than one maximum in its first derivative (Clevers&Jongschaap 2006). Another method was developed by Guyot & Baret (1988) which applies a linear model to the red-NIR slope. This method has been reported to be robust when it was applied to various data sets (Clevers et al. 2002). A third method identifies the red-edge inflection point as the maximum of a curve fitted to the first derivative of the reflectance spectrum. This method has been closely related to chlorophyll content per unit area at leaf and canopy level (Blackburn 1998b) and has shown sensitivity to detect vegetation stress by quantifying changes in chlorophyll content (Smith;Steven & Colls 2004).

3.2 Materials and methods

3.2.1 Study area and sites

Fieldwork was undertaken from April to Jul 2012 at three sites in the Amazon tropical rainforest of Ecuador (Figure 3.1). The first and second study sites are located in a lowland evergreen secondary forest in Sucumbios province, Tarapoa region (0°11' S, 76°20' W). Mean annual rainfall is 3,800 mm and the average annual temperature is 23°C with relative humidity close to 90% (Fitton 2000). The area is located at 232-238m above mean sea level. The third study site is a highly diverse lowland evergreen primary forest located in the Orellana province, in the northern section of Yasuní National Park (0°41' S, 76°24' W). The area lies 216-248m above mean sea level and receives an annual average of 3081mm rainfall with peaks in October and November. Mean monthly temperatures vary from 22°C to 34°C (Valencia 2004). In this site, the Pontifical Catholic University of Ecuador established and manages permanent forest dynamics plots of 50

hectares where over 150,000 mapped trees $\geq 1\text{cm}$ in diameter at breast height (dbh) from over 1,100 species have been identified (Valencia et al. 2004). A detailed description of the sites is shown in Table 3.2

In spite of the study site are located in the lowland Amazon forest, there are substantial differences in plant species and forest structure. Site 1 and Site 2 are disturbed forest that was exposed to selective logging, agricultural activities, petroleum industry impacts and secondary forest regrowth over the last 20 years following diminishing human influence. Site 3 is a pristine primary tropical rainforest with legal protection status where a research project on plant and animal species diversity is currently conducted. Studies consider that the plant species richness in this area is among the highest in the world (Tedersoo et al. 2010).

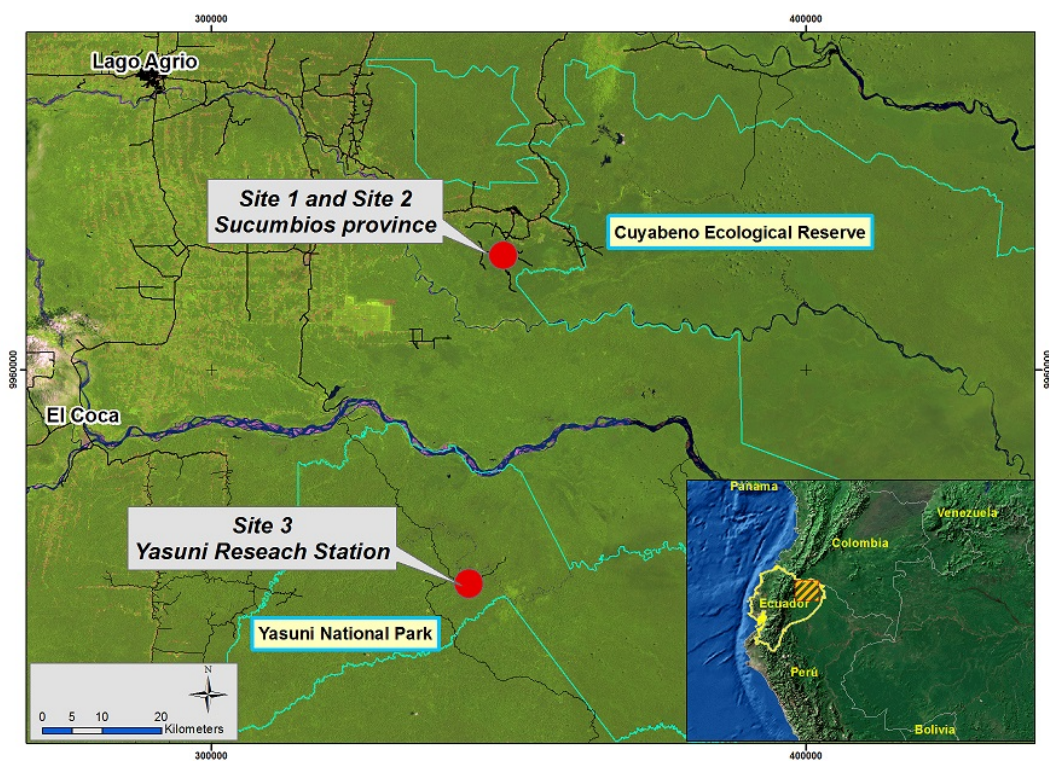


Figure 3.1 Map of the study area-North-east Amazon region of Ecuador. Site 1 and Site 2 are located in Sucumbios province and Site 3 is located in Orellana province. Background is a Landsat image. Source of zoom-in map: Colour Shaded Relief Image, WorldSat International, Inc.

The fieldwork campaign of this project was granted with the appropriate permits and approvals from the Environmental Ministry of Ecuador and the Non-Renewable Resource Ministry of Ecuador.

Table 3.2 Description of the sites in the study area

| | Site 1 | Site 2 | | Site 3 |
|-------------------------------|--|---------------------------|---------|--------------------------------------|
| | | Site 2a | Site 2b | |
| Forest classification | Aseasonal-Lowland evergreen rainforest | | | |
| Forest type | Secondary /regrowth following abandoning farming | | | Pristine Forest |
| Pollution | Petroleum-Hydrocarbon pollution | Not affected by pollution | | Not affected by pollution |
| Coordinates System | UTM-WGS84-Z18N | | | |
| Latitude | 9979706 | 9980060 | 9978875 | 9924894 |
| Longitude | 348523 | 348694 | 347525 | 344220 |
| Altitude (m. above sea level) | 232 | 238 | 229 | 235 |
| Mean annual temperature (°C) | 27 | | | 28 |
| Mean annual rainfall (mm) | 3300 | | | 3081 |
| Soil type | Histosols/Fibrils/Tropofibrils | | | Inceptisols/ Tropots/ Distrops |

Site 1 – Oil Spill

This site is an area located near to a non-operative petroleum platform where abandoned, open and unlined pits have been found. The pits contain crude oil that has been discharging to the environment or leaching out as the pits degrade or overflow from rainwater. It is not clear when the pits were constructed but it is estimated that they have been there for at least 15 years. The site is covered by a secondary forest (see Figure 3.2a).



a)



b)



c)

Figure 3.2 Site 1 affected by oil spill. **a)** Forest canopy; **b)** Oil spill; **c)** vegetation growing on the crude oil

The crude oil that has not migrated from the pits has formed a viscose stratum of approximately 1.5m deep where there is no major vegetation growth (see Figure 3.2b). A thin layer of organic matter from leaf decomposition covers the crude oil where some shrubs and grass have found a growing base (see Figure 3.2c). The volatility process of lighter hydrocarbons (gaseous and liquid components $< C_{18}$) may happen in time after the crude oil has been disposed in these open pits (approximately 15 years ago). Hydrocarbons have migrated from the open pits by infiltration into the soil and dissolution in water. These processes may have

occurred more intensively in the upper layer of the oil spill, but in the interior of the viscose stratum of crude oil there is still a mixture of liquid hydrocarbons and gases. When we drilled a hole of 1.5m deep, an odour of diesel/gasoline escaped together with oily liquids. Temperatures and moisture in the site probably stimulated the bacterial decomposition of hydrocarbons in the upper layers of the spill. Biodegradation has decomposed part of the hydrocarbons, especially in areas where the concentration of crude oil in the soil is low (e.g. in the areas where the hydrocarbons migrate for the action of the runoff water) but the concentration of crude oil in the pits is very high with very low oxygen concentration which has limited biodegradation. Another drawback for the slow biodegradation process of hydrocarbons remaining in the open pits is the acidic characteristics of the soils and the low concentrations of nitrogen and phosphorus in the soils (see results of soil analysis in Table 4.1). All of this suggests that the source of pollution is still active and hydrocarbons will continue migrating to the environment. The high levels of TPH in soil reported by the laboratory analysis supports this argument (See Table 4.1).

Site 2 - Not affected by hydrocarbons

This site is composed of two sub-sites carefully selected where there is no direct influence of hydrocarbons. Site 2a is located at 400 meters distance from the oil spill described in Site 1, and Site 2b is located at 1,250 meters distance. There are no open pits or signs of petroleum spills, and soil samples from those sites did not report hydrocarbon pollution according to the TPH and HAPs results reported by laboratory analysis (see results of the laboratory analysis of soils in Table 4.1). Since their proximity, Site 1, Site 2a and 2b share the same environment conditions related to soils type, weather, forest type and anthropogenic influence.



a)



b)

Figure 3.3 Secondary forest not affected by oil pollution. a) Site 2a b) Site 2b

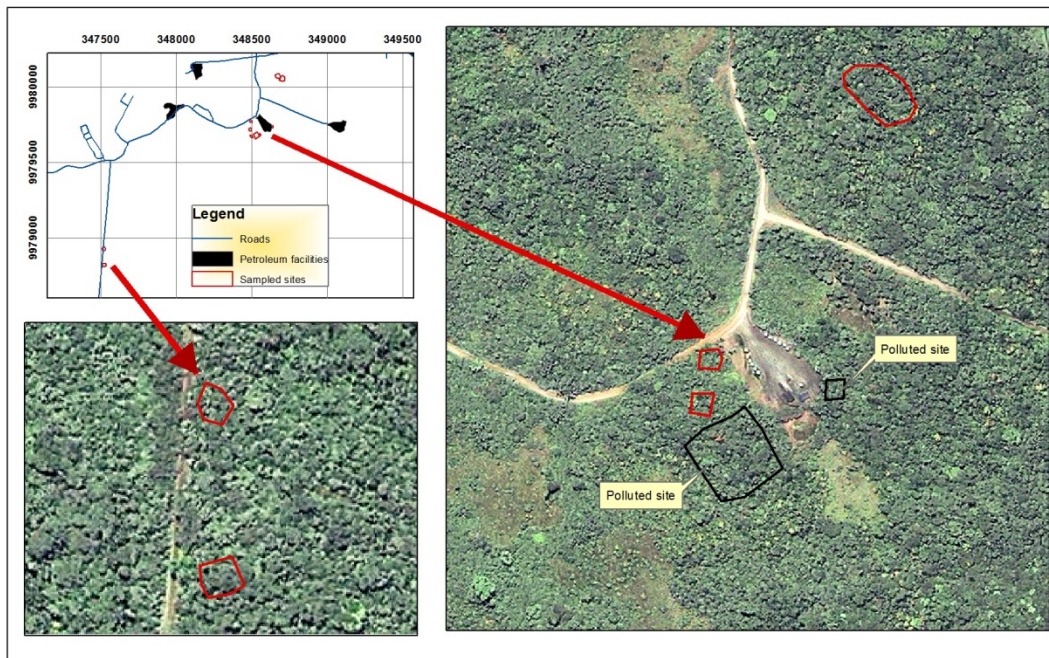


Figure 3.4 Location of sampled areas. Black polygons = polluted site; Red polygons = Non polluted secondary forest. Ikonos image as background

Site 3 - Pristine forest

Site 3 is located in a pristine lowland rainforest in Yasuni National Park (see Figure 3.1 and Figure 3.5). We developed our fieldwork in some parcels of a 50-ha forest dynamic plot managed by the scientific research station of the Pontifical Catholic University of Ecuador where over 150,000 mapped trees ≥ 1 cm in diameter at breast height (dbh) from over 1,100 species are permanently registered for biological and forest dynamic studies (Valencia 2004).



Figure 3.5 Pristine forest in Yasuni National Park

Fieldwork camping in Yasuni National Park was conducted in an area of 4800 m² divided in 12 parcels, each parcel represents 20 x 20 m. Figure 3.6 shows the 3167 trees surveyed trees in area (green circles) and the 280 sampled trees (orange circles). Every circle in the figure represents a tree crown as a function of the (Diameter at Breast Height) DBH in cm.

According to the results of soil analysis, HAPs and TPH show reading below the standard laboratory method which proves there are no petroleum pollutants in the area (see Table 4.1).

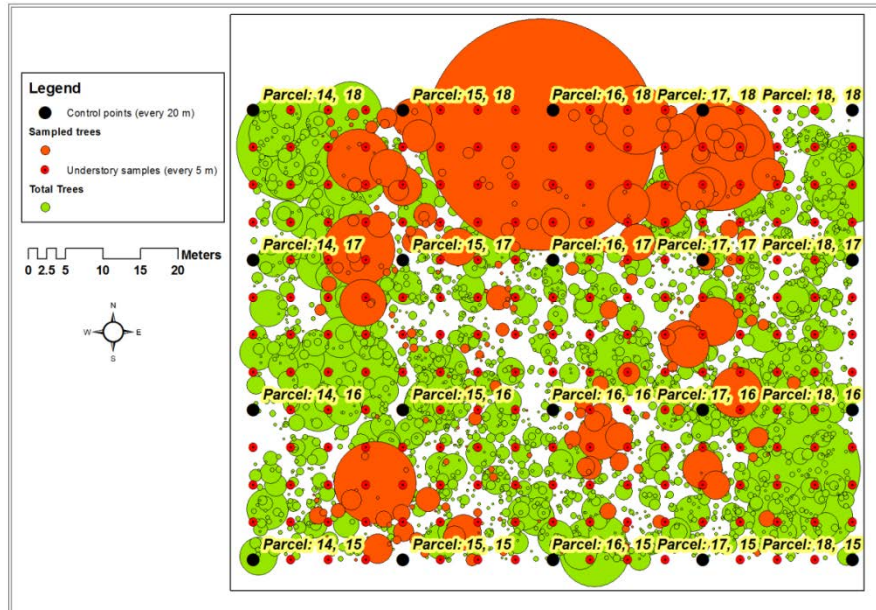


Figure 3.6. Map of the sampled parcels of the Yasuni plot.

3.2.2 Sampling process

Well-developed branches were carefully selected and collected by using a telescopic pruner, tree-climbing techniques and canopy towers at different levels of the vertical profile of the forest (Figure 3.7). The collected branches were sealed in large polyethylene bags to maintain their moisture content and stored in ice coolers. The foliar material was transported to a local site, and fully expanded mature leaves with no damage by herbivorous or pathogens were selected for analysis. A total of 1.134 samples were collected in the three fieldwork sites. The sampling process accounted for three levels of the vertical profile and included a wide range of vegetation heterogeneity related to species distribution, phenological stage and leaf structure. A list of vegetation species sampled in the study sites are detailed in Annex 1 and Annex 2.



a)



b)



c)



d)



e)

Figure 3.7 Photographs of leaf sampling process. **a)** Collecting leaves using the telescopic pruner **b)** Climbing trees **c)** Telescopic pruner nine meters long **d)** Climbing trees techniques **e)** Canopy towers in the study area

3.2.3 Chlorophyll meter readings

Depending on the size and shape of the leaf, different cork borers of variable size between 2.5 to 8.5 centimetres diameter were used to clip a leaf disk from the central and widest portion of the leaf blade, avoiding the major veins (Figure 3.8).



Figure 3.8 Leaf samples and clipped disks from plants of different species and health status. The last photo shows the SPAD-502 meter

All leaf disks were clipped from the midpoint of the leaves since it has been documented that it is the best position from which to take chlorophyll readings (Hoel 1998). Three readings were taken from each disk using a portable SPAD-502 chlorophyll meter at different positions of each leaf disk, and a mean index value was used in further analysis.

For each leaf sample, an average of three SPAD-502 chlorophyll meter readings was calculated. Different readings per leaf took into account any possible variations in leaf thickness. The histogram of the dataset shows a normal distribution and the boxplot identified values outside the 95% confidence interval considered as outliers (Figure 3.9). Table 3.3 shows descriptive statistics of the dataset.

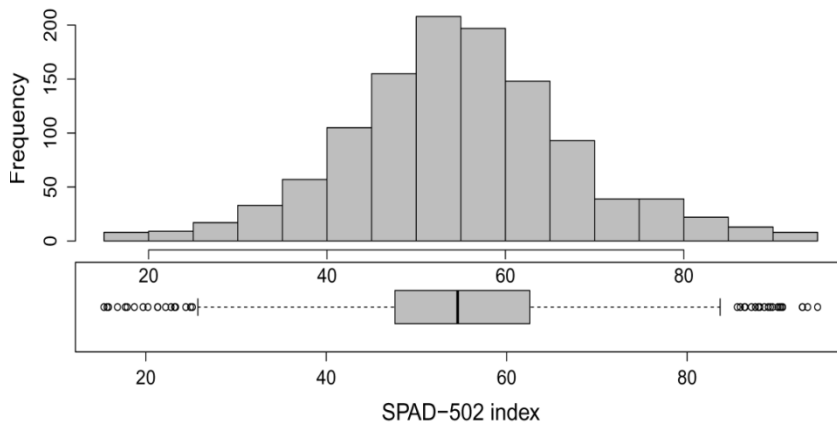


Figure 3.9 Histogram and boxplot of the SPAD-502 chlorophyll meter. Total samples collect in both sites of the Amazon forest in Ecuador

Table 3.3 Number of foliar samples and descriptive statistics of the SPAD-502 chlorophyll meter readings from two sites of the study area

| Number of Samples | Maximum | Minimum | Mean | SD |
|-------------------|---------|---------|-------|-------|
| 1134 | 94.47 | 15.37 | 54.88 | 12.83 |

3.2.4 Spectroradiometer measurements

Reflectance and ‘trans-flectance’ (a term used in this study to describe the measurement of ‘double’ transmittance) were measured for each leaf disk using an ASD FieldSpec HandHeld-2 spectroradiometer (Analytical Spectral Devices Inc., Boulder, Colorado). This instrument provides a wavelength range of 325-1,075 nm with a resolution of full width at half maximum of 3.5 nm and sampling interval of 1 nm. The spectrometer is attached with a plant probe to an internal 4.05-W halogen light source and a leaf clip that includes rotating head with both white and black reference panels (Figure 3.10).



Figure 3.10. a) ASD HandHeld 2 spectrophotometer, b) plant probe + leaf clip

This mechanism holds the leaves, excludes ambient direct and scattered light and ensures a constant field of view (FOV) of 10 mm geometry for the target sample. Reflectance was estimated by recording the radiance reflected from the leaf with the black reference panel, and trans-flectance was estimated by recording the radiance reflected from the leaf with the white panel. Spectrum averages of ten scans were taken for each leaf disk and to the white reference radiance panel. The appropriate number of scans was established based on a compromise between the time required for each spectrum collection and noise reduction. We tested the measured differences in the specific wavelength range used by reflectance indices for the estimation of chlorophyll content. The difference between 10 and 20 scans in the range of 700-750 was 2.0% and in the range 751-800 nm it was 0.9%. Differences between 10 and 30 scans in the same ranges were 3.3% and 1.8% respectively. These low differences were considered acceptable for the reflectance index calculation. This can be considered an advantage of using the plant probe and leaf clip mechanism which provides a constant light source in a closed

environment to allow us to reduce the numbers of scans and keep a comparable signal-to-noise ratio.

3.2.5 Chlorophyll indices based on SPAD-502 readings (transmittance)

Several published calibration models based on SPAD-502 readings were applied in this study. Table 3.4 describes seven published polynomial, exponential or homographic calibration models for chlorophyll content estimation from SPAD-502 chlorophyll meter readings. Selected calibration models cover a heterogeneous range of plants species, plant physiology, phenology and growing conditions which is a characteristic of the vegetation in tropical forests. All selected models have shown good agreement with traditional methods applied in a laboratory. Some models tested in this study over perform or underperform chlorophyll content estimations and therefore were excluded from this analysis (see details of these models in Annex 3, page 215). The models used in this study are briefly introduced in this section.

Six Amazonian tree species growing in open conditions in Manaus, Brazil were considered to assess the accuracy of a general calibration model to convert SPAD-502 readings into absolute chlorophyll content (Marenco;Antezana-Vera & Nascimento 2009). Per each species, 30 to 50 leaves at different stages of development, from very young to fully expanded sun leaves, were analysed. Chlorophyll content obtained in a laboratory using traditional methods was used to validate several models, one for each species and a general species-independent model for the six species together. Determination coefficients (r^2) between SPAD-502 readings and chlorophyll content were in the range of 0.81 to 0.95 for the six species-specific. From the six models, a generalised model that considers the six plant species was computed and exhibited a determination coefficient of 0.79. This generalised published model was selected in this study and is described in Table 3.4 as Model 3.1.

An experiment under greenhouse conditions was conducted in French Guiana where 13 tropical rainforest tree species of the lowland forest were selected to cover a broad range of leaf structural characteristics (Coste et al. 2010). For each species, 30 leaf samples growing in different illumination gradients were selected. Traditional laboratory extraction techniques were applied to derive chlorophyll content for validation SPAD-502 readings. The approach proposed a new homographic calibration model for a wide range of tropical species that has a natural asymptote, something that is not taken into account, the often-used linear, polynomial and exponential models. The idea behind this model is that the performance of chlorophyll meters degrades at high chlorophyll contents since they are unable to measure very low transmittances precisely. The accuracy of the homographic model was higher than the accuracy of linear, polynomial and exponential models. Additionally, the performance of the model to predict independent datasets gathered on other species was similar to the original models developed specifically for these species. The study concludes that foliar chlorophyll content can be reliably estimated using the proposed homographic model, despite the broad range of SPAD-502 readings and the chlorophyll content intrinsic of the tropical tree species. The resulting model is described in Table 3.4 Model 3. 2.

Hawkins et al. (2009) assessed foliar chlorophyll content across a range of plant ages, growing conditions and genotypes of *Lindera melissifolia* (a shrub) using a SPAD-502 chlorophyll meter. Transformation models were presented for each plant group as well as a general model (Table 3.4, Model 3.3).

Richardson (2002) compared the performances of two chlorophyll meters with several reflectance indices for chlorophyll estimation. Readings between the two meters showed a very high consistency of $r^2=0.97$. Chl_{NDI} (chlorophyll normalized difference index) (Gitelson&Merzlyak 1994), R_{II} (reflectance integral index) and D_{730} (first difference of the reflectance spectrum at 730 nm) performed better than the chlorophyll meters. The SPAD-502 chlorophyll estimation performed better

than the red-edge position (REP), vegetation index or simple ratio (VI), normalised difference vegetation index (NDVI) and the yellowness index (YI). The resulting model is described in Table 3.4 as Model 3.4.

Table 3.4 Indices of chlorophyll content estimation based on SPAD-502 chlorophyll meter models applied in this study

| ID | Model | Units | Tested in | #of sampl es | SPAD-502 range | Chl range ($\mu\text{m cm}^{-3}$) | R^2 |
|-----|---|------------------------|-----------------------------|-------------------------|----------------|-------------------------------------|-------|
| 3.1 | $\text{Chl} = 62.05e^{(X*0.0408)}$ | mg cm^{-2} | 6 Amazonian trees species | 30-50 leaves per specie | 3-80 | ~0-100 | 0.79 |
| 3.2 | $\text{Chl} = (117.1*X) / (148.84-X)$ | $\mu\text{g cm}^{-2}$ | 13 Amazonian trees species | 391 | 0-80 | 0-150 | 0.89 |
| 3.3 | $\text{Chl} = 2E-05X^2 + 1E-04X + 0.0038$ | mg cm^{-2} | <i>Lindera melissifolia</i> | 145 | 3.8 - 47.3 | 4-50 | 0.90 |
| 3.4 | $\text{Chl} = 5.52E-04 + 4.04E-04X + 1.25E-05X^2$ | mg cm^{-2} | Paper birch | 100 | ~ 0-45 | 0.4-45.5 | 0.96 |
| 3.5 | $\text{Chl} = 10.6 + 7.39X + 0.114X^2$ | $\mu\text{mol m}^{-2}$ | Soybean and maize | na. | 0-70 | ~0-90 | 0.96 |
| 3.6 | $\text{Chl} = 10(X^{0.265})$ | $\mu\text{mol m}^{-2}$ | Soybean and maize | na. | na. | ~0-90 | 0.94 |
| 3.7 | $\text{Chl} = 10(X^{0.264})$ | $\mu\text{mol m}^{-2}$ | Maize | na. | na. | na. | 0.79 |

Source: 3.1) (Marenco;Antezana-Vera & Nascimento 2009) 3.2) (Coste et al. 2010) 3.3) (Hawkins;Gardiner & Comer 2009) 3.4) (Richardson;Duigan & Berlyn 2002) 3.5) (Marwell;Osterman & Mitchell 1995) 3.6) (Marwell;Osterman & Mitchell 1995) 3.7) (Marwell;Osterman & Mitchell 1995). na. = Not available

A variety of lines of soybean and maize representing a diverse range of chlorophyll concentrations were used by Marwell et al. (1995) to define a calibrated relationship between chlorophyll extracted from chemical methods and SPAD-502 readings. Their results showed, that for both plant species, an exponential equation provided a more accurate approximation of chlorophyll content than a polynomial equation (Table 3.4, Model 3.5 and Model 3.6). For single specie (maize) a very similar exponential model was proposed (Model 3.7).

3.2.6 Chlorophyll index based on reflectance indices.

Five reflectance indices for chlorophyll content estimation found in the literature are described in Table 3.5. They considered the visible, red edge and near infrared ranges. Chlorophyll content was estimated by applying linear or polynomial models for specific plant species when deriving these models. Selection criteria for reflectance indices was based on their ability to estimate chlorophyll content in a wide range of plant species, plant physiology, phenology and growing conditions which is a characteristic of the vegetation in tropical forests. Some indices reported extremely low estimations therefore were excluded for further analysis (see Annex 4).

Feret *et al.* (2011) compiled a global vegetation dataset composed of 17 independent sets including a wide range of leaf spectra, chemical and structural properties. They included 1417 leaves corresponding from about 120 species from various growing conditions and developmental stages that represent a wide range of terrestrial ecosystems around the world. The study assessed the performance of radiative transfer model and vegetation indices for estimating leaf pigments (chlorophyll and carotenoids) and leaf biophysical structure parameters (equivalent water thickness and leaf mass per area). Three generalized optimal chlorophyll indices to estimate chlorophyll content in a wide range of plant species, ecological conditions and phenological stages were proposed and are presented in Table 3.5 (Models 4.1, 4.2 and 4.3).

In 2005, Gitelson *et al.* (2005) proposed a three-band conceptual model based on the ratio of Near Infrared range (750-800 nm) and red edge index (710-730 nm), shown as Model 4.4 in Table 3.5. The optimal spectral bands are found in a stepwise linear regression of the model against total chlorophyll content in maize and soybean canopies.

Ciganda *et al.* (2009) applied the red edge chlorophyll index (CI_{red edge}) to accurately estimate chlorophyll content at leaf and canopy level. The sampling process took into account the variability in chlorophyll content within and among

leaves in the canopy. A total of 2300 samples of 154 maize plants were collected during two consecutive years (Table 3.5, Model 4.5).

Table 3.5 Chlorophyll content indices based on reflectance derived from spectroradiometer data.

| ID | Index | Model | Units | Tested in | Samples | Chl range ($\mu\text{m cm}^{-2}$) | RMSE | R ² |
|---|---|---|-----------------------|---|---------|-------------------------------------|------|----------------|
| 4.1 | $[1/(R_{680-730})] - [1/(R_{780-800})]*R_{755-780}$ | $\text{Chl} = 3.96*X^2 + 23.86*X - 3.31$ | $\mu\text{g cm}^{-2}$ | Temperate and tropical tree species and crops | 1417 | 0.3 - 106.7 | 6.53 | na |
| 4.2 | R_{708} / R_{775} | $\text{Chl} = 96.8*X^2 - 209.76*X + 115.08$ | $\mu\text{g cm}^{-2}$ | Temperate and tropical tree species and crops | 1417 | 0.3 - 106.7 | 6.6 | na |
| 4.3 | $(R_{780} - R_{712}) / (R_{780} + R_{712})$ | $\text{Chl} = 40.65*X^2 + 121.88*X - 0.77$ | $\mu\text{g cm}^{-2}$ | Temperate and tropical tree species and crops | 1417 | 0.3 - 106.7 | 6.25 | na |
| 4.4 | $(R_{750-800}) / (R_{710-730}) - 1$ | $\text{Chl} = 716.32 * X$ | mg m^{-2} | Maize and soybean | 82 | ~ 0 - 100 | 6.07 | 0.95 |
| 4.5 | $(R_{770-800}) / (R_{720-730}) - 1$ | $\text{Chl} = 37.904 + 1353.7X$ | mg m^{-2} | Maize | 2300 | 1 - 80.5 | 3.8 | 0.94 |
| Source: 4.1) (Féret et al. 2011); 4.2) (Féret et al. 2011); 4.3) (Féret et al. 2011); 4.4) (Gitelson et al. 2005); 4.5) (Ciganda;Gitelson & Schepers 2009). na. = Not available | | | | | | | | |

It is important to highlight the wide range of species and phenological conditions included in the high number of samples used by Models 4.1, 4.2 and 4.3 which includes 1,417 samples from 120 plant species from around the world (Féret et al. 2011).

3.2.7 PROSPECT model

The inversion of the PROSPECT model using leaf reflectance and transmittance was applied in this chapter in order to estimate chlorophyll concentration. First, a Savitzky-Golay filter was computed to reflectance and trans-flectance signals in order to smooth the signals and increase the signal-to-noise ratio. Second, the measurements of trans-flectance (or double reflectance) obtained from the leaf-clip attached to the ASD FieldSpec HandHeld-2 spectroradiometer (see details of

in section “Spectroradiometer measurements” in pag.70) were transformed to transmittance based on a procedure developed for this research. This was founded on the Kubeika-Munk theory of light scattering and light absorption based on the communications with Professor Stephane Jacquemoud and Dr. Sebastien Marcq from the Institute of Physique du Globe of Paris & Universidad Paris Diderot (ISO 2012, Jacquemoud&Marcq 2012).

$$L_1 = R_W * L_{inc} \quad (1)$$

$$L_{inc} = \frac{L_1}{R_W} \quad (2)$$

$$L_2 = R_b * L_{inc} \quad (3)$$

$$L_3 = R_w^{each} * L_{inc} \quad (4)$$

$$L_4 = R_b^{each} * L_{inc} \quad (5)$$

$$R(\lambda)_b = \frac{L_2 R_W}{L_1} \quad (6)$$

$$R(\lambda)_w^{each} = \frac{L_3 R_W}{L_1} \quad (7)$$

$$R(\lambda)_b^{each} = \frac{L_4 R_W}{L_1} \quad (8)$$

$$R_{est} = \frac{R(\lambda)_b R(\lambda)_w^{each} - R(\lambda)_b^{each} R_W}{R(\lambda)_b - R_W + R_W R(\lambda)_b (R(\lambda)_w^{each} - R(\lambda)_b^{each})} \quad (9)$$

$$T = \sqrt{\frac{(R(\lambda)_w^{each} - R_{measured}) (1 - R_{measured} R_W)}{R_W}} \quad (10)$$

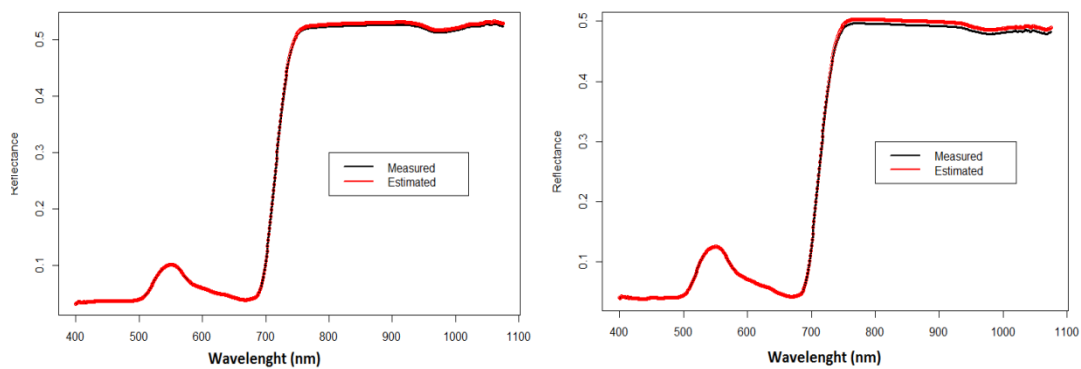
Where

- L₁: luminance measured with the white background disk only
- L₂: luminance measured with the black background disk only
- L₃: luminance of the leaf mounted on the white background disk
- L₄: luminance of the leaf mounted on the black background disk
- R_{measured}: leaf reflectance measured

- R_{est} : leaf reflectance estimated
- T : leaf transmittance
- R_b : reflectance of blank background disk
- R_w : reflectance of the white background disk
- R_w^{each} : reflectance of each leaf + white background disk
- R_b^{each} : reflectance of each leaf + black background disk.
- L_{inc} : Lamp luminance

An automatic process to apply this procedure was developed in R® programming language and is presented in Annex 5.

Reflectance was estimated by applying Eq.8 in order to test the procedure applied to estimate transmittance. Figure 3.11 illustrates the close agreement between measured and estimated reflectance spectral.



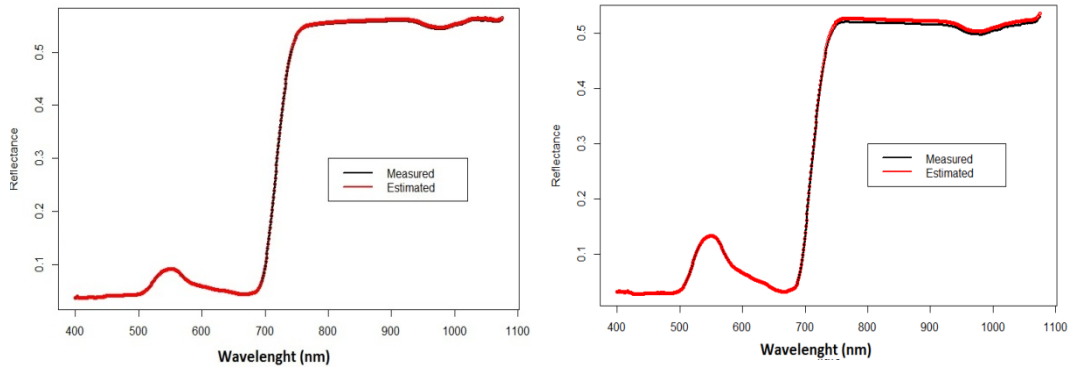


Figure 3.11 Measured and estimated reflectance of some representative samples of the foliar dataset

Foliar chlorophyll content (C_{ab}) was computed by the inversion process of PROSPECT 5 which was modified by its author (Jacquemoud&Marcq 2012) to work in the range of 400-1,075 nm using reflectance and transmittance in the sampling interval of 1 nm for the 1,134 leaf samples. Annex 6 shows the MATLAB® code of the modified inversion process of the PROSPECT model. Brown pigments (C_{bp}) and water content (C_w) were neutralised since foliar samples are green vegetation and the spectra does not show water absorption features. Figure 3.12 illustrates the process to estimate chlorophyll content at leaf.

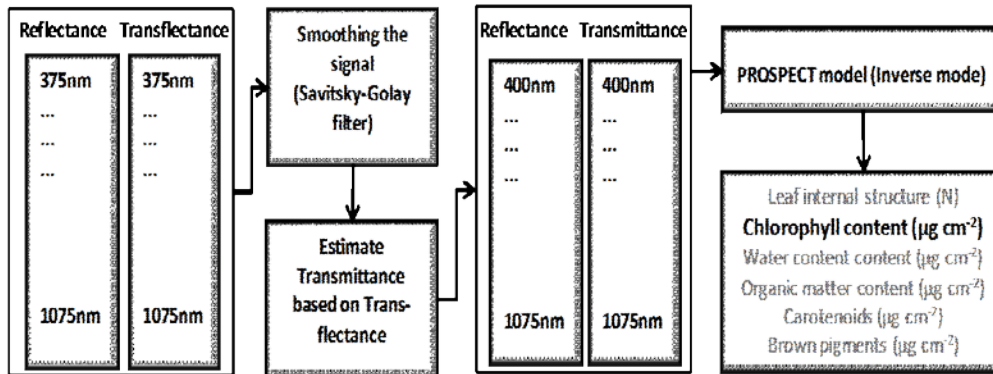


Figure 3.12. Process to estimate Chlorophyll content ($\mu\text{g cm}^{-2}$) applying the inversion process of PROSPECT leaf reflectance model

3.2.8 MTCI Index

In this study, MTCI was applied to foliar reflectance data collected at leaf level by the following equation:

$$MTCI_{foliar\ reflectance\ data} = \frac{R_{754} - R_{709}}{R_{709} - R_{681}} \quad (10)$$

Where R_{754} , $R_{709.75}$ and R_{681} are the foliar reflectance at wavelength 754 nm, 709 nm and 681 nm respectively.

3.2.9 REP (first derivative method)

The red-edge inflection point was estimated by the first derivative method:

$$D_{\lambda(i)} = \frac{R_{\lambda(i)} - R_{\lambda(i-1)}}{\Delta\lambda} \quad (11)$$

Where $R_{\lambda(i)}$ and $R_{\lambda(i-1)}$ are reflectance at wavelength i and $(i-1)$ respectively.

3.3 Results

3.3.1 Chlorophyll content based on SPAD-indices

Models 3.1 to 3.7 shown in Table 3.4 were applied to the SPAD-502 chlorophyll meter readings from the tropical forest study sites and the descriptive statistics of the estimates are shown in Table 3.6.

Table 3.6 Descriptive statistics of leaf chlorophyll content ($\mu\text{g cm}^{-2}$) based on seven published SPAD-502 chlorophyll meter models.

| Model | Reference | Max. | Min. | Mean | SD |
|-------|---|--------|-------|-------|-------|
| 3.1 | (Marenco;Antezana-Vera & Nascimento 2009) | 292.83 | 11.62 | 67.02 | 39.70 |
| 3.2 | (Coste et al. 2010) | 203.45 | 13.48 | 72.16 | 28.30 |
| 3.3 | (Hawkins;Gardiner & Comer 2009) | 191.73 | 10.06 | 72.82 | 30.21 |
| 3.4 | (Richardson;Duigan & Berlyn 2002) | 150.27 | 9.71 | 62.43 | 23.21 |
| 3.5 | ((Marwell;Osterman & Mitchell 1995) | 154.04 | 13.48 | 69.46 | 23.10 |
| 3.6 | (Marwell;Osterman & Mitchell 1995) | 194.22 | 10.31 | 72.78 | 29.87 |
| 3.7 | (Marwell;Osterman & Mitchell 1995) | 187.56 | 10.18 | 70.80 | 28.82 |

Figure 3.13 illustrates the chlorophyll content estimations for each model, its average values across models and the confidence interval of 95% for the binned SPAD-502 readings. Estimations for the first six bins (range 15-80 SPAD-502 index) reported similar values. Average values at the higher SPAD index bin (80-95) show increase differences between models.

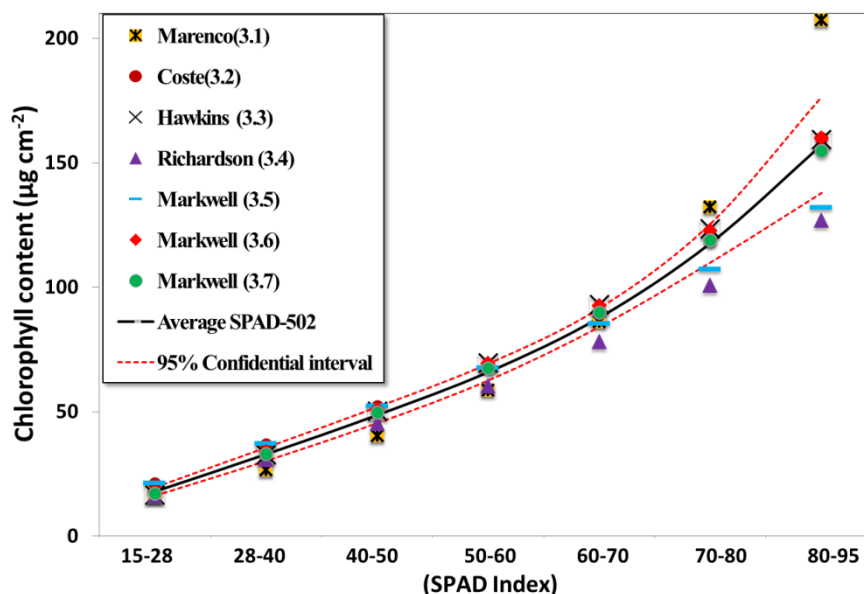


Figure 3.13. Estimated chlorophyll content for each SPAD-502 calibration model applied to the total samples of our dataset. The black line represents the average value across models and its confidential interval of 95% for the binned SPAD-502 readings.

3.3.2 Chlorophyll content based on reflectance indices

Reflectance indices and their respective models were applied to the reflectance spectra to the samples collected for this study. The resulting descriptive statistics are shown in Table 3.7.

Figure 3.14 illustrates the chlorophyll content estimations for each reflectance model, its average values across models and the confidence interval of 95% for the binned SPAD-502 readings. It is interesting to observe that chlorophyll estimations become insensitive for SPAD reading greater than 80.

Table 3.7 Descriptive statistics of chlorophyll concentration ($\mu\text{g cm}^{-2}$) from the reflectance models based on the spectroradiometer Data.

| Model | Reference | Max | Min | Mean | SD |
|-------|------------------------------------|--------|-------|-------|-------|
| 4.1 | (Féret et al. 2011) | 126.82 | 1.06 | 57.92 | 17.48 |
| 4.2 | (Féret et al. 2011) | 78.63 | 5.05 | 53.17 | 11.26 |
| 4.3 | (Féret et al. 2011) | 85.80 | 6.22 | 54.37 | 12.29 |
| 4.4 | (Gitelson et al. 2005) | 101.66 | 5.86 | 50.05 | 14.59 |
| 4.5 | (Ciganda;Gitelson & Schepers 2009) | 136.69 | 12.51 | 65.77 | 18.91 |

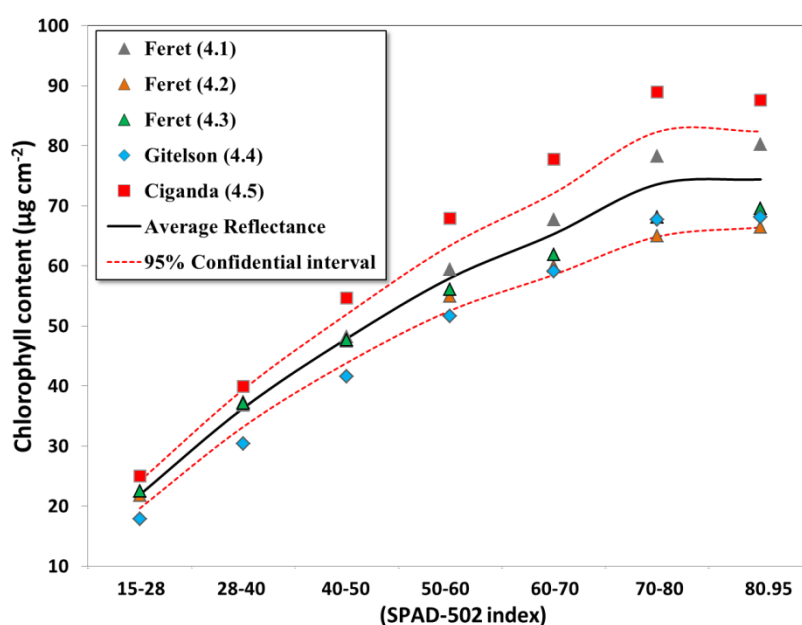


Figure 3.14 Average chlorophyll content estimates from five reflectance models (errors bars at 1.96 standard deviations) compared to estimated ground truth chlorophyll content based on SPAD-502 chlorophyll meter readings (error bars at 1.96 standard deviations)

3.3.3 Comparison between the three methods for chlorophyll estimation

Figure 3.15 shows the comparison between average chlorophyll estimations from the three methods used in this study. Estimations until bin 50-60 are relatively similar. Estimation from SPAD then increased exponentially while estimations

from reflectance and PROSPECT model are close to each other until bin 70-80, differences then increased since the asymptotic behaviour of reflectance models estimations.

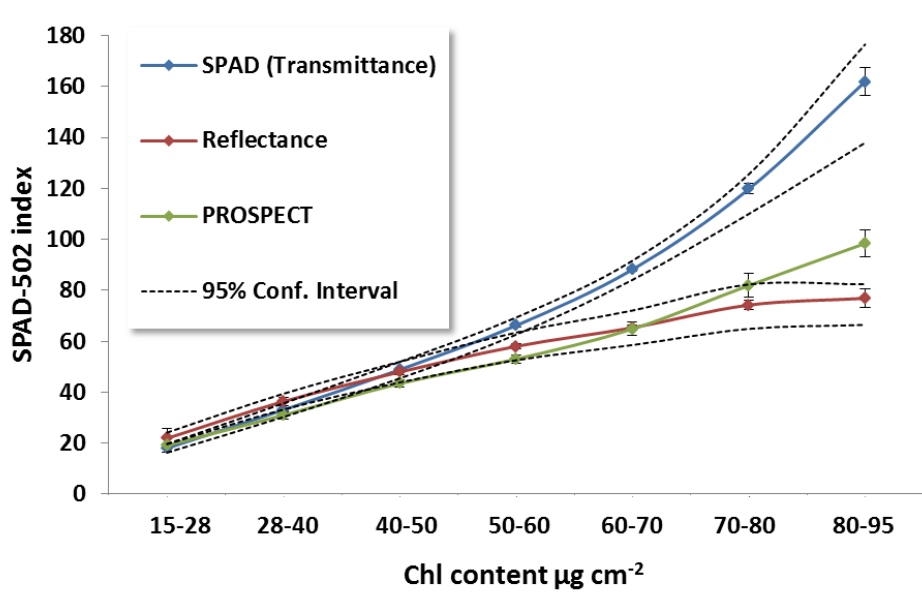


Figure 3.15 Comparison of average chlorophyll content estimates from the SPAD-502 chlorophyll meter index and the averages of all spectroradiometer-based chlorophyll estimates (error bars at 1.96 standard deviations).

Table 3.8 shows the descriptive statistics and Figure 3.16 illustrates the correspondent boxplots for the three approaches used in this study.

Table 3.8 Descriptive statistics of average chlorophyll content estimates (µg Cm⁻²) from all SPAD-502 models and spectroradiometer reflectance models

| | SPAD-502 indices average | Reflectance indices average | PROSPECT model |
|---------|--------------------------|-----------------------------|----------------|
| Maximum | 196.30 | 105.21 | 175.28 |
| Minimum | 11.26 | 6.14 | 3.14 |
| Mean | 69.64 | 56.26 | 54.27 |
| SD | 28.89 | 14.34 | 22.40 |

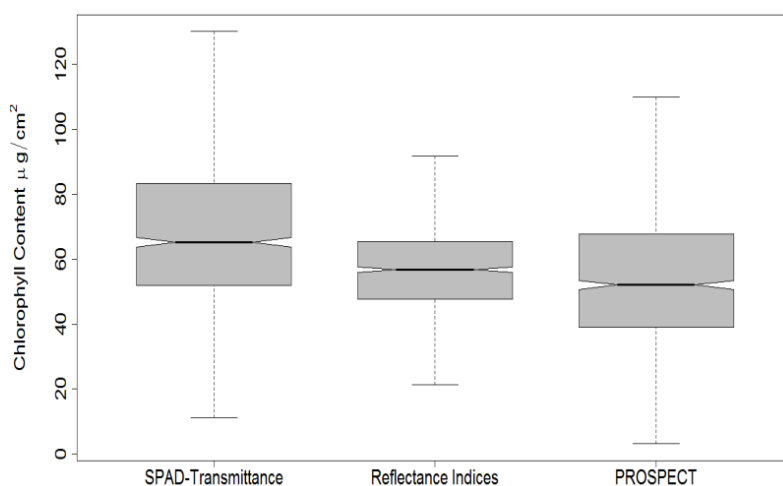


Figure 3.16 Boxplots of the three estimation of chlorophyll content (outliers not included)

Figure 3.17 shows the correlations between the three chlorophyll estimations (SPAD-502, reflectance and PROSPECT) applied in this study. Additionally, correlations with MTCI and REP are presented.

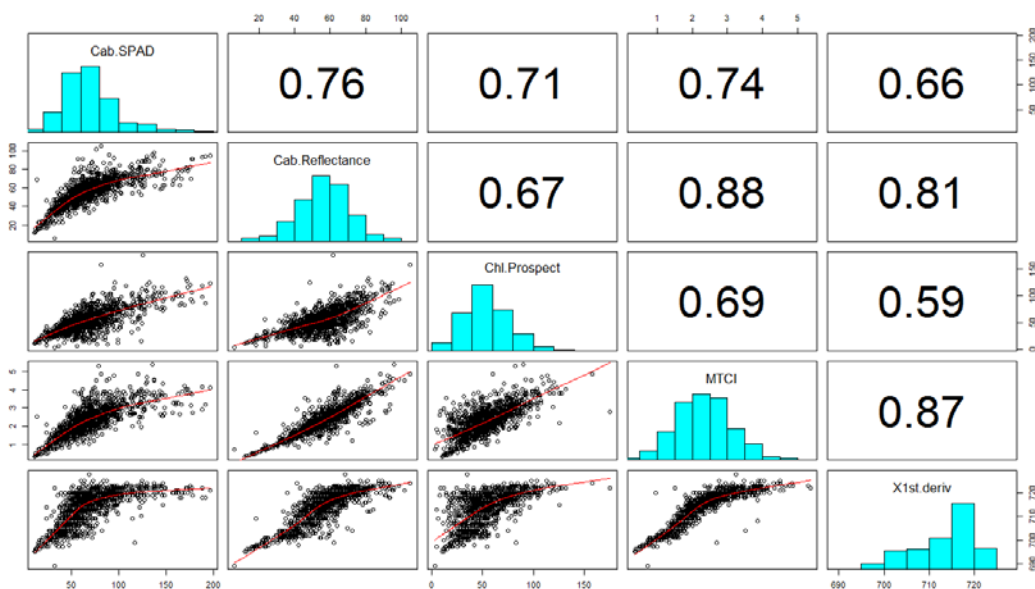


Figure 3.17 Scatter plots, histograms and Pearson correlation between three chlorophyll estimations (SPAD, Reflectance and PROSPECT) and MTCI index and REP

3.4 Discussion

Three methods for the estimation of chlorophyll content were applied to the collection of over 1,100 leaf samples from the Ecuadorian Amazon rainforest, which represents a wide range of vegetation species growing in a disturbed and a pristine lowland rainforest. The first method is an optical method based on transmittance from the SPAD-502 chlorophyll meter index, the second method, also optical, and is based on reflectance measurements collected by a spectroradiometer and the third method is based on radiative transfer approach using the inversion process of PROSPECT model.

For the first method, seven models that account for a wide range of vegetation species, phenological stage and leaf structure showed close estimations between them until 80 SPAD-502 index (Table 3.6 and Figure 3.13). At higher indices the differences increase. This can be explained by the fact that the calibration models considered a maximum SPAD-502 range of 80 units, meanwhile our database register readings beyond this range until 95 units. As discussed above (Section 3.1.1 in page 54), the best accuracy claimed by the instrument reaches its maxima until 50 units; therefore higher values may be less accurate.

Based on the results of the seven SPAD-502 published calibration models we compute their average in order to obtain a general model for chlorophyll content estimation which accomplish for a wide range of vegetation species and physiological stage. The resulting general model is a second order polynomial in a range of 15 to 95 SPAD index readings. This general model is proposed as ground truth chlorophyll which is assessed by comparing it to a reference published generalized model based on SPAD-502 readings and traditional methods in a laboratory. The first reference model is a homographic model proposed by Cerovic et al. (2012) and computed from seven (polynomial, exponential and homographic) models applied to a variety of plant species. The second model is the generalised homographic model for tropical trees proposed by

Coste et al. (2010) which was discussed before as Model 3.2. Figure 3.18 illustrates the comparison of the three models.

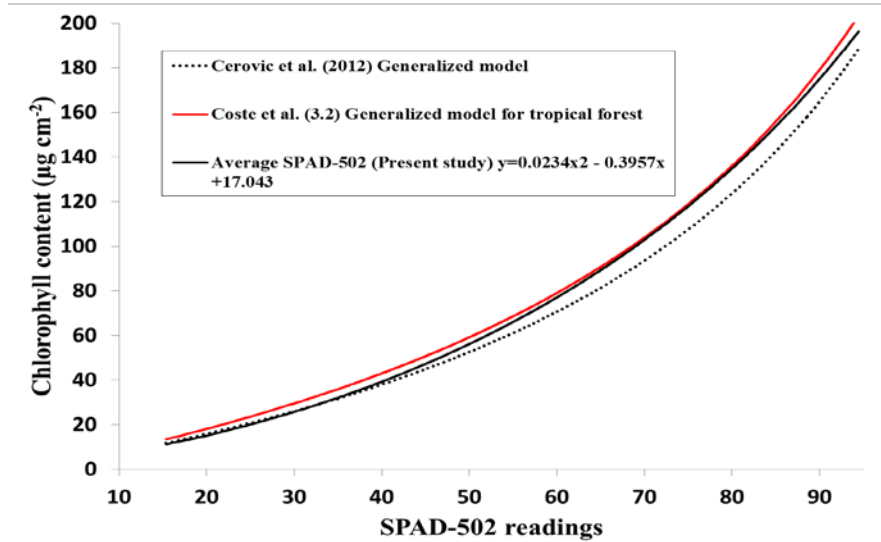


Figure 3.18 Comparison of three generalized models derived from SPAD-502 readings. The second order polynomial model proposed in this study (black line), the homographic model proposed by Cerovic et al. (2012) (dotted line) and the homographic model proposed by Coste et al. (2012) for a trees from the Amazon forest.

The proposed second order polynomial model has the same concave shape and very close chlorophyll estimations along the range 15-95 SPAD-502 readings than the two homographic models. Homographic models have the generalised equation proposed by Cerovic et al.(2012) and claims to be probably more accurate and certainly more rapid and portable than wet methods when used in crop plants. The model proposed by Coste et al. (2010) was developed for the tropical forest from the Amazon region and has been a reference model for estimating chlorophyll content based on SPAD-502 readings.

Indeed, published SPAD-502 models applied to tropical rainforest vegetation are rare. A literature search by the author only found two models (Model 3.1 and Model 3.2) developed for several species of the Amazon forest. Both experiments with tropical trees of the Amazon exhibited higher SPAD-502 readings which are comparable with our dataset. Those models account for a wide range of species, leaf structure and phenology and claim good accuracy for chlorophyll content

estimation in multi species forest stands. The homographic model proposed by Coste et al. (2010) (Model 3.2) has been used to estimate chlorophyll content in a study that considered 1,084 trees from 758 species across a broad environment gradient of 13 sites (seasonal flooded, clay terra firme and white-sand forest) at opposite ends of Amazonia in Guiana and Peru (Fortunel;Fine & Baraloto 2012). The study relies on chlorophyll estimations based on the SPAD-502 model without considering traditional methods in a laboratory which prove the ability of a rapid and portable method of chlorophyll content in remote areas where analysis in a laboratory is not available.

Based on the comparison to published homographic models for multi-species, it is derived that the second order polynomial calibration model offers a good approximation of chlorophyll content in tropical forest species. This is because of its close performance compared to the models proposed by Cerovic et al. (2012) and Coste et al. (2010) (Figure 3.18), and its homographic nature takes into consideration the reduced performance of chlorophyll meters at high chlorophyll contents. Indeed a homographic nature of SPAD-502 model has been applied to a wide range of tropical species from the Amazonia (Fortunel;Fine & Baraloto 2012).

Estimations from the second method based on five reflectance models illustrate good agreements along all range of SPAD-bins (15-95 units). Table 3.7 and Figure 3.14 illustrate the results of these methods showing a saturation curve at the higher SPAD bind (80-95).

The observed maximum values of chlorophyll estimation from SPAD-502 (Table 3.6) are considerably higher than maximum values from reflectance indices (Table 3.7) which reflect the exponential increase of SPAD-502 models after 80 SPAD-502 units and the asymptotic nature of reflectance indices after this range. Differences between average estimations are less distinctive.

The first two methods are compared versus the third method which is based on the inversion process of the PROSPECT model. Figure 3.15 illustrates that the mean values are close to each other until 50-60, and after that the estimations based on SPAD-502 models increase faster than the other two methods. The method based on reflectance models and the PROSPECT model show close mean values until bin 70-80. Analysis of variance ANOVA and pairwise comparison between the three methods showed in Table 3.9 indicates significant difference between methods. Results from the lower SPAD-502 bin reported no differences between methods.

Table 3.9 ANOVA and pairwise comparison between the three chlorophyll methods for chlorophyll estimation based on the binned SPAD-502 index

| | ANOVA | Pairwise comparisons between chlorophyll estimation methods (Holm adjustment) | | |
|-------------|---------|---|------------------|-------------------------|
| | p-value | SPAD vs Reflectance | SPAD vs PROSPECT | Reflectance vs PROSPECT |
| All dataset | *** | *** | *** | * |
| < 28 | ns | ns | ns | ns |
| 28-40 | *** | ** | . | *** |
| 40-50 | *** | ns | *** | *** |
| 50-60 | *** | *** | *** | *** |
| 60-70 | *** | *** | *** | ns |
| 70-80 | *** | *** | *** | ** |
| 80 > | *** | *** | *** | *** |

*** Strongly significant (0.1%) . Lowest significant (10%)
 ** Highly significant (1%) ns Non-significant
 * Significant(5%)

Pearson correlation demonstrates a strong correspondence between the three methods. Chlorophyll content estimates by the second order polynomial based on SPAD-502 models and reflectance models agree in 0.76 while SPAD-502 models and PROSPECT agreed in 0.71. The lowest correlation ($r=0.67$) is presented by estimations from reflectance models and PROSPECT model despite the fact that both methods are estimated from reflectance measurements.

In addition, correlations between MTCI and REP (first derivative) are presented. A strong correlation between them was found. MTCI and SPAD-502 correlate in 0.74, MTCI and reflectance models correlate in 0.88 and MTCI and PROSPECT correlate in 0.69. Correlation coefficients between REP and SPAD-502 model, reflectance models, PROSPECT and MTCI are 0.66, 0.81, 0.59 and 0.87 respectively.

3.5 Conclusion

Generalised calibration equations for estimation of chlorophyll and other plant pigments based on spectra readings (reflectance and transmittance) accounting for a wide range of vegetation species, leaf spectra, chemical and structural properties have been proposed in the past (Coste et al. 2010, Marengo;Antezana-Vera & Nascimento 2009, Féret et al. 2011, Cerovic et al. 2012). They offer a viable and accurate alternative to measure plant pigments in heterogeneous forests.

Three optical methods for estimation of chlorophyll content were applied to the collection of over 1,100 leaf samples collected in the Ecuadorian Amazon rainforest, which represents a wide range of vegetation species growing in a disturbed and a pristine lowland rainforest. The first method is based on transmittance from the SPAD-502 chlorophyll meter index, the second method is based on reflectance measurements collected by a spectroradiometer and the third method estimates chlorophyll content from the radiative transfer PROSPECT model. For the first method, seven models that account for a wide range of vegetation species showed similar average leaf chlorophyll contents until 80 units of SPAD-502. An average of the results of these models was computed and used as ground truth from where a generalised second order polynomial model was created. For the second method, five chlorophyll indices based on reflectance measurements provided similar chlorophyll content estimations for all SPAD range (15-95 units). The third method estimates chlorophyll content based on the inversion process of the PROSPECT model.

Comparison between the three methods shows that estimations until bin 50-60 are relatively similar, and estimations from SPAD increased exponentially. Estimations from reflectance and the PROSPECT model are close to each other until bin 70-80, after that differences increased since the asymptotic behaviour of reflectance models estimations. A strong coefficient of correlations between the proposed generalised model and reflectance and PROSPECT approaches result in 0.76 and 0.71 respectively. Comparison with MTCI and REP indicate correlations of 0.74 and 0.66 respectively.

Chlorophyll content estimates in the tropical rainforest are rare. A published generalised homographic model for trees of the Amazon region (Coste et al. 2010) has been used as standard model to estimate chlorophyll content for more than 700 Amazonian tree species. A comparison of chlorophyll estimation between the homographic model and the second order polynomial model proposed in this study illustrates good agreement for a wide range of SPAD-502 reading (15-95 units).

The accuracy of the SPAD-502 decreases at high chlorophyll index readings. When applying the proposed second order polynomial model, caution should be taken for readings higher than 80 where estimation increases markedly compared to other optical methods (reflectance indices and PROSPECT) assessed in this study.

The results of this study show that the relatively light-weight handheld field spectroradiometer can be used to estimate leaf chlorophyll content in remote tropical rainforest ecosystems that are difficult to access. They provide a rapid and portable method for such remote areas where traditional chemical extraction methods for chlorophyll estimation are not viable. A general second order polynomial calibration model for chlorophyll content estimation which accounts for a wide range of plant species, phenological stage and leaf structure based on spectral measures offers an alternative approach for chlorophyll estimation.

Chapter 4. Evidence of Vegetation Stress Caused by Hydrocarbons

This chapter investigates the effects of hydrocarbon pollution on the biophysical and biochemical parameters of tropical forest. Those effects are assessed in the vertical profile of the tropical forest.

4.1 Introduction

The high diversity and intrinsic complex biological interactions of the tropical forest are challenging when we try to understand the effects of petroleum-hydrocarbons in vegetation health. The vertical structure of the forest plays a particular role in the interaction of light which is the primary source of energy for the most important biochemical process on the earth, photosynthesis. In this environment, plant species have developed their own mechanisms for adaptation through adjustments in leaf thickness, leaf structure, photosynthetic plant pigments content, foliar water content, organic matter content, leaf size and angle distribution. Those parameters are critical variables in plant ecology and vegetation health assessment (Féret et al. 2011).

4.1.1 Foliar biophysical and biochemical parameters

This section describes some of the more widely used leaf parameters used to evaluate vegetation health in forest.

Plant pigments

Chlorophylls are the most important plant pigment since they are essential during the photosynthesis process and are responsible for the absorption of violet-blue and red light: green light is not absorbed for photosynthesis. Light is the key factor to power the photosynthetic process. When irradiance is below a certain level ($10-40 \mu\text{mol photon m}^{-2} \text{ s}^{-1}$), CO_2 uptake is balanced by CO_2 loss during respiration therefore net assimilation is zero. Increasing irradiance also increases photosynthesis rates until light saturation -when increasing light no longer

increases photosynthesis (Bonan 2008). When the amount of light reaches high irradiance levels, photoinhibition of photosynthesis reduces the photosynthetic capacity by lowering the electron transport activity and alters chlorophyll characteristics (Kamaluddin&Grace 1992). Photoinhibition occurs also when plants adapted to shade are exposed to high irradiance levels

Foliar Nitrogen is another important factor in plant growth physiology. It has been used to evaluate vegetation health due to its close relation to photosynthetic activity and leaf chlorophyll content (Percival;Keary & Noviss 2008). Broadleaf trees species have shown a strong relationship between maximum photosynthetic capacity and leaf nitrogen content (Reich et al. 1995). The majority of foliar N is contained in chlorophyll molecules, indeed there is a close relationship between chlorophyll content and foliar N content. Greater amounts of nitrogen allow for more chlorophyll and rubisco, fuelling greater rates of photosynthesis (Torres-Netto et al. 2005, Marengo;Antezana-Vera & Nascimento 2009, Bonan 2008, Percival;Keary & Noviss 2008, White&Montes-R 2005). Expressed in area basis, foliar N decreases as canopy height decreases in the Amazon rainforest (Carswell et al. 2000a).

Vegetation optical properties are influenced by plant pigment concentrations, water content and leaf structure (Terashima&Saeki 1983). Besides photosynthetic pigments, leaf water content and dry matter content are critical variables in plant ecology, especially in forest fire risk assessment, water stress, net ecosystem exchange and carbon storage estimations (Féret et al. 2011).

Foliar water content (Cw)

The water content of leaves is regulated by the water loss during transpiration and water uptake from soil. During photosynthesis the stomata of the leaves are open to allow CO₂ uptake, but at the same time water vapour is lost from the leaf during transpiration. Stomata tend to close when the leaf water potential drops below a certain point (Bonan 2008): water content of the leaf affects stomata opening and hence respiration. Water content is closely correlated to leaf

thickness, intercellular space and infrared reflectance and transmittance (Castro-Esau et al. 2006).

Dry matter content (Cm)

Dry matter content is associated with leaf density and leaf thickness and can also be estimated by the product of leaf density and thickness. It includes two compounds: the first one is a non-nitrogenous compound (cell walls, membranes and storage carbohydrates and lipids) and the second are nitrogenous compounds (proteins and chlorophyll). Dry matter content is closely correlated to photosynthetic rates and atmospheric CO₂ (White&Montes-R 2005).

Dry matter content is considered to reflect relative carbon accumulation and it is sensitive to variations in nutrients and/or moisture availability, light intensity, temperature, atmospheric CO₂ and SO₂ concentrations; leaf pubescence, season and leaf age. In the vertical profile of the forest, dry matter content decreases through the canopy in response to the decline in light intensity (Witkowski&Lamont 1991).

Specific leaf area (SLA)

SLA represents the amount of carbon (dry mass) investment in photosynthesising unit area. Species with high specific leaf area have thin leaves with a large surface area per unit mass. *SLA* is positively correlated to maximum net photosynthesis. (Bonan 2008). It has a close association to potential growth rate and decrease in the upper levels of the canopy high (Carswell et al. 2000b). SLA values in our three study sites show the same tendency. Reich et al, (1995) demonstrate that SLA is positively correlated to leaf nitrogen expressed in mass basis in deciduous hardwood vegetation moreover, Carswell et al. (2000b) showed no correlation expressed in mass basis but a strong negative correlation when N is expressed in area basis in an undisturbed Amazon rainforest.

Leaf thickness or leaf succulent (Lt)

Leaf thickness is associated with leaf carbon assimilation rate, leaf size, canopy structure and light interception (Vile et al. 2005), and consequently it has an important effect in reflectance and transmittance (White&Montes-R 2005). Leaves represent a huge variation of leaf morphology, and thickness is not uniform along a single leaf. An estimation of leaf thickness equates with Specific Leaf Mass (Ws), but this approximation ignores differences in true thickness due to the variation in water, air and organic content. Vile et al. (2005) found that leaf thickness in laminar leaves can be adequately estimated by $SLA * \text{Leaf dry matter content}^{-1}$ (LDMC), alternatively, Lt could also be assessed by the ratio Fresh weight (Fw) to surface area (Marenco;Antezana-Vera & Nascimento 2009). Chlorophyll and nitrogen concentrations may show higher values in thicker leaves due the increased tissue per unit area (White&Montes-R 2005).

4.1.2 Vertical profile of tropical forest

The high diversity of the tropical forest and its complex structure plays a particular role in the interaction with light which is the principal source of energy in the forest. The light is reflected, absorbed and transmitted at different levels in the vertical profile. The upper layer receives 25-100% of the relative irradiance, lower down the irradiance decreases until it reaches 1-3% in the lower layers of the forest (Longman 1987, Chazdon&Fetcher 1984). Canopy height and vegetation density cause steep vertical gradients of the microclimate specially related to temperature and humidity and a consequently differentiation in CO_2 concentrations (Roberts;Cabral & Ferreira De Aguiar 1990, Grace 1999).

Stomatal conductance declines steadily down through the canopy in tropical rainforest environments (Roberts;Cabral & Ferreira De Aguiar 1990). Dolman et al, (1991) demonstrated that mean stomatal conductance in the top layers of the rainforest in the Amazon canopy reach a maximum of around $300 \text{ mmol m}^{-2} \text{ s}^{-1}$ while in the lower levels of the canopy the values drop to $100 \text{ mmol m}^{-2} \text{ s}^{-1}$. Photosynthetic rates of tropical rainforest C_3 trees are low compared to C_4 plant

species but also compared to herbaceous C₃ species (Bonan 2008, Grace 1999). Net photosynthesis in trees of the Amazon forest varies with species, but also with phenological status and growing conditions. Sunlit leaves show higher net photosynthesis rates than shaded leaves (Bonan 2008).

Relationships between net photosynthetic rates and foliar nitrogen are variable among species, but the tropical trees species as a whole showed a strong, positive relationship. Five sites of the upper Rio Negro region of the Amazon basin reported the steepest slopes growing in high resources disturbed and secondary sites. The slope of the relationship tends to decrease in trees growing in undisturbed sites showing lower net photosynthesis for the same leaf nitrogen content (Reich et al. 1994).

Sunlit leaves in the Amazon forest have an N content of 100-200 mmol m² and a phosphorus content of 1-2 mmol m², this falls by half in the lower canopy (Lloyd; Grace & Miranda 1995).

4.2 Materials and Methods

4.2.1 Study area and sites

A detailed description of the study area is presented in Chapter 3, section 3.2.1.

4.2.2 Soil samples

Soil samples were taken from all sites and analysed in certified laboratories. Parameters related to physical properties, petroleum hydrocarbons, metals and soil nutrients were considered. Table 4.1 shows the results of the soil samples in the three study sites together with the standard methods used for analysis and accreditations of the laboratory. Site 1 shows a high value of TPHs which confirms the area is an active source of hydrocarbons. pH values are low for all cases, which confirm the acidic characteristics of the soils in the Amazon region. Acidic soils cause the mobilisation of minerals which is reflected in the values of aluminium, zinc and magnesium of Sites 1 and 2.

Table 4.1 Results of laboratory analysis of soils for the three study sites

| | Parameters | Standard method | Units | Site 1 Pollution | Site 2 No pollutes areas | | | Site 3 Pristine Forest - Yasuni National Park | | | |
|--|---------------------------------------|--------------------|-------|---------------------|--------------------------|--------|--------|--|--------|--------|--------|
| | | | | | | | | | | | |
| Hydrocarbons | Hydrocarbons Aromatic Polycyclic-HAPs | CP-PEE-S001 | mg/kg | <0.5 | <0.5 | <0.5 | <0.5 | <0.5 | <0.5 | <0.5 | <0.5 |
| | Total Petroleum Hydrocarbons - TPH | CP-PEE-S003 | mg/kg | 8876.6 | <200 | <200 | <200 | <200 | <200 | <200 | <200 |
| Metals | Iron | EPA 3051/7000A | mg/kg | 18,905 | 17,635 | 12,598 | 15,460 | 15,108 | 14,569 | 13,692 | 18,916 |
| | Aluminium | EPA 3051/ APHA 350 | mg/kg | 36 | 36 | 36 | 36 | <10 | <10 | <10 | <10 |
| | Zinc | EPA 3051/7000A | mg/kg | 28.7 | 47 | 50 | 31.5 | 38.1 | 80.9 | 34.2 | >100 |
| | Magnesium | EPA 3051/7000A | mg/kg | 372.5 | >500 | >500 | 445 | 386.7 | 383.3 | 380.3 | 389.2 |
| | Manganese | EPA 3051/7000A | mg/kg | 116.3 | >500 | >500 | 90.5 | 836.7 | 836.1 | 156.6 | 232.5 |
| | Barium | EPA 3051/ Hach 801 | mg/kg | <50 | 83.2 | 87.6 | 113 | <50 | <50 | 53.5 | 88.8 |
| Physical properties | Electrical conductivity | SM 2010 B | uS/cm | 32 | 56.6 | 62.6 | 85.6 | 38.4 | 34.4 | 32 | 28.9 |
| | pH | CP-PEE-S004 | | 4.6 | 5.5 | 5.5 | <4.0 | 5.3 | 4.8 | 4.6 | 4.2 |
| Nutrients | Organic matter | Gravimetric | % | 43.3 | 62.1 | 52.6 | 41.9 | 60.3 | 64.6 | 60.4 | 64 |
| | Total N | SM 4500-N C | mg/kg | 22 | 50 | 110 | 46 | 27 | 36 | 78 | 44 |
| | Total P | SM 4500 P B-C | mg/kg | >450 | 400 | >450 | >450 | >500 | >500 | >500 | 150 |
| | Potassium (K) | EPA 3051/7000A | mg/kg | 280 | >500 | >500 | 420 | 189 | 188.1 | 201.2 | 201.5 |
| The laboratory has the follow accreditations: National Accreditation Office from Spain (ENAC No. 415/LE 929). Ecuadorian Accreditation Office (OAE No. LE2 C 04-001 and OAE LE C 10-011) | | | | | | | | | | | |

4.2.3 Foliar sampling

The sampling process considered three height levels of the forest: upper canopy, medium canopy and understory. Details of the vegetation sampling is presented in Chapter 3, from section 3.2.1, page 59. Table 4.2 shows the number of samples available for foliar biophysical and biochemical analysis in each study site.

Table 4.2 Number of samples according to the three samples sites and vertical profile of the forest

| | Site1 Forest affected by oil spill | Sites 2 Forest not affected by hydrocarbons | Site 3 Pristine forest (Yasuni park) | Total |
|---------------|---|--|---|--------------|
| Upper canopy | 154 | 62 | 197 | 413 |
| Medium canopy | 128 | 45 | 192 | 365 |
| Understory | 106 | 17 | 156 | 279 |
| TOTAL | 388 | 124 | 545 | 1057 |

The number of samples was defined by the permission granted to access each of the sampled sites. Site 1 and Site 3 reflect a greater number of samples which is explained by the permissions granted by the petroleum company operated in the area and Yasuni Research Station, respectively. Meanwhile Site 2 shows a reduced number of samples due to the limited permissions granted by the farmers owning the land.

4.2.4 Foliar biophysical and biochemical measurements

Vegetation health was assessed through key biochemical and biophysical leaf traits widely applied to investigate vegetation stress and vegetation physiology.

Chlorophyll content in $\mu\text{g cm}^{-2}$ was obtained by applying the generalised chlorophyll model based on SPAD-502 chlorophyll meter index for a tropical forest which is explained in Chapter 3. According to the conclusions in Chapter 3, chlorophyll content estimations are less accurate for the higher SPAD-502

reading, therefore a decision was taken to remove the outliers. The histogram of the SPAD-502 reading shown in Figure 4.1 illustrates a normal distribution with values outside 95% confidential interval considered outliers illustrated in the box plot.

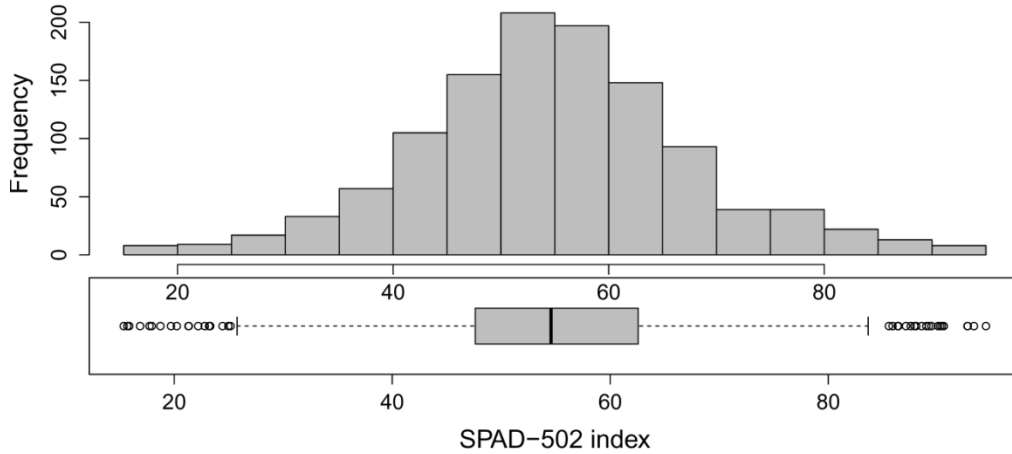


Figure 4.1 Histogram of the SPAD-502 chlorophyll meter readings and boxplot showing the outliers. Total samples collected in the study sites.

Using the same leaf disks of known *surface* (S) (described in Section 3.2.3, page 68), *Fresh weight* (Fw) was measured with a precision weighing balance, and then the samples were dried at approximately 60 °C for a period of at least 48 hours. They were then reweighted to get the *dry weight* (Dw).

Water content in g cm^{-2} (Cw) (Gerber et al. 2011) or Equivalent water thickness (Féret et al. 2011, Datt 1999, Hunt Jr&Rock 1989a) was estimated by the following equations:

$$Cw = \frac{Fw - Dw}{S} \quad (4.1)$$

$$Ewt = \frac{Fw - Dw}{dw * S} \quad (4.2)$$

where dw is the density of water = 1 g ml⁻¹

Dry matter content (Cm) in g cm⁻² (Féret et al. 2011, Datt 1999, Gerber et al. 2011) also known as Specific leaf mass (Ws) (Marenco;Antezana-Vera & Nascimento 2009) or Leaf specific mass (LSM) (White&Montes-R 2005) or Leaf mass per area (Wright et al. 2004) was computed by:

$$Cm = \frac{Dw}{S} \quad (4.3)$$

Specific leaf area (SLA) in cm² g⁻¹ (Sánchez-Azofeifa et al. 2009, Marenco;Antezana-Vera & Nascimento 2009, White&Montes-R 2005, Vile et al. 2005) was estimated by:

$$SLA = \frac{1}{Cm} \quad (4.4)$$

Leaf water content (LWC) (Marenco;Antezana-Vera & Nascimento 2009) in percentage was computed as follow:

$$LWC = \frac{(Fw-Dw)}{Fw} \quad (4.5)$$

Leaf dry matter content ($LDMC$) (Vile et al. 2005) expressed in percentage was estimated by:

$$LDMC = \frac{Dw}{Fw} \quad (4.6)$$

Leaf thickness (Lt) (Vile et al. 2005) and Leaf succulent (Ls) (Marenco;Antezana-Vera & Nascimento 2009) expressed in g cm⁻² was computed as follow:

$$Lt = \frac{1}{SLA*LDMC} \quad (4.7)$$

$$LS = \frac{Fw}{S} \quad (4.8)$$

4.3 Results

The results of the analysis of foliar biophysical and biochemical parameters are differentiated per each site and vertical profile of the forest.

4.3.1 Results per site

Results of foliar parameters for each study site are represented by the descriptive statistics in Table 4.3. Histograms and boxplots of the foliar parameters are detailed in Annex 7. Mean values of chlorophyll content indicate a clear reduction of the photosynthetic pigment in the site affected by the oil spill. For the other parameters, the mean value from descriptive statistics does not explain important differences.

Table 4.3 Descriptive statistics of foliar parameters for the three study Sites

| | Chl ($\mu\text{g cm}^{-2}$) | Cw (g cm^{-2}) | Cm (g cm^{-2}) | SLA ($\text{cm}^2 \text{g}^{-1}$) | Lt (g cm^{-2}) | LWC (%) | LDMC (%) |
|---------------------------------|----------------------------------|------------------------------|------------------------------|--|------------------------------|------------|-------------|
| Site 1 - Oil Spill | | | | | | | |
| Mean | 60.15 | 0.012 | 0.007 | 188.6 | 0.019 | 63.4 | 36.6 |
| Maximum value | 126.34 | 0.057 | 0.022 | 1,256.6 | 0.062 | 94.4 | 85.7 |
| Minimum value | 17.96 | 0.001 | 0.001 | 44.7 | 0.006 | 14.3 | 5.6 |
| SD | 21.01 | 0.006 | 0.003 | 127.3 | 0.009 | 11.2 | 11.2 |
| Site 2 - No polluted | | | | | | | |
| Mean | 73.99 | 0.011 | 0.008 | 164.1 | 0.019 | 59.2 | 40.8 |
| Maximum value | 132.18 | 0.027 | 0.026 | 804.2 | 0.053 | 87.5 | 80.0 |
| Minimum value | 32.88 | 0.002 | 0.001 | 38.3 | 0.006 | 20.0 | 12.5 |
| SD | 24.04 | 0.004 | 0.004 | 104.7 | 0.006 | 12.4 | 12.4 |
| Site 3 - Pristine forest | | | | | | | |
| Mean | 71.33 | 0.011 | 0.007 | 172.7 | 0.017 | 61.2 | 38.8 |
| Maximum value | 127.35 | 0.025 | 0.016 | 1,396.3 | 0.035 | 94.4 | 66.7 |
| Minimum value | 32.88 | 0.003 | 0.001 | 61.9 | 0.004 | 33.3 | 5.6 |
| SD | 20.46 | 0.003 | 0.002 | 90.8 | 0.005 | 9.9 | 9.9 |

Analysis of ANOVA I showed in Table 4.4 illustrates that the differences between means for all sites are statistically significant for *SLA* (95%), highly significant for *Cm* (99%) and strongly significant for *C_{ab}*, *C_w*, *Lt*, *LWC* and *LDMC* (99.9%).

Table 4.4 ANOVA I test for the seven leaf traits

| | <i>C_{ab}</i> | <i>C_w</i> | <i>C_m</i> | <i>SLA</i> | <i>Lt</i> | <i>LWC</i> | <i>LDMC</i> |
|--------------|-----------------------|----------------------|----------------------|------------|-----------|------------|-------------|
| ANOVA | 2.0E-16 | 4.2E-07 | 1.7E-03 | 2.8E-02 | 2.2E-05 | 1.5E-05 | 1.5E-04 |
| | *** | *** | ** | * | *** | *** | *** |

*** Strongly significant (99.9%) ** Highly significant (99%) * Significant (95%) No significant difference

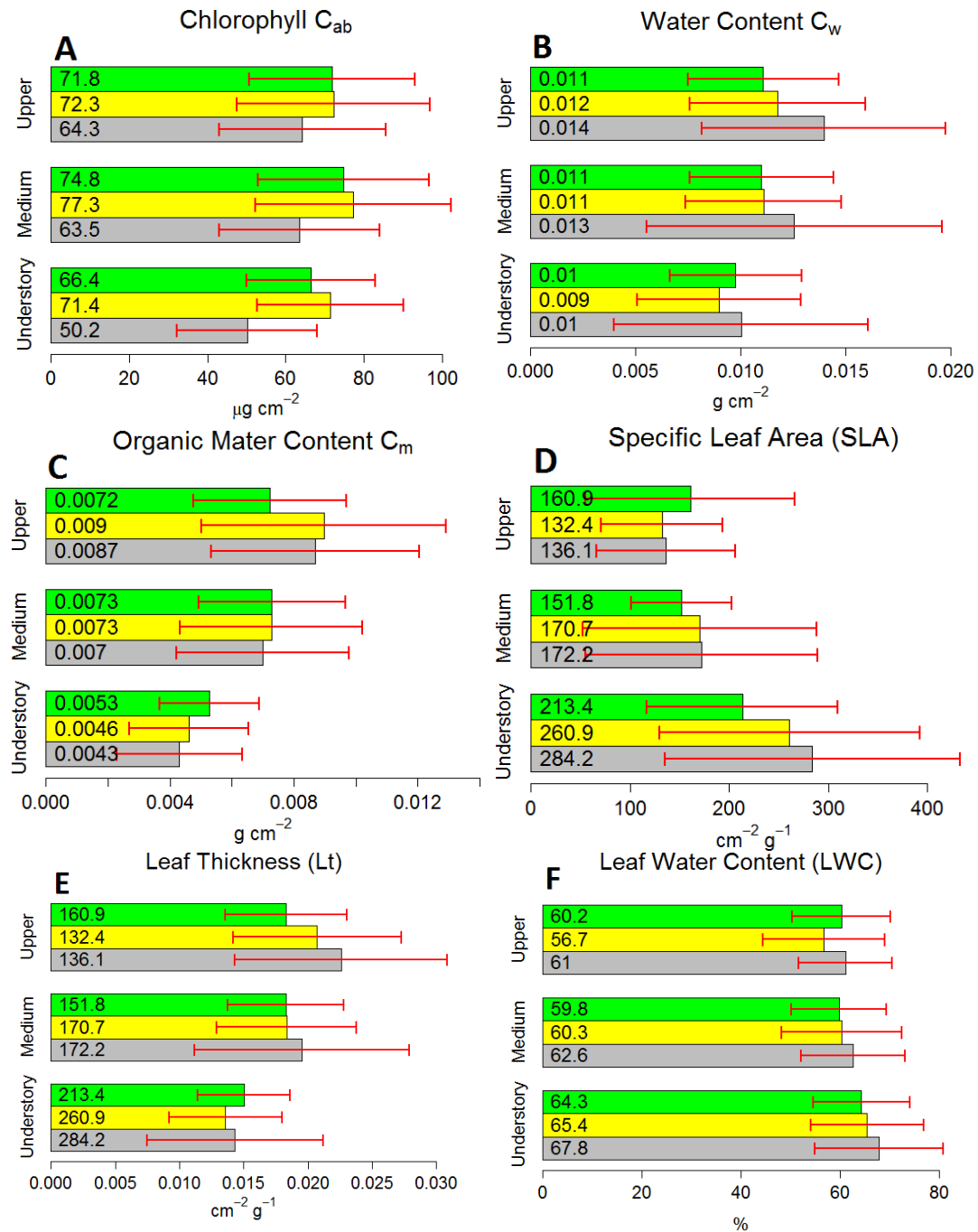
In order to explain the differences between sites, we conducted a pairwise comparison of *p-values* by applying the adjustment method of Holm (see Table 4.5). Strongly significantly differences (99.9%) between the oil spill site and the two other sites were found for most of leaf parameters (*C_{ab}*, *C_w*, *Lt*, *LWC* and *LDMC*). The non-polluted site and the pristine forest only differ in *C_m* (highly significant) and *Lt* (significant). For the remaining traits there are no differences between those two forest sites. *SLA* is the only trait which has shown no significant differences for all sites and layers of the vertical profile.

Table 4.5 Pairwise comparison of *p-values* with holm adjustment method

| | <i>C_{ab}</i> | <i>C_w</i> | <i>C_m</i> | <i>SLA</i> | <i>Lt</i> | <i>LWC</i> | <i>LDMC</i> |
|--------------------------------------|-----------------------|----------------------|----------------------|------------|-----------|------------|-------------|
| Oil spill-No Polluted | 6.2E-10 | 2.1E-02 | 1.5E-02 | 7.8E-02 | 5.0E-01 | 4.4E-04 | 4.4E-04 |
| Oil spill-Pristine forest | 1.2E-14 | 2.2E-07 | 2.3E-01 | 7.8E-02 | 2.0E-05 | 4.2E-03 | 4.2E-03 |
| No polluted - Pristine forest | 2.1E-01 | 3.5E-01 | 1.1E-03 | 4.2E-01 | 4.3E-02 | 5.8E-02 | 5.8E-02 |
| Significant codes | | | | | | | |
| Oil spill-No Polluted | *** | * | * | | | *** | *** |
| Oil spill-Pristine forest | *** | *** | | | *** | ** | ** |
| No polluted - Pristine forest | | | ** | | * | | |

4.3.2 Results per site and vertical profile of the forest

Figure 4.2 illustrates a comparison of foliar parameters in the vertical profile for the three study sites.



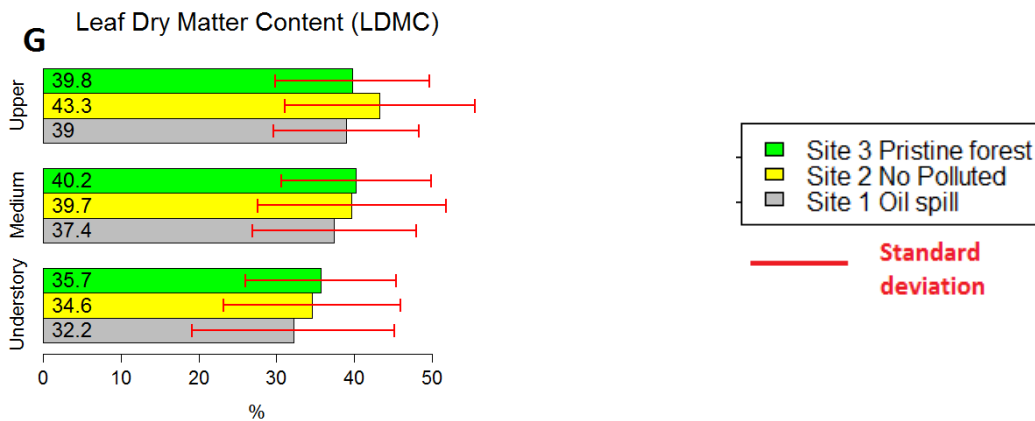


Figure 4.2 Leaf parameter in the vertical profile for the three study sites

The vertical profile of the forest exhibits a clear tendency for specific parameters. C_w , C_m , L_t and $LDMC$ decrease as the height of the forest profile decreases, meanwhile SLA and LWC increase as the vertical height decreases. In the site affected by the oil spill, C_w , L_t , SLA and LWC display apparent higher values across the vertical profile.

The results show lower values of C_{ab} across the vertical profile and considerable low chlorophyll content in the polluted area (Figure 4.2A). Foliar water content is higher in the upper canopy and decreases with the high of the forest. Vegetation in the area affected by the oil spill shows higher C_w than the two other sites (Figure 4.2B). Organic matter content expressed in area basis also shows a clear tendency to decrease with the high of the forest. C_m values in the oil spill site are lower than the other sites (Figure 4.2C). Results of SLA in the study sites reported a decreasing tendency across the canopy height and particularly higher values in the understory of the oil spill area (Figure 4.2D). L_t values in our study sites show a decreasing tendency in the vertical profile of the forest with thicker leaves in the area affected by the oil spill (Figure 4.2E). The percentage of water content (LWC) is higher in the lower levels of the forest and decrease with canopy high. The highest values of LWC are shown in the oil spill site. Dry matter content ($LDMC$) values are lower in the lower levels of the forest and increase with canopy high. Lower values of $LDMC$ are shown in the oil spill site (Figure 4.2F

and Figure 4.2G). Descriptive statistics and histograms for each site and vertical profile are presented in Annex 8, Annex 9, Annex 10 and Annex 11 respectively.

In order to explain if the differences are statistically significant, Table 4.6 presents a pairwise comparison of *p-values* by the adjustment method of Holms. Chlorophyll content in the polluted site illustrates strongly, high and significant differences in all levels of the vertical profile of the forest. On the other hand, the two parameters expressed in mass basis (*LWC* and *LDWC*) did not highlight significant differences between sites and canopy layers.

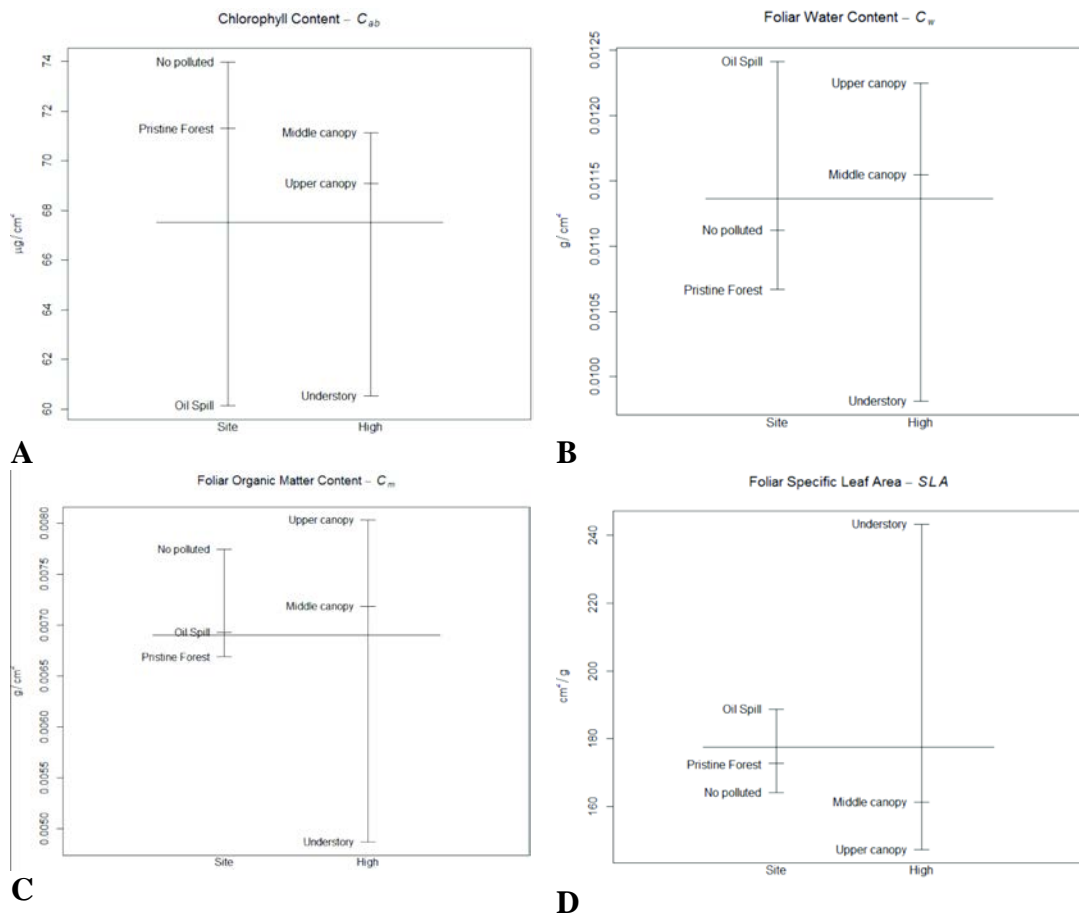
The pairwise comparison of *C_w*, *C_m*, *SLA* and *Lt* indicated significant differences between the polluted site and pristine forest site for the upper and understory layers only. Significant differences between the non-polluted site and pristine forest site are shown only for *C_m*. Annex 12 presents more detailed results of the ANOVA II and the pairwise comparison.

Table 4.6 Pairwise comparison of *p-values* by the adjustment method of holms for each site and the vertical profile of the forest

| Sites | <i>C_{ab}</i> | | | <i>C_w</i> | | |
|---|-----------------------|--------|------------|----------------------|--------|------------|
| | Upper | Medium | Understory | Upper | Medium | Understory |
| Site1 (Oil spill)-Site2 (No Polluted) | * | *** | *** | | | |
| Site1 (Oil spill)-Site3 (Pristine forest) | *** | *** | *** | *** | | |
| Site2 (No polluted) – Site3 (Pristine forest) | | | | | | |
| | <i>C_m</i> | | | <i>SLA</i> | | |
| Site1 (Oil spill)-Site2 (No Polluted) | | | | | | |
| Site1 (Oil spill)-Site3 (Pristine forest) | *** | | * | | | *** |
| Site2 (No polluted) – Site3 (Pristine forest) | *** | | | | | |
| | <i>Lt</i> | | | <i>LWC and LDMC</i> | | |
| Site1 (Oil spill)-Site2 (No Polluted) | | | | | | |
| Site1 (Oil spill)-Site3 (Pristine forest) | | | *** | | | |
| Site2 (No polluted) – Site3 (Pristine forest) | | | | | | |

*** Strongly significant (99.9%) ** highly significant (99%) * Significant (95%)
 No significant difference

Figure 4.3 supports those findings. It displays the plots of the univariate effects of sites and canopy height factors for each leaf parameter. Figure 4.3A illustrates a significantly reduced level of chlorophyll content in the understory of the oil spill site. Water content (C_w) is higher in the upper canopy of the polluted site (Figure 4.3B). Specific leaf area (SLA) is considerably higher in the understory of the polluted site (Figure 4.3D). Leaves from the upper canopy of the polluted site seem to be thicker (Figure 4.3E).



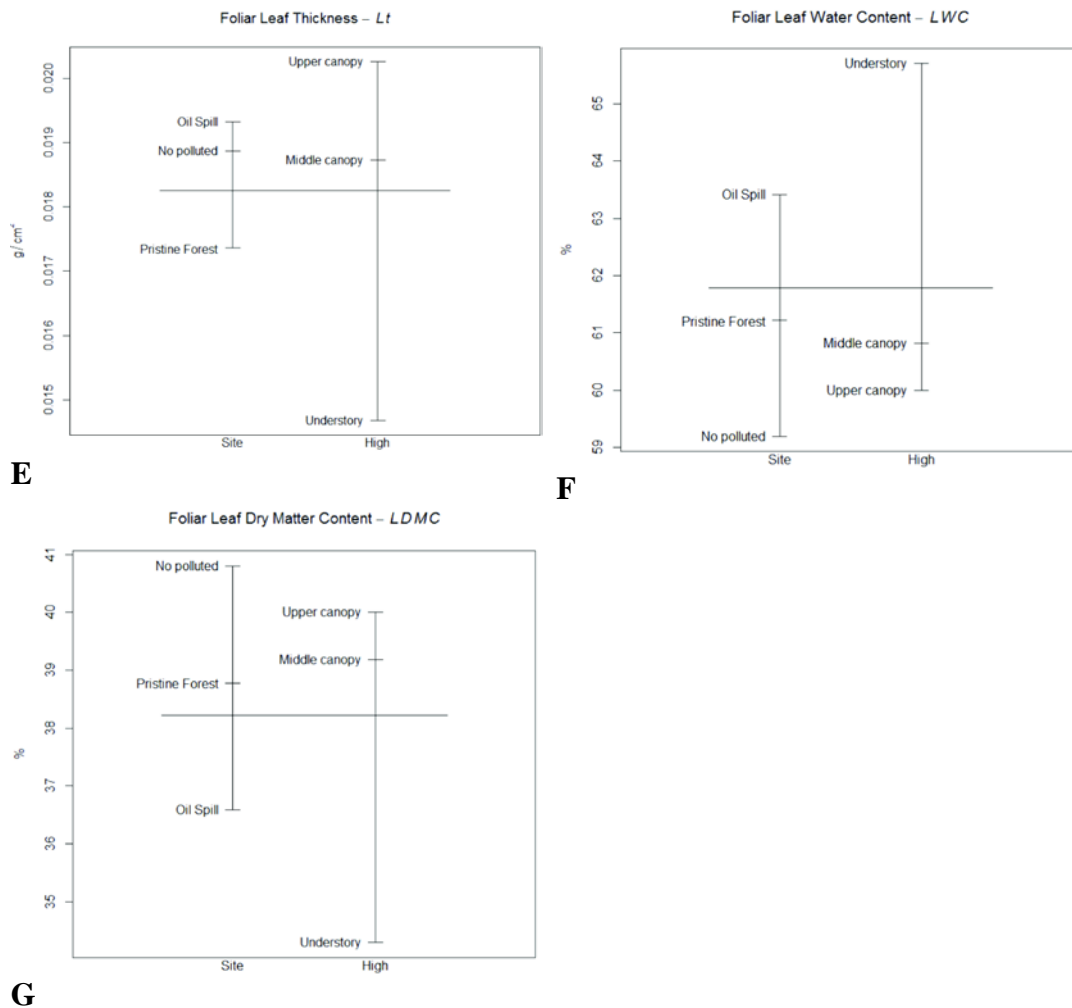


Figure 4.3 Plots of mean weight gain for each level of the two factors. The horizontal line represents the mean value for each trait and the vertical lines the location of the mean for the corresponding factor (Site and Canopy High)

4.4 Discussion

4.4.1 Leaf traits analysis per site

Major differences were shown between the oil spill site and the sites not affected by hydrocarbons excepting the leaf parameters based on organic matter content (*SLA* and *Cm*). This finding suggests that foliar organic matter content is not significantly affected in areas affected by hydrocarbon pollution. The two leaf parameters expressed on mass basis (% *LWC* and % *LDMC*) showed to be highly

and strongly significant in the oil pollution site. Due to the fact that these parameters are not normalised by the leaf area, these differences can be explained by the high species diversity of the sample sites where leaves vary greatly in morphology, anatomy and physiology in response to their growing conditions.

Chlorophyll seems to be a distinctive parameter of vegetation stress. It showed significant differences for the polluted site across the canopy levels.

Most of the leaf parameters in the areas not affected by petroleum pollution (Site 2 and Site 3) do not show statistical differences between them, the exceptions are *Cm* (99%) and *Lt* (95%) which indicate that biophysical and biochemical parameters of vegetation in the secondary and pristine forest do not change significantly compared to vegetation from a forest growing under the effects of hydrocarbons.

4.4.2 Leaf parameters analysis per site and vertical profile

As stated in 4.1.1 (page 90), the gradient in the light availability is closely related to the photosynthetic capacity in the vertical profile of the forest (Carswell et al. 2000b) and this explains that chlorophyll levels in the upper canopy are higher and decreases with canopy height (Kamaluddin&Grace 1992, Kamaluddin&Grace 1993). This behaviour is not evident in the study sites of this research, but we found that chlorophyll content levels in the oil spill are significantly lower than the sites not affected by pollution, particularly in the understory where vegetation is close to the hydrocarbon influence (Figure 4.2A). These results confirm the discussion of the effects of hydrocarbons on vegetation presented in Chapter 2 which state that hydrocarbons reduce the rate of photosynthetic activity and the cell injury caused by the accumulation of hydrocarbons in the chloroplasts which in turn explains the reduction of chlorophyll content.

A close correlation was observed between water content and leaf thickness which also has been suggested by Castro-Esau et al (2006). Indeed, those two parameters are the result of the intercellular space and leaf architecture which are responsible

of the spectral response of vegetation in the infrared reflectance and transmittance. Higher foliar water content was identified in the polluted site across all layers of the vertical profile and the pairwise comparison highlighted significantly higher water content on leaves of the upper canopy.

In the vertical profile of the forest, dry matter content (C_m) decreases through the canopy in response to the decline in light intensity which supports the findings of Witkowski (1991). Significant differences were detected between pristine forest and the two secondary forests (polluted and non-polluted) which may explain relative changes of carbon accumulation and leaf density in the forest sites.

Specific leaf area (SLA) consistently decreases across the vertical profile. Significant differences found in the understory illustrate that thinner leaves in the polluted area may reflect a major impact of hydrocarbons in young or early stage plants growing close to the source of pollution. Indeed these results support the finding that SLA is closely associated to leaf potential growth rate and decrease in the upper levels of the canopy high (Carswell et al. 2000b). In the low light environment of the understory, plants produce more leaf area per mass showing high SLA and thinner leaves. Studies conducted in the Amazon forest near Manaus reported that SLA varied from $50 \text{ cm}^2 \text{ g}^{-1}$ in the top of the canopy to $200 \text{ cm}^2 \text{ g}^{-1}$ in the understory (Roberts; Cabral & Ferreira De Aguiar 1990, Grace 1999).

Thicker leaves in the upper canopy were identified in all the study sites. Indeed, leaves in the upper canopy are thicker than those in the understory with a higher maximum stomata conductance and rate of photosynthesis (Grace 1999). Thicker leaves in the top of the canopy are the result of adaptation of leaves exposed to high irradiance levels showing an extra or thicker palisade mesophyll layer than leaves growing under low irradiance (Grace 1999).

We conclude that there is strong evidence that chlorophyll content (C_{ab}) levels are significantly lower in the site affected by hydrocarbons in all levels of the vertical

profile. Levels of water content (C_w) of the upper canopy in the site affected by hydrocarbons are significantly greater than in the pristine forest. Organic matter content (C_m) levels in the sites near to petroleum facilities (oil spill and not polluted sites) are higher compared to the pristine forest. This can be explained by the fact that C_m is closely correlated to atmospheric CO_2 and SO_2 concentrations (White&Montes-R 2005, Witkowski&Lamont 1991), which are considerably higher and near to petroleum facilities. In the understory of the site affected by the oil spill, specific leaf area (SLA) is significant higher than in the pristine forest. This means that leaves close to the source of pollution are significantly thinner than in the pristine forest. This fact is also explained by the significantly lower values of Lt in the understory of the oil spill compared to the pristine forest. On the other hand, leaves of the upper canopy in the oil spill site are significant thicker than in the pristine forest. Finally, the traits expressed in percentage of mass basis (LWC and $LDMC$), do not evidence any differences between sites and cannot be used as an indicator of vegetation stress.

4.5 Conclusions

The analysis of biophysical and biochemical parameters in the vertical profile of the tropical forest have revealed important differences in the vegetation growing in the oil spill compared with areas without the influence of hydrocarbons.

Lower levels of chlorophyll content, higher levels of water content, thicker leaves in the upper canopy and thinner leaves in the understory are key indicators of vegetation affected by hydrocarbons reported in this study.

The reduced levels of chlorophyll content can be explained by the findings presented in the literature in Chapter 2 which state that hydrocarbons reduce the rate of photosynthetic activity and the cell injury caused by the accumulation of hydrocarbons in the chloroplasts, which in turn explains the reduction of chlorophyll content.

Increasing levels of water content, especially in the upper canopy, may be explained by the reduction of transpiration rates cited in Chapter 2. It is not clear how the respiration rates are affected. Thicker leaves are probably the result of increased levels of foliar water content per unit area, but also possible adaptations by some species to grow in polluted environments. It is hypothesised that the vegetation growing in the oil spill have been experimenting changes and adaptations to the particular reduced environment but also there has been a shift in the specie composition because some species have been replaced by invasive species which are more resistant to the hydrocarbons influence. This shift in specie composition has also been reported in vegetation affected by gases from hydrocarbon seepages (Noomen;van der Werff & van der Meer 2012).

Thinner leaves in plants growing in the understory can reflect a major impact of hydrocarbons in young or early stage plants growing close to the source of pollution.

According to these finding, the oil spill is an active source of hydrocarbons to the environment where hydrocarbons penetrate the plants through the root system.

Since leaf and canopy reflectance and transmittance are sensitive to changes in plant pigments in the visible region of the electromagnetic spectrum, water content and leaf structure in the infrared regions, vegetation indices computed from remote sensing techniques can be applied to detect vegetation stress caused by hydrocarbons. These techniques can contribute to detect oil spills covered by tropical vegetation but also to remotely detect vegetation affected by hydrocarbon seepages as a key indicator of petroleum reservoirs in the underground, and in this way reduce the environmental impact and costs of the exploration projects.

Chapter 5. Response of Vegetation Indices from Hyperion to Petroleum Pollution in the Amazon Rainforest

In this chapter several vegetation indices derived from hyperspectral satellite images are computed in order to assess vegetation stress based on changes of biophysical and biochemical parameters identified in the previous chapter. New vegetation indices are explored to identify vegetation stress caused by hydrocarbon pollution. Vegetation stress is mapped and provides evidence of hydrocarbon pollution. Finally a method to estimate canopy chlorophyll content from leaf chlorophyll concentrations is discussed.

5.1 Introduction

In the previous chapter it was shown that hydrocarbon pollution affects some biophysical and biochemical parameters of the vegetation of the tropical forest growing near sources of hydrocarbon leakage. At leaf level, vegetation affected by hydrocarbon pollution shows decreasing levels of foliar chlorophyll content which suggests a reduced photosynthetic activity of the vegetation surrounding an oil spill, higher levels of water content which may explain the thicker leaves in the upper canopy, and thinner leaves in the understory.

Various vegetation indices (VIs) have been developed and applied to remotely sensed images to quantitatively characterise the physiological status of vegetation. VIs are dimensionless measures that indicate relative abundance and activity of green vegetation, including leaf-area-index (LAI), percentage green cover, chlorophyll content, green biomass and absorbed photosynthetically active radiation (APAR) (Jensen 2007). VIs are obtained by adding, multiplying or taking ratios of reflectances in two or more spectral bands of a pixel. According to the spectral resolution, VIs can be classified into broadband which can be derived from multispectral/hyperspectral data, and narrow band VIs from hyperspectral data.

5.1.1 Vegetation indices for vegetation stress caused by hydrocarbons

Some VIs have been specifically developed and tested to identify chlorophyll content across multiple vegetation species by using specific spectral bands sensitive to chlorophyll content changes. Other indices have been applied to remote sensing images to detect the effects of hydrocarbon pollution on vegetation. Some of these indices are explained here.

Three primary types of vegetation indices (simple ratio, normalized difference and red edge) have been developed for estimation of chlorophyll content, however in most cases these indices have been tested for few species only and therefore it is not clear whether they can be applied across a range of species with varying leaf structure as well as phenology. Sims and Gamon (2002) developed specific indices to estimate chlorophyll across species and found that indices based on reflectance at 680 nm, like the PSSRa index (also called SR_{680}), were largely insensitive to variations in chlorophyll content. On the other hand, normalised difference indices $NDVI_{705}$ using the reflectance at 705 nm is sensitive to the variation of chlorophyll content across several species ($r^2=0.65$), moreover vegetation indices mSR_{445} and $mNDVI_{445}$ using the reflectance at 445 nm produced substantially better correlation with total chlorophyll content ($r^2=0.74$ and $r^2=0.83$ respectively). This improved performance was attributed to the suppression of the surface reflectance at R_{445} which appears to be the most important factor in the variation of chlorophyll content derived from remote sensing across species.

Narrow-band vegetation indices have been applied to detect the effects of hydrocarbon pollution on the vegetation (Yang 1999, Smith;Steven & Colls 2004, Noomen et al. 2008, Zhu et al. 2013). It is assumed that hydrocarbon pollution affects vegetation adversely by displacement of the soil oxygen needed for respiration. This causes changes in plant and canopy reflectance. Noomen, *et al* (2008) applied 54 vegetation indices based on canopy characteristics and chlorophyll content in a simulated natural hydrocarbon gas leak in order to detect

changes in plants of maize (*Zea mays*) and wheat (*Triticum aestivum*). Six vegetation indices performed better: NDVI₇₀₅, mNDVI₇₀₅, CTR2, LIC1, LIC3 and OSAVI.

In another study, 20 vegetation indices were applied to detect the detrimental effects of oil pollution in reed (*Phragmites australis*) communities around oil wells that have been producing petroleum for approximately 10 years in the Yellow River Delta, eastern China (Zhu et al. 2013). Two vegetation indices best estimated soil TPH (Total Petroleum Hydrocarbons) concentrations: the modified chlorophyll absorption ratio index (MCARI) had the highest coefficient of determination ($r^2=0.73$) followed by the NDVI ($r^2=0.70$).

The red-edge position (REP) is a unique feature of green plants related to leaf chlorophyll content and to LAI. REP is defined as the inflection point (or sharp change) of the low red reflectance caused by chlorophyll absorption near 680 nm and high infrared reflectance governed by the internal structure of leaves near 750 nm (Clevers&Jongschaap 2006). Smith *et al* (2004) applied derivative analysis to locate the position and height of the inflection point of the red-edge that may indicate stress in plants (decreases in growth and chlorophyll content reduction) caused by hydrocarbon gases in the soil.

REP has been used as an indicator of vegetation stress in areas affected by hydrocarbon gases (hydrocarbon seepages and leaks from pipelines). Noomen and Skidmore (2009) found that REP moved to the shorter wavelengths in vegetation growing in a polluted soil. On the other hand, Yang et al. (1999, 2000) reported a shift of the red-edge towards longer wavelengths in an agricultural field located in a hydrocarbon seepage area. In that study, a linear interpolation method was applied to estimate the REP. The method first estimated the midpoint between the NIR at 780 nm and the reflectance minimum of the chlorophyll absorption feature at about 670 nm. Secondly, a linear interpolation was applied between the measurements at 700 nm and 740 nm for estimating the wavelength at the inflection point.

In this chapter, several vegetation indices derived from the atmospherically corrected Hyperion and CHRIS-Proba images of study areas are investigated to explore those slight changes of biophysical and biochemical parameters detected at leaf level can be detected at canopy level by using hyperspectral satellite images. The following questions are addressed: i) Which vegetation indices can best identify vegetation stress caused by hydrocarbon pollution? ii) Can new vegetation indices sensitive to detecting tropical rainforest affected by hydrocarbon pollution be derived? iii) Can chlorophyll content maps be derived from hyperspectral satellite images and can they highlight vegetation stress caused by hydrocarbons?

5.2 Materials and Methods

5.2.1 Study sites

A detailed description of the study area and sites is presented in Chapter 3, section 3.2.1, page 59. Vegetation biophysical, biochemical parameters and spectra data (reflectance and transmittance as described in Section 3.2.4, page 70) were collected from three study sites in the Amazon forest of Ecuador (Figure 5.1).

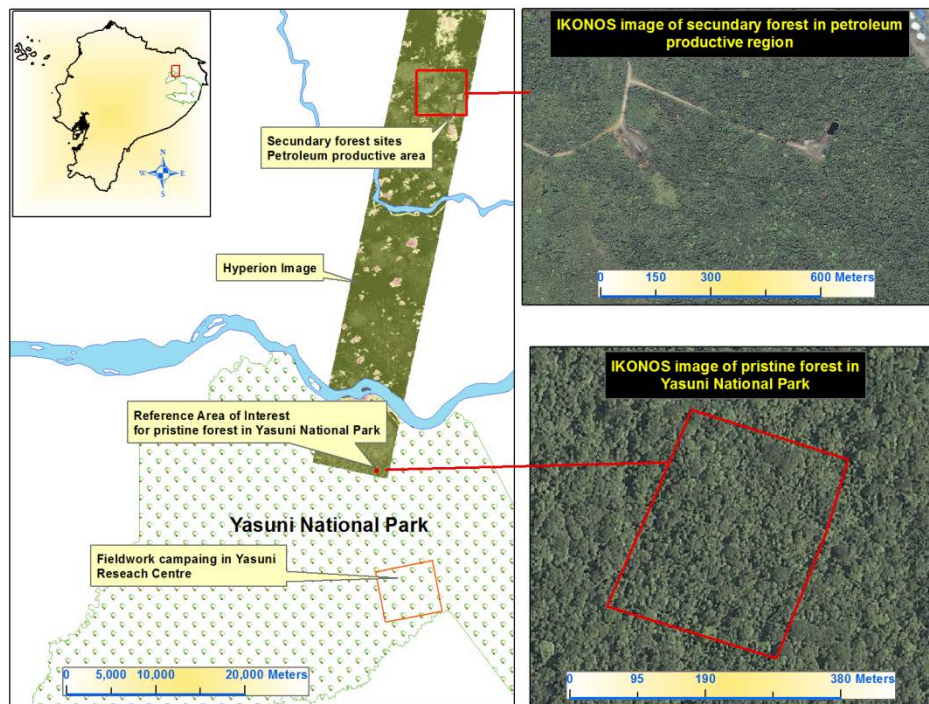


Figure 5.1 Location of sampled sites in the Amazon region of Ecuador which correspond to the three sampled sites described in Chapter 3

Two sites are secondary forests located in a petroleum productive area; the first site corresponds to a polluted area where, for a long time, (probably more than 15 years) an open pit containing crude oil has been discharging hydrocarbons to the environment. The second site integrates eight sampled sub-sites of the secondary forest where no evidence of hydrocarbon pollution was found during the soil sampling (see Chapter 4, section 4.2.1). Figure 5.2 and Figure 5.3 show a map of the sampled sites located in the petroleum productive area which included petroleum infrastructure: platforms, stations and other petroleum facilities which may be sources of hydrocarbon pollution. The former one describes open pits or facilities where polluted soils are remediated. According to environmental studies and audits those sites were identified as a source of pollution (Walsh Environment Scientists and Engineers 2005).

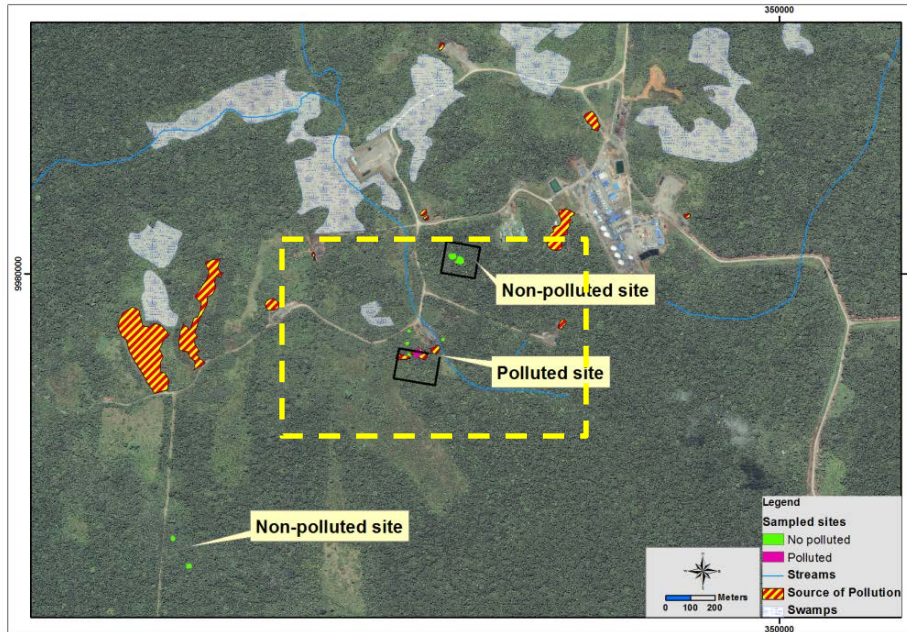


Figure 5.2 Study area and sampled sites in the petroleum productive region in the Amazon region of Ecuador. Background an IKONOS image accessed from Google Earth. The yellow square is zoomed in the next Figure.

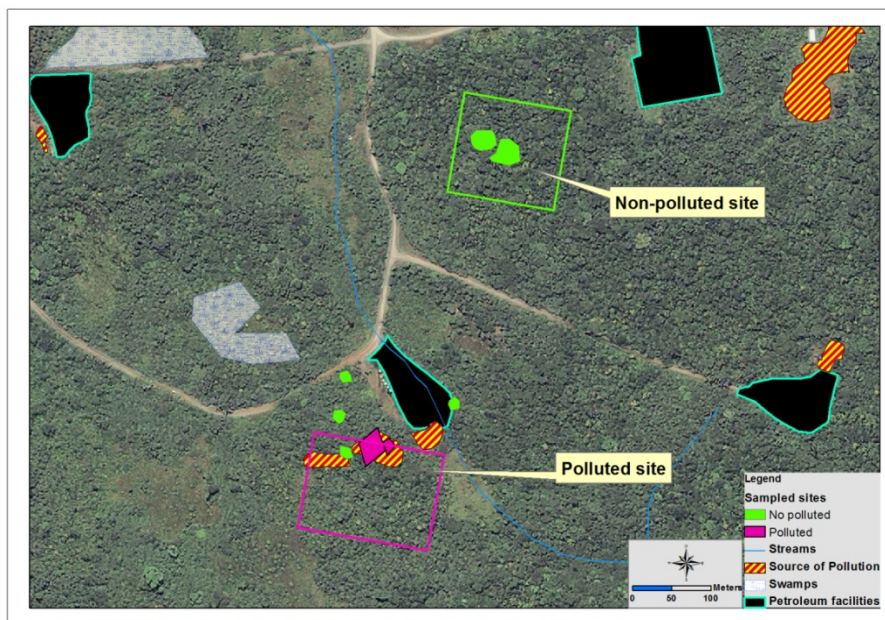


Figure 5.3 Sampled fieldwork sites in secondary forest of petroleum productive region. Polluted site (pink areas) and non-polluted sites (green circles). Squares represent areas of interest from where statistics and vegetation indices are derived.

The third site is a pristine forest located at the Yasuni National Park where a forest dynamic plot is managed by the Research Centre of the Pontifical Catholic University of Ecuador. Soil samples of this site show no hydrocarbon pollution. Unfortunately, there is not coverage of hyperspectral sensor for this site. A request for the acquisition of a new Hyperion image was submitted to USGS-NASA (United States Geological Survey-National Aeronautics and Space Administration) in 2011. Unfortunately, cloudy conditions have not allowed new image acquisitions until now therefore a reference area covered by Hyperion images was chosen as explained in the next page.

A fieldwork campaign was conducted in the above described three study sites. An extra study site is included in this study where no fieldwork campaign was implemented due to the lack of permissions from the petroleum company operating in the area. This fourth study site called the Pungarayacu oil field, where a vast hydrocarbon seepage produced by a geological uplift, has exposed crude oil to the surface (Figure 5.4).

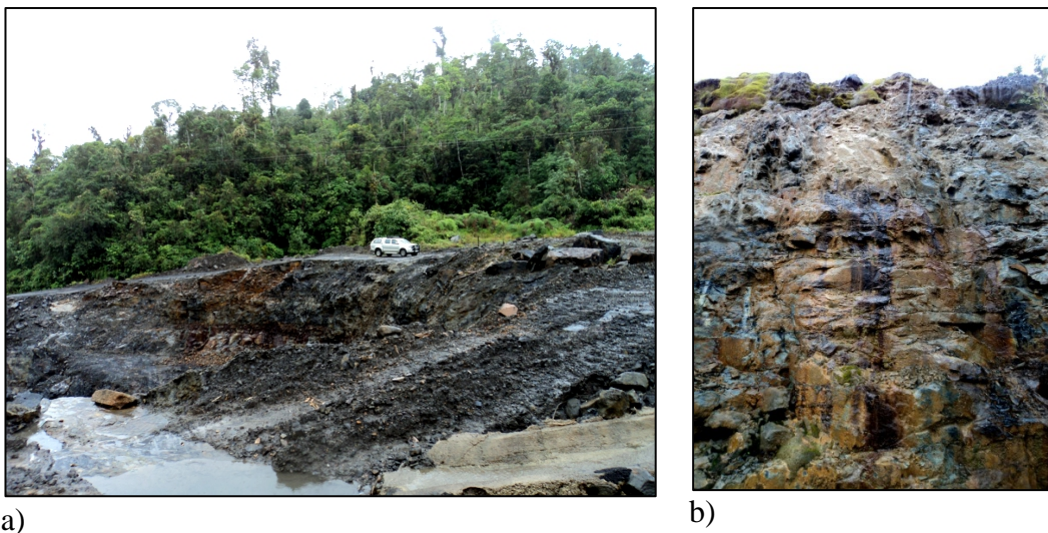


Figure 5.4 Pungarayacu hydrocarbon seepage located in Napo province in the Amazon region of Ecuador a) Crude oil on the surface b) Crude oil leaking from rocks

The Pungarayacu oil field is part of a geological structure known as Napo uplift. This is an extensive deformation zone along the Andean range as a result of tectonic stress of the Nazca and Continental plates. See Annex 13 for details of the geological structure of Napo uplift and Pungarayacu field.

5.2.2 Satellite images

EO-1 Hyperion image from NASA-USGS and CHRIS-Proba from ESA were used in this research.

Hyperion images

A Hyperion image provided by NASA-USGS covers the two sites located in a petroleum productive area. Unfortunately none of the Hyperion images provided cover the sampled area in the pristine forest, therefore a reference area of interest located 13km north from the sampled area was chosen inside the Yasuni National Park. It is assumed that this site represents the same conditions as the pristine forest (see Figure 5.1).

Hyperion is a hyperspectral instrument on board of the Earth-Observing 1 (EO-1) spacecraft launched in November of 2000 as part of the National Aeronautics and Space Administration (NASA) New Millennium Program. The EO-1 is in a sun-synchronous orbit with an altitude of 705 km and a 10:01 AM descending node. The orbit inclination is 98.2 degrees, the orbital period is 98.9 minutes, and equatorial crossing time is one minute behind Landsat-7 (Barry 2001). Figure 5.5 shows a schematic representation of the EO-1 orbit and its instruments footprint.

Hyperion is a pushbroom imaging spectrometer which provides radiometrically calibrated spectra. The swath is 7.7 km wide (cross-track) by 185 km long (along track). Each pixel covers an area of 30 m x 30 m on the ground. The full spectrum covers a range from 400 nm to 2500 nm distributed in 242 bands at bandwidth of approximately 10-nm full-width at half-maximum (FWHM).

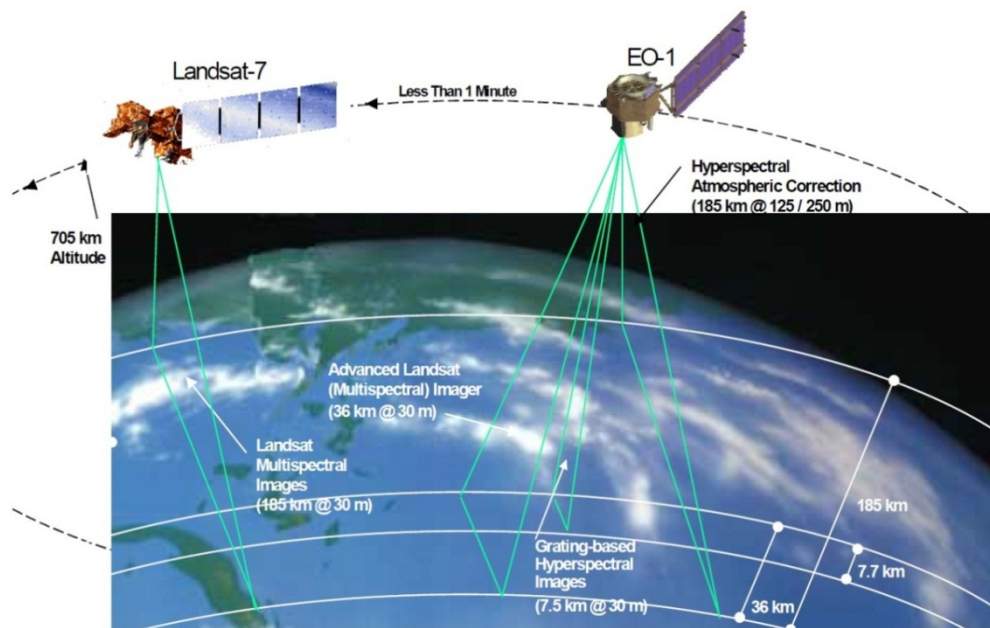


Figure 5.5 Schematic representation of the satellite orbit and sensors footprint of the instruments: Hyperion, (Advanced Landsat Imager). From EO-1/Hyperion Science Data User's Guide (Barry 2001)

Hyperion has a single telescope and two spectrometers, one covers the visible near-infrared region (VNIR) between 357-1055 nm and one covers the short-wave infrared region (SWIR) between 851-2576 nm.

Hyperion images have the dimensions of 256 pixels 6925 pixels x 242 bands. The span of the field-of-view is represented by the first number which defines the swath width. The swath length is represented by the second number. There is one pixel shift between the VNIR and SWIR cross-track co-registration, resulting in a 255 VNIR-SWIR coincident field-of-view locations. For each pixel location, 242 bands of data are obtained. Bands from 1-70 are collected from the VNIR, and bands 71-242 are collected from the SWIR. Some spectral bands in the overlap region are not calibrated due to their low signal and to avoid duplication. The 'no calibrated bands' are kept in the dataset but are set to zero. Other 'no calibrated bands' correspond to bands 1 to 7 and 225 to 242. Table 5.1 and Figure 5.6 illustrate the 'calibrated' and 'not calibrated' spectral bands of Hyperion images.

Table 5.1 Hyperion images calibrated and un-calibrated bands

| Array | Calibrated bands | | Uncalibrated bands | |
|-------|------------------|-----------------|--------------------|-----------------|
| | Band # | Wavelengths(nm) | Band # | Wavelengths(nm) |
| VNIR | 8-57 | 427 to 925 | 1-7 | 356-417 |
| SWIR | 77-224 | 912 to 2396 | 58-76 | Overlap region |
| | | | 225-242 | 2405-2577 |

A drawback affected Hyperion images is linked to the spectral and spatial artefacts related to the array malfunction of some sensors (see next section ‘Hyperion Level L1-R images’). Another is the relatively low signal to noise ratio (Hyperion signal to noise ratio (SNR), page 121). A third drawback is a significant smile effect (‘Smile effect correction-Vertical de-stripping’, page 138) (Datt et al. 2003, Goodenough et al. 2003, Dadon; Ben-Dor & Karnieli 2010).

Hyperion Level L1-R images

Since the first images taken by the Hyperion sensor, several products have been generated according to the evolution of the pre-processing levels applied. Previous levels were: Level 1 after April 1, 2001; Level 1A from July 1, 2001 and Level 1A1 from October 12, 2001; Level 1B1 and L1-R which became effective from December 2001. In this study, the radiometrically corrected L1-R product has been used: no geometric corrections have been applied to this level. Radiometric corrections involved in L1-R level consist in the following process:

- Flag pixels > 4095 which represent pixels affected by echo and smear.
- Smear correction to SWIR data which is the leakage of a signal from one pixel into the next readout pixel in the spectra direction.
- Echo removal from SWIR data which occurs when the signal from one image echoes into the neighbour pixels.
- Dark current and background removal of the residual charge in the detector.

- Sensor bias affects.
- Repair known bad pixels.
- Applying sensor gain values that are based on post-launching calibration coefficients. The radiometrically corrected image is then re-scaled for DN output by 40 for the VNIR and 80 for the SWIR (Barry 2001).

The resulting Level L1-R image has digital values of 16-bit radiances stored as a 16-bit signed integer. The units are $W/m^2 SR \mu m$.

Hyperion atmospheric windows

The solar irradiance curve or spectrum at the surface shows various absorption bands due to aerosol scattering and the absorption by gases of the atmosphere. Therefore some Hyperion bands are strongly affected by the atmospheric absorption features and show very low radiance signals. These will be removed during the image pre-processing (Section 5.2.3). Three principal water vapour (H₂O) absorption areas are located about 1350-1480 nm, 1800-1970 nm and >2480 nm. Oxygen (O₂) absorption features located at 690 nm, 760 nm, and 1260 nm. Carbon dioxide (CO₂) at 1600-1610 nm and 1950-2050 nm. Additionally, other gases with minor effects include carbon monoxide (CO), nitrous oxide (N₂O), and methane (CH₄). Table 5.2 and Figure 5.6 illustrate the Hyperion bands affected by absorption features caused by atmospheric gases.

Table 5.2 Hyperion bands affected by atmospheric absorption features

| Wavelengths (nm) | Hyperion Bands | Absorption Feature |
|------------------|----------------|--------------------|
| 690, 760, 1260 | 34, 41, 112 | Oxygen "notch" |
| 932-953 | 79-81 | Water vapour |
| 1115-1150 | 98-101 | Water vapour |
| 1350-1480 | 121-133 | Water vapour |
| 1600-1610 | 146-146 | CO ₂ |
| 1800-1970 | 165-182 | Water vapour |
| 1950-2050 | 180, 190 | CO ₂ |
| >2480 | Un-calibrated | Water vapour |

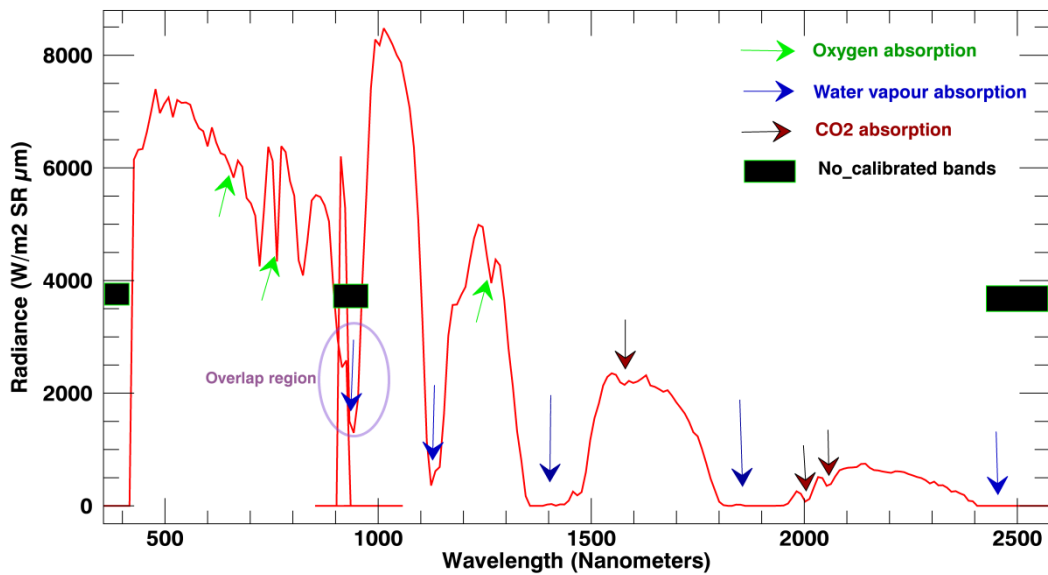


Figure 5.6 Radiance signal from a cloud pixel of Hyperion image. Spectral absorption features show very low values. No calibrated bands are set to zero.

Hyperion signal to noise ratio (SNR)

The signal to noise ratio (SNR) is a dimensionless measure that reflects the quality of the remote sensing data through the noise levels and signal strength. The noise in a satellite image depends on internal factors such as sensor sensitivity, spatial/spectra resolution and electronics of the system. External factors can also contribute to the noise and signal relationship: solar zenith angle, atmospheric attenuation and scattering and surface reflectance (Kruse; Boardman & Huntington 2003).

The predicted (SNR) of Hyperion images is in the range of 190 to 40 as the wavelength increases (Beck 2003). Table 5.3 illustrates the on-board SNR of the Hyperion images.

Table 5.3 Signal to Noise Ratio of Hyperion images

| Array | Spectral Range | On-Orbit SNR |
|--------------|-----------------------|---------------------|
| VNIR | 550 nm | 192 |
| VNIR | 650 nm | 140 |
| VNIR | 700 nm | 140 |
| SWIR | 1025 nm | 65 |
| SWIR | 1225 nm | 96 |
| SWIR | 1575 nm | 64 |
| SWIR | 2125 nm | 38 |

Several methods for estimating the SNR in satellite images have been proposed:

- Laboratory methods use the signal mean and its standard deviation of a few spectral bands located in an area covered by a bright surface. This method in most cases overestimates the SNR due to high values of the bright surface.
- Dark current methods measure the noise based on the variations in the signal dark current
- Image method computes the signal mean and its standard deviation for a homogeneous area within the scene. This method is widely used but in most cases underestimates the SNR since the inter-pixel variability contributes to the noise compound represented by the standard deviation, then suppressing the SNR (van der Meer;de Jong & Bakker 2006).

The image method was applied to the Hyperion image of the study area in order to estimate the SNR. Four homogeneous windows of 4x4 pixels were created and considered four land cover types: water body, dense vegetation (vegetation 1), no-dense vegetation (vegetation 2) and infrastructure. For each window, the signal average was computed (S_m). The noise was estimated by the standard deviation of the signal window (S_{sd}). SNR was estimated by the ratio of the estimated signal mean and the noise.

$$S_m = \bar{X} \quad (5.1)$$

$$S_{sd} = \sqrt{\frac{\sum_1^n (S_{ij} - S_m)^2}{n}} \quad (5.2)$$

$$SNR = \frac{S_m}{S_{sd}} \quad (5.3)$$

Where, n = windows pixel size and S_{ij} = Pixel signal at ij location in the homogeneous window

For the four homogeneous windows, the higher SNR is reported in the VNIR where it ranges from 0 to 112. Maximum SNR is located in band 10. Figure 5.7 shows the measured SNR of Hyperion images in the study area.

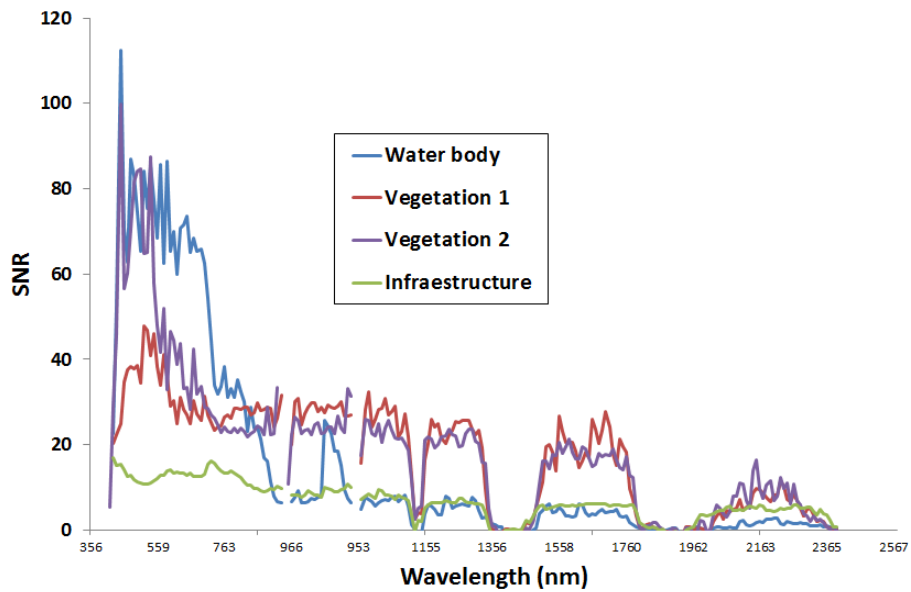


Figure 5.7 Signal to Noise Ratio (SNR) measured in the study area

CHRIS-Proba images

An image acquisition over the Pungarayacu hydrocarbon seepage was requested from the European Space Agency (ESA) for this research study. On 30th of July

2012, a CHRIS-Proba image was acquired under cloud-free conditions (Figure 5.8 shows the footprint of CHRIS-Proba image in the study area)

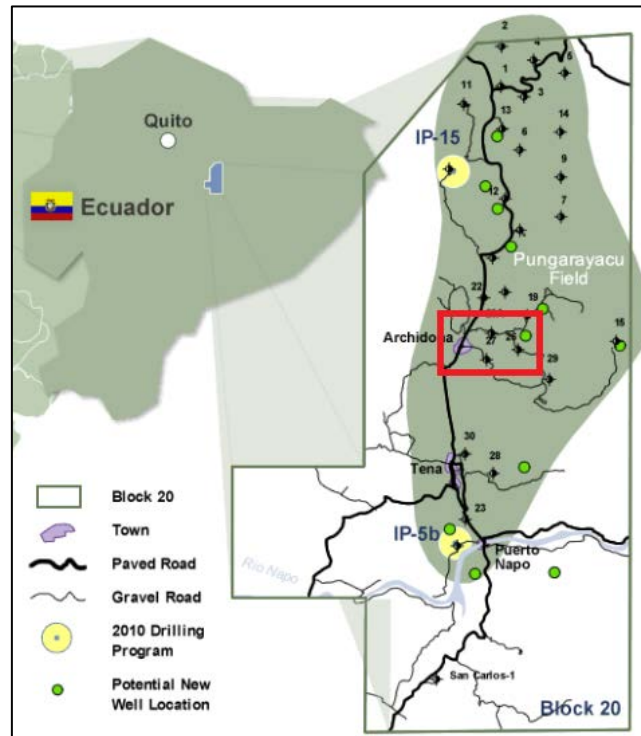


Figure 5.8. Location of the Chris-PROBA image in the hydrocarbon seepage area (read rectangle). Petroleum Block 20 is operated by Ivanhoe Energy Company. Data source: <http://footprintsOfEcuador.weebly.com/> accessed on: 14th April 2014.

The Compact High Resolution Imaging Spectrometer (CHRIS) on board the European Space Agency (ESA) Project for On-Board Autonomy (PROBA) satellite provides the option of both hyperspectral and multispectral observations. CHRIS acquires high spatial resolution (17-20 m or 34-40 m) images up to 62 narrow band channels in the visible and near infrared range. It also obtains images in five different view angles: +55°, +36°, 0°, -36° and -55° (Barnsley et al. 2004).

The acquired scene was recorded as Level 1A Mode 1 with 62 spectral bands in the range 400-1036 nm at spatial resolution of 34 m. Spectral sampling varies

from 2nm at the blue end of the spectrum, to about 12nm at 1050nm. In the red-edge (~690-740nm) sampling is about 7nm. Due to operational constraints, only three view angles were recorded: +55°, +36° and -55°.

5.2.3 Hyperion image pre-processing

This section describes the procedure for pre-processing Hyperion images which was followed in this study. Figure 5.9 displays the steps.

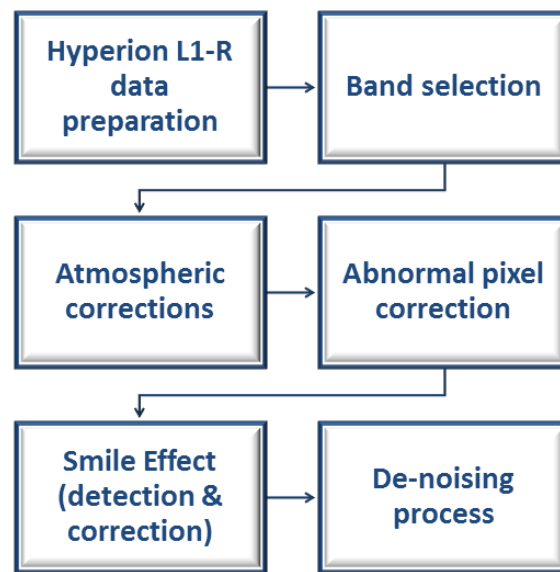


Figure 5.9 Process for pre-processing Hyperion images developed in this study

Hyperion L1-R data preparation

Hyperion images are distributed by USGS-NASA in Hierarchical Data Format (HDF) which contains the image data, spectral centre wavelengths, spectral bandwidths, gain coefficients and a flag mask.

An ENVI® (ENVI® version 4.4 and 5.0, Exelis Visual Information Solutions, Boulder, Colorado) plug-in called Hyperion Tool was applied to unpack the HDF files. During this process, geographic coordinates for the four corners of the image contained into the metadata file (*.met) are applied to perform a pseudo-geographic projection.

Some Hyperion detectors were malfunctioning, which often results in vertical striping in the image. The vertical striping is correlated on the fly by the referred tool, replacing the bad values with ones linearly interpolated from the remaining good values of the same scan line, based on the post-launching information on malfunctioning sensors. A mask file is created (1=good data, 0=bad data) for the whole image.

A text file is created which contains the wavelength and the full-width half maximum values (FWHM) for the 242 bands of Hyperion. Additionally, another text file is created containing the scale factor for every band.

Each detector in the Hyperion pushbroom array has a slightly different band centre and FWHM values for each band. A linear (or quadratic) interpolation is performed across all detectors on a pixel by pixel, spectrum by spectrum basis to a common set of wavelengths. The resulting file includes wavelengths representing the new common set of band centres.

Band Selection

From the 242 spectral bands of Hyperion images, 44 uncalibrated bands were removed for the next steps. From the remaining 198 bands, there are four bands overlapping in the VNIR and SWIR regions. These are band 56 (915.7 nm), band 57 (925.9 nm), band 77 (912.5 nm) and 78 (922.6 nm) (see Figure 5.6). So to avoid duplications, the former two bands (77 and 78) were eliminated to obtain 196 unique bands.

Another criterion for band selection was to eliminate bands strongly affected by water vapour absorption. Those bands are easily identified due to their very low signal values (see Table 5.2 and Figure 5.6). The final band selection accounts for 96 non-usable bands and 146 usable bands listed in Table 5.4.

Atmospheric corrections

Calibrated radiance data have the appearance of the solar irradiance curve and exhibit spectral discontinuities due to the scattering and absorption features caused by H₂O and gases in the atmosphere (see Table 5.2 and Figure 5.6). DN radiance values are quantities of radiation that are recorded by the imaging spectrometer within a given solid angle. The Hyperion sensor records radiance expressed in $W.m^{-2} sr^{-1} \mu m^{-1}$ (Watts per steradian per micrometre). Atmospheric corrections are needed to remove the effects of the atmosphere and transform the raw radiance data to rescaled reflectances from the Earth's surface. These can be compared to reflectance spectra acquired in the field or in the laboratory. Relative and absolute atmospheric correction methods have been developed.

Table 5.4 Unusable and usable Hyperion bands

| Non-usable bands | | | Usable bands | |
|------------------|----------------------------|----------------------------|-------------------------|---------|
| Range (nm) | Bands | Affected by | Range | Bands |
| 355-427 | 1-8 | Not-calibrated | 488-925 | 14-57 |
| 437-478 | 9-13 | Noise | 933 | 79 |
| 935-922 | 58-78 | Not-calibrated/Overlap | 973-1114 | 83-97 |
| 943-963 | 80-82 | Water absorption | 1155-1336 | 101-119 |
| 1124-1144 | 98-100 | Water absorption | 1477-1790 | 133-164 |
| 1346-1467 | 120-132 | Water absorption | 1981-1991 | 183-184 |
| 1800-1972 | 165-182 | Water absorption | 2032-2355 | 188-220 |
| 2002-2012 | 185-187 | CO ₂ absorption | | |
| 2365-2577 | 221-242 | Not-calibrated | | |
| TOTAL | 96 not-usable bands | | 146 usable bands | |

Absolute methods are the most effective and most common. These methods request a specific description of the components of the atmosphere and provide a recalibrated image that matches the reflectance of the ground with a maximum

estimated error of 10% if the parameters of the atmospheric profile are chosen correctly (Tempfli et al. 2009).

These methods use the radiative transfer models (RTM) for the assessment of the atmospheric contribution to the at-satellite signal by modelling the radiation pathway from the source (in this case the sun) to the target on the Earth's surface and back to the sensor. RTM require a full description of the atmospheric components at fixed altitudes throughout the atmosphere. LOWTRAN, MODTRAN, Code 5S and 6S are well known models. From these algorithms, MODTRAN has become the standard for research studies.

FLAASH

FLAASH (Fast Line-of-sight Atmospheric Analysis of Spectral Hypocubes) is a MODTRAN4-based radiative transfer model for atmospheric corrections developed by Spectral Sciences, Inc., under the sponsorship of the US Air Force Research Laboratory. FLAASH operates in the 0.4-2.5 micrometre spectral range and produces accurate, physics-based derivations of apparent surface reflectance through derivation of atmospheric properties such as surface albedo, surface altitude, water vapour columns, aerosol and cloud optical depths, surface and atmospheric temperatures.

ENVI® version 4.4 includes a licence of FLAASH which has been used in this study.

FLAASH incorporates a method for retrieving aerosol/haze from selected dark land pixels in the scene of a nearly fixed ratio between the reflectances for such pixels at 660 nm and 2100 nm. FLAASH retrieves the aerosol amount by iterating over a series of visible ranges which are later used to perform a second and final MODTRAN4 calculation loop over water.

Atmospheric correction of Hyperion images

Table 5.5 describes the parameters applied to FLAASH for atmospheric corrections.

When using the **water retrieval** option, the column water vapour amount for each pixel is estimated. This technique produces a more accurate correction than using a constant water amount for the entire scene. It was decided to use the 820 nm water feature as reference since it produced better reflectance curve results.

Table 5.5 FLAASH parameters for atmospheric corrections

| Image parameters | | Atmospheric parameters | |
|------------------------------------|--------------|----------------------------|---------------|
| Parameter | Value | Parameter | Value |
| Latitude (degrees) | 0.4 | Atmospheric model | Tropical |
| Longitude (degrees) | -76.2286 | Water retrieval | Yes |
| Flight data | Feb, 15 2005 | Water absorption feature | 820 nm |
| Flight time | 15:15:00 | Aerosol model | Rural |
| Sensor altitude (km) | 705 | Aerosol retrieval | 2-Band(K-T) |
| Ground elevation (km) | 0.240 | Initial visibility (km) | 40 |
| Pixel size (m) | 30 | Spectral Polishing | Yes |
| Zenith angle (degrees) | 161.42199 | Width (# of bands) | 9 |
| Azimuth angle (degrees) | 98.2 | Wavelength recalibration | No |
| Advanced Settings | | | |
| Aerosol Scale Height (km) | 1.5 | Reuse MODTRAN calculations | No |
| CO ₂ Mixing Ratio (ppm) | 390 | MODTRAN resolution | 15 cm-1 |
| Use Square Slit Function | No | MODTRAN multiscatter model | Scaled Disort |
| Use Adjacency Correction | Yes | Number of DISORT streams | 8 |

The **Aerosol retrieval** option estimates the scene average visibility using a dark pixel reflectance ratio which requires the presence of sensor channels around 660 nm and 2100 nm. A dark-pixel is defined when reflectance at 2100 nm is 0.1 or less and a 660:2100 reflectance ratio is 0.45 approximately. An additional check is performed for the ratio 800:420 nm. If the result of this ratio is 1 or less, then the

pixels are marked as shadows and water bodies. 2-Band (K-T) option uses this particular method. If a suitable dark pixel is not found, then the value in the **Initial Visibility** field is used.

Spectral polishing is a linear normalisation method that reduces spectral artefacts in hyperspectral data using data itself. It is based on the following assumptions:

- The linear transformation is channel-dependent gain factors and offsets.
- Spectrally smooth reference pixels (example, soil or pavement) can be found within the scene.
- The true spectra of the reference pixels can be approximated by applying a spectral smoothing operation.

A FLAASH spectral polishing algorithm is performed with a smoothing running average over n adjacent bands defined in the width number of bands field. A low n value is useful for removing residual saw-tooth noise caused by a dark current offset between odd-number and even-number bands. A higher n value (for example 5 to 11) is better for removing larger-scale artefacts such as atmospheric absorption band residuals. A value of $n=9$ is recommended for the 10-nanometer resolution in hyperspectral sensors.

Wavelength recalibration is closely related to the water retrieval process to produce accuracy reflectance results. The process consists of finding accuracy locations of the band centre wavelength. Hyperion is one of the sensors which automatically support wavelength recalibration in FLAASH. When wavelength recalibration was enabled, the results of the reflectance produced two disconnected peaks located between 950-1300 nm (see Figure 5.10). It was decided to disable this option in order to avoid this issue.

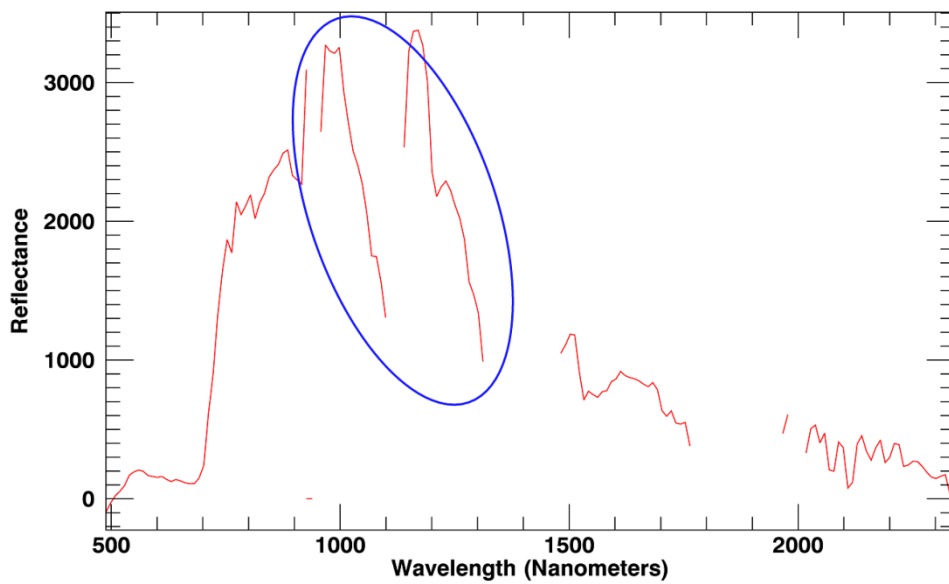


Figure 5.10 Spectra reflectance results from FLAASH. The blue oval highlights two peaks disconnected in the range of 950-1300 nanometres. This unusual result is shown when wavelength recalibration option is enabled.

Abnormal pixels

If a detector for a column in the VNIR or SWIR arrays is not calibrated properly, a vertical “stripe” will result for an image band. The most extreme case of a failed calibration are the “abnormal pixels” or “bad pixels”. According to Goodenough et al. (2003), abnormal pixels are classified in four categories:

- Continuous with atypical DN values.
- Continuous with constant DN values.
- Intermittent with atypical DN values.
- Intermittent with lower DN values.

The first three abnormal pixel categories are corrected during the pre-processing of Level L1-R (see page 119). The last category, intermittent with lower DN value, still exists affecting a full column of the scene. Additionally abnormal pixels may occur due to the pixel saturation, which makes the correction for

sensor “echo” inoperable and other times extra abnormal pixels may be associated with events of space environment such as high-energy particles. Table 5.6 shows the pre-launch and the remaining abnormal pixels (columns) in the Hyperion images.

Table 5.6 Identification of pre-launch and remaining abnormal pixels (columns) in L1-R Hyperion images

| Pre-launch | | Remaining | |
|-------------------|---------------|------------------|------------------------|
| BAND | COLUMN | BAND | COLUMN |
| 8-36 | 1 | 8-11 | 6, 68 |
| 94 | 92 | 8-35 | 114 |
| 101 | 91 | 8 | 237 |
| 116 | 137 | 9 | 229 |
| 119-120 | 239 | 10,11 | 199 |
| 165 | 147 | 12 | 176 |
| 169 | 22 | 13 | 158 |
| 168 | 255 | 14 | 247 |
| 190 | 112 | 27-28 | 47 |
| 203 | 114 | 37 | 128 |
| 200-201 | 7 | 55-56 | 8,13,17,20,32,35,37,39 |
| | | 56 | 147 |

Assuming that the nearby pixels have the highest spatial autocorrelation, abnormal pixels-columns were corrected by replacing their DN value with the average value of their immediate neighbour columns. Figure 5.11 shows the abnormal pixels (column) remaining in Band 16 before and after corrections.

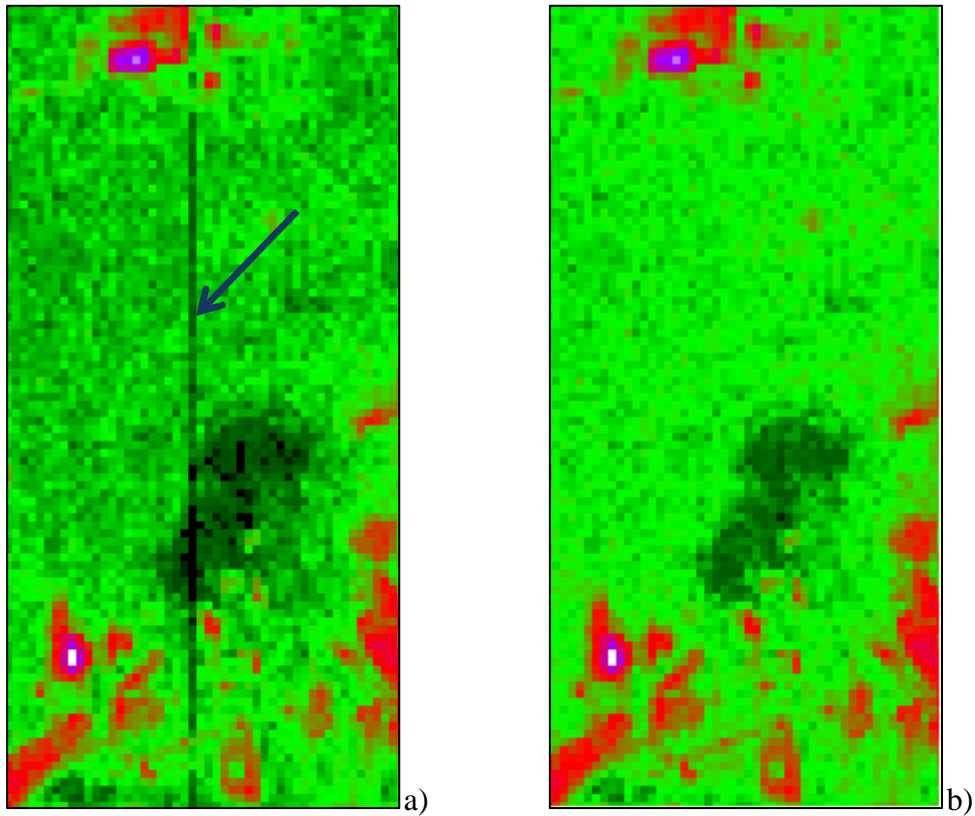


Figure 5.11 Subset of Hyperion image (Band 16) in the study area. Colour representation is arbitrary to highlight the abnormal pixel-column (arrow). **a)** Before correction and **b)** after correction.

Smile effect detection

The smile effect refers to an across-track wavelength shift from the central wavelength, which is due to change of dispersion angle with field position. In VNIR bands the shift range is between 2.6- to 3.5 nm, with the maximum shift occurring at column 256 in band 10. In SWIR bands, the spectral shift is less than 1 nm and is not significant for forest applications (Goodenough et al. 2003).

The first smile correction was applied to the Hyperion sensor based on pre-launch parameters of the detector arrays, but the procedure did not properly correct the effect and, in fact, significant errors were increased specially in the first VNIR bands (Dadon; Ben-Dor & Karnieli 2010).

The smile effect may affect Hyperion images in different degrees of the spectral range and may vary from scene to scene. Spectral smile is not obvious to the naked eye, so an indicator is necessary to make it visible. There are two methods to detect images affected by the smile effect; the first is through the effects of the absorption features of O₂ in specific spectra regions and the second is the Minimum Noise Fraction (MNF) transformation.

Gas absorption features

Absorption features caused by O₂ around 760 nm (VNIR) located at band 41 and CO₂ around 2012 nm (SWIR) located at band 186 can be used as internal indicators of spectral smile. It is assumed that the absorption features of those gases affect the signal received by the sensor relatively similarly across the detector line array, and (columns) therefore do not exhibit pronounced changes in depth. However, the smile effect can be observed as a notable change in the angle of slopes in both sides of the absorption curve (shoulder) at different columns across the image (Figure 5.12). This research takes advantage of the higher SNR of the O₂ absorption feature for smile effect detection. Therefore, in order to detect possible cross-track variation in O₂ absorptions due smile, the first derivative of the right hand side shoulder (B') is estimated by Equation (5.4) as follow:

$$B' = \frac{B_2 - B_1}{fwhm} \quad (5.4)$$

where B_1 is the O₂ absorption feature band, B_2 is the right shoulder at the next two bands (Dadon; Ben-Dor & Karnieli 2010).

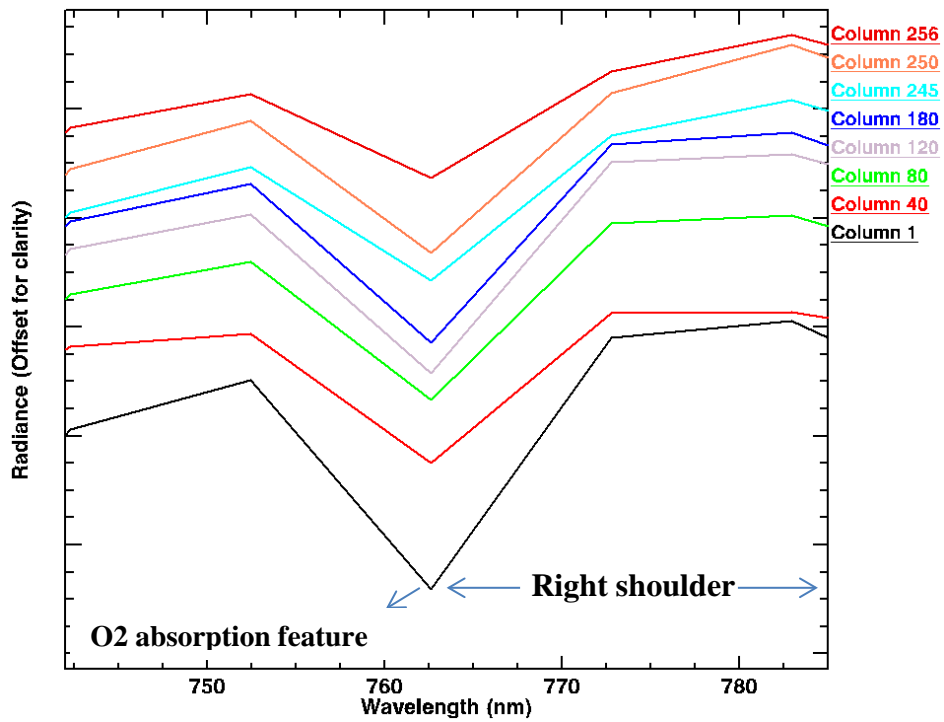


Figure 5.12 O₂ absorption curve at different columns across the image. Note the changes in the angles of the slope in the shoulders of the absorption feature.

The resulting derivative image (B') exhibits a spectra gradient on the right side of the scene (Figure 5.13a), and a section across columns display lower values in the midsection of the scene and higher values at the right hand of the scene which represent the smile effect (Figure 5.13b).

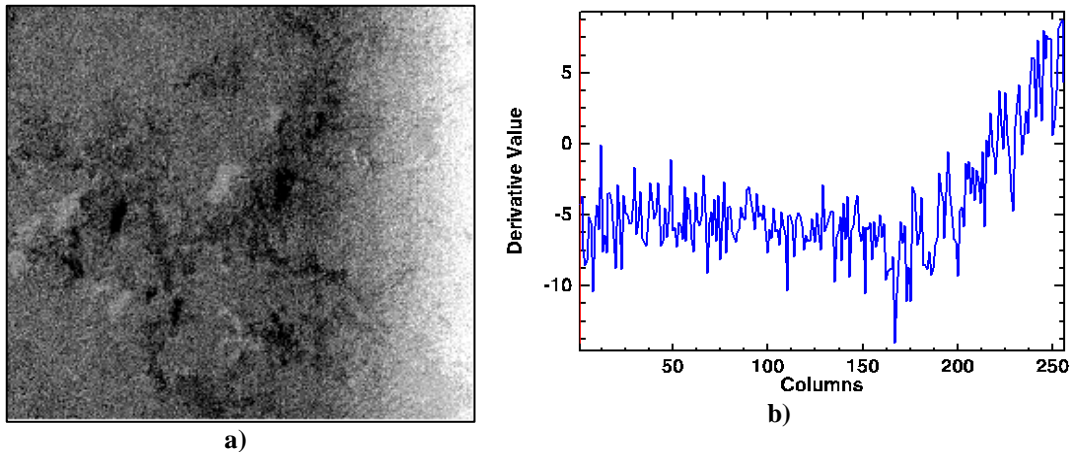


Figure 5.13 a) Derivative image estimated in the O₂ absorption feature around 760. b) Section across columns (horizontal profile) of the derivative image where the smile effect is clearly identified.

MNF transformation

The MNF transformation is an algorithm used for ordering data cubes into components of image quality using a two-cascade-principal-components-transform which selects new components in order to decreasing signal to noise ratio. The first transform based on an estimated noise covariance matrix, decorrelates and rescales the noise in the data. The first step result is transformed data in which the noise has unit variance and no band-to-band correlations. The second step is a standard principal component transformation of the noise-whitened data (van der Meer;de Jong & Bakker 2006)(van der Meer;de Jong & Bakker 2006)(van der Meer;de Jong & Bakker 2006)(van der Meer, de Jong & Bakker 2006)(van der Meer;de Jong & Bakker 2006).

The spectral dimensionality of the data set can be determined by its associated eigen-values and eigen-images. The data space is divided into two parts: one part associated with large eigen-values and coherent eigen-images, and a second part of MNF bands having near-unity eigenvalues and noise dominated images.

Figure 5.14 represents the MNF procedure in ENVI® software. First the noise is estimated from three sources: a) dark current image acquired with data, b) noise statistics calculated from data, or c) from statistics saved from previous transform. Both, the eigen-values and eigen-images are used to evaluate the dimensionality of the data.

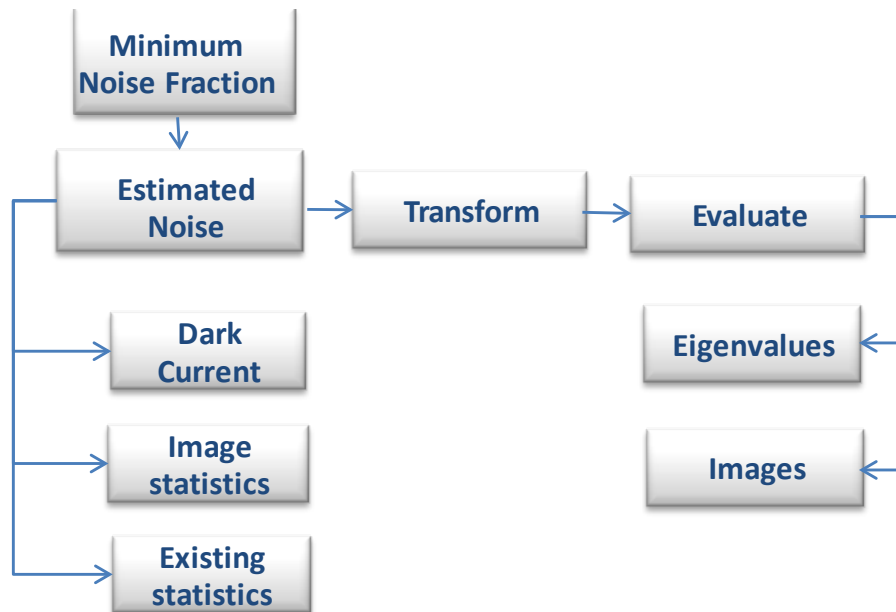


Figure 5.14 Minimum Noise Fraction (MNF) procedure in ENVI® software.

MNF transformation was applied to the radiance Hyperion image. The results are illustrated in Figure 5.15. The band MNF-1 has a strong spatial gradient that corresponds to the spectral smile.

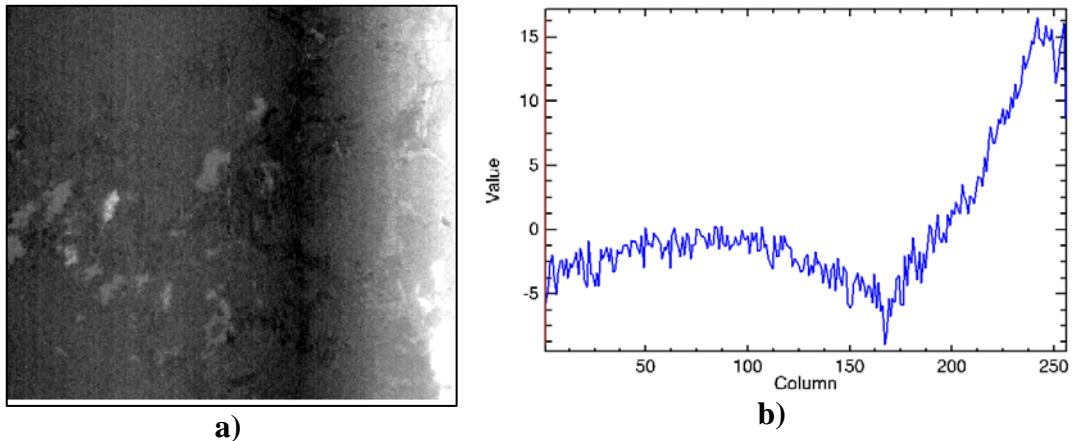


Figure 5.15 Minimum Noise Fraction transformation of the Hyperion image. a) MNF band 1 shows a spectra gradient on the right side of the image. b) Section across columns (horizontal profile) of the MNF band 1 where the smile effect is detected.

Smile effect correction-Vertical de-striping

Vertical stripes are the less severe effects of the pushbroom sensor calibration problems. Those pixels are effectively spatially, and possibly temporally, varying at scales determined mainly by array structure rather than the Earth's surface structure. According to Datt *et al.* (2003), at one level a single detector in one of the arrays may have an anomaly calibration. If such pixels have no association with other detectors they will create pixel-level and pixel-dependent vertical stripes in the image data. Several Hyperion bands are affected by vertical stripes, especially the first 12 bands of VNIR and many SWIR bands.

A method for de-striping Hyperion images was proposed by (Datt, et al.2003). This method relies on the significantly modified gain and offset values of columns affected by vertical stripes, which are relatively stable over the image collection but not necessarily between image collections. It is similar to other methods for removing horizontal stripes in satellite images in mirror scanner by histogram equalisation or balance detectors in airborne pushbroom sensors.

In the de-striping method applied in this study, the statistical moments for each column are modified to match those for the whole image for each band.

$$X'_{ijk} = \alpha_{ik} \cdot X_{ijk} + \beta_{ik} \quad (5.5)$$

Gains and offsets are computed by:

$$\alpha_{ik} = \frac{\bar{S}_{ik}}{S_{ik}} \quad (5.6)$$

$$\beta_{ik} = \bar{m}_{ik} - \alpha_{ik} \cdot m_{ik} \quad (5.7)$$

Where:

m_{ik} = mean of the detector at i th column for band k .

\bar{m}_{ik} = mean reference value.

S_{ik} = within column standard deviation.

\bar{S}_{ik} = within column standard deviation reference value.

The method takes into account the reference mean to be the total image mean and the reference standard deviation to be the whole image within column standard deviation.

$$\bar{m}_{ik} = \bar{m}_k \quad (5.8)$$

$$\bar{S}_{ik} = \bar{S}_k \quad (5.9)$$

An algorithm for de-stripping a hyperspectral cube was implemented using the software package MATLAB®, R2011b (The MathWorks Inc., Natick, MA, 2011) (see Annex 14 for the code). Figure 5.16 shows the results of the de-stripping method applied to several bands of the VNIR. The first three bands (a, b, c) correspond to bands 8, 9 and 10 which are strongly affected by stripes. Band number 37 is not affected by stripes. The extreme high DN values of clouds alter the statistics of every column then introduce artefacts along columns containing clouds except for the band 37.

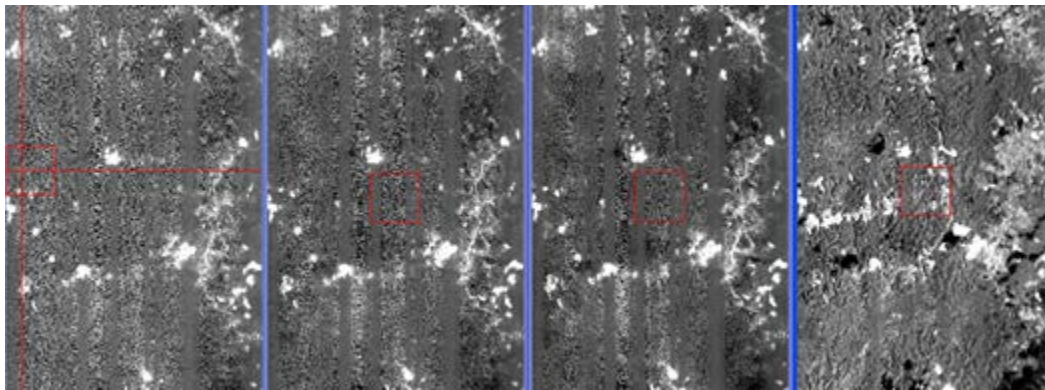
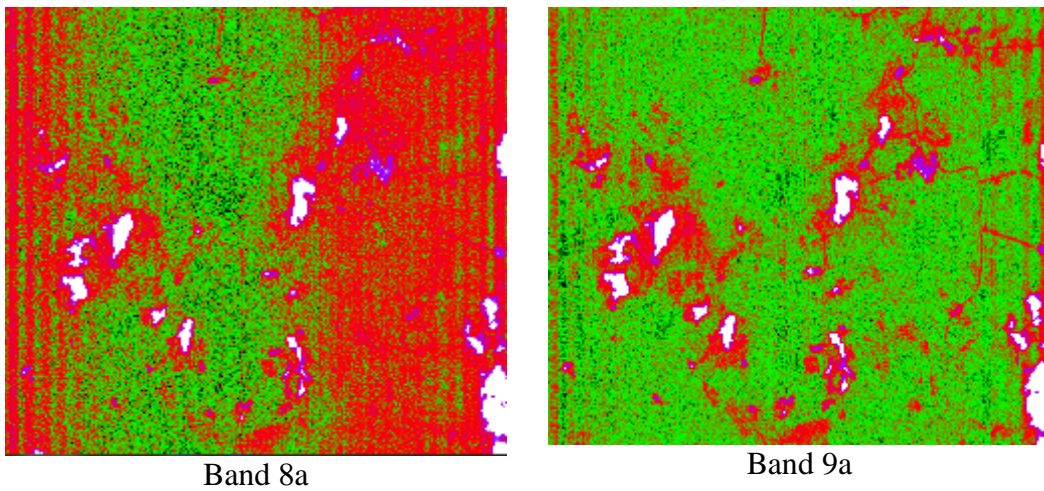


Figure 5.16 Results of the de-stripping method for bands **a)** 8, **b)** 9 **c)** 10 and **d)** 37. The first three are bands strongly affected by stripes. Results show artefacts introduced by the method along columns affected by clouds.

A specific algorithm for de-stripping Hyperion images was created in order to exclude the influence of clouds/shadows in the statistics of the image by introducing a cloud-shadows-threshold. Figure 5.17 illustrates the results of the de-stripping procedure excluding the influence of clouds/shadows.



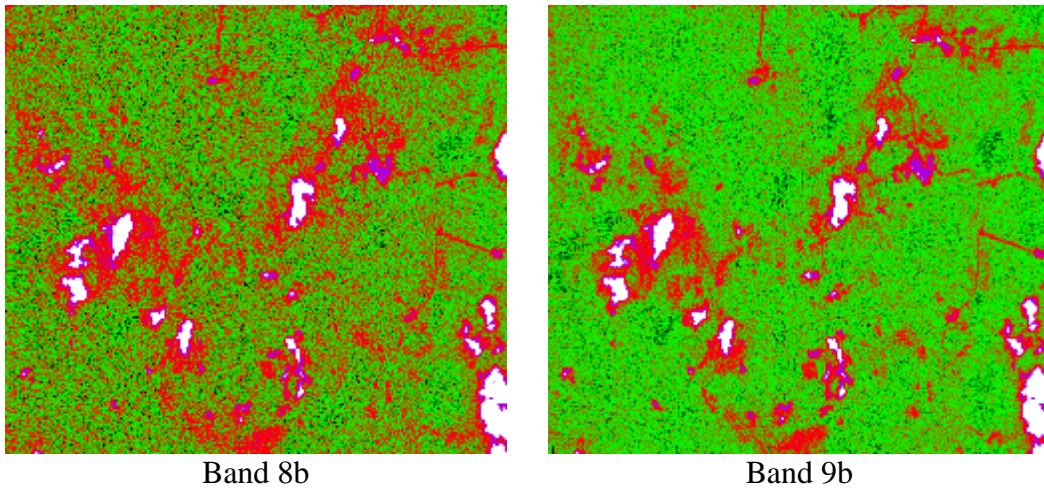


Figure 5.17 Band 8a and 9a before de-stripping. Band 8b and 9b after de-stripping. Selection of colours are arbitrary to demonstrate the effects of the de-stripping process

Figure 5.18 represents the horizontal spectral profile of the resulting image which shows that the smile effect has been corrected.

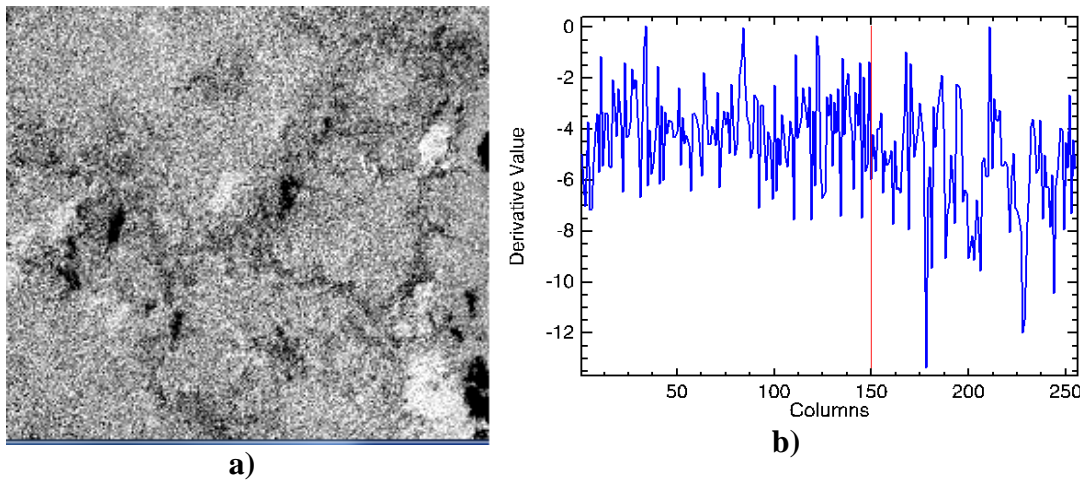


Figure 5.18 a) Derivative image estimated in the O_2 absorption feature (bands 42 and 43 of Hyperion) after the de-stripping correction. **b)** Horizontal profile of the derivative image where the smile effect has been removed.

De-noising process

MNF (Minimum Noise Fraction) is a widely applied method for reducing data dimensionality and removing noise (Goodenough et al. 2011, Apan et al. 2004). Section “MNF transformation”, in page 136, offers an introduction about MNF transformation which relies on an estimation of noise and a subsequent PCA (Principal Component Analysis) of the noise covariance matrix through the spatial domain. In contrast to PCA analysis, where eigenvectors are ranked by eigenvalues, the MNF eigenvectors are ranked by a signal to noise ratio (SNR) defined as the noise variance divided by total variance. The components corresponding to low SNR and unstructured spatial statistics can often be eliminated from the data by putting the transformation back together without them (Datt et al. 2003). This process is called the Inverse MNF transformation.

Forward MNF process

Forward MNF transformation was applied to the resulting image from the previous step. At this point the number of bands in the Hyperion image has been reduced to 146 bands (see Table 5.4). Figure 5.19 plots the resulting eigenvalues versus the band number. Higher eigenvalues are shown around band 15. Visual inspection of the first 15 MNF bands shows that most of the information is contained within the first 15-MNF bands (see Figure 5.20). The resulting bands do not contain spatial information.

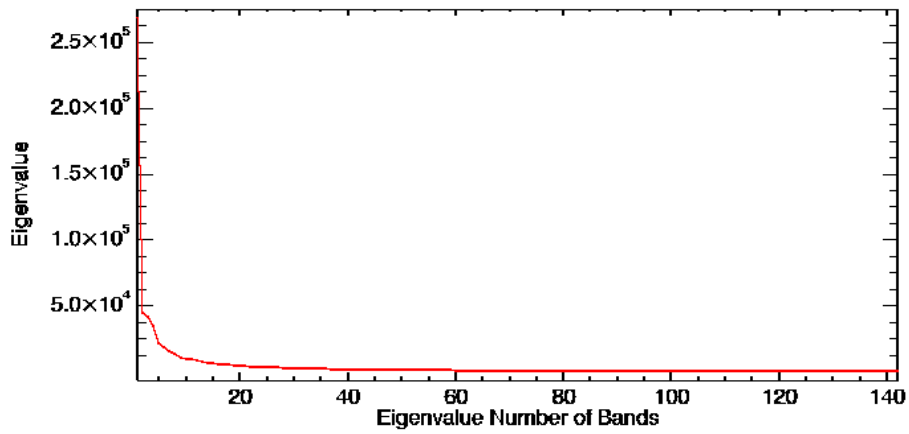


Figure 5.19 Eigenvalues for the MNF transformation of the Hyperion image

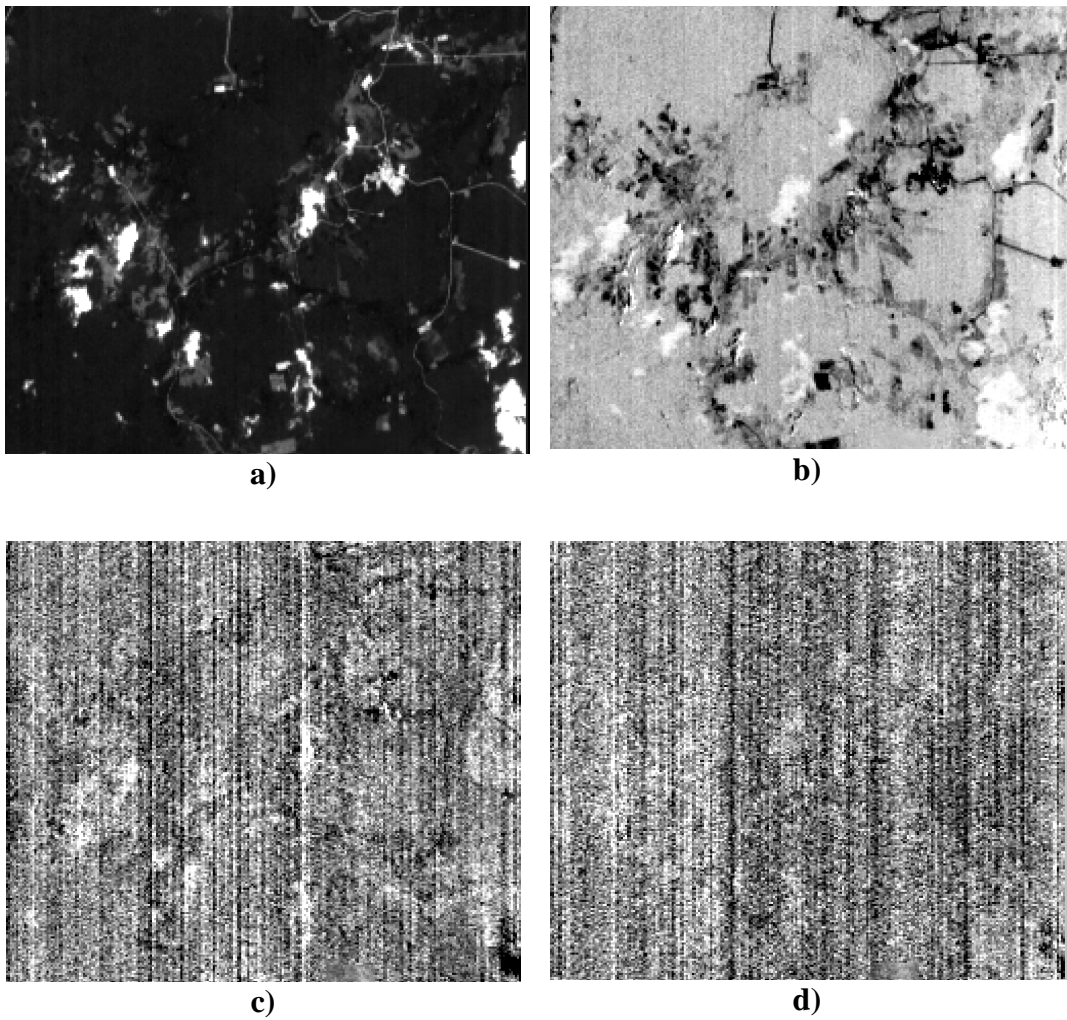


Figure 5.20 MNF transformation results of Hyperion image. a) MNF-1, b) MNF-2, c) MNF-10 and d) MNF-15

Analysis of the first 15 MNF bands shows that 83% of the information is contained in the first 15 MNF bands, and so consequently these bands are used during the MNF inversion process. Figure 5.21 presents the reflectance signal before and after MNF inverse transformation to remove noise. As a reference, Datt *et al* (2003) found a good method to remove noise by using the first 20 MNF band for Hyperion images.

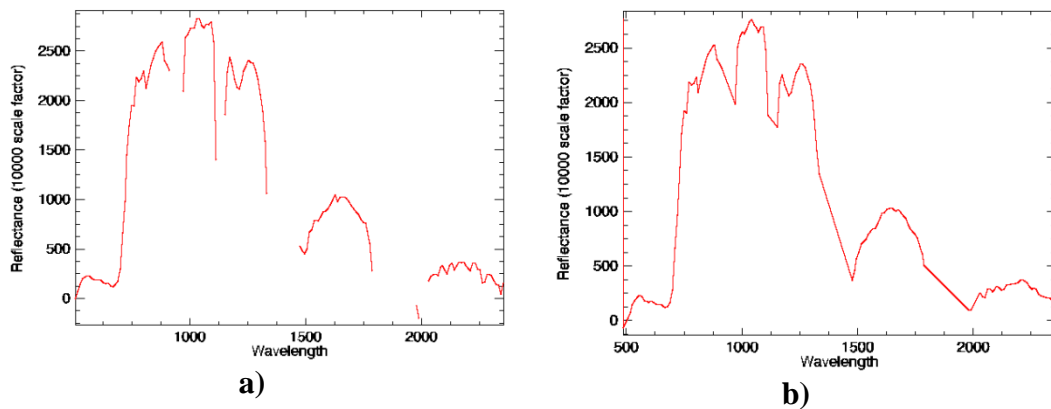


Figure 5.21 a) Reflectance signal before the inverse MNF process to remove noise; b) Reflectance signal after remove noise (same pixel for both figures)

5.2.4 CHRIS-Proba image pre-processing

Image pre-processing was carried out using the open source software BEAM 4.11 Toolbox® which is a collection of executable tools developed by ESA to facilitate image processing (<http://www.brockmann-consult.de/cms/web/beam/>). CHRIS-Proba pre-processing was performed using the following specific tools: noise reduction, atmospheric corrections and geometric corrections.

A noise reduction algorithm faces the problem of removing coherent noise, known as ‘drop-out’, and vertical striping which are frequently reported in push-broom sensors:

- Drop-out noise is anomalous odd pixels in image rows due to errors in transmission of channel 2 (drop-outs).

- Vertical striping consist of the multiplicative noise in image columns due to the irregularities of the entrance slit and CDD elements in the across-tracking direction (Gomez-Chova et al. 2008).

The atmospheric correction module for CHRIS-Proba images included in BEAM® 4.11 Toolbox is an automatic process independent of the acquisition mode. The number of processing steps are given by the spectral resolution and sampling of each mode and consists of the characterisation of spectral calibration, aerosol optical thickness (AOT) retrieval, column water vapour (CWV) retrieval, reflectance retrieval and data recalibration (Guanter et al. 2008).

The geometric corrections module is based on the parametric modelling of the acquisition process. It makes use of the satellite position, velocity and pointing at the moment of line acquisition, projecting the line of sight onto the Earth's surface to calculate the geographical coordinates of each pixel. The inputs needed by the algorithm are contained in the telemetry file which included the satellite position, velocity and image timing, target centre coordinate and local Digital Elevation Model (DEM) Alonso&Moreno (2004, 2005).

5.2.5 Vegetation indices

Several vegetation indices, which are related to the described parameters, affected by hydrocarbon pollution were selected from the literature and grouped in broad-band indices, narrow-band-greenness/chlorophyll, narrow-band-other pigments and narrow-band-water indices. Table 5.7 and Table 5.8 describe the vegetation indices applied in this study.

Table 5.7 Vegetation indices applied to Hyperion images in the study area

| INDEX | REFERENCE | EQUATION | Eq. Number |
|---|--|---|------------|
| BROAD-BAND VEGETATION INDICES | | | |
| Simple Ratio (SR) | (Rouse;Haas & Schell 1974) | $\frac{\rho_{NIR}}{\rho_{Red}}$ | 5.10 |
| Normalised Difference Vegetation Index (NDVI) | (Rouse;Haas & Schell 1974) | $\frac{\rho_{NIR} - \rho_{Red}}{\rho_{NIR} + \rho_{Red}}$ | 5.11 |
| Green Normalised Difference Vegetation Index (GNDVI) | (Gitelson; Kaufman & Merzlyak 1996) | $\frac{\rho_{NIR} - \rho_{Green}}{\rho_{NIR} + \rho_{Green}}$ | 5.12 |
| Enhanced Vegetation Index (EVI) | (Huete et al. 1997) | $2.5 \frac{\rho_{NIR} - \rho_{Red}}{\rho_{NIR} + 6\rho_{Red} - 7.5\rho_{Blue} + 1}$ | 5.13 |
| Atmospherically Resistant Vegetation Index (ARVI) | (Kaufman & Tanre 1992) | $\frac{\rho_{NIR} - (2\rho_{Red} - \rho_{Blue})}{\rho_{NIR} + (2\rho_{Red} - \rho_{Blue})}$ | 5.14 |
| Sum Green (SG) | (Gamon & Surfus 1999) | $\sum_{600nm}^{500nm} \rho_{Green}$ | 5.15 |
| NARROW-BAND VEGETATION INDICES | | | |
| GREENNESS / CHLOROPHYLL | | | |
| Pigment Specific Simple Ratio-Chla (PSSRa) | (Blackburn 1998a) | $\frac{\rho_{800}}{\rho_{680}}$ | 5.16 |
| Red-Edge Normalised Difference Index (NDVI ₇₀₅) | (Sims & Gamon 2002) | $\frac{\rho_{750} - \rho_{705}}{\rho_{750} + \rho_{705}}$ | 5.17 |
| Modified Red-Edge Simple Ratio (mSR ₇₀₅) | (Sims & Gamon 2002) | $\frac{\rho_{750} - \rho_{445}}{\rho_{705} + \rho_{445}}$ | 5.18 |
| Modified Red-Edge Normalised Difference Index (mNDVI ₇₀₅) | (Sims & Gamon 2002) | $\frac{\rho_{750} - \rho_{705}}{\rho_{750} + \rho_{705} + 2\rho_{445}}$ | 5.19 |
| Carter Index 2 (CTR2) | (Carter 1994) | $\frac{\rho_{695}}{\rho_{760}}$ | 5.20 |
| Lichtenthaler Index 1 (LIC1) or Pigment Specific Normalised Difference - Chla (PSNDa) | (Blackburn 1998a, Lichtenthaler et al. 1996) | $\frac{\rho_{800} - \rho_{680}}{\rho_{800} + \rho_{680}}$ | 5.21 |
| Optimised Soil-Adjusted Vegetation Index (OSAVI) | (Rondeaux; Steven & Baret 1996) | $1 + 0.16 \frac{\rho_{800} - \rho_{670}}{\rho_{800} - \rho_{670} + 0.16}$ | 5.22 |
| Modified Chlorophyll Absorption Ratio Index (MCARI) | (Daughtry et al. 2000) | $\frac{\rho_{700}}{\rho_{670}} [(\rho_{700} - \rho_{670}) - 0.2(\rho_{700} - \rho_{550})]$ | 5.23 |
| Ratio of derivatives at 725 and 702 nm (Der ₇₂₅₋₇₀₂) | (Smith; Steven & Colls 2004) | $\frac{dp/d\lambda_{725}}{dp/d\lambda_{702}}$ | 5.24 |

| | | | |
|--|---------------------------------------|---|------|
| Red-Edge Position (REP) | (Guyot;Baret & Major 1988) | $\rho_{re} = \frac{\rho_{670} + \rho_{780}}{2}$ $700 + 40 \frac{\rho_{re} - \rho_{700}}{\rho_{740} - \rho_{700}}$ | 5.25 |
| Vogelmann Red-Edge Index (VOG1) | (Vogelmann;Rock & Moss 1993) | $\frac{\rho_{740}}{\rho_{720}}$ | 5.26 |
| Chlorophyll Index (CI ₅₉₀) | (Gitelson&Merzlyak 1997) | $\frac{\rho_{880}}{\rho_{590}} - 1$ | 5.27 |
| MERIS Terrestrial Chlorophyll Index (MTCI) | (Curran&Dash 2005) | $\frac{\rho_{753.75} - \rho_{708.75}}{\rho_{708.75} - \rho_{681.25}}$ | 5.28 |
| OTHER PIGMENTS | | | |
| Structure Insensitive Pigment Index (SIPI) | (Penuelas et al. 1995) | $\frac{\rho_{800} - \rho_{445}}{\rho_{800} - \rho_{680}}$ | 5.29 |
| Red Green Ratio (RG) | (Gamon&Surfus 1999) | $\frac{\sum \rho_{Red}}{\sum \rho_{Green}}$ | 5.30 |
| Anthocyanin Reflectance Index 1 (ARI1) | (Gitelson;Merzlyak & Chivkunova 2001) | $\frac{1}{\rho_{550}} - \frac{1}{\rho_{700}}$ | 5.31 |
| Anthocyanin Reflectance Index 2 (ARI2) | (Gitelson;Merzlyak & Chivkunova 2001) | $\rho_{800} \left[\frac{1}{\rho_{550}} - \frac{1}{\rho_{700}} \right]$ | 5.32 |
| WATER INDICES | | | |
| Water Band Index (WBI) | (Peñuelas et al. 1997) | $\frac{\rho_{900}}{\rho_{970}}$ | 5.33 |
| Normalised Difference Water Index (NDWI) | (Gao 1996) | $\frac{\rho_{857} - \rho_{1241}}{\rho_{857} + \rho_{1241}}$ | 5.34 |
| Moisture Stress Index (MSI) | (Hunt Jr&Rock 1989b) | $\frac{\rho_{1599}}{\rho_{819}}$ | 5.35 |
| Normalised Difference Infrared Index (NDII) | (Hardisky;Klema s & Smart 1983) | $\frac{\rho_{819} - \rho_{1649}}{\rho_{819} + \rho_{1649}}$ | 5.36 |
| Normalised Heading Index (NHI) | (Pimstein et al. 2009) | $\frac{\rho_{1100} - \rho_{1200}}{\rho_{1100} + \rho_{1200}}$ | 5.37 |
| ρ = reflectance expressed in nanometres | | | |

Table 5.8 Description of the vegetation indices applied in this study

| INDEX | DESCRIPTION | RANGE |
|---------------------------------------|--|--|
| BROAD-BAND VEGETATION INDICES | | |
| SR | It is the ratio between the strong reflection in NIR by mesophyll tissue and the low reflection of red light produced by chlorophyll absorption. It is sensitive to LAI and biomass in high biomass vegetation such as forests. | 0 - 30 2 - 8 green vegetation |
| NDVI | Equivalent to SR index but the combination of its normalised differences reduces many forms of multiplicative noise (sun illumination, differences, cloud shadows, some atmospheric attenuation, and some topographic variation). | -1 to 1 0.2 to 0.8 green vegetation |
| GNDVI | Modification of NDVI apparently more sensitive at higher LAI, particularly good detecting chlorophyll as it increases over a much wider range of chlorophyll than does NDVI. | nd |
| EVI | Developed to improve NDVI index in high biomass regions by using the blue reflectance to correct for soil background and reduce atmospheric influences. | -1 to 1 0.2 to 0.8 green vegetation |
| ARVI | Less sensitive to atmospheric effects (example, aerosol) by normalising the radiance in the blue, red and NIR. It is more useful in regions of high atmospheric aerosol content, including tropical regions contaminated by soot from slash-and-burn agriculture. | -1 to 1 0.2 to 0.8 green vegetation |
| SG | It accounts for the reflected signal in the green region which is highly sensitive to small changes in vegetation canopy opening, such as forest disturbances. Increase SG values indicate less chlorophyll content and a reduced photosynthetic activity. | 0 to 50 10 to 25 green vegetation |
| NARROW-BAND VEGETATION INDICES | | |
| GREENNESS / CHLOROPHYLL | | |
| PSSRa | Good for estimating Chlorophyll a at leaf level. | nd |
| NDVI ₇₀₅ | Modification of NDVI by using bands along the red-edge, instead of the main absorption and reflectance peaks. It is highly sensitive to changes in canopy foliage content, gap fraction and senescence. Applications include forest monitoring, vegetation stress and precision agriculture. | -1 to 1 0.2 to 0.9 green vegetation |
| mSR ₇₀₅ | Modification of SR by using bands in the red-edge and a correction for leaf specular reflection. It is suitable for applications of forest monitoring and vegetation stress and precision agriculture. | 0 to 30 2 to 8 green vegetation |
| mNDVI ₇₀₅ | Modification of the NDVI ₇₀₅ by incorporating a correction of leaf specular reflection. The sensitivity of the red-edge is used to highlight small changes in canopy foliage content, gap fraction and senescence. | -1 to 1 0.2 to 0.7 green vegetation |

| | | |
|------------------------|---|--|
| CRT2 | Sensitive to vegetation stress in several plant species and stress agents. | nd |
| LIC1 or PSNDa | Sensitive to the red and far-red chlorophyll fluorescence providing information about environmental changes or a decline in photosynthetic quantum. | nd |
| OSAVI | Optimisation of the SAVI (Soil- Adjusted Vegetation Index) family which minimise the effects of different soil backgrounds highlighting vegetation vigour. | nd |
| MCARI | Modification of the Chlorophyll Absorption in Reflectance Index (CARI) for minimising the effects of nonphotosynthetic materials on the estimation of the absorbed photosynthetic active radiation. The MCARI index is the depth of the chlorophyll absorption at 670 nm relative to the reflectance at 550 nm and 700 nm. | nd |
| Der ₇₂₅₋₇₀₂ | Responds to natural gas contamination of soils. First derivative method | nd |
| REP | It estimates the point of maximum slope within the range 690 to 740 nm (linear model method). REP is strongly correlated to foliar chlorophyll content then it is sensitive to vegetation stress. Increased chlorophyll concentration moves the red-edge to longer wavelengths. Applications include photosynthesis modelling, canopy stress, ecosystems disturbance detection, yield production (Clevers&Jongschaap 2006). | 700 to 730 nm green vegetation |
| VOG1 | It is sensitive to the combined effects of foliage chlorophyll concentration, canopy leaf area, and water content. Applications include vegetation phenology, vegetation productivity modelling, precision agriculture. | 0 to 20 4 to 8 green vegetation |
| CI ₅₉₀ | More sensitive to canopy Nitrogen status than is NDVI. | nd |
| MTCI | Sensitive to a wide range of chlorophyll contents. It is independent of soil-atmospheric conditions, spatial resolution, illumination and observation geometry. | nd |
| OTHER PIGMENTS | | |
| SIPI | Sensitive to the ratio of bulk carotenoids (alpha carotene and beta-carotene) to chlorophyll while decreasing sensitivity to variation in canopy structure (LAI). Increase in SIPI is an indicator of canopy stress (carotenoid pigment). | 0 to 2 0.8 to 1.8 green vegetation |
| RG | Sensitive to the ratio of leaf redness caused by anthocyanin to chlorophyll. It has been used to estimate the course of foliage development in canopies and is an indicator of leaf production and stress. | 0.1 to 8 0.7 to 3 |
| ARI1 | Sensitive to anthocyanins. Increase values indicate canopy changes in foliage via new growth or death. | 0 to 0.2 0.001 to 0.1 green vegetation |
| ARI2 | Modification of ARI1. This index detects higher concentrations of anthocyanins in vegetation. | 0 to 0.2 0.001 to 0.1 green vegetation |
| WATER INDICES | | |

| | | |
|------|--|---|
| WBI | Sensitive to changes in canopy water status. As the water content increases, the strength of absorption around 970 nm increases relative to that of 900 nm. | 0.8 to 1.2 |
| NDWI | Sensitive to changes in canopy water status. Reflectance at 857 nm and 1241 nm has slightly different liquid water absorption properties. The scattering of light by vegetation canopies enhances the weak absorption at 1241 nm. | -1 to 1 -0.1 to 0.4 green vegetation |
| MSI | As the water content of leaves increases, the strength of the absorption around 1599 nm increases. Absorption at 819 nm used as reference is unaffected by changes in water. Higher values indicate greater water stress and less water content. | 0 to 3 0.4 to 2 green vegetation |
| NDII | Uses a normalised relationship instead of a simple ratio. The index values increase with increasing water content. | -1 to 1 0.02 to 0.6 |
| NHI | Respond to heading in wheat, with values >0.18 indicating spike emergency. | nd |

5.2.6 Exploring new vegetation indices for detecting hydrocarbon pollution in the tropical rainforest

The methodology of this section is based on the studies presented by (Inoue et al. 2012, Stratoulas et al. in press). Two types of spectral indices (SIs) approaches are applied in this study to explore the suitable band combination of hyperspectral data to detect changes in biophysical and biochemical parameters of vegetation affected by hydrocarbon pollution in the tropical forest. The first approach considers a Ratio Spectral Index (RSI):

$$RSI = \frac{R_i}{R_j}$$

Where R_i and R_j are the reflectance response for bands i and j respectively. The second approach explores a Normalised Difference Spectral Index (NDSI) which is effective in reducing the influence of errors or uncertainty due to sensor specifications, atmospheric and background differences. NDVI is a widely used normalised vegetation index applied for studies of plant growth, vegetation cover, biomass and vegetation vigour. It is defined by:

$$\text{NDSI} = \frac{R_i - R_j}{R_i + R_j}$$

RSI and NDSI were estimated from reflectance samples collected at leaf level and correlated with biophysical and biochemical parameters from the same leaves. The parameters considered are: a) chlorophyll content estimated from the SPAD-502 readings (Chapter 3), b) Chlorophyll content derived from the inversion of the PROSPECT model, c) foliar water content and d) foliar organic matter content. The approach computes the coefficient of determination (R^2) for all possible combinations of available bands and the corresponding plant parameters. The computational process used an R programming language (R Core Team) generated by Stroulia et al. (in press). In order to reduce the computer processing time, a subset of 127 foliar samples were selected, which represent a multispecies tropical rainforest of the Amazon region. For each sample, reflectance signal at leaf level was averaged every three channels. Results are presented as raster maps of coefficient of determination (R^2) between the SIs and specific biophysical and biochemical parameters of vegetation.

5.3 Results

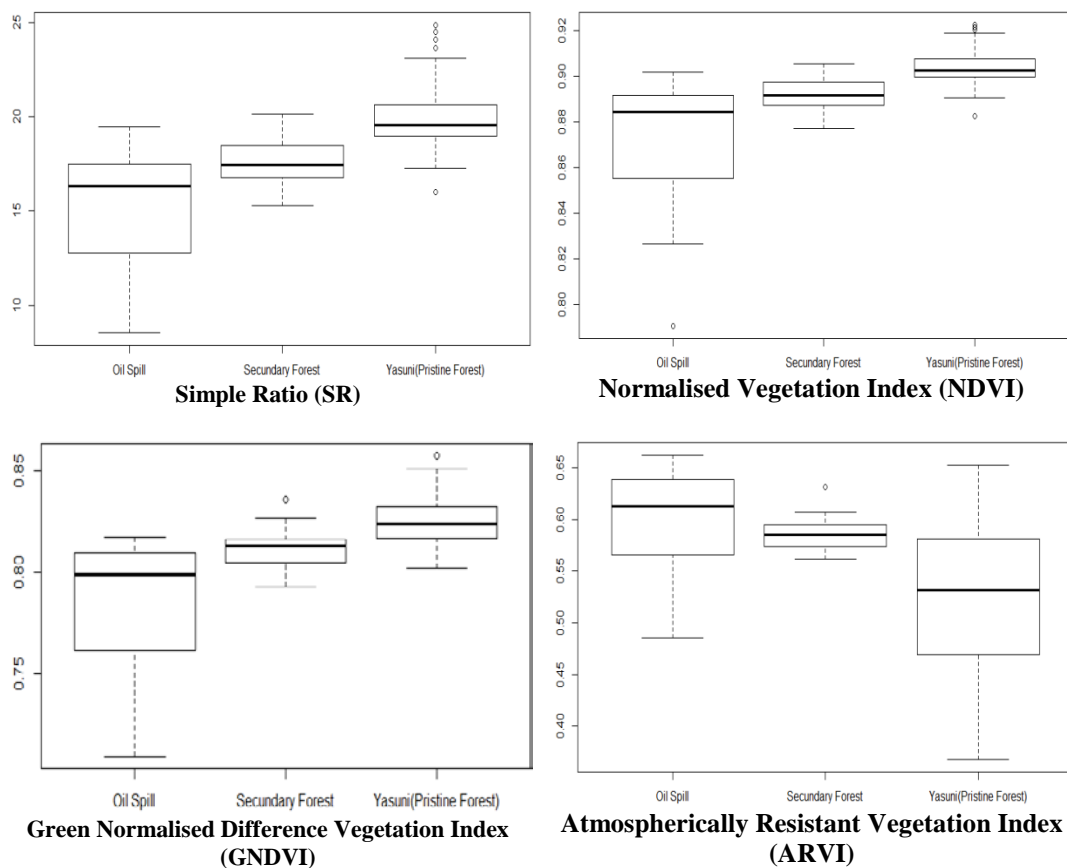
Sampled areas during the fieldwork campaign were used to define a region of interest in the Hyperion images from where statistics are derived. Figure 5.3 illustrates details of the sampled areas in the secondary forest of the petroleum productive area where polluted and non-polluted sites were considered. The region of interest for the pristine forest is defined in Figure 5.1.

5.3.1 Broad-band Indices

Figure 5.22 illustrates the boxplots for vegetation broad-band indices related to the three study sites. SR, NDVI and GNDVI indices show lowest values for the area affected by the oil spill, followed by the secondary forest area. Those two areas are located close each other, around 400 meters away (Chapter 3, section 3.2.1) and share the same environmental conditions and vegetation characteristics. The only difference between them is the influence of petroleum pollution in the

first one; therefore the differences between the oil spill and the secondary forest (not affected by hydrocarbons) can only be attributed to the effects of hydrocarbon pollution on the biophysical and biochemical parameters of vegetation. As expected, pristine forest presents the highest values for those three indices which suggest their sensitivity to discriminate between the secondary and pristine forest.

Vegetation indices which use the blue range of the spectrum (EVI and ARVI) to reduce atmospheric effects also clearly discriminate between the secondary and pristine forest, showing lower values for pristine forest. This behaviour can be explained by the extremely low reflectance signal in the blue range of the Hyperion image (see Figure 5.10).



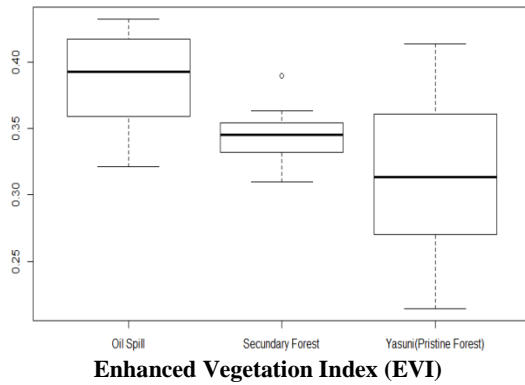
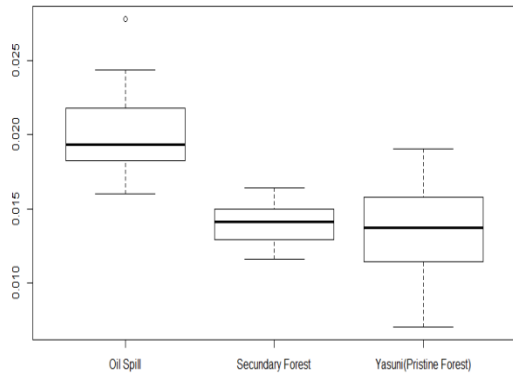


Figure 5.22. Box plots of the calculated Broad-band vegetation indices

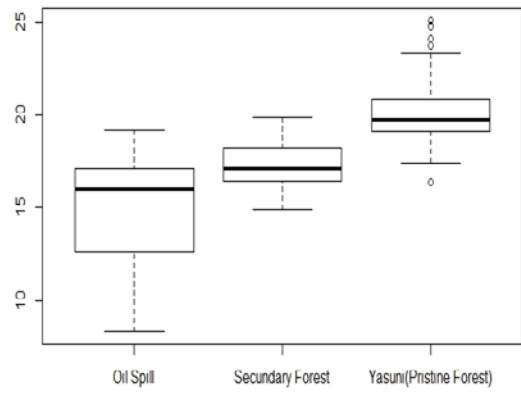
5.3.2 Narrow-band-greenness/chlorophyll

Figure 5.23 presents the boxplots of narrow-band indices. The SG index displays a large difference between the polluted sites compared to the two other sites. This index accounts for the energy which is not absorbed by the vegetation in the green range of the spectrum. Higher SG values indicate less chlorophyll content and a reduced photosynthetic activity which suggests reduced levels of chlorophyll content in the site affected by hydrocarbon pollution as reported in the results of Chapter 4.

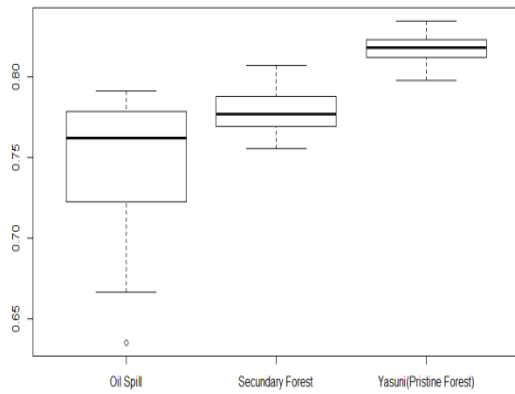
PSSRa and NDVI₇₀₅ clearly discriminate between the higher levels of chlorophyll contents in the pristine forest site and lower chlorophyll content in the site affected by hydrocarbons. Boxplots for mSR₇₀₅ and mNDVI₇₀₅ do not exhibit sensitivity to the effects of the hydrocarbon pollution site compared to the non-polluted secondary forest site. The explanation for this fact is that those indices use R₄₄₅ of the Hyperion image which has extremely low values in this spectral range.



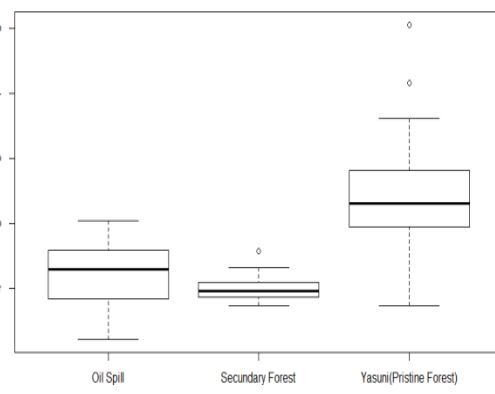
Sum Green Vegetation Index (SG)



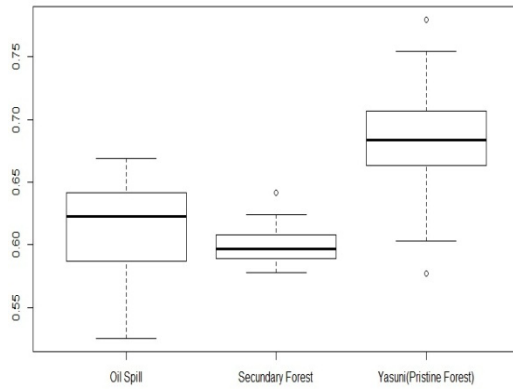
Pigment Specific Simple Ratio (PSSRa)



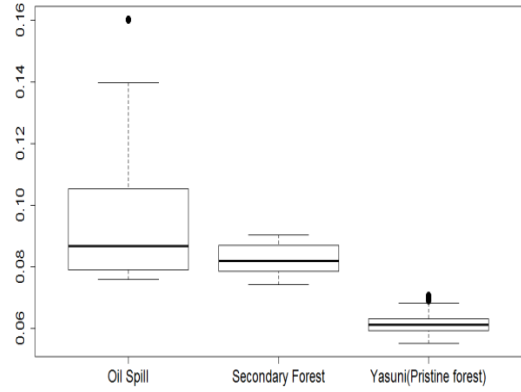
Red-Edge NDVI (NDVI₇₀₅)



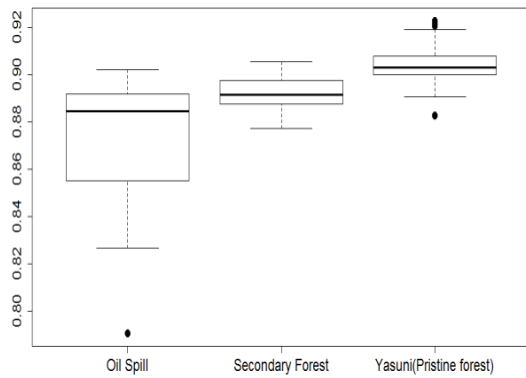
Modified Red-Edge Simple Ratio (mSR₇₀₅)



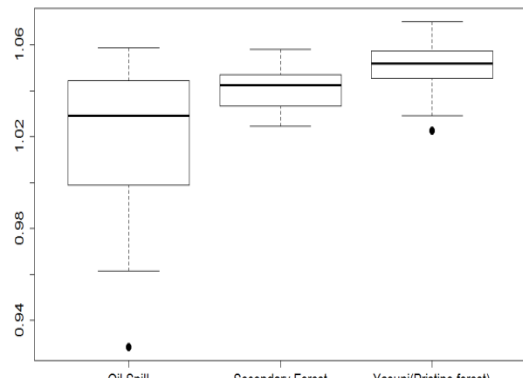
Modified Red-Edge Normalised Difference Index (mNDVI₇₀₅)



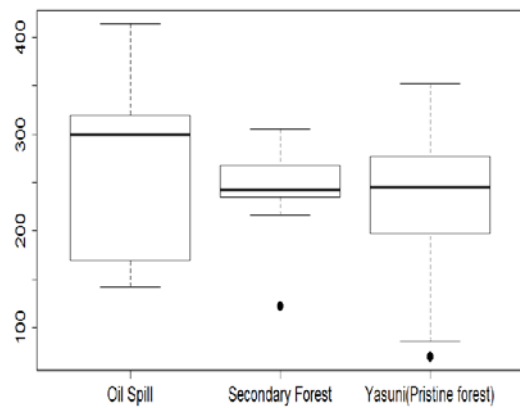
Carter Index 2 (CTR2)



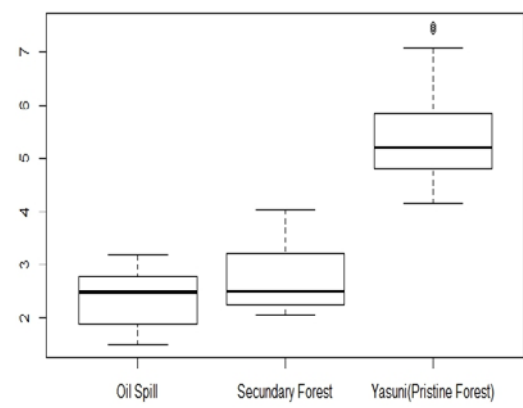
Lichtenthaler Index 1 (LIC1) or Pigment Specific Normalized Difference (PSNDa)



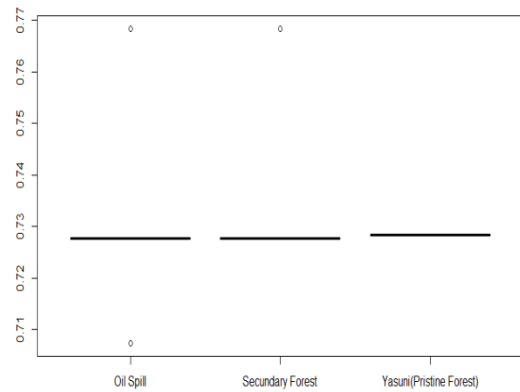
Optimised Soil-Adjusted Vegetation Index (OSAVI)



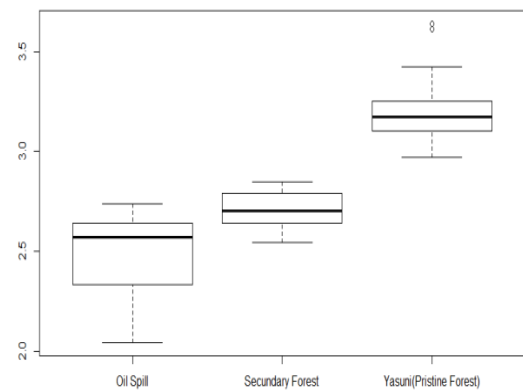
Modified Chlorophyll Absorption Ratio Index (MCARI)



Ratio of Derivatives (Der_725-702) (first derivative)



Red-Edge Position (REP-linear model method)



Vogelmann Red-Edge Index (VOG1)

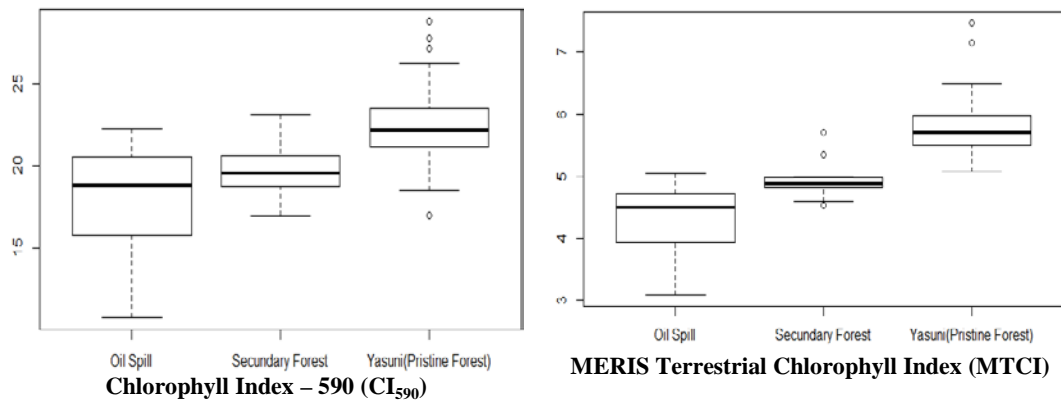


Figure 5.23. Box plots of the calculated Narrow-Band Vegetation Indices: Greenness / Chlorophyll

Five of the six narrow band vegetation indices (NDVI705, MNDVI705, CTR2, LIC1, OSAVI) which best detected vegetation affected by hydrocarbons in the study of Noomen et al (2008) also clearly discriminate between the three study sites in this study. LIC3 (Lichtenthaler 3 = R_{440}/R_{740}) was not applied in this study since reflectance in the blue range is extremely low for the Hyperion image.

MCARI index was also calculated in our study sites but it could not show differences between our study areas (see boxplot in Figure 5.23).

The REP position was determined by computing the ratio of the first derivatives at 725 nm and 702 nm ($Der_{725-702}$). Figure 5.23 shows the boxplot of the index which clearly discriminates between the very dense pristine forest and secondary forest sites but is unable to discriminate between the oil spill site and non-polluted secondary forest site.

The results of the REP calculated by the linera model method for the three study sites do not show sensitivity to detect vegetation stress (see Figure 5.23). Indeed, the REP is not an accurate indicator of chlorophyll content at high levels because of the asymptotic relationship between REP and chlorophyll content (Jago;Cutler & Curran 1999, Munden;Curran & Catt 1994).

Vogelmann et al. (1993) developed three vegetation indices related to the relationship of the REP and foliar chlorophyll content. The results exhibited by the three indices were highly correlated with variation of total chlorophyll content. In this study one of those indices (VOG1) was applied as a reference. Its boxplot shows the ability of the index to differentiate between the site affected by the oil spill and the secondary forest.

CI₅₉₀ is a modification of the original chlorophyll index developed by Gitelson and Merzlyak (1997) since reflectance at 590 nm is now used in preference to the original reflectance at 540 nm (Jones&Vaughan 2010). The boxplot for this index illustrates a good discrimination between the study sites.

MERIS Terrestrial Chlorophyll Index (MTCI) uses data in three red/NIR wavelengths centred at 681.25, 708.75 and 753.75 (bands 8, 9 and 10 of the MERIS-ENVISAT instrument) in order to detect chlorophyll content at a global scale. MTCI has shown a better sensitivity to chlorophyll content variation than SR, NDVI and REP indices. The boxplot associated with MERIS in Figure 5.23 shows the ability of the index to differentiate our three study sites.

5.3.3 Other pigments indices

The first two indices (SIPI and RG) are related to carotenoid and the other two (ARI1 and ARI2) are related to anthocyanin pigments. The corresponding boxplots shown in Figure 5.24 illustrate lower values for the pristine forest site and higher values for the secondary forest site. It is not clear how carotenoids and anthocyanin pigments may vary in vegetation from the tropical forest, nor the behaviour of those pigments in areas affected by hydrocarbons. More research is needed in this subject.

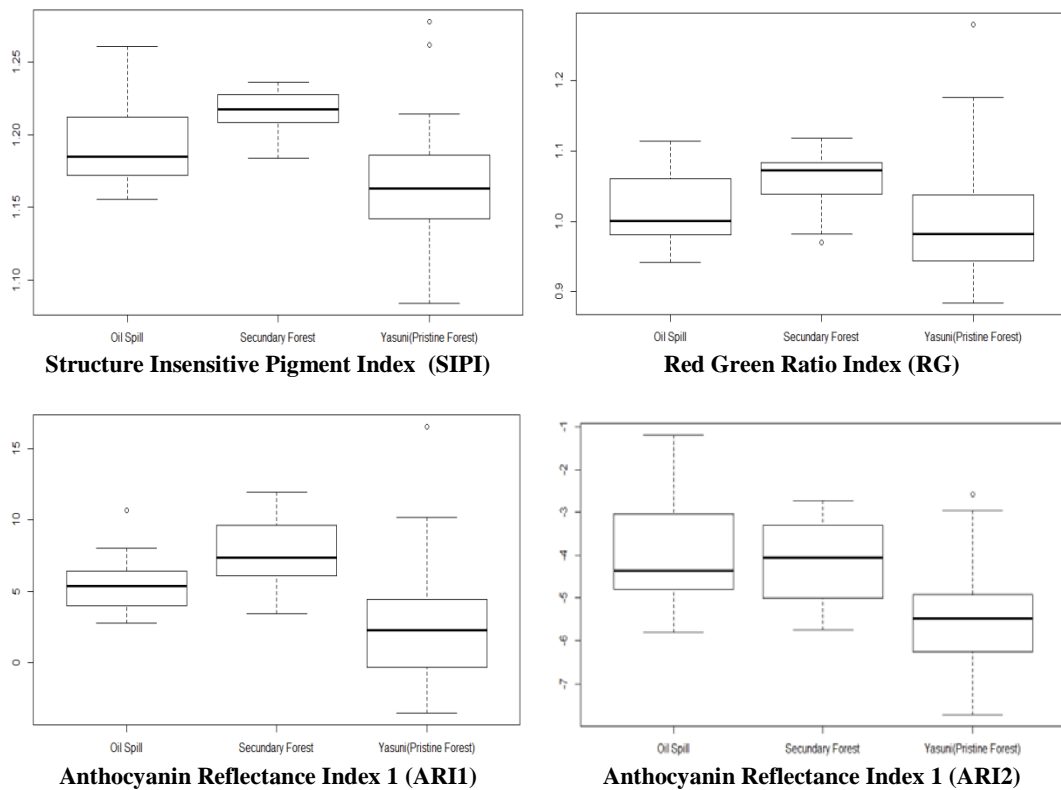


Figure 5.24. Box plots of the calculated Narrow-Band Vegetation Indices: Other pigments

5.3.4 Water indices

According to the results of Chapter 4, vegetation affected by hydrocarbon pollution showed increased levels of foliar water content which in turn can be related to the thicker leaves found in the polluted site.

Vegetation indices for foliar water content are based on the near to mid-infrared regions where there are strong water-absorption features (see Figure 5.6 for details of the water absorption features) and the lower signal-to-noise-ratio is reported for the Hyperion images (see Table 5.3 and Figure 5.7). Figure 5.25 demonstrates the boxplots resulting from several water indices applied to the Hyperion images in the three study sites. There is not a clear discrimination of foliar water content between sites; moreover there is contradiction between the estimate indices.

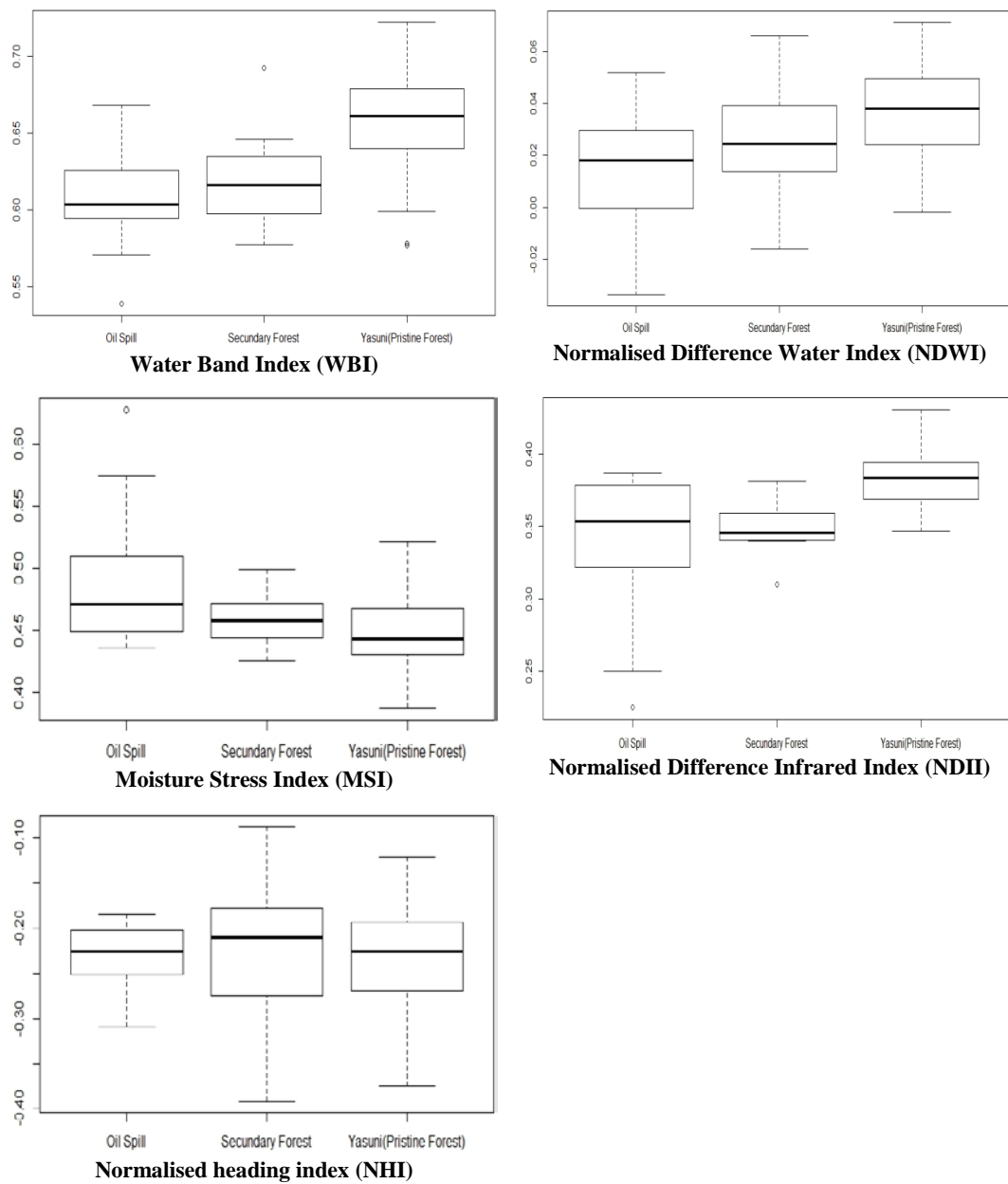


Figure 5.25. Box plots of the calculated Narrow-Band Vegetation Indices: Water Indices

Annex 15, Annex 16 and Annex 17 present the descriptive statistics for each vegetation index applied and for each study site.

5.3.5 Vegetation indices suitable to detect hydrocarbon pollution

In order to understand how significant the results from the vegetation indices are, analysis of variance of means considering the three study sites was conducted by

an ANOVA test. Table 5.9 exhibits the results of the ANOVA test which illustrates a strong significant difference for most vegetation indices.

Table 5.9 ANOVA comparison of means and significance

| | INDEX | | ANOVA | Significance |
|--|--|------------------------|----------|--------------|
| BROAD-BAND VEGETATION INDICES | | | | |
| 1 | Simple Ratio | SR | 2.19E-15 | *** |
| 2 | Normalized Difference Vegetation | NDVI | 4.42E-14 | *** |
| 3 | Green Normalized Difference Vegetation Index | GNDVI | 5.09E-15 | *** |
| 4 | Atmospherically Resistant Vegetation Index | ARVI | 2.81E-07 | *** |
| 5 | Enhanced Vegetation Index | EVI | 2.26E-09 | *** |
| NARROW-BAND VEGETATION INDICES: Greenness / Chlorophyll / REP | | | | |
| 6 | Sum Green | SG | 7.09E-15 | *** |
| 7 | Pigment Specific Simple Ratio-Chla | PSSRa | <2e-16 | *** |
| 8 | Red Edge Normalized Difference Index | NDVI ₇₀₅ | <2e-16 | *** |
| 9 | Modified Red Edge Simple Ratio | mSR ₇₀₅ | <2e-16 | *** |
| 10 | Modified Red Edge Normalized Difference Index | mNDVI ₇₀₅ | <2e-16 | *** |
| 11 | Carter Index 2 | CRT2 | <2e-16 | *** |
| 12 | Lichtenthaler Index 1/Pigment Specific Normalized Difference | LIC1/PSNDa | 4.42E-14 | *** |
| 13 | Optimized Soil-Adjusted Vegetation Index | OSAVI | 1.35E-10 | *** |
| 14 | Modified Chlorophyll Absorption Ratio Index | MCARI | 2.16E-01 | ns |
| 15 | Ratio of derivatives at 725 and 702 nm | Der ₇₂₅₋₇₀₂ | <2e-16 | *** |
| 16 | Red Edge Position | REP | 5.05E-03 | ** |
| 17 | Vogelmann Red Edge Index | VOG1 | <2e-16 | *** |
| 18 | Chlorophyll Index | CI ₅₉₀ | 1.77E-12 | *** |
| 19 | MERIS Terrestrial Chlorophyll Index | MTCI | <2e-16 | *** |
| NARROW-BAND VEGETATION INDICES: Other Pigments | | | | |
| 20 | Structure Insensitive Pigment Index | SIPI | 1.56E-08 | *** |
| 21 | Red Green Ratio | RG | 3.57E-03 | ** |
| 22 | Anthocyanin Reflectance Index 1 | ARI1 | 5.15E-08 | *** |
| 23 | Anthocyanin Reflectance Index 2 | ARI2 | 6.59E-08 | *** |
| NARROW-BAND VEGETATION INDICES: Water Indices | | | | |
| 24 | Water Band Index | WBI | 3.66E-11 | *** |
| 25 | Normalized Difference Water Index | NDWI | 5.92E-06 | *** |
| 26 | Moisture Stress Index | MSI | 1.44E-05 | *** |
| 27 | Normalized Difference Infrared Index | NDII | 1.32E-08 | *** |
| 28 | Normalized Heading Index | NHI | 5.42E-01 | ns |

*** Strongly significant (0.1%)

** Highly significant (1%)

ns No significant

Differences explained by MCARI and NHI are not significant. REP and RG show high significant (99%) differences, meanwhile the rest of the vegetation indices illustrated strongly (99.9%) significant differences which means that vegetation indices are able to discriminate between the three study sites.

The interest of this research is to identify vegetation indices which are able to detect vegetation stress in areas affected by hydrocarbon pollution, and then a post-hoc pairwise comparison was performed after significant differences were found by the ANOVA. The pair-wise comparison of means using the adjustment method of Holm displays significant differences between the three study sites: the secondary forest affected by oil spill, the secondary forest not affected by oil spill and the pristine forest (see Table 5.10).

Most indices were able to discriminate between the two most dissimilar sites in terms of forest structure, plant species and conservation: oil spill and pristine forest (second column) where the differences are strongly significant (99.9%) for most of them. Differences between MCARI and NHI were no significant. Furthermore the comparison between the secondary forest (not affected by oil spill) and the pristine forest (last column) were also identified as strongly (99.9%) and highly (99.0%) significant. These results clearly proved the ability of the chosen vegetation indices to discriminate between the secondary and pristine forest.

Table 5.10 Analysis of variance and pairwise comparison of means using Holm adjustment method for the study sites (oil pollution, secondary forest and pristine forest)

| | INDEX | | Oil Spill vs. Secondary forest | Oil Spill vs. Pristine forest (Yasuni) | Secondary forest vs. Pristine forest (Yasuni) |
|--|--|------------------------|--------------------------------|--|---|
| BROAD-BAND VEGETATION INDICES | | | | | |
| 1 | Simple Ratio | SR | *** | *** | *** |
| 2 | Normalized Difference Vegetation | NDVI | *** | *** | ** |
| 3 | Green Normalized Difference Vegetation Index | GNDVI | *** | *** | ** |
| 4 | Atmospherically Resistant Vegetation Index | ARVI | ns | *** | *** |
| 5 | Enhanced Vegetation Index | EVI | ** | *** | * |
| NARROW-BAND VEGETATION INDICES: Greenness / Chlorophyll / REP | | | | | |
| 6 | Sum Green | SG | *** | *** | ns |
| 7 | Pigment Specific Simple Ratio-Chla | PSSRa | *** | *** | *** |
| 8 | Red Edge Normalized Difference Index | NDVI ₇₀₅ | *** | *** | *** |
| 9 | Modified Red Edge Simple Ratio | mSR ₇₀₅ | ns | *** | *** |
| 10 | Modified Red Edge Normalized Difference Index | mNDVI ₇₀₅ | ns | *** | *** |
| 11 | Carter Index 2 | CRT2 | *** | *** | *** |
| 12 | Lichtenthaler Index 1/Pigment Specific Normalized Difference | LIC1/PSNDa | *** | *** | ** |
| 13 | Optimized Soil-Adjusted Vegetation Index | OSAVI | *** | *** | * |
| 14 | Modified Chlorophyll Absorption Ratio Index | MCARI | ns | ns | ns |
| 15 | Ratio of derivatives at 725 and 702 nm | Der ₇₂₅₋₇₀₂ | ns | *** | *** |
| 16 | Red Edge Position | REP | ** | ns | ** |
| 17 | Vogelmann Red Edge Index | VOG1 | *** | *** | *** |
| 18 | Chlorophyll Index | CI ₅₉₀ | * | *** | *** |
| 19 | MERIS Terrestrial Chlorophyll Index | MTCI | *** | *** | *** |
| NARROW-BAND VEGETATION INDICES: Other Pigments | | | | | |
| 20 | Structure Insensitive Pigment Index | SIP1 | * | *** | *** |
| 21 | Red Green Ratio | RG | ns | ns | ** |
| 22 | Anthocyanin Reflectance Index 1 | ARI1 | * | ** | *** |
| 23 | Anthocyanin Reflectance Index 2 | ARI2 | ns | *** | *** |
| NARROW-BAND VEGETATION INDICES: Water Indices | | | | | |
| 24 | Water Band Index | WBI | ns | *** | *** |
| 25 | Normalized Difference Water Index | NDWI | . | *** | * |
| 26 | Moisture Stress Index | MSI | * | *** | ns |
| 27 | Normalized Difference Infrared Index | NDII | ns | *** | *** |
| 28 | Normalized Heading Index | NHI | ns | ns | ns |

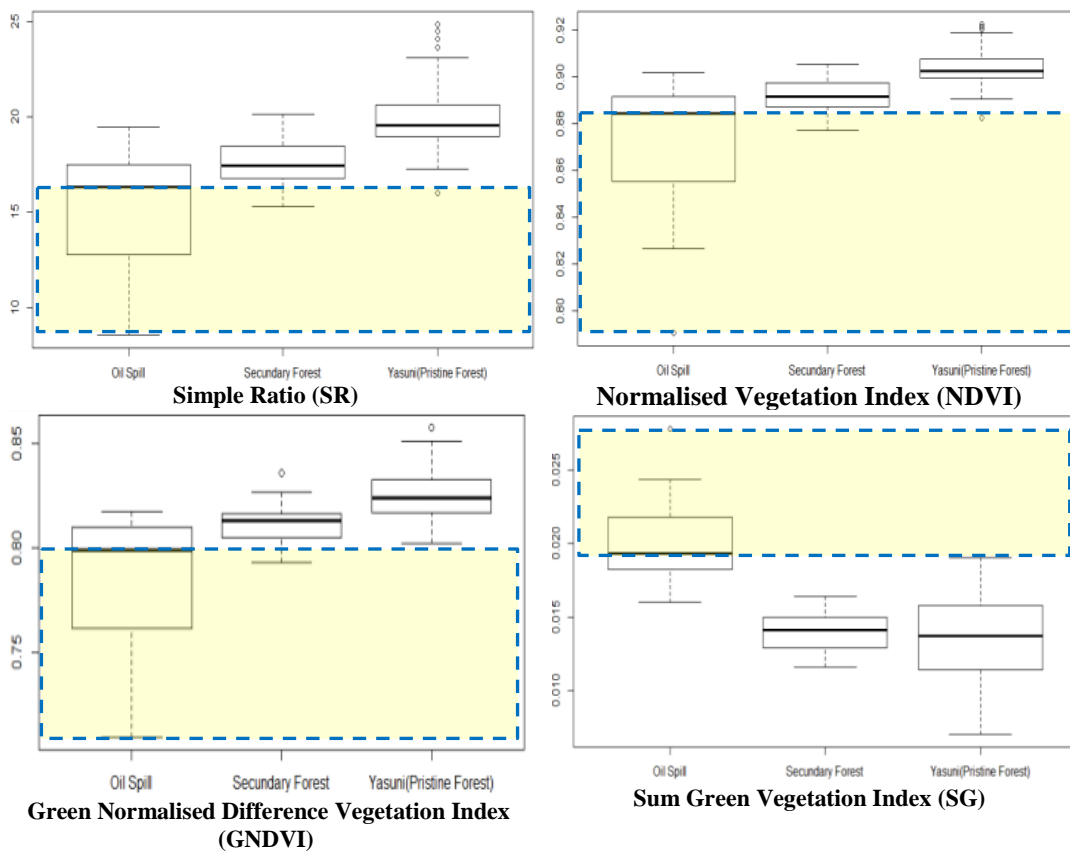
*** Strongly significant (0.1%)
 ** Highly significant (1%)
 * Significant(5%)
 . Lowest significant (10%)
 ns No significant

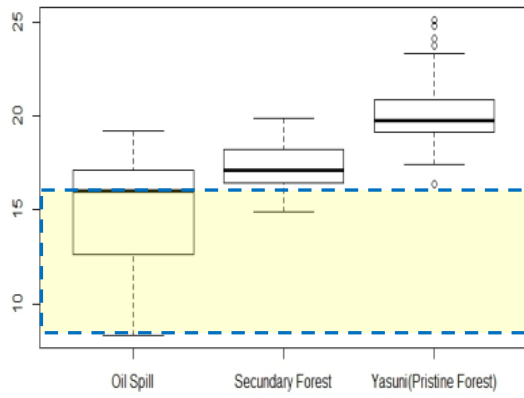
Eleven vegetation indices were able to discriminate as strongly significant (99.9%) the difference between the two sampled secondary forests (oil spill and secondary forest), all of them corresponding to broad-band indices and narrow-band-greenness-chlorophyll-red-edge index groups. Lower and no-significance were found in indices grouped under other pigments and water indices. As mentioned in Chapter 4, these two forests are located close to each other (400 meters away) and share the same environmental conditions and vegetation characteristics. The only difference between them is the influence of petroleum

pollution in the first one, therefore the differences between the oil spill and secondary forest (not affected by hydrocarbons) can only be attributed to the effects of hydrocarbon pollution on the biophysical and biochemical parameters of vegetation.

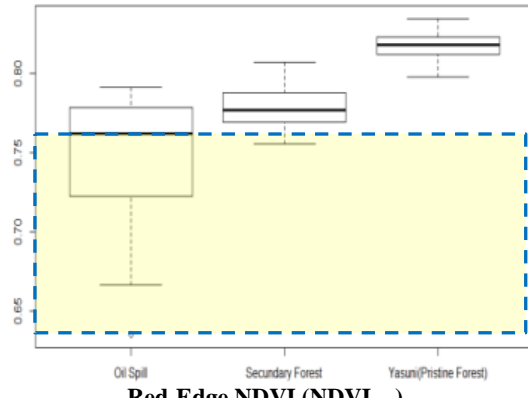
5.3.6 Mapping vegetation stress

Based on the ability of the 11 vegetation indices to discriminate the area affected by hydrocarbons and the secondary forest not polluted, threshold values were defined for every vegetation index based on the median and the min /max value which better characterise the area affected by oil spill. Figure 5.26 illustrates the threshold range for every vegetation index and Table 5.11 details the threshold values for each selected index.

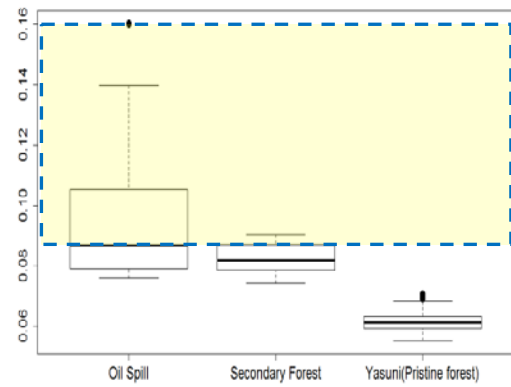




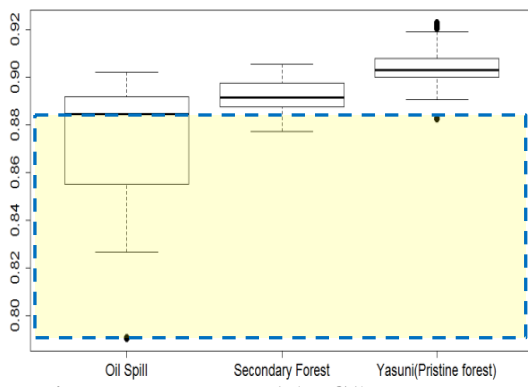
Pigment Specific Simple Ratio (PSSRa)



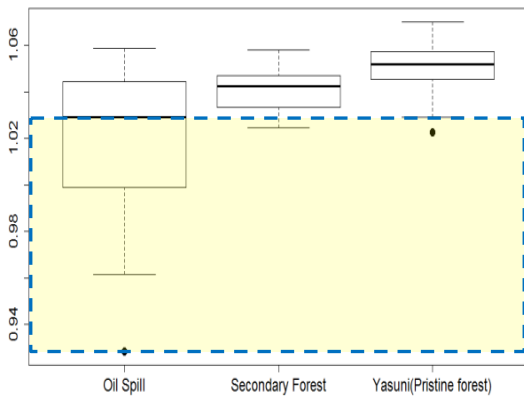
Red-Edge NDVI (NDVI₇₀₅)



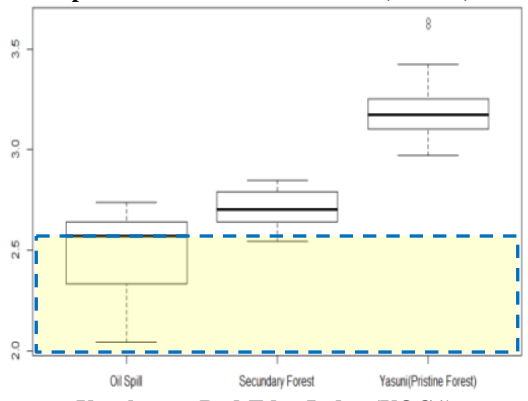
Carter Index 2 (CTR2)



Lichtenthaler Index 1 (LIC1) or Pigment Specific Normalised Difference (PSNDa)



Optimised Soil-Adjusted Vegetation Index (OSAVI)



Vogelmann Red-Edge Index (VOG1)

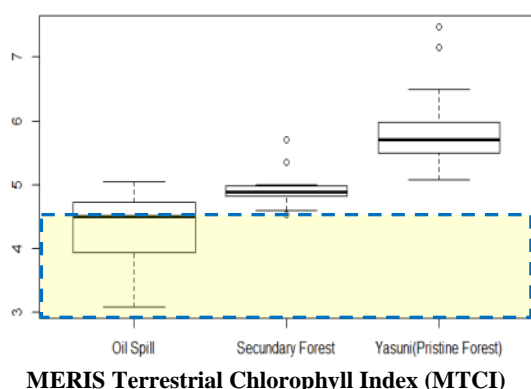


Figure 5.26. Boxplots of selected vegetation indices highlighting the threshold (yellow area) defined by the median and the min/max values of the oil-spill site.

Based on the defined threshold values, a mask was created for each selected vegetation index. A value of 1 was assigned if the pixel value is inside the threshold range, otherwise 0 (zero). Finally, an image of vegetation stress was computed by summing the masks of the selected vegetation indices. If a pixel value in the resulting image has a value of 11 it means that all vegetation indices detected that pixel as vegetation stress; on the other hand if the pixel value is 0 (zero) then it means that none of the indices detected that specific pixel as vegetation stress. Figure 5.27 illustrates the results of the areas detected as vegetation stress based on the selected vegetation indices.

Table 5.11. Threshold values defined for selected vegetation indices in the area affected by hydrocarbon pollution

| Index | Median | Min/Max value |
|---------------------|---------|---------------|
| SR | 16.3065 | 8.5502 (min.) |
| NDVI | 0.8844 | 0.7906 (min.) |
| GNDVI | 0.7987 | 0.7096 (min.) |
| SG | 0.0193 | 0.0278 (max.) |
| PSSRa | 16.0014 | 8.3391 (min.) |
| NDVI ₇₀₅ | 0.7620 | 0.6351 (min.) |
| CTR2 | 0.08669 | 0.1603 (max.) |
| LIC1 | 0.8844 | 0.7906 (min.) |
| OSAVI | 1.0290 | 0.9284 (min.) |
| VOG1 | 2.5724 | 2.0433 (min.) |
| MTCI | 4.4889 | 3.0824 (min.) |

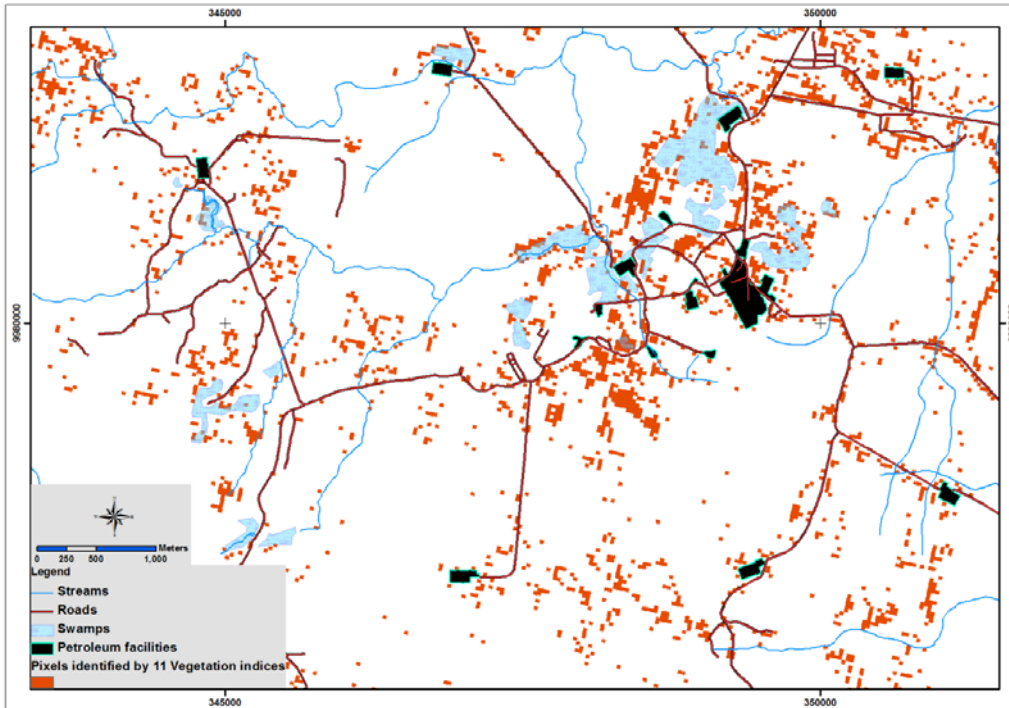


Figure 5.27. Areas identified as vegetation stress based on the eleven vegetation indices (orange)

A discriminant function analysis was computed to identify the differences between sites on the basis of the 11 vegetation indices and investigate which vegetation index contributes most to the group's separation. Figure 5.28 shows the first and second linear discrimination plot which illustrate a clear differentiation between sites based on the selected vegetation indices.

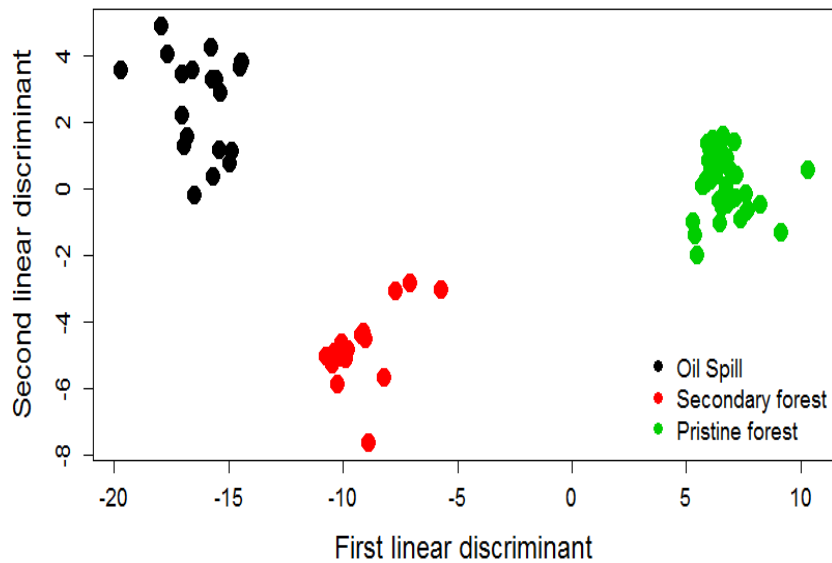


Figure 5.28. Discriminant function analysis results applied to the three study sites based on the selected vegetation indices.

Table 5.12 displays the coefficients of linear discriminants LD1 and LD2 for each vegetation indices which explains 95% and 5% of the variance between and within sites respectively (trace proportion) and 69 and 16 standard deviations on the linear discriminant variables (eigenvalues). According to the relative weight of the linear discriminant 1 (LD1), SG index has the strongest contribution to the group separation (53%) followed by NDVI index (21.6%) and NDVI₇₀₅ (8.4%). These three indices represent 83% of the group separation which can be explained by the fact that high values of SG index is an indicator of lower chlorophyll content and a reduced photosynthetic activity. On the other hand, high values of NDVI are sensitive to high LAI and biomass.

Following the same approach, detection of vegetation stress was applied based on the results of the discriminant function analysis using the first three indices (SG, NDVI and NDVI₇₀₅) which explain 83% of the sites separability (see results in Figure 5.29).

Table 5.12. Results of discrimination function analysis

| Vegetation indices | LD1 | LD2 | Relative weight (LD1) |
|-----------------------------|------------|------------|------------------------------|
| SG | 592.0 | -735.9 | 53.0% |
| NDVI | -241.2 | 115.5 | 21.6% |
| NDVI ₇₀₅ | 94.1 | 18.7 | 8.4% |
| CTR2 | 51.7 | -23.7 | 4.6% |
| GNDVI | -51.1 | -146.7 | 4.6% |
| LIC1 | 39.3 | 5.9 | 3.5% |
| VOG1 | 27.4 | 24.5 | 2.4% |
| OSAVI | -9.8 | -22.6 | 0.9% |
| MTCI | -3.7 | -4.8 | 0.3% |
| PSSRa | 3.5 | 1.9 | 0.3% |
| SR | -2.6 | -3.2 | 0.2% |
| Trace proportion (variance) | 95.0% | 5.0% | |
| Eigenvalues | 69.3 | 16.0 | |

Vegetation stress caused by hydrocarbon pollution detected by both approaches (11 and three indices) illustrates a very close agreement. A greater number of pixels were identified as stressed by the three indices which can be explained by their contribution to the sites separability (83%).

The results from this approach indicate the potential of using a combination of few multispectral and hyperspectral vegetation indices to map plant stress in areas potentially affected by hydrocarbons. In this study, vegetation stress detected by three indices provides similar results than using a combination of 11 indices. The selection of indices is based on their contribution to the site separability and to their ability to highlight lower levels of photosynthetic pigments, in particular chlorophyll (SG index) and dense vegetation with high LAI (NDVI) characteristic of tropical forest environments.

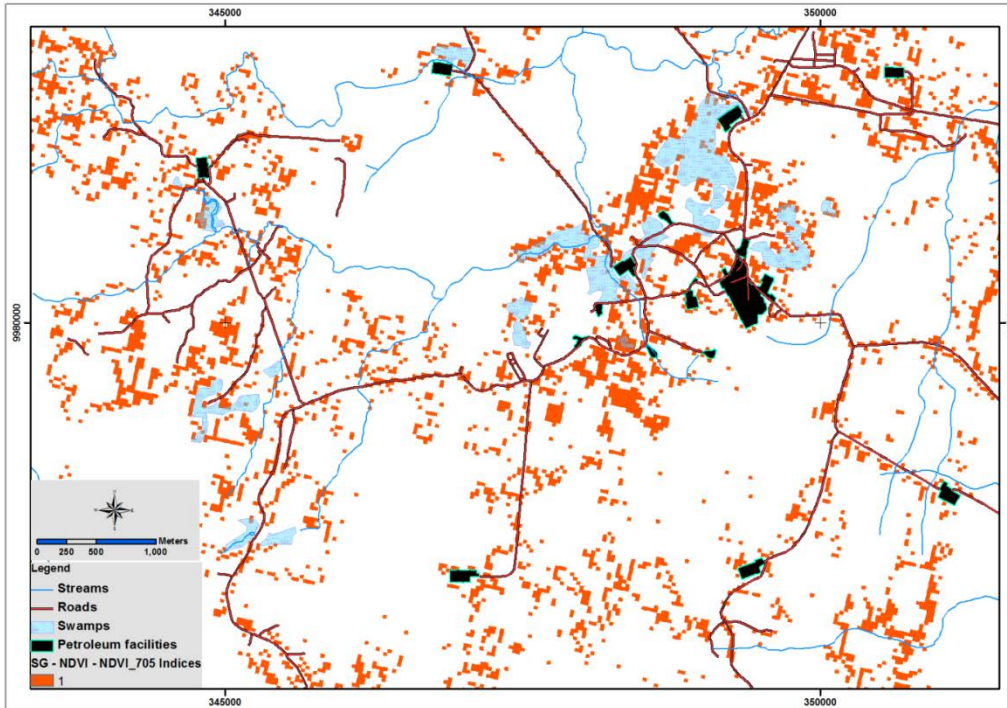


Figure 5.29. Areas identified as vegetation stress based on the SG, NDVI and NDVI₇₀₅ indices which together contribute to 83% of the site separability

Based on the results, this approach was applied to an area which historically has been exposed to hydrocarbons. The Pungarayacu study site is a hydrocarbon seepages and active source of hydrocarbons into the soil as was reported in this research (see Chapter 1, section 1.2.2 and 1.2.5 and Chapter 4, section 4.1.1). SG, NDVI and NDVI₇₀₅ indices were calculated using a CHRIS-Proba satellite image and masked according to the threshold values defined on Table 5.11 for the corresponding indices. Figure 5.30 show the areas (in red) detected as vegetation stress where hydrocarbons exposed to the surface may be affecting the surrounding vegetation.

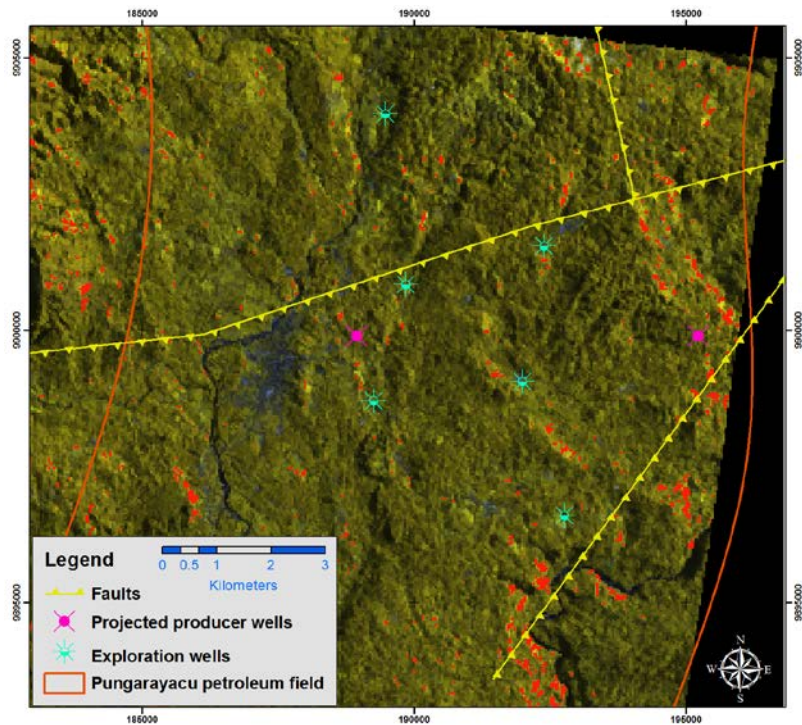


Figure 5.30 Results of vegetation stress detection in Pungarayacu site using a CHRIS-Proba image. The red areas correspond to pixels detected as vegetation stress based on the proposed approach

The selected pixels represent dense vegetation with high LAI, detected by the two thresholds of NDVI. Those pixels have the highest reflectance values in the green range of the spectrum, characteristic of low levels of chlorophyll content detected by SG index. Figure 5.30 displays information of petroleum exploration activities in the area which include exploration wells, producing wells and geological faults from seismic projects. The average depth of the exploration wells drilled in the Pungarayacu field is 220 meters deep (Ministerio de Energia y Minas 2002) which confirms the shallow location of petroleum reservoirs.

Unfortunately, it is not possible to assess the accuracy of the results in the Pungarayacu study site since the petroleum company operating in the area did not allow to carry out fieldwork in the area. However, the selected areas detected as vegetation stress agree with the location of wells and geological faults as an indicator of shallow petroleum reservoirs.

5.3.7 Exploring new vegetation indices for vegetation affected by petroleum pollution

Maps of coefficient of determination (R^2) for foliar parameters and the SIs (RSI and NDSI) are presented in Figure 5.31 and Figure 5.32 respectively. The maps use a complete combination of two wavebands at i and j nm for the foliar dataset from the Amazon forest. The results highlight the most significant regions of the spectrum to assess foliar parameters.

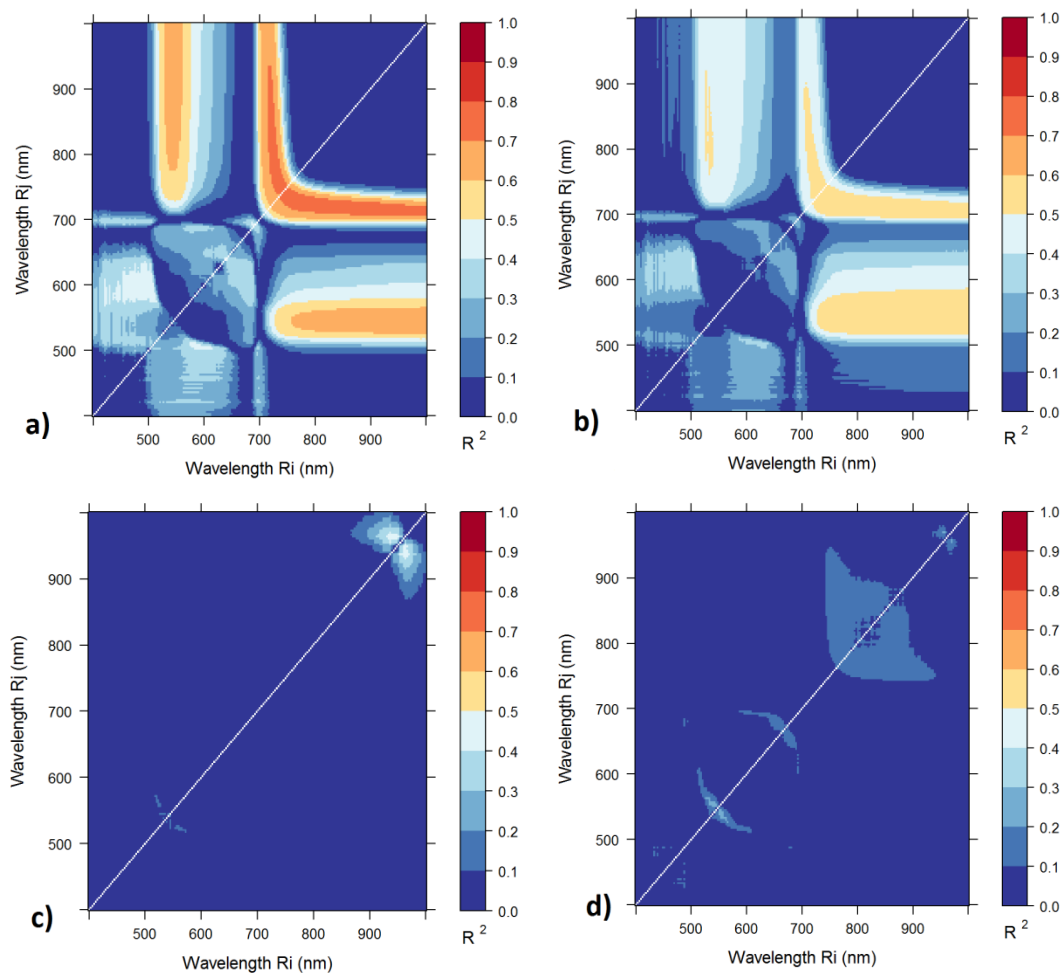


Figure 5.31 Coefficient of determination (R^2) for each wavelength combination between RSI and foliar parameters: **a)** Chlorophyll content from SPAD-502 readings, **b)** Chlorophyll content from PROSPECT model, **c)** Water content and **d)** Organic matter content.

The results of coefficient of determination for RSI and NDSI show similar patterns. Higher correlations are observed for chlorophyll content from SPAD-502 ($R^2=0.74$ and $R^2=0.73$ respectively), followed by chlorophyll content from PROSPECT ($R^2=0.59$ and $R^2=0.53$ respectively). Lower coefficient of determination are illustrated for water content ($R^2=0.47$ and $R^2=0.47$ respectively) and organic matter content ($R^2=0.25$ and $R^2=0.25$ respectively). Table 5.13 presents the maximum coefficient of determination (R^2) and the corresponding R_i and R_j wavelength bands.

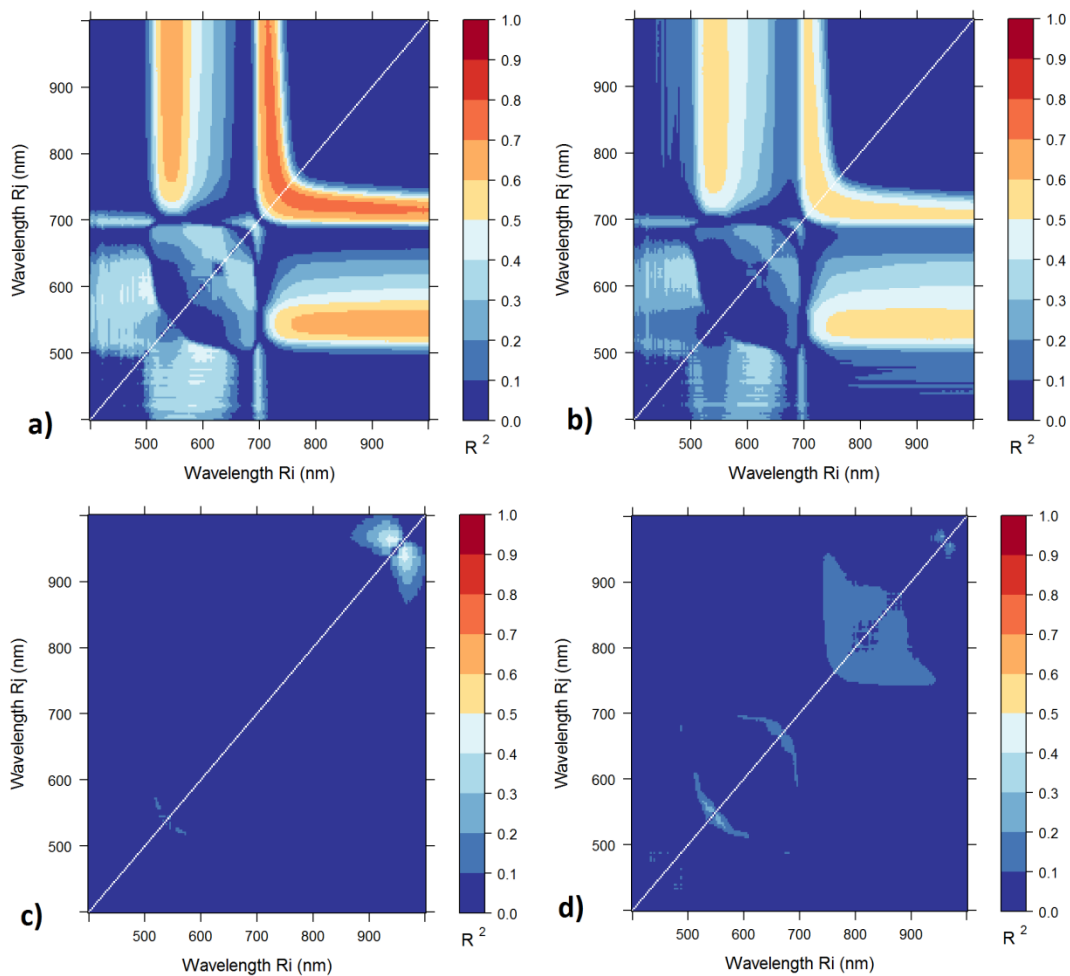


Figure 5.32 Coefficient of determination (R^2) for each wavelength combination between NDSI and foliar parameters: **a)** Chlorophyll content from SPAD-502 readings, **b)** Chlorophyll content from PROSPECT model, **c)** Water content and **d)** Organic matter content.

Table 5.13 Maximum R² and spectral bands for RSI and NDSI indices for foliar biophysical and biochemical parameters of tropical forest.

| | RSI=x/y | | NDSI=(x-y)/(x+y) | |
|--|----------------|----------------------|------------------|----------------------|
| | R ² | @ spectral range(nm) | R ² | @ spectral range(nm) |
| Chlorophyll content (µg cm ⁻²) from SPAD-502 | 0.74 | x=900; y=716 | 0.73 | x=726; y=797 |
| Chlorophyll content (µg cm ⁻²) from PROSPECT model | 0.59 | x=927; y=704 | 0.53 | x=711; y=803 |
| Foliar water content | 0.47 | x=948; y=962 | 0.47 | x=948; y=962 |
| Foliar organic matter content | 0.25 | x=555; y=542 | 0.25 | x=543; y=554 |

The higher coefficients of determination (RSI=0.74 and NDSI=0.73) shown by chlorophyll content from SPAD-502 were selected to assess the chlorophyll content at canopy level in vegetation of the tropical rainforest in the study area using the reflectance spectral data from Hyperion images.

Figure 5.33 illustrates the band combination of RSI adapted to the Hyperion bands (band 36 and Band 55) and Figure 5.34 shows the NDSI band combination (band 37 and band 45 of Hyperion) in the areas of interest. The figures show a clear differentiation between forested areas affected and not affected by hydrocarbon pollution.

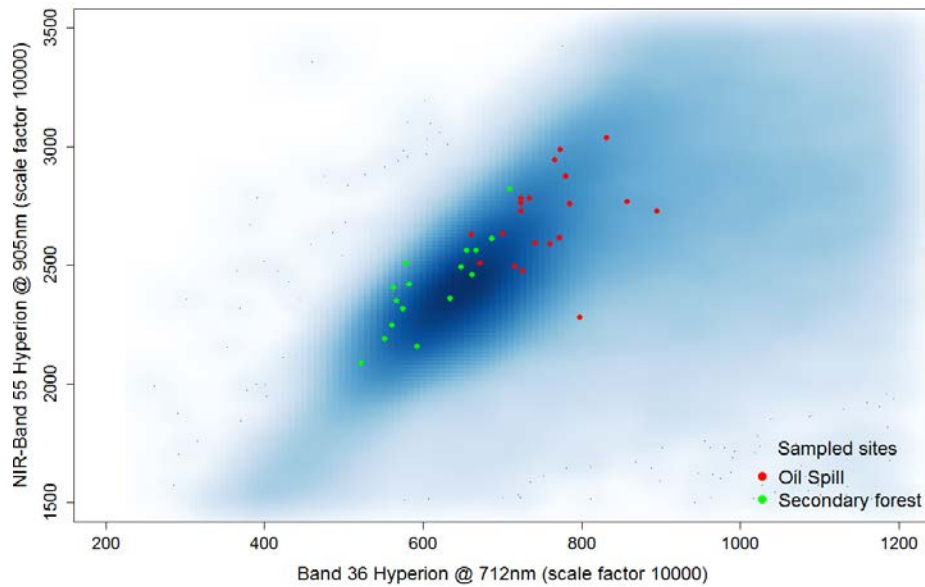


Figure 5.33 RSI band combination. Smooth blue region represents a scatter plot of Band 36 (712 nm) and Band 55 (905 nm) of Hyperion image (red dots = polluted site; green dots = non-polluted site)

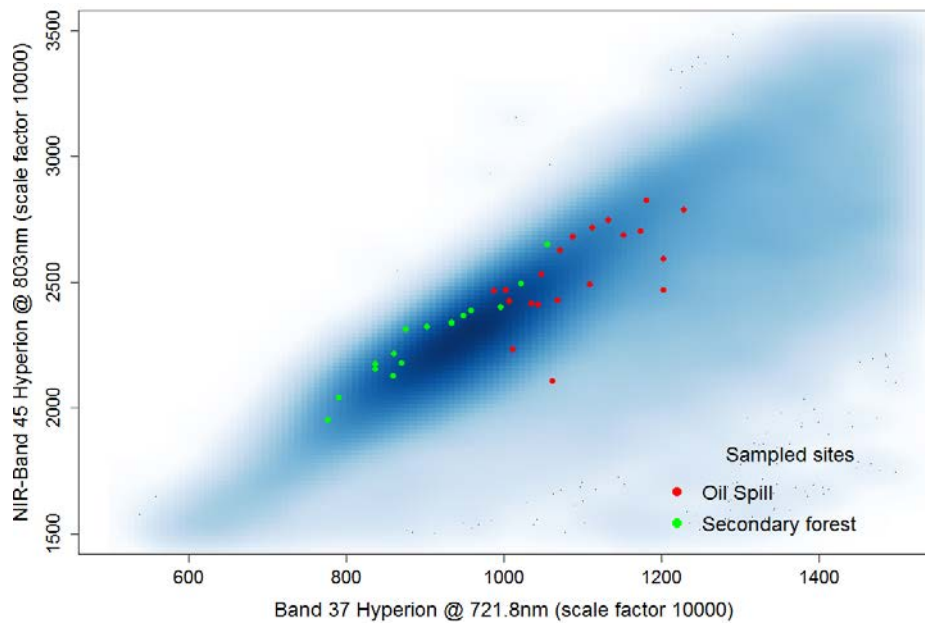


Figure 5.34 NDSI band combination. Smooth blue region represents a scatter plot of Band 37 (721 nm) and Band 45 (803 nm) of Hyperion image (red dots = polluted site; green dots = non-polluted site)

Plotting the relationship of spectral response of RSI and NDSI band combinations for the three study sites highlights an important difference between them (see Figure 5.35). The pristine forest has a strong relationship for RSI and NDSI ($R^2 = 0.92$ and $R^2 = 0.96$ respectively) followed by the secondary non-polluted site ($R^2 = 0.76$ and $R^2 = 0.93$ respectively), and finally the polluted site has a low relationship ($R^2 = 0.10$ and $R^2 = 0.40$ respectively). This suggests that in the tropical forest of pristine environments the increase of RED reflectance is associated with an increase in NIR reflectance, meanwhile in polluted environments this relationship is not clear.

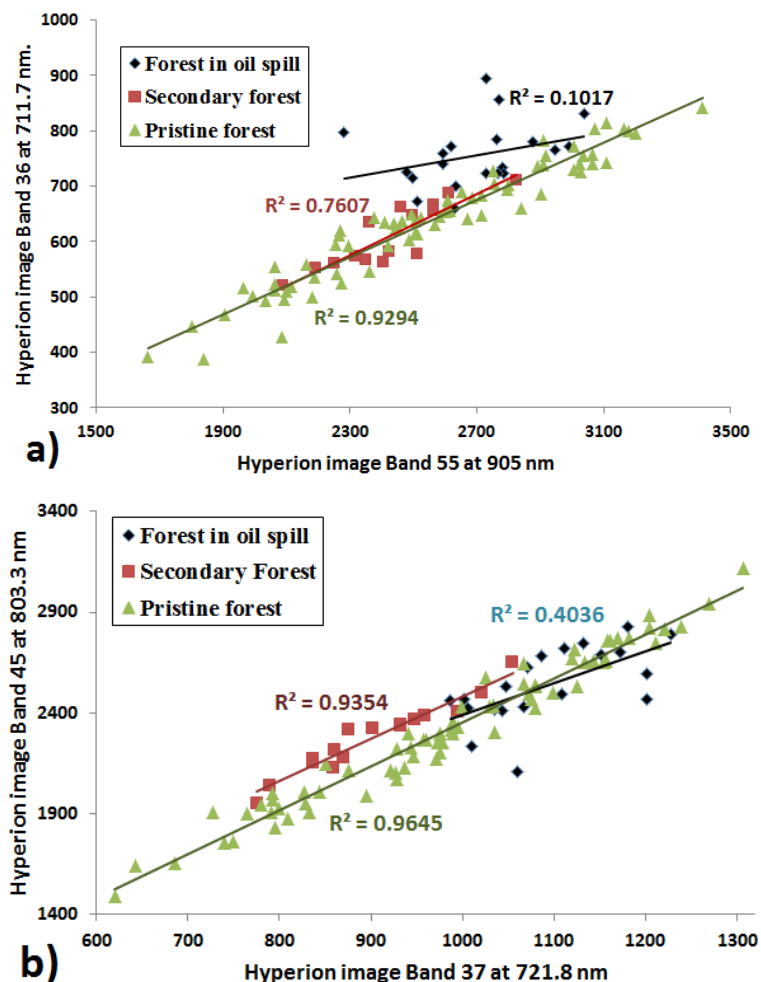
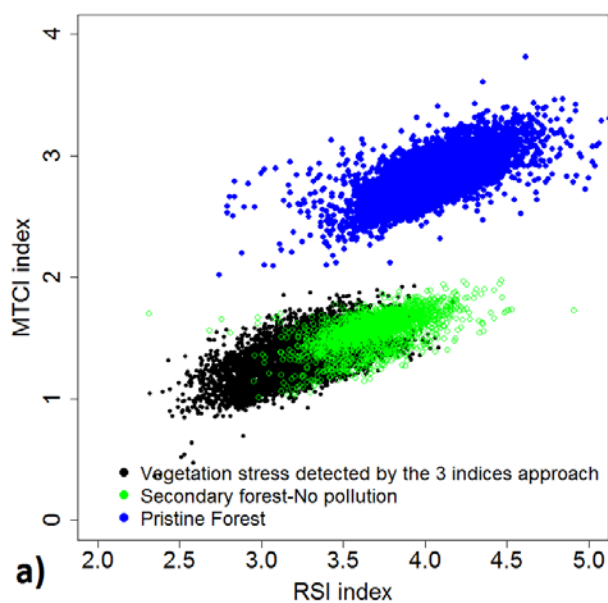


Figure 5.35 Correlation between band combinations applied to Hyperion images bands in the study area for: **a)** RSI band combination **b)** NDSI band combination

Tropical rainforest health, based on vegetation stress detected by the three-indices approach used in the previous section (see Figure 5.29) was tested by a combination of the new vegetation indices proposed in this study (SIs) and MTCI, which is a standard product of the European Space Agency (ESA) and provides estimates of chlorophyll content of vegetation (amount of chlorophyll per unit area of ground) at global level. A hyperspectral Hyperion image was used to identify three statuses of the tropical rainforest: a) vegetation stress caused by hydrocarbon pollution (detected by the three indices approach), b) secondary forest non-polluted by hydrocarbons and c) pristine tropical rainforest of Yasuni National Park.

Figure 5.36 displays the sensitivity of RSI and MTCI indices to detect the three levels of tropical forest status. The MTCI index clearly differentiates higher chlorophyll levels from pristine forest, but showed less sensitivity to polluted and non-polluted secondary forests. Meanwhile RSI showed better sensitivity to detect pristine forest than NSDI (see the same range of NSDI index for pristine and secondary forest). On the other hand, NSDI provides a better identification of polluted and non-polluted secondary forest.



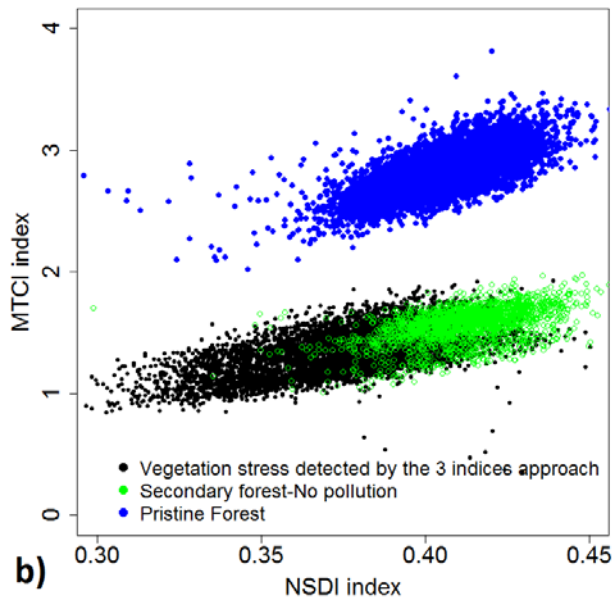


Figure 5.36 Identification of tropical rainforest health based on the vegetation indices proposed in this study and MTCI. **a)** RSI vs MTCI **b)** NSDI vs MTCI

5.3.8 Mapping chlorophyll content

Chlorophyll content at canopy level is the combination of the area of leaves per unit area of ground (Leaf Area Index-LAI) and the chlorophyll concentration of those leaves. Therefore the high LAI values of vegetation in the tropical forest are directly related to higher chlorophyll content levels. REP has been considered as an important predictor of chlorophyll content derived from satellite images. However, as indicated earlier, REP is relatively insensitive to chlorophyll content at high values of chlorophyll content (Dash et al. 2010).

An alternative standard level 2 product (atmospherically corrected top-of canopy reflectance) from the European Space Agency (ESA) is the Medium Resolution Imaging Spectrometer (MERIS) which is described in Chapter 3, section 3.1.4, page 57. In this research, application of MTCI to the Hyperion images was performed according to the follow band settings:

$$MTCI_{hyperion} = \frac{\rho_{Band40} - \rho_{Band36}}{\rho_{Band36} - \rho_{Band33}} = \frac{\rho_{752.4} - \rho_{711.7}}{\rho_{711.7} - \rho_{861.2}} \quad (5.10)$$

Figure 5.37 shows the band combination used by MTCI and the equivalent bands combination for Hyperion images.

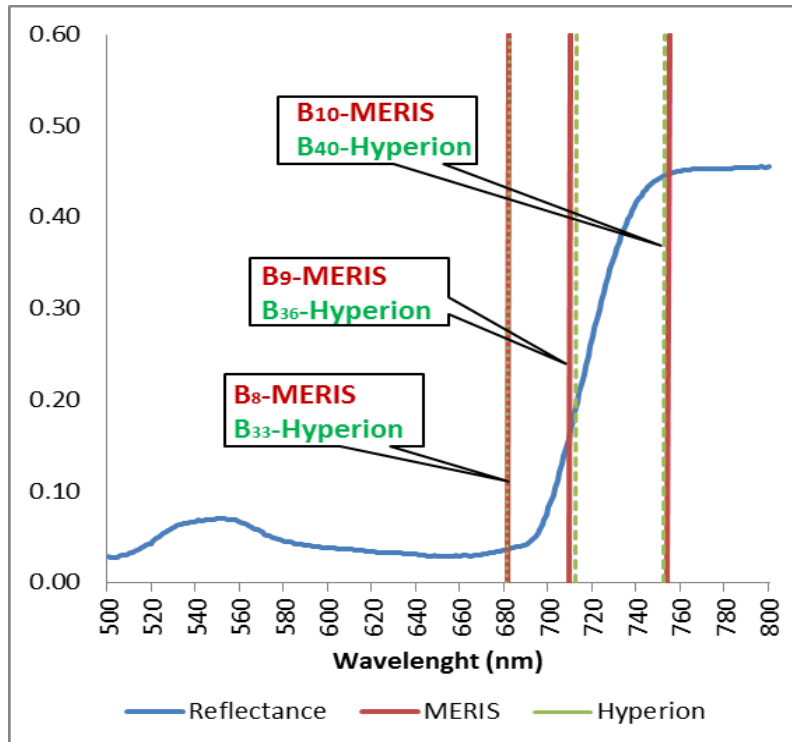


Figure 5.37 MTCI bands comparing with MTCI applied to Hyperion image

Chapter 3 details the steps taken to estimate ground truth foliar chlorophyll content in $\mu\text{g cm}^{-2}$ based on the SPAD-502 chlorophyll meter index for the sampled sites in the study area. Truth foliar chlorophyll content is based on seven SPAD-502 index models which account for a wide range of vegetation species. On the other hand, reflectance data collected by a spectrophotometer for each leaf sampled at the upper canopy level (see Chapter 3) was used to compute MTCI at leaf level for all sampled sites. The relationship between MTCI at foliar level and ground truth foliar chlorophyll content expressed in $\mu\text{g cm}^{-2}$ was established for sampled leaves collected from the upper layer of the canopy only in all sampled sites (polluted, non-polluted and pristine forest). As discussed in Chapter 3, it is

not clear how the accuracy of the SPAD-502 chlorophyll meter varies in high chlorophyll content readings. Then, in this section, the results were evaluated from the foliar dataset including all samples but also excluding the SPAD-502 outliers. The following equations show these relationships for samples including outliers (Equation 5.40) and samples after excluding outliers (Equation 5.41):

$$y = 33.886x^{0.8802} \quad (5.40)$$

$$y = 36.894x^{0.5658} \quad (5.41)$$

The results in Figure 5.38 show strong positive power regression models before ($R^2=0.68$) and after outlier removal ($R^2=0.57$). A stronger correlation was found when the regression model was tested in the whole dataset including outliers.

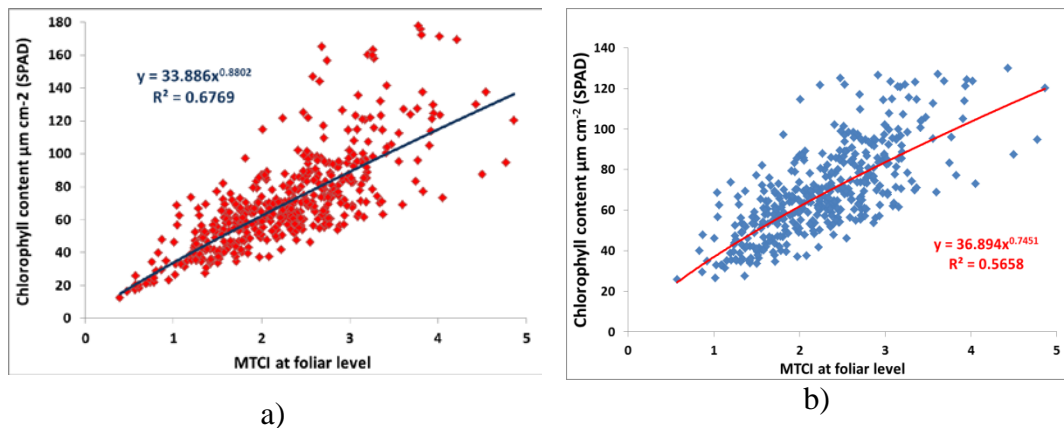


Figure 5.38 Regression model MTCI and chlorophyll content at foliar level for samples at the upper canopy. a) including outliers and b) excluding outliers

In order to estimate chlorophyll content (expressed in $\mu\text{g cm}^{-2}$) at canopy level using satellite images, the equations defined at leaf level (Figure 5.38) were applied to MTCI derived from the Hyperion images. A vegetation mask defined by $\text{NDVI} > 0.1$ was applied to the chlorophyll content maps for excluding non-vegetated pixels. Figure 5.39 and Figure 5.40 show the maps of the estimation of chlorophyll content at canopy level in the petroleum productive area and pristine forest.

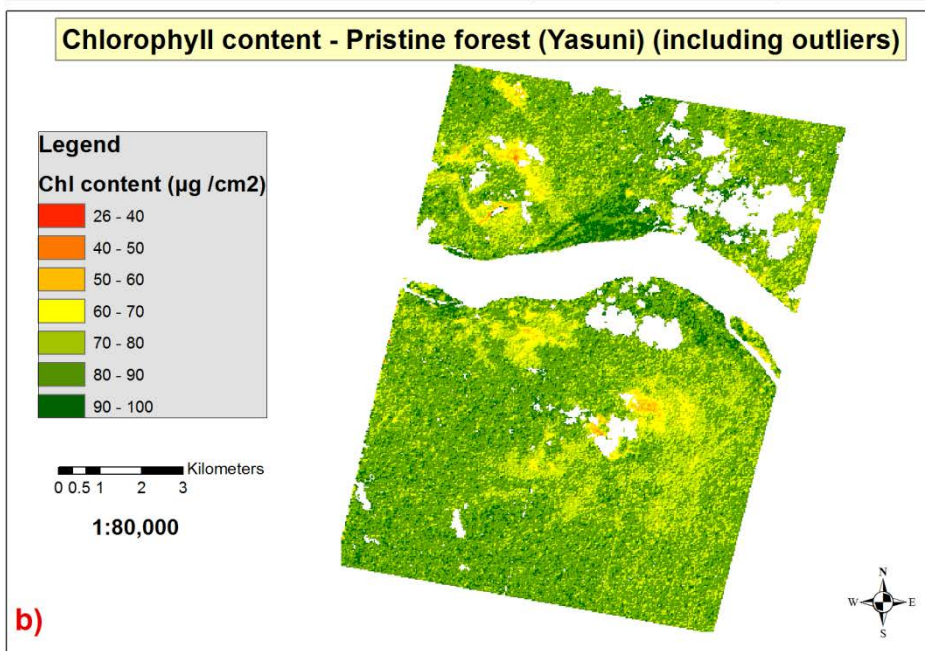
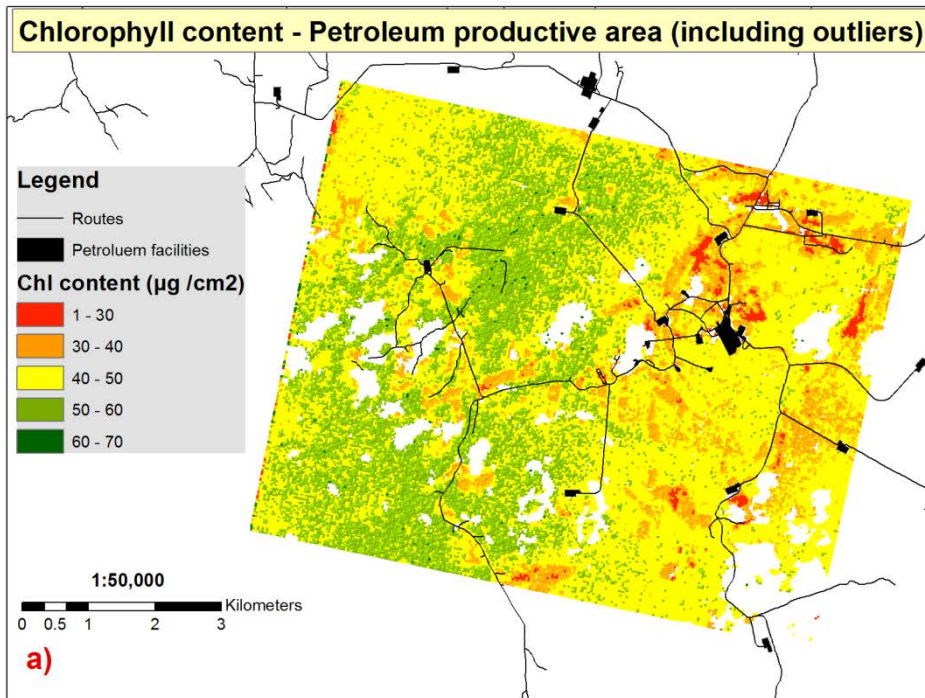


Figure 5.39. Maps of the estimations of chlorophyll content at canopy level before outlier removal a) petroleum productive area b) Pristine forest (Yasuni)

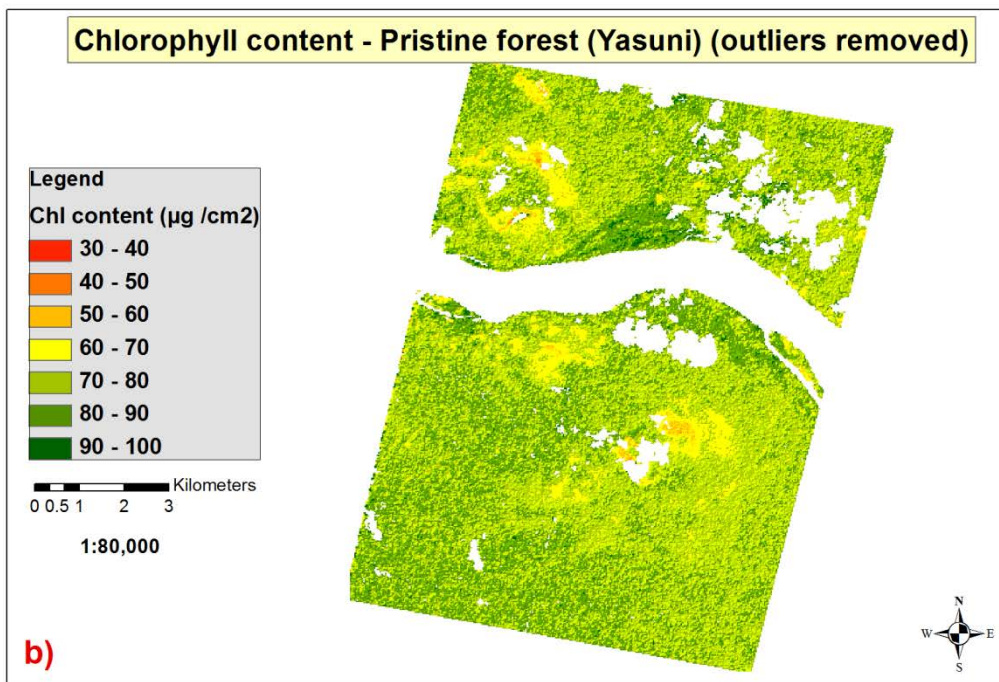
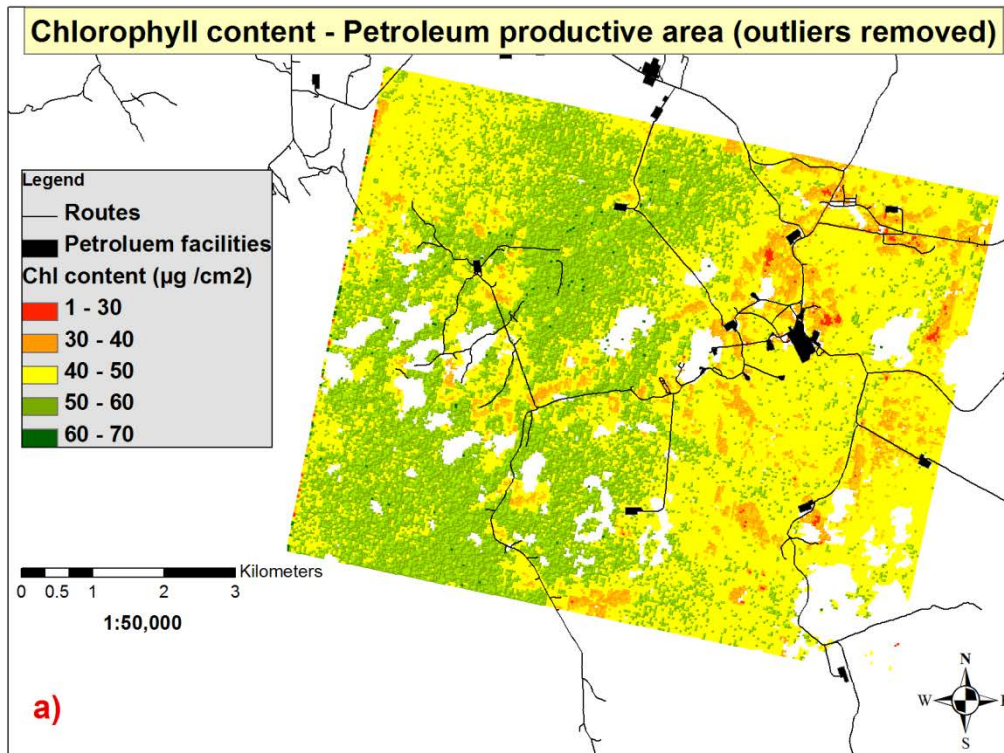


Figure 5.40 Maps of the estimations of chlorophyll content at canopy level after outlier removal **a)** petroleum productive area **b)** Pristine forest (Yasuni)

A diagram of the explained process to estimate chlorophyll content from leaf to canopy level proposed in this research is shown in Figure 5.41

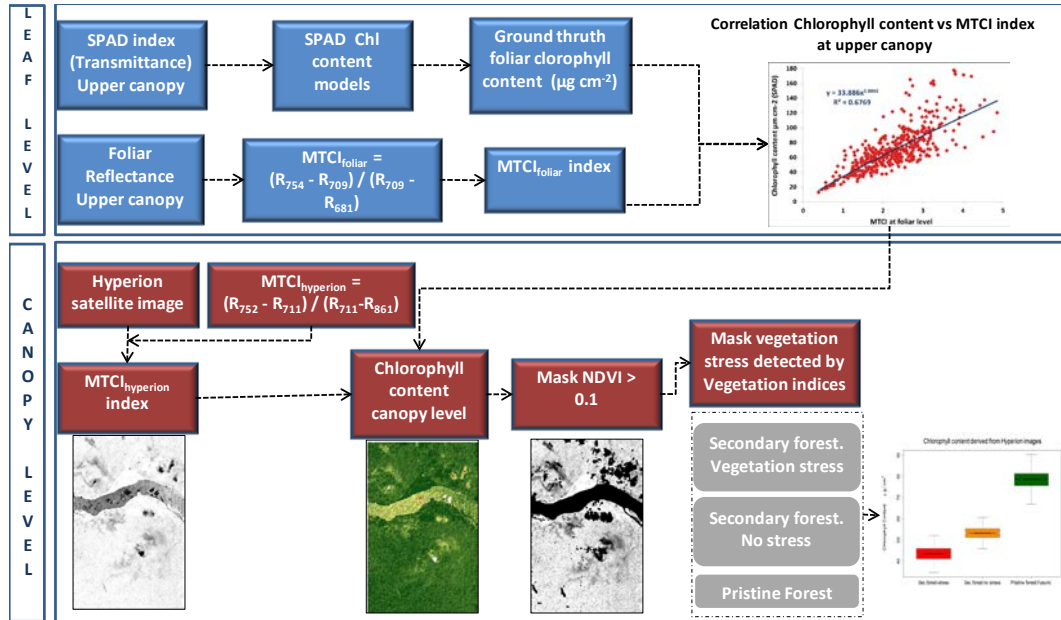


Figure 5.41 Diagram of the process followed to estimate chlorophyll content from leaf to canopy level

The resulting chlorophyll content images were used to compute chlorophyll levels in the areas detected as vegetation stress based on the 11 vegetation indices (see subsection Mapping vegetation stress in page 163). The computed chlorophyll content at canopy level based on final results are shown in Figure 5.42

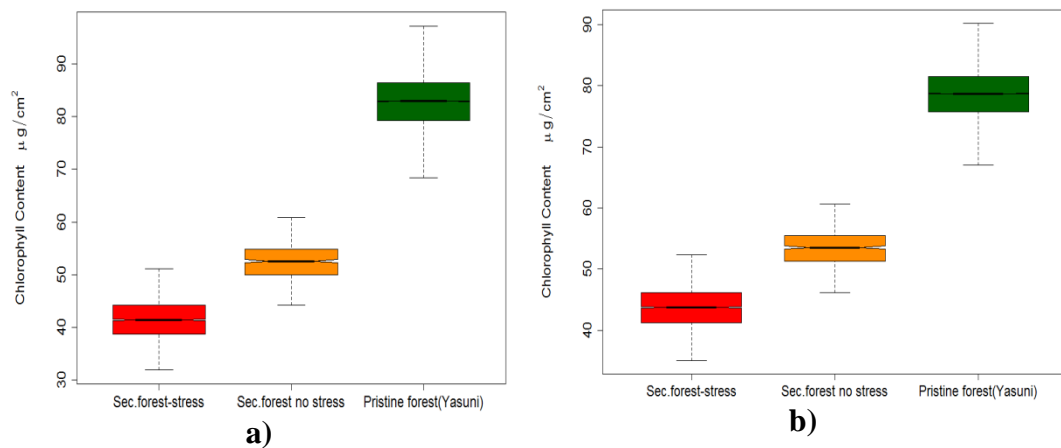


Figure 5.42 Chlorophyll content levels for the three study sites based on the MTCI index applied from leaf to canopy level. a) all leaf samples and b) samples excluding outliers

5.4 Discussion

Several vegetation indices were applied to the atmospherically corrected Hyperion image in order to find out their ability to discriminate biophysical and biochemical changes in vegetation affected by hydrocarbon pollution. The results show almost all indices clearly differentiate secondary forest and pristine forest. The interest of this research is to explore vegetation indices suitable to discriminate between the secondary tropical forest affected by hydrocarbon pollution and the secondary tropical forest not affected by pollution. From 29 indices applied to the study sites, the pair-wise comparison of means using the adjustment method of Holm established 11 indices which proved strong significant differences (99.9%) between the two secondary forests (polluted and non-polluted); three indices are broad-band and eight are narrow-band indices.

5.4.1 Vegetation indices suitable to detect hydrocarbon pollution

Broad-band and narrow-band vegetation indices related to the traditional NDVI (SR, GNDVI, NDVI₇₀₅) showed significant differences in the area affected by hydrocarbons. This result endorses the conclusions of Zhu et al. (2013) which

found a strong negative correlation between NDVI and vegetated areas affected by hydrocarbon pollution.

The Sum Green vegetation index (SG) clearly identified an increased reflectance signal in the visible spectral region of the area affected by hydrocarbon pollution which confirms the findings presented in Chapter 4 related to reduced chlorophyll content levels in the polluted site.

The two indices, developed to estimate chlorophyll content across species (PSSRa and NDVI₇₀₅), clearly exhibited lower chlorophyll content for the forest affected by hydrocarbons which suggest their sensitivity for vegetation from tropical forests. These findings in one hand contradict with Sims and Gamon's (2002) conclusions which suggested that PSSRa was largely insensitive to variations in chlorophyll content in a multispecies forest. But on the other hand, this thesis agrees with their findings related to the sensitivity of NDVI₇₀₅ to variations of chlorophyll content across several species.

The narrow-band indices NDVI₇₀₅, CTR2, LIC1 and OSAVI showed strong significant differences in the polluted site. These results agree with another study for detecting vegetation stress due to natural hydrocarbon gases leakage (Noomen&Skidmore 2009), where these four indices correctly identified vegetation stress.

Narrow-bands indices developed to identify shifts of the red-edge position caused by vegetation stress applied in this study (REP and ratio of derivatives-Der₇₂₅₋₇₀₂) did not show a strong significant difference in polluted and non-polluted sites which contradicts the findings presented in other studies (Smith;Steven & Colls 2004, Yang et al. 1999, Smith;Steven & Colls 2004, Noomen&Skidmore 2009, Yang et al. 2000). This can be explained by the fact that REP is relatively insensitive to chlorophyll content when values are high in tropical forest environments (Jago;Cutler & Curran 1999, Munden;Curran & Catt 1994). This is

explained by the chlorophyll content at canopy level being a combination of the LAI and foliar chlorophyll concentration (Dash et al. 2010).

VOG1 vegetation index explores the relationship between REP and foliar chlorophyll content. This index showed strong significant differences between polluted and non-polluted sites.

MTCI index provided good evidence to detect reduced chlorophyll content in areas affected by hydrocarbons. These results open the possibility to extend the use of MTCI to other space and aircraft hyperspectral sensors.

Vegetation indices related to other plant pigments and water content were not able to detect the symptoms of vegetation stress in areas affected by hydrocarbons. Low signal-to-noise-ratio in the near-middle infrared regions and a relatively coarse spatial resolution of Hyperion images (30 m) may be the most likely factors for this. Airborne hyperspectral data may provide an adequate spatial resolution and appropriate SNR to investigate changes in foliar water content and other leaf pigments.

Discriminant function analysis applied to areas detected as vegetation stress by the 11 vegetation indices showed that three indices (SG, NDVI and NDVI₇₀₅) explain 83% of the separability between the three study sites. Indeed, detection of vegetation stress by applying those three indices illustrated very similar results than the 11 indices approach. This suggests that applying indices related to chlorophyll and NDVI are suitable to detect areas which are affected by hydrocarbon pollution. Those three indices were applied to the CHRIS-Proba image of the fourth study site where hydrocarbons are exposed to the surface or near-surface. The areas detected as vegetation stress agree with the location of wells and geological faults as an indicator of shallow petroleum reservoirs.

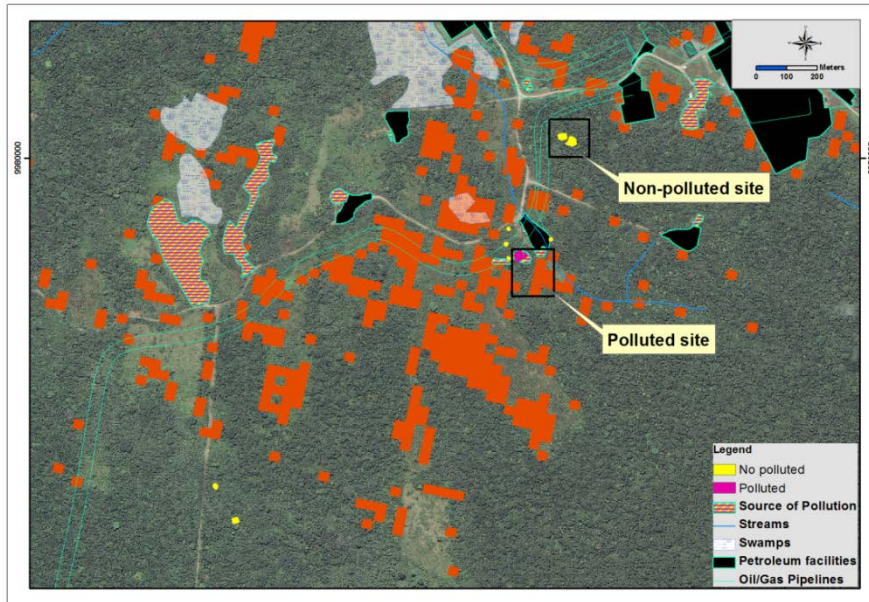
5.4.2 Mapping vegetation stress

Figure 5.43 illustrates pixels identified as vegetation stress based on two approaches: a) 11 vegetation indices and b) three vegetation indices explaining 83% of the sites separability. Results from the latest approach increase the number of pixels detected as vegetation stress which can be explained by the percentage of separability cover by the three indices. In order to assess the accuracy of these approaches, we overlapped the pixels identified as vegetation stress over a very high, one meter resolution IKONOS image (accessed from Google Earth), where sampled areas during fieldwork are identified (yellow circles) and also the pixels sampled in the Hyperion image (black squares) for vegetation indices calculation.

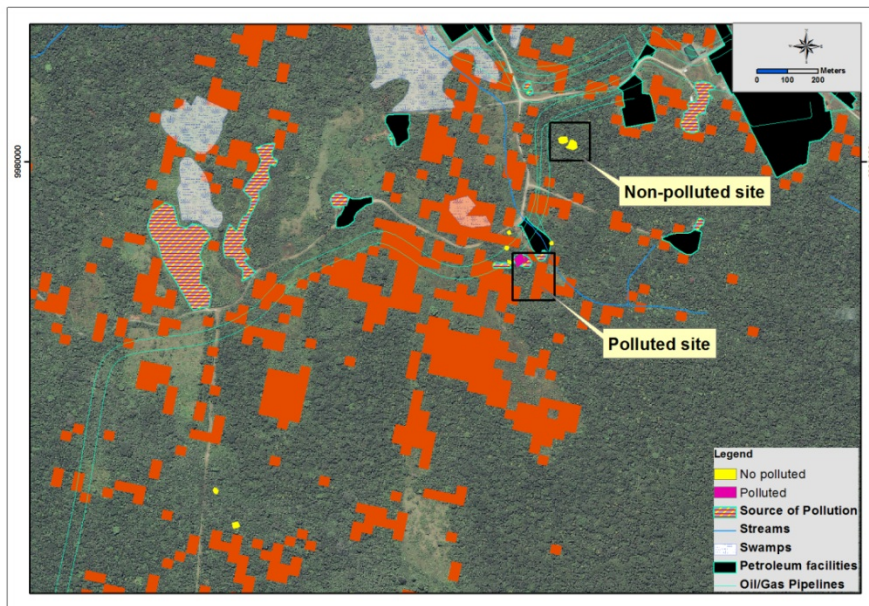
In both approaches, the eight sampled sites of the secondary forest not affected by pollution (yellow circles) were correctly identified as non-polluted pixels in both maps. Several pixels inside the polluted site were correctly identified by the two approaches.

The identified polluted pixels are plotted together with petroleum infrastructure: platforms, stations and oil/gas pipelines (Figure 5.43). Areas identified as a source of pollution are open pits where polluted soils have been stocked for remediation. Most of the polluted pixels are grouped around petroleum facilities, pipelines and areas that have been identified as a source of pollution. As it is discussed in Chapter 4, open pits contain crude oil that has been discharging to the environment or leaching out as the pits degrade or overflow from rainwater. It is not clear when the pits were constructed but it is estimated that they have been a source of pollution for at least the least 15 years. According to environmental studies and governmental environmental audits (Walsh Environment Scientists and Engineers 2005), those areas are active sources of hydrocarbons pollutants. Water discharges from the source of pollution, and transport hydrocarbon pollutants which are deposited and accumulated in the nearest swamps. As we observed in Figure 5.27 and Figure 5.29, a cluster of pixels identified as

vegetation stress are located in forested areas around swamps where water runoff from those facilities bring hydrocarbons and other pollutants to the environment.



a)



b)

Figure 5.43. Areas identified as vegetation stress by a) eleven selected indices and b) three selected indices representing 83% of the site separability. The eight yellow areas represent sampled sites during fieldwork and black squares the sampled areas to estimate vegetation indices.

5.4.3 Exploring new vegetation indices for vegetation affected by petroleum pollution

From all possible combinations of two wavelengths, RSI (R_{900}/R_{716}) has the most significant relationship with chlorophyll content ($R^2 = 0.74$) followed by NDSI combination ($(R_{726}-R_{797})/(R_{726}+R_{797})$) with chlorophyll content ($R^2 = 0.73$). Those are the new chlorophyll indices proposed in this study. As shown in Table 5.13, a least significant relationship was found for chlorophyll content derived from the PROSPECT model ($R^2=0.59$ and $R^2=0.53$ for RSI and NDSI respectively) which may be explained by the fact that the transmittance signal used for the inverse process of the model could not be collected from the field and was inferred from “trans-flectance” as explained in Materials and methods section in Chapter 3.

A significant relationship between SIs and foliar water content were $R^2=0.47$ for both cases, which is related to reflectance response driven by water content around 834 nm in the NIR region. The low relationship of $R^2=0.25$ of organic matter content can be explained by the fact that the spectral range used for mapping coefficient correlations (400 and 1000 nm) is poorly correlated to vegetation parameters.

Figure 5.33, Figure 5.34 and Figure 5.35 illustrate higher reflectance values in the visible range of the polluted area, and are related to decreased levels of foliar chlorophyll content which was reported in Chapter 4. On the other hand, higher reflectance values in the NIR region in the polluted site suggests lower foliar water content which apparently contradicts the reported higher values of foliar water content findings of Chapter 4. Indeed, the internal structure of the leaves defines the air-water spaces and it has been proven that higher levels of intercellular water in leaves causes increased transmittance and reduced reflectance (Kumar;Schmidt & Dury 2006). However, an increased NIR reflectance signal has been found in plants growing in soils with high levels of pollution caused by heavy metals such as copper, lead and zinc (Howard;Watson

& Hessin 1971, Press 1974), which confirm the increased foliar water content found in the polluted site presented in Chapter 4.

A comparison of sensitivity to detect different statuses of tropical forest based on chlorophyll content levels showed that MTCI better identifies pristine forest than secondary forest. Meanwhile, NSDI and RSI illustrated a major sensitivity to differentiate between the polluted and non-polluted secondary forest (Figure 5.36).

Figure 5.44 shows the scatter plots of the best band combination of Hyperion images (band 37 and band 45) resulting from the NSDI index which best differentiates between the polluted and non-polluted secondary forest. Red dots represent the polluted area and green dots represent non-polluted pixels. This figure confirms that vegetation growing in areas affected by hydrocarbons experience changes in biophysical and biochemical parameters which can be detected by using hyperspectral satellite images. Higher reflectance in the visible range stands for reduced levels of chlorophyll content and higher reflectance in the NIR region which is related to changes in the internal structure of the leaves in the area affected by pollution. The increased reflectance in the NIR has been reported to be correlated to a decrease of water content, but the results of this study indicate that higher levels of water content reported in the polluted area correlates with higher reflectance in the NIR. The increased reflectance in the polluted site agrees with other studies of plants growing in soils with high levels of pollution caused by heavy metals such as copper, lead and zinc (Howard;Watson & Hessin 1971, Press 1974).

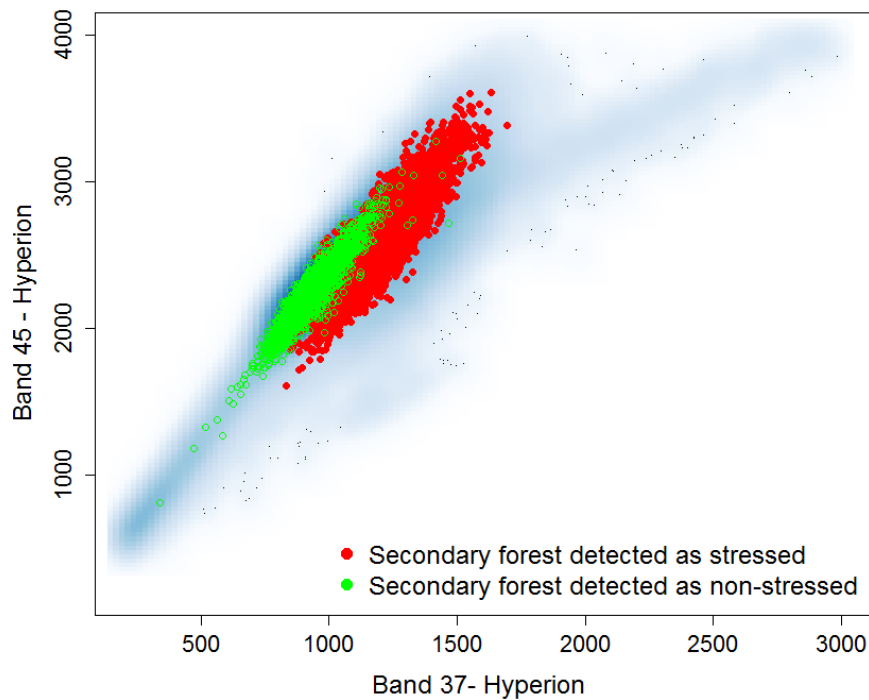


Figure 5.44 Scatter plot of Hyperion NSDI index band combination (blue smoothed). Secondary forest detected as polluted by the three vegetation indices (SG-NDVI-NDVI₇₀₅) in red; vegetation non-polluted in green

5.4.4 Mapping chlorophyll content

The resulting chlorophyll content maps in the petroleum productive area (Figure 5.39a and Figure 5.40a) illustrate lower levels of chlorophyll content, around 40 and 50 $\mu\text{g cm}^{-2}$ along the western side of the study area with some patches ranging between 30 and 40 $\mu\text{g cm}^{-2}$. The same pattern can be seen at the upper left corner of the study area. Along the central region of the image higher levels of chlorophyll content between 50 and 60 $\mu\text{g cm}^{-2}$ are reported.

Estimations of chlorophyll content in the pristine forest (Figure 5.39b and Figure 5.40b) are without question higher than in the petroleum productive area. Since it is an area with little or no human intervention, the forest may be considered as a healthy mature forest with relatively constant, high chlorophyll levels between 70 and 90 $\mu\text{g cm}^{-2}$ along the study area. In the upper left corner of the image, which is located outside the protected area (Yasuni), agricultural activities and illegal

logging have been reported, therefore lower chlorophyll content ranges between 50-70 $\mu\text{g cm}^{-2}$. Same chlorophyll content values are detected due south of the Napo River (white region across the image) which corresponds to a forest regularly affected by floods.

The secondary forest affected by stress reported the lowest chlorophyll content levels followed by the secondary forest not affected by stress. Significant highest chlorophyll content is reported in the pristine forest. Using the method proposed in this research, differences between before and after outlier removal from the SPAD-502 readings are not critical as we can see in Table 5.14.

Table 5.14. Average chlorophyll ($\mu\text{g cm}^{-2}$) content estimations for the three study sites

| | Secondary forest Vegetation stress | Secondary forest Non-stressed | Pristine Forest |
|--|---|--------------------------------------|------------------------|
| Before remove outliers (all samples from the upper canopy for the three study sites) | 41.4 | 52.5 | 82.5 |
| After remove outliers | 43.7 | 53.5 | 78.7 |

The method presented in this thesis for chlorophyll estimation at canopy level in tropical forest has highlighted different levels of conservation of tropical forest. Areas close to petroleum facilities and probably exposed to some kind of pollution presented the lower chlorophyll content levels (around 42 $\mu\text{g cm}^{-2}$). Secondary forest exposed to human intervention but not hydrocarbon pollution reported chlorophyll levels around 53 $\mu\text{g cm}^{-2}$. Chlorophyll content maps in pristine forest allowed to differentiate levels of forest degradation. En Yasuni National Park, the chlorophyll content at canopy level reported values around 80 53 $\mu\text{g cm}^{-2}$, however, swats of forest presented lower chlorophyll content values which correspond to areas where forest has been exposed to human intervention, illegal logging, agricultural practices and flooding.

5.5 Conclusions

Several vegetation indices related to vegetation density, plant pigments and water content were applied to the atmospherically corrected Hyperion and CHRIS-Proba images of the study area in order to identify vegetation stress in areas influenced by petroleum/hydrocarbon pollution.

Vegetation indices related to LAI, canopy density and vigour (NDVI family) and vegetation indices related to chlorophyll content and photosynthetic activity were suitable to identify vegetation stress in areas affected by hydrocarbon pollution in the study area. From the 28 vegetation indices applied in this study, 11 indices were able to discriminate changes between the secondary forest affected and not-affected by pollution. Almost all indices (24) differentiate the secondary forest and pristine forest.

Vegetation indices for other plant pigments different to chlorophyll (carotenoids, anthocyanins) and canopy water content were not suitable to detect differences in polluted and non-polluted areas. This can be explained by the low signal-to-noise-ratio of the Hyperion images in the near to mid-infrared regions where there are strong water-absorption features. Furthermore, the very low signal recorder by Hyperion images in the blue range of the spectrum limited the performance of some vegetation indices using the blue range (for example EVI, ARVI, mNDVI₇₀₅, mSR₇₀₅).

The effects of hydrocarbon pollution in vegetation of the tropical forest are expressed in reduced levels of chlorophyll content, increased foliar water content (Chapter 4 of this study) and, according to the literature, an important decrease in LAI and vegetation vigour. Therefore detection of vegetation stress caused by hydrocarbon pollution should be based on a combination of several specific vegetation indices. As observed in our results, the application of the 11 selected vegetation indices identified vegetation stress in areas where hydrocarbons have been leaking to the environment.

This research has confirmed the applicability of some vegetation indices that detected vegetation stress caused by hydrocarbons in the past. NDVI, CTR2, LIC1 and OSAVI were also successfully applied in previous studies. On the other hand, the red-edge-position indices were not sensitive enough to detect vegetation stress in the study area despite their good performances in other studies. This can be explained by the fact that REP is relatively insensitive to chlorophyll content at high values in tropical forest environments (Jago;Cutler & Curran 1999, Munden;Curran & Catt 1994). This is explained by the chlorophyll content at canopy level being a combination of the LAI and foliar chlorophyll concentration (Dash et al. 2010).

Satellite data from the Hyperion images shows that in the tropical forest of pristine environments the increase of RED reflectance (reduced chlorophyll content) is associated to an increase in NIR reflectance, while in polluted environments this relationship is not clear. This is a key finding, we have further confirmed that vegetation exhibits stress symptoms at leaf level. As discussed in Chapter 2, hydrocarbon pollution causes changes of biophysical and biochemical parameters of vegetation which can be expressed in the vegetation morphology (size, thickness and leaf structure) and functionality (reduces transpiration, changes in respiration rates and reduced photosynthetic activity). Results from Chapter 4 confirm reduced levels of photosynthetic activity explained by the lower chlorophyll content levels, increased levels of foliar water content and thicker leaves. We can now exploit the opportunity to use specific vegetation indices for monitoring tropical forest environments using a wide range of satellite data sets.

The approach enabled the detection of stressed vegetation located near swamps and in the vicinity of petroleum processing, storage and transport facilities (platforms, pipelines, and open pits). Water runoff from those facilities brings hydrocarbons (and probably other pollutants) to the swamps.

Discriminant function analysis has showed that the results of the vegetation stress detected by the selected 11 vegetation indices were able to distinguish between the three study sites. Moreover, the relative weight of the linear discriminant 1 (LD1) showed that SG index has the strongest contribution to the group separation (53%) followed by NDVI index (21.6%) and NDVI₇₀₅ (8.4%). These three indices represent 83% of the group separation which can be explained by the fact that high values of SG index indicate less chlorophyll content and reduced photosynthetic activity. Meanwhile, high values of NDVI are sensitive to high LAI and biomass. SG, NDVI and NDVI₇₀₅ were applied to the Hyperion image of the study area. The results showed accurate identification of polluted and non-polluted sites.

Based on these results, the approach was applied to an area where vast seepage has been exposing hydrocarbons to the surface covered by tropical rainforest. SG, NDVI and NDVI₇₀₅ were applied to an atmospherically corrected CHRIS-Proba image and the results showed areas densely covered by vegetation with high NDVI values and high reflectance in the visible range which suggest lower levels of chlorophyll content. The selected areas suggest vegetation affected by some kind of stress, maybe related to hydrocarbons on the surface. Validation of these results in the field was not possible because permissions were not granted by the petroleum company operating in the area.

New vegetation indices were explored for the detection of vegetation stress caused by hydrocarbon pollution. Maps of coefficient of determination (R^2) between foliar parameters and two spectral indices (Ratio Spectral Index-RSI and Normalized Difference Spectral Index-NDSI) were computed. The maps use a complete combination of two wavebands at i and j nm for the foliar dataset from the Amazon forest. The results highlight the most significant regions of the spectrum to assess foliar parameters.

Higher correlations were observed between RSI, NDSI and chlorophyll content derived from SPAD-502 ($R^2=0.74$ and $R^2=0.73$ respectively), followed by

chlorophyll content from PROSPECT ($R^2=0.59$ and $R^2=0.53$ respectively). Lower coefficient of determination are illustrated for water content ($R^2=0.47$ and $R^2=0.47$ respectively) and organic matter content ($R^2=0.25$ and $R^2=0.25$ respectively). Based on that, two new indices sensitive to chlorophyll content in the tropical rainforest are proposed in this study: RSI (R_{900}/R_{716}) and NDSI ($(R_{726}-R_{797})/(R_{726}+R_{797})$).

The new indices were applied to a Hyperion satellite image in order to assess the chlorophyll content at canopy level in vegetation of the tropical rainforest. In the pristine forest sampled during fieldwork, the results revealed a strong correlation of 0.92 and 0.96 by RSI and NDSI respectively. Followed by the secondary non-polluted site ($R^2 = 0.76$ and $R^2=0.93$ respectively). In the secondary forest polluted site, the correlation of band combination is weak ($R^2= 0.10$ and $R^2=0.40$ respectively). This suggests that the effects of hydrocarbon pollution in the tropical forest can be detected by Hyperion satellite images by observing an increase of RED reflectance (reduce chlorophyll content), associated to an increase in NIR reflectance.

A comparison of the new indices with MTCI revealed that MTCI is more sensitive for detecting the differences between pristine and secondary forest. On the other hand, NSDI provides a better identification of polluted and non-polluted secondary forest.

Furthermore, a scaling-up method to estimate chlorophyll content from leaf to canopy level was developed. A chlorophyll index based on transmittance measurements was used to compute ground truth chlorophyll content (Chapter 3) which was correlated to MTCI index based on reflectance measurements from the same leaves. A strong correlation of $R^2=0.68$ was found for the whole dataset without removing outliers. Meanwhile, the correlation was $R^2=0.57$ after removing outliers from the dataset which suggests that using the method proposed in this chapter, extreme high and low SPAD-502 readings are sensitive to chlorophyll content compared to the sensitivity of MTCI index based on reflectance measurements. Based on these correlations, chlorophyll content at

canopy level was computed by applying MTCI index to the hyperspectral Hyperion images. Chlorophyll content maps confirmed lower mean chlorophyll content values of $42 \mu\text{g cm}^{-2}$ in the secondary forest affected by hydrocarbons (vegetation stress), followed by mean chlorophyll concentrations of $52 \mu\text{g cm}^{-2}$ in the secondary forest not affected by hydrocarbons and highest mean chlorophyll contents of $80 \mu\text{g cm}^{-2}$ in the pristine forest of Yasuni National Park.

Applications of airborne hyperspectral images with a higher spatial resolution and higher signal-to-noise-ratio will definitely improve detection of vegetation stress caused by petroleum pollution. In addition, LiDAR data can contribute favourably to estimate biophysical and biochemical parameter in the tropical forest.

Chapter 6. Conclusions, Limitations and Further Research

6.1 Conclusions

The aim of this research was to understand the effects of hydrocarbon pollution in the vegetation of the tropical forest and define a method to detect vegetation stress caused by hydrocarbon pollution through the evaluation of biophysical and biochemical parameters measured at leaf level and then scaling-up to canopy level using spectral hyperspectral remote sensing data. A fieldwork campaign was conducted in areas of the Amazon forest of Ecuador affected by petroleum pollution and in the pristine forest of the Yasuni National Park.

This chapter discusses the results of the three research questions with regards to their implications for the remote sensing detection of vegetation stress using hyperspectral methods.

6.1.1 Conclusions for Research Question 1

Research Question 1: As knowledge and in-situ observations about chlorophyll levels in tropical forests are limited, what alternative method based on non-destructive and portable instruments can provide rapid and accurate estimations of chlorophyll content in diverse tropical rainforest environments?

The findings from Chapter 3 provide the answer to the Research Question 1.

Non-destructive and portable methods provide accurate chlorophyll content estimations based on the calibration model for specific vegetation species, however generalised calibration models have been proposed for a wide range of vegetation species accounting for heterogeneous leaf structure, plant physiological, plant phenology and growing conditions.

Three optical non-destructive methods for the estimation of chlorophyll content were applied to the collection of over 1,100 leaf samples from the Amazon

rainforest, which represents a wide range of vegetation species growing in a disturbed and a pristine lowland rainforest. The first method is based on transmittance from the SPAD-502 chlorophyll meter index; the second method is based on reflectance measurements collected by a spectroradiometer and the third method estimates chlorophyll content from the inversion process of the radiative transfer PROSPECT model

For the first method, seven models that account for a wide range of vegetation species, some of them specific for vegetation tropical forest species, showed similar leaf chlorophyll content estimations until 80 units of SPAD-502. An average of the results of these models was computed and used as ground truth from where a generalised second order polynomial model was derived for the range of 15 to 95 SPAD-502 units. For the second method, five chlorophyll indices based on reflectance measurements provided similar chlorophyll content estimations for all SPAD range (15-95 units).

Chlorophyll content estimations based on the proposed ground truth second order polynomial shows a strong positive correlation of 0.76 compared to estimations derived from reflectance indices. The correlation of the ground truth estimations and the inverse process of PROSPECT model reported a strong positive correlation of 0.71. The comparison with MTCI and REP indicate correlations of 0.74 and 0.66 respectively. These results provide strong evidence of the ability of the model proposed in this study to estimate chlorophyll content for several species in the Amazon forest.

Moreover, a generalised homographic model for a variety of tree species from the Amazon region has been published in the past and has been used as the standard model to estimate chlorophyll content for more than 700 Amazonian tree species. A comparison of chlorophyll estimation between the homographic model and the second order polynomial model proposed in this study illustrates a good agreement for a wide range of SPAD-502 reading (15-95 units).

Estimations of chlorophyll content for vegetation from the tropical forest are rare therefore a better knowledge of leaf chlorophyll content in the tropical forest is required to contribute to detecting and modelling vegetation stress during drought or forest degradation. This can be done by using satellite data to better understand the potential of photosynthetic capacity and its implications in regional and global carbon cycle and climate models.

The results of this chapter show that the relatively light-weight handheld field spectroradiometer can be used to estimate leaf chlorophyll content in remote tropical rainforest ecosystems that are difficult to access. They provide a rapid and portable method for such remote areas where traditional chemical extraction methods for chlorophyll estimation are not viable. A general second order polynomial calibration model for chlorophyll content estimation which accounts for a wide range of plant species, phenological stage and leaf structure based on spectral measures offers an alternative approach for chlorophyll estimation.

6.1.2 Conclusions for Research Question 2

Research Question 2: Are biophysical and biochemical foliar parameters across the vertical profile of the tropical rainforest affected by hydrocarbon pollution?

The findings from Chapter 4 provide the answer to the Research Question 2.

Several foliar parameters were assessed in order to identify the effects of hydrocarbon pollution in the study area. The foliar parameters considered are: chlorophyll content ($\mu\text{g cm}^{-2}$), organic matter content (g cm^{-2}), foliar water content (g cm^{-2}), specific leaf area ($\text{cm}^2 \text{g}^{-1}$), leaf thickness (g cm^{-2}), leaf water content in mass basis (%) and leaf dry matter content (%). This study reveals for the first time that tropical forests exposed to hydrocarbon pollution show reduced levels of chlorophyll content, higher levels of foliar water content and leaf structural changes.

The analysis considered three vertical layers of the forest: upper canopy, medium canopy and understory. The results are the first of their kind, showing a vertically differentiated response of rainforest canopy structure to hydrocarbon pollution.

An important finding of this research is that chlorophyll content is a key indicator of vegetation which is affected by hydrocarbon pollution. Reduced levels of the plant pigment were found across all layers of the vertical profile of the forest growing in a site polluted by hydrocarbons. Reduced levels of chlorophyll content is an indicator of a reduced photosynthetic activity caused by the hydrocarbons from the polluted site. Indeed, laboratory experiments conducted in the past have reported that reduced levels of chlorophyll content is an indicator of vegetation stress caused by hydrocarbon pollution. Those experiments considered few plant species, generally crops. It was not clear how hydrocarbons affect vegetation in a heterogeneous tropical forest.

Increased levels of foliar water content were found in the polluted site. It is not clear why but a possible explanation is that the reduced photosynthetic rate affects the respiration process. Another explanation of increased foliar water is that stomata tend to close in vegetation under stress conditions. Another conclusion from this research indicated that thicker leaves in the upper canopy and thinner leaves in the understory are key indicators of vegetation affected by hydrocarbons.

This research has found that, despite the fact that hydrocarbons were disposed in the polluted site many years ago, it is still a potential source of pollution which has been effecting the vegetation. Indeed, part of hydrocarbons have been evaporated and biodegraded. Liquid hydrocarbons have migrated from the open pits by infiltration into the soil and dissolution in water, but in the interior of the viscose stratum of crude oil from the open pits there is still a mixture of liquid hydrocarbons and gases.

The result of this chapter significantly advances scientific understanding by providing evidence of leaf chemical and physical alterations in the rainforest

caused by hydrocarbon pollution and has implications for global rainforest monitoring satellite missions in that it identifies the leaf chemical properties that can be detected from a space-borne sensor.

6.1.3 Conclusions for Research Question 3

Research Question 3: What is the potential of hyperspectral satellite images for detecting changes of biophysical and biochemical parameters of the tropical rainforest affected by hydrocarbon from oil spills or hydrocarbon seepages? In this context, this research question can be split in the following parts:

- Which vegetation indices can best identify vegetation stress caused by hydrocarbon pollution?
- Can new vegetation indices sensitive to detecting tropical rainforest affected by hydrocarbon pollution be derived?
- Can chlorophyll content maps be derived from hyperspectral satellite images and can they highlight vegetation stress caused by hydrocarbons?

The findings from Chapter 5 provide the answer to the Research Question 3.

Which vegetation indices can best identify vegetation stress caused by hydrocarbon pollution?

From 28 vegetation broad-band and narrow-band vegetation indices, 11 indices effectively identified the effects of hydrocarbon pollution in the tropical forest. Those indices are sensitive to detection changes of photosynthetic activity of the forest based on chlorophyll content and indices related to canopy density and vegetation vigour. On the other hand, vegetation indices sensitive to foliar water content were not able to detect changes at canopy level. Most of the vegetation indices (24) were able to discriminate between secondary and pristine forests.

Based on the 11 suitable vegetation indices to detect vegetation stress, a vegetation stress map was computed in the petroleum productive site. The results distinguished stressed vegetation located near swamps and in the vicinity of

petroleum processing, storage and transport facilities (platforms, pipelines, and open pits). Water runoff from those facilities brings hydrocarbons (and probably other pollutants) to the swamps.

Discriminant function analysis has indicated that from the 11 vegetation indices, three of them contribute with 83% of the group separability. SG index contributes with 53%, followed by NDVI index with 21.6% and NDVI₇₀₅ with 8.4%. The contribution of the other indices is relatively low.

Mapping vegetation affected by hydrocarbon pollution by the three indices approach identified practically the same areas as using the 11 indices approach which demonstrates that effectiveness of the SG and NDVI indices to detect vegetation stress in tropical forest.

The applicability of the three indices approach was tested in a CHRIS-Proba image from an area where crude oil has been naturally exposed to the surface in vast hydrocarbon seepage. It is assumed that tropical vegetation growing in this reduced environment has been exposing to stress conditions. The areas detected as vegetation stress intersect with geological faults and commercial reservoirs that the oil industry has identified through exploratory wells and seismic projects. That is a potential application of the results of this research in the petroleum industry which can considerable reduce cost during exploration projects in inaccessible or environmental sensitive areas.

Can new vegetation indices sensitive to detect tropical rainforest affected by hydrocarbon pollution be derived?

Two new vegetation indices were derived from the higher correlation observed between foliar reflectance and foliar chlorophyll content. The new indices sensitive to chlorophyll content in the tropical rainforest proposed in this study are: RSI (R_{900}/R_{716}) and NDSI ($(R_{726}-R_{797})/(R_{726}+R_{797})$). Correlations between RSI and chlorophyll content reported $R^2=0.74$ and NDSI reported $R^2=0.73$.

The new indices highlighted that higher reflectance values in the visible range of the polluted area are related to decreased levels of foliar chlorophyll content which was reported in Chapter 4. On the other hand, the indices highlighted higher reflectance values in the NIR region, which has been reported in vegetation growing in soils with high levels of pollution.

RSI and NDSI indices were applied to a Hyperion satellite image in order to assess the chlorophyll content at canopy level in vegetation of the tropical rainforest. In the pristine forest sampled during fieldwork, the results revealed a strong correlation of 0.92 and 0.96 by RSI and NDSI respectively. Followed by the secondary non-polluted site ($R^2 = 0.76$ and $R^2=0.93$ respectively). In the secondary forest polluted site, the correlation of band combination is weak ($R^2=0.10$ and $R^2=0.40$ respectively). This suggests that the new vegetation indices can effectively differentiate the effects of hydrocarbon pollution in the tropical forest using Hyperion satellite images by observing an increase of RED reflectance (reduce chlorophyll content), associated to an increase in NIR reflectance.

A comparison of the new indices with MTCI revealed that is more sensitive for detecting the differences between pristine and secondary forest. On the other hand, NSDI provides a better identification of polluted and non-polluted secondary forest. These findings can be applied to exploit the opportunity to use specific vegetation indices for monitoring tropical forest environments using a wide range of satellite data sets.

Do chlorophyll content maps can be derived from hyperspectral satellite images and they can highlight vegetation stress caused by hydrocarbons?

In this study it was demonstrated that chlorophyll content is an indicator of vegetation health in a tropical forest. Then an approach to estimate chlorophyll content at canopy level was presented based on information collected at leaf level using transmittance and reflectance measurements applied to MTCI index and scaling-up to canopy level using a hyperspectral Hyperion image. This method

was able to map chlorophyll content at canopy level showing low concentrations around petroleum facilities which may indicate vegetation stress and very high concentrations in the pristine forest.

The sensitivity of the SPAD-502 chlorophyll meter in extreme high and low readings was tested in this study. The ground-truth chlorophyll content from the SPAD-502 before and after outliers were removed was correlated to the sensitivity chlorophyll content of MTCI index at leaf level. The results showed a strongest correlation without outlier removal ($R^2=0.68$). When applied to canopy level, chlorophyll maps shows close estimations of chlorophyll content which suggest that using the method proposed in this study, SPAD-502 readings are sensitive for mapping chlorophyll content in vegetation of tropical forest.

6.2 Contribution to knowledge

A calibration model to estimate chlorophyll content in a heterogeneous tropical forest using SPAD-502 chlorophyll meter has been proposed. This approach significantly contributes to estimate chlorophyll content in remote areas of the tropical rainforest where laboratory facilities are not available.

This study reveals for the first time that a tropical forest exposed to hydrocarbon pollution shows reduced levels of chlorophyll content, higher levels of foliar water content and leaf structural changes. Furthermore the effects of pollution have been distinguished at different layers of the vertical profile of the tropical forest. These findings can effectively contribute to investigations of forest health and vegetation stress in areas affected by pollution and in this way assesses forest degradation.

Mapping vegetation affected by hydrocarbon pollution by the three indices approach (SG, NDVI and NDVI₇₀₅) provided 83% of the separability between different forest groups and identified practically the same areas than using the 11 indices approach, which demonstrates the effectiveness of the SG and NDVI indices to detect vegetation stress in tropical forest.

Two new vegetation indices (RSI and NSDI) able to detect changes of biophysical and biochemical parameters of tropical rainforest are presented. Those indices are based on the strong correlation shown by chlorophyll content and reflectance at leaf level. The NSDI index has shown sensitivity to differentiate between the polluted and non-polluted secondary forest. This is a normalised difference index which is effective in reducing the influence of errors or uncertainty due to sensor specifications, atmospheric and background differences.

Chlorophyll content is a key photosynthetic pigment which is closely related to vegetation health. This study present an alternative method to estimate chlorophyll content at canopy level based on optical data collected at leaf level and scale-up at canopy level throughout the MTCI index applied to hyperspectral remote sensing images. This approach makes it possible to map chlorophyll content at canopy level in the tropical forest of the Amazon region.

In summary, this research significantly advances scientific understanding by providing evidence of leaf chemical alterations in the tropical rainforest caused by hydrocarbon pollution and has implications for global rainforest monitoring satellite missions in that it identifies the leaf chemical properties that can be detected from a space-borne sensor. The implication of this finding is that we can start to develop remote sensing methods to detect swaths and sections of forest that have been exposed to enhanced levels of hydrocarbons which may contribute to detecting hydrocarbon seepages as well as significant pollution spills in forest ecosystems.

6.3 Limitations

Some assumptions and limitations in this study have been discussed in detail in the respective chapters with recommendations for further research. Here the limitations are summarized:

In spite of the efforts to sample biophysical and biochemical parameters of vegetation in the Pungarayacu site (hydrocarbon seepage site), the petroleum

company operating in the area denied the permission for data collection which did not allow accurate assessment of vegetation stress in areas affected by hydrocarbons from the seepage.

We have a limited number of Hyperion satellite images from the study sites. A request for new Hyperion images was submitted to NASA-USGS but the cloudy conditions of the study area did not allow for new acquisitions.

A scaling-up process for estimating chlorophyll content from leaf to canopy level was applied by using the DART model. It is a 3D model that simulates radiative transfer in complex 3-D scenes of forest stands. The model uses a specific module for simulation of reflectance at leaf level which relies on the PROSPECT model. The forward process of the model was successfully applied in the study sites, but the inverse mode to estimate chlorophyll content at canopy level was not operative at the time of this research.

6.4 Further research

- Several authors have discussed the “sieve effect” which appears to be the principal factor for a reduced accuracy of the SPAD-502 meter in high chlorophyll content plants. The sieve effect states that in leaves with high chlorophyll concentrations, the chloroplasts may contain an increased density of chlorophyll rather than an increased density of chloroplasts. It is recommended to investigate the impact of the sieve effect in vegetation of tropical forests which has shown high chlorophyll content and very high SPAD-502 readings.
- Foliar samples in this study represent sites of the low land tropical forest of Ecuador. It is advisable to test the calibration model proposed in this study on vegetation of tropical forest of different latitudes. Biochemical foliar datasets of tropical forests may be used, for instance the Carnegie Spectranomics dataset (<http://spectranomics.stanford.edu/>).

- Higher levels of foliar water content were found in vegetation growing in the polluted site. It is not clear why foliar water content increases in vegetation affected by hydrocarbon pollution. More research needs to be done in this area.
- A better understanding of a possible shift in the specie composition in tropical forest affected by hydrocarbons is needed because some species may be replaced by invasive species more resistant to the hydrocarbons influence.
- The implication of the findings may contribute to the development of remote sensing methods to detect swaths and sections of forest that have been exposed to enhanced levels of hydrocarbons at the Earth's surface, therefore methods of detecting hydrocarbon seepages as well as significant pollution spills in forest ecosystems can now be developed. Petroleum exploration projects may benefit from the application of hyperspectral remote sensing techniques in order to detect hydrocarbon seepages as evidence of commercial petroleum/gas reservoirs. In addition, the findings of this research can be tested and applied to investigate the possible environmental effects of gas production using fracking techniques.
- Tests of the new vegetation indices in different hyperspectral sensors and study areas of the tropical rainforest affected by hydrocarbons will provide a more accurate assessment of the proposed indices.
- Applications of airborne hyperspectral images with a higher spatial resolution and higher signal-to-noise-ratio will definitely improve detection of vegetation stress caused by petroleum pollution. The Unmanned Aerial Vehicles (UAV) may also provide an alternative to investigate biophysical and biochemical parameters of vegetation at tree level. In addition, LiDAR data can contribute favourably to estimate biophysical and biochemical parameter in the tropical forest.

- The complex composition of the tropical forest, due its high diversity and physiological composition, requires more specific vegetation indices developed and tested for this particular environment. Most research needs to be done in this subject.

ANNEXES

Annex 1 Vegetation species sampled in Site 1 and Site 2-Petroleum productive area

This list represents the plant species that were identified during fieldwork. Some samples were no identified.

| | Family | Genus/Specie | | Family | Genus/Specie |
|----|------------------|------------------------------|----|-----------------|---------------------------------|
| 1 | Acanthaceae | <i>N.I. *</i> | 39 | Melastomataceae | <i>Miconia sp</i> |
| 2 | Anacardiaceae | <i>Tapirira guianensis</i> | 40 | Melastomataceae | <i>Miconia bubalina</i> |
| 3 | Anacardiaceae | <i>N.I. *</i> | 41 | Melastomataceae | <i>Maietia sp</i> |
| 4 | Annonaceae | <i>Gutteria sp.</i> | 42 | Melastomataceae | <i>Blackea sp</i> |
| 5 | Annonaceae | <i>Gutteria glaberrima</i> | 43 | Meliaceae | <i>Guarea sp</i> |
| 6 | Araliaceae | <i>Shefflera morottotoni</i> | 44 | Moraceae | <i>Ficus sp.</i> |
| 7 | Araliaceae | <i>Dendropanax sp</i> | 45 | Moraceae | <i>Ficus tonduzzi</i> |
| 8 | Boraginaceae | <i>Cordia nodosa</i> | 46 | Moraceae | <i>Pseudolmedia lperbea</i> |
| 9 | Boraginaceae | <i>Cordia sp</i> | 47 | Moraceae | <i>Pseudolmedia sorocea</i> |
| 10 | Burseraceae | <i>Protium nodulosum</i> | 48 | Moraceae | <i>Sorocea sp</i> |
| 11 | Cecropiaceae | <i>Cecropia scyadophylla</i> | 49 | Myristiaceae | <i>Otoba sp</i> |
| 12 | Chrysobalanaceae | <i>Licania sp</i> | 50 | Myristiaceae | <i>Otoba glycyarpa</i> |
| 13 | Clusiaceae | <i>Clusia sp</i> | 51 | Myristiaceae | <i>Virola sp</i> |
| 14 | Clusiaceae | <i>Tovomita sp</i> | 52 | Myrtaceae | <i>N.I. *</i> |
| 15 | Clusiaceae | <i>Vismia sp</i> | 53 | Nyctaginaceae | <i>Neea sp</i> |
| 16 | Clusiaceae | <i>Vismia baccifera</i> | 54 | Ochnaceae | <i>Cespedecia sp.</i> |
| 17 | Combretaceae | <i>N.I. *</i> | 55 | Piperaceae | <i>Piper sp</i> |
| 18 | Euphorbiaceae | <i>Acalypha sp</i> | 56 | Piperaceae | <i>Piper arboreum</i> |
| 19 | Euphorbiaceae | <i>Croto lechleri</i> | 57 | Poaceae | <i>Olyra latifolia</i> |
| 20 | Euphorbiaceae | <i>Aparisthmium cordatum</i> | 58 | Polygonaceae | <i>Coccoloba desifrons</i> |
| 21 | Euphorbiaceae | <i>Hevea guianensis</i> | 59 | Proteaceae | <i>Roupala sp.</i> |
| 22 | Fabaceae | <i>Inga sp.</i> | 60 | Pteridophyta | <i>Ferns</i> |
| 23 | Fabaceae | <i>Inga ciliata</i> | 61 | Rubiaceae | <i>Psychotria poeppigiana</i> |
| 24 | Fabaceae | <i>Swartzia sp</i> | 62 | Rubiaceae | <i>Pentagonia spmacrophylla</i> |
| 25 | Fabaceae | <i>Brownea grandiceps</i> | 63 | Rubiaceae | <i>Rudgea sp</i> |
| 26 | Fabaceae | <i>Zygia</i> | 64 | Sapindaceae | <i>Paullinia sp</i> |
| 27 | Fabaceae | <i>Dussia sp.</i> | 65 | Sapindaceae | <i>Allophyllus sp</i> |
| 28 | Fabaceae | <i>Dussia tessmannii</i> | 66 | Sapindaceae | <i>Serjania sp</i> |
| 29 | Fabaceae | <i>Macrolobium</i> | 67 | Sapotaceae | <i>Pouteria torta</i> |
| 30 | Fabaceae | <i>Parkia baslevii</i> | 68 | Sapotaceae | <i>Micropholis venulosa</i> |
| 31 | Flacourtiaceae | <i>Banara sp</i> | 69 | Sloaneaceae | <i>Sloanea sp.</i> |
| 32 | Lecythidaceae | <i>N.I. *</i> | 70 | Sterculiaceae | <i>Theobroma o Sterculia</i> |
| 33 | Maranthaceae | <i>Calathea sp</i> | 71 | Sterculiaceae | <i>Sterculia sp.</i> |
| 34 | Malvaceae | <i>Matisia sp</i> | 72 | Tiliaceae | <i>Apeiba membranacea</i> |

| | | | | | |
|----|----------------------|-----------------------------|----|---------------|-------------------------|
| 35 | Malvaceae | <i>Matisia obliquifolia</i> | 73 | Violaceae | <i>Leonia glycyarpa</i> |
| 36 | Malvaceae | <i>Ochroma pyramidale</i> | 74 | Staphyleaceae | <i>Huerteia sp</i> |
| 37 | Malvaceae | <i>Patinoa sp</i> | 75 | Vochysiaceae | <i>Qualea sp</i> |
| 38 | Melastomataceae | <i>Clidemia o Miconia</i> | | | |
| | * N.I. No identified | | | | |

Annex 2 Vegetation species sampled in Site 3-Pristine forest

This list represents the plant species sampled in an area of 4800 m² where data collection was carry on during fieldwork. This area represents 12 subplots inside the permanent plot of the Yasuni Research Station managed by the Catholic University of Ecuador. The list of species was provided by Dr Renato Valencia.

| | Family | Genus/Species | | # of trees sampled |
|----|------------------|---------------------|-------------------------|--------------------|
| 1 | ANACARDIACEAE | <i>Spondias</i> | <i>mombin</i> | 1 |
| 2 | ANACARDIACEAE | <i>Tapirira</i> | <i>guianensis</i> | 4 |
| 3 | ANNONACEAE | <i>Guatteria</i> | <i>recurvisepala</i> | 1 |
| 4 | ANNONACEAE | <i>Trigynaea</i> | <i>triplinervis</i> | 1 |
| 5 | ANNONACEAE | <i>Unonopsis</i> | <i>veneficiorum</i> | 1 |
| 6 | ARALIACEAE | <i>Dendropanax</i> | <i>caucanus</i> | 1 |
| 7 | ARECACEAE | <i>Iriartea</i> | <i>deltoidea</i> | 1 |
| 8 | BIGNONIACEAE | <i>Memora</i> | <i>cladotricha</i> | 2 |
| 9 | BOMBACACEAE | <i>Matisia</i> | <i>bracteolosa</i> | 2 |
| 10 | BOMBACACEAE | <i>Matisia</i> | <i>huallagensis</i> | 2 |
| 11 | BOMBACACEAE | <i>Matisia</i> | <i>malacocalyx</i> | 18 |
| 12 | BOMBACACEAE | <i>Matisia</i> | <i>obliquifolia</i> | 2 |
| 13 | BURSERACEAE | <i>Protium</i> | <i>aracouchini</i> | 2 |
| 14 | BURSERACEAE | <i>Protium</i> | <i>brillanodu</i> | 2 |
| 15 | BURSERACEAE | <i>Protium</i> | <i>grannodu</i> | 1 |
| 16 | BURSERACEAE | <i>Protium</i> | <i>nodulosum</i> | 1 |
| 17 | BURSERACEAE | <i>Protium</i> | <i>sagotianum</i> | 3 |
| 18 | CECROPIACEAE | <i>Pourouma</i> | <i>bicolor</i> | 2 |
| 19 | CECROPIACEAE | <i>Pourouma</i> | <i>deeplob</i> | 1 |
| 20 | CECROPIACEAE | <i>Pourouma</i> | <i>tomentosa</i> | 1 |
| 21 | CELASTRACEAE | <i>Maytenus</i> | <i>cilindrica</i> | 1 |
| 22 | CHRYSOBALANACEAE | <i>Licania</i> | <i>longipedicellata</i> | 7 |
| 23 | DICHAPETALACEAE | <i>Tapura</i> | <i>peruviana</i> | 3 |
| 24 | ELAEOCARPACEAE | <i>Sloanea</i> | <i>fragrans</i> | 1 |
| 25 | ELAEOCARPACEAE | <i>Sloanea</i> | <i>granalargada</i> | 1 |
| 26 | ELAEOCARPACEAE | <i>Sloanea</i> | <i>rufisessi</i> | 1 |
| 27 | ELAEOCARPACEAE | <i>Sloanea</i> | <i>tomentosa</i> | 2 |
| 28 | EUPHORBIACEAE | <i>Alchornea</i> | <i>triplinervia</i> | 1 |
| 29 | EUPHORBIACEAE | <i>Caryodendron</i> | <i>orinocense</i> | 1 |
| 30 | EUPHORBIACEAE | <i>Mabea</i> | <i>superbrundu</i> | 2 |
| 31 | EUPHORBIACEAE | <i>Pausandra</i> | <i> trianae</i> | 2 |
| 32 | EUPHORBIACEAE | <i>Richeria</i> | <i>racemosa</i> | 1 |
| 33 | FABACEAE | <i>Apuleia</i> | <i>leiocarpa</i> | 1 |
| 34 | FABACEAE | <i>Brownea</i> | <i>grandiceps</i> | 8 |
| 35 | FABACEAE | <i>Inga</i> | <i>auristella</i> | 1 |

| | | | | |
|----|------------------|-----------------------|---------------------|---|
| 36 | FABACEAE | <i>Inga</i> | <i>bourgonii</i> | 2 |
| 37 | FABACEAE | <i>Inga</i> | <i>cordatoalata</i> | 1 |
| 38 | FABACEAE | <i>Inga</i> | <i>marginata</i> | 1 |
| 39 | FABACEAE | <i>Inga</i> | <i>microcoma</i> | 2 |
| 40 | FABACEAE | <i>Inga</i> | <i>nobilis</i> | 1 |
| 41 | FABACEAE | <i>Inga</i> | <i>ruiziana</i> | 2 |
| 42 | FABACEAE | <i>Inga</i> | <i>tenuistipula</i> | 1 |
| 43 | FABACEAE | <i>Inga</i> | <i>umbratica</i> | 3 |
| 44 | FABACEAE | <i>Swartzia</i> | <i>arborescens</i> | 1 |
| 45 | FABACEAE | <i>Zygia</i> | <i>heteroneura</i> | 1 |
| 46 | FLACOURTIACEAE | <i>Carpotroche</i> | <i>longifolia</i> | 1 |
| 47 | FLACOURTIACEAE | <i>Casearia</i> | <i>arborea</i> | 1 |
| 48 | FLACOURTIACEAE | <i>Casearia</i> | <i>sylvestris</i> | 1 |
| 49 | FLACOURTIACEAE | <i>Lindackeria</i> | <i>paludosa</i> | 1 |
| 50 | FLACOURTIACEAE | <i>Lozania</i> | <i>klugii</i> | 2 |
| 51 | FLACOURTIACEAE | <i>Ryania</i> | <i>speciosa</i> | 1 |
| 52 | FLACOURTIACEAE | <i>Tetrathylacium</i> | <i>macrophyllum</i> | 6 |
| 53 | LAURACEAE | <i>N.I.</i> | <i>lisagroovy</i> | 2 |
| 54 | LAURACEAE | <i>Cryptocarya</i> | <i>yasuniensis</i> | 3 |
| 55 | LAURACEAE | <i>Endlicheria</i> | <i>formosa</i> | 1 |
| 56 | LAURACEAE | <i>Endlicheria</i> | <i>sericea</i> | 1 |
| 57 | LAURACEAE | <i>Licaria</i> | <i>cannella</i> | 2 |
| 58 | LAURACEAE | <i>Licaria</i> | <i>chiquita</i> | 1 |
| 59 | LAURACEAE | <i>Mezilaurus</i> | <i>trunca</i> | 1 |
| 60 | LAURACEAE | <i>Ocotea</i> | <i>alamembra</i> | 1 |
| 61 | LAURACEAE | <i>Ocotea</i> | <i>cernua</i> | 1 |
| 62 | LAURACEAE | <i>Ocotea</i> | <i>javitensis</i> | 1 |
| 63 | LAURACEAE | <i>Ocotea</i> | <i>laurita</i> | 1 |
| 64 | LAURACEAE | <i>Ocotea</i> | <i>luis</i> | 2 |
| 65 | LECYTHIDACEAE | <i>Eschweilera</i> | <i>coriacea</i> | 1 |
| 66 | LECYTHIDACEAE | <i>Eschweilera</i> | <i>gigantea</i> | 1 |
| 67 | LECYTHIDACEAE | <i>Eschweilera</i> | <i>rufifolia</i> | 1 |
| 68 | LECYTHIDACEAE | <i>Grias</i> | <i>neuberthii</i> | 1 |
| 69 | LECYTHIDACEAE | <i>Gustavia</i> | <i>hexapetala</i> | 2 |
| 70 | LECYTHIDACEAE | <i>Gustavia</i> | <i>longifolia</i> | 2 |
| 71 | MAGNOLIACEAE | <i>Talauma</i> | <i>ovata</i> | 1 |
| 72 | MELASTOMATAACEAE | <i>Miconia</i> | <i>acutipetala</i> | 1 |
| 73 | MELASTOMATAACEAE | <i>Miconia</i> | <i>fosteri</i> | 1 |
| 74 | MELASTOMATAACEAE | <i>Miconia</i> | <i>peqdorada</i> | 2 |
| 75 | MELASTOMATAACEAE | <i>Miconia</i> | <i>tipica</i> | 7 |
| 76 | MELASTOMATAACEAE | <i>Mouriri</i> | <i>grandiflora</i> | 1 |
| 77 | MELIACEAE | <i>Guarea</i> | <i>carinata</i> | 1 |
| 78 | MELIACEAE | <i>Guarea</i> | <i>fistulosa</i> | 7 |
| 79 | MELIACEAE | <i>Guarea</i> | <i>gomma</i> | 1 |

| | | | | |
|-----|---------------|---------------------|------------------------|---|
| 80 | MELIACEAE | <i>Guarea</i> | <i>guentheri</i> | 1 |
| 81 | MELIACEAE | <i>Guarea</i> | <i>guenthfuzzy</i> | 1 |
| 82 | MELIACEAE | <i>Guarea</i> | <i>kunthiana</i> | 2 |
| 83 | MELIACEAE | <i>Guarea</i> | <i>macrophylla</i> | 1 |
| 84 | MELIACEAE | <i>Guarea</i> | <i>pteriorhachis</i> | 1 |
| 85 | MELIACEAE | <i>Guarea</i> | <i>silvatica</i> | 1 |
| 86 | MELIACEAE | <i>Trichilia</i> | <i>poepigii</i> | 2 |
| 87 | MELIACEAE | <i>Trichilia</i> | <i>rubra</i> | 1 |
| 88 | MELIACEAE | <i>Trichilia</i> | <i>septentrionalis</i> | 2 |
| 89 | MONIMIACEAE | <i>Mollinedia</i> | <i>killipii</i> | 1 |
| 90 | MONIMIACEAE | <i>Mollinedia</i> | <i>spinilarga</i> | 1 |
| 91 | MONIMIACEAE | <i>Siparuna</i> | <i>biglí</i> | 1 |
| 92 | MONIMIACEAE | <i>Siparuna</i> | <i>cuspidata</i> | 3 |
| 93 | MONIMIACEAE | <i>Siparuna</i> | <i>decipiens</i> | 4 |
| 94 | MORACEAE | <i>Ficus</i> | <i>gomelleira</i> | 1 |
| 95 | MORACEAE | <i>Maquira</i> | <i>calophylla</i> | 1 |
| 96 | MORACEAE | <i>Perebea</i> | <i>mollis</i> | 1 |
| 97 | MORACEAE | <i>Perebea</i> | <i>xanthochyma</i> | 1 |
| 98 | MORACEAE | <i>Pseudolmedia</i> | <i>laevigata</i> | 2 |
| 99 | MORACEAE | <i>Pseudolmedia</i> | <i>laevis</i> | 1 |
| 100 | MORACEAE | <i>Sorocea</i> | <i>pubivena</i> | 2 |
| 101 | MORACEAE | <i>Sorocea</i> | <i>steinbachii</i> | 1 |
| 102 | MYRISTICACEAE | <i>Iryanthera</i> | <i>grandis</i> | 1 |
| 103 | MYRISTICACEAE | <i>Iryanthera</i> | <i>hostmannii</i> | 5 |
| 104 | MYRISTICACEAE | <i>Otoba</i> | <i>glycycarpa</i> | 3 |
| 105 | MYRISTICACEAE | <i>Virola</i> | <i>dixonii</i> | 1 |
| 106 | MYRISTICACEAE | <i>Virola</i> | <i>pavonis</i> | 2 |
| 107 | MYRISTICACEAE | <i>Virola</i> | <i>xx</i> | 1 |
| 108 | MYRTACEAE | <i>N.I.</i> | <i>smedpubicost</i> | 2 |
| 109 | MYRTACEAE | <i>Eugenia</i> | <i>granvariable</i> | 1 |
| 110 | MYRTACEAE | <i>Eugenia</i> | <i>longisepala</i> | 1 |
| 111 | MYRTACEAE | <i>Eugenia</i> | <i>membranegra</i> | 1 |
| 112 | MYRTACEAE | <i>Eugenia</i> | <i>schunkei</i> | 2 |
| 113 | MYRTACEAE | <i>Plinia</i> | <i>pseudomouriri</i> | 1 |
| 114 | MYRTACEAE | <i>Plinia</i> | <i>unop</i> | 1 |
| 115 | NYCTAGINACEAE | <i>Neea</i> | <i>aniboid</i> | 1 |
| 116 | NYCTAGINACEAE | <i>Neea</i> | <i>claudia</i> | 1 |
| 117 | NYCTAGINACEAE | <i>Neea</i> | <i>comun</i> | 1 |
| 118 | NYCTAGINACEAE | <i>Neea</i> | <i>fuzzy</i> | 1 |
| 119 | NYCTAGINACEAE | <i>Neea</i> | <i>gigante</i> | 1 |
| 120 | NYCTAGINACEAE | <i>Neea</i> | <i>granredonda</i> | 1 |
| 121 | OPIACEAE | <i>Agonandra</i> | <i>peruviana</i> | 1 |
| 122 | PIPERACEAE | <i>Piper</i> | <i>obchic</i> | 1 |
| 123 | POLYGONACEAE | <i>Coccoloba</i> | <i>densifrons</i> | 1 |

| | | | | |
|-----|---------------|----------------------|----------------------|----|
| 124 | QUIINACEAE | <i>Quiina</i> | <i>florida</i> | 1 |
| 125 | QUIINACEAE | <i>Quiina</i> | <i>grandifolia</i> | 1 |
| 126 | RUBIACEAE | <i>Agouticarpa</i> | <i>isernii</i> | 1 |
| 127 | RUBIACEAE | <i>Alseis</i> | <i>lugonis</i> | 2 |
| 128 | RUBIACEAE | <i>Calycophyllum</i> | <i>megistocaulum</i> | 1 |
| 129 | RUBIACEAE | <i>Chomelia</i> | <i>tenuiflora</i> | 1 |
| 130 | RUBIACEAE | <i>Duroia</i> | <i>hirsuta</i> | 1 |
| 131 | RUBIACEAE | <i>Faramea</i> | <i>capillipes</i> | 1 |
| 132 | RUBIACEAE | <i>Pentagonia</i> | <i>amazonica</i> | 1 |
| 133 | RUBIACEAE | <i>Pentagonia</i> | <i>subauric</i> | 1 |
| 134 | RUBIACEAE | <i>Posoqueria</i> | <i>latifolia</i> | 2 |
| 135 | RUBIACEAE | <i>Simira</i> | <i>rubescens</i> | 1 |
| 136 | RUBIACEAE | <i>Warszewiczia</i> | <i>coccinea</i> | 2 |
| 137 | RUBIACEAE | <i>Warszewiczia</i> | <i>cordata</i> | 1 |
| 138 | RUTACEAE | <i>Zanthoxylum</i> | <i>brillante</i> | 1 |
| 139 | SAPINDACEAE | <i>Allophylus</i> | <i>glabra</i> | 1 |
| 140 | SAPOTACEAE | <i>Ecclinusa</i> | <i>guianensis</i> | 2 |
| 141 | SAPOTACEAE | <i>Pouteria</i> | <i>glomerata</i> | 1 |
| 142 | SAPOTACEAE | <i>Pouteria</i> | <i>guianensis</i> | 1 |
| 143 | SAPOTACEAE | <i>Pouteria</i> | <i>redondita</i> | 1 |
| 144 | SAPOTACEAE | <i>Pouteria</i> | <i>torta</i> | 1 |
| 145 | SAPOTACEAE | <i>Pouteria</i> | <i>vernica</i> | 1 |
| 146 | SAPOTACEAE | <i>Sarcaulus</i> | <i>romolerouxii</i> | 1 |
| 147 | SAPOTACEAE | <i>Sarcaulus</i> | <i>vestitus</i> | 1 |
| 148 | STERCULIACEAE | <i>Sterculia</i> | <i>tessmannii</i> | 1 |
| 149 | STERCULIACEAE | <i>Theobroma</i> | <i>subincanum</i> | 3 |
| 150 | TILIACEAE | <i>Apeiba</i> | <i>membranacea</i> | 1 |
| 151 | ULMACEAE | <i>Ampelocera</i> | <i>edentula</i> | 1 |
| 152 | ULMACEAE | <i>Celtis</i> | <i>schippii</i> | 1 |
| 153 | VIOLACEAE | <i>Rinorea</i> | <i>apiculata</i> | 2 |
| 154 | VIOLACEAE | <i>Rinorea</i> | <i>lindeniana</i> | 9 |
| 155 | VIOLACEAE | <i>Rinorea</i> | <i>viridifolia</i> | 12 |

Annex 3 Chlorophyll indices based on SPAD-502 readings excluded from the analysis

| ID | Model | Units | Tested in | Samples | SPAD-502 range | Chl range ($\mu\text{m cm}^{-2}$) | R ² | Source |
|------|--|------------------------|--------------------|---------|----------------|-------------------------------------|----------------|--------------------------------------|
| 3.8 | $\text{Chl} = -2366 + 97.5 X - 0.7237X^2$ | $\mu\text{mol m}^{-2}$ | Maize | na. | na. | na. | 0.89 | (Marwell ; Osterman & Mitchell 1995) |
| 3.9 | $\text{Chl} = (63.92 * X) / (82.85 - X)$ | $\mu\text{g cm}^{-2}$ | Oak and beech | 70 | 10-90 | ~10-90 | 0.94 | (Demarez et al. 1999) |
| 3.10 | $\text{Chl} = 525.99154 / (1 + 29.9566 e^{-0.08719X})$ | $\mu\text{mol m}^{-2}$ | Papaya (2 species) | 50 | 4 - 60 | 0 - 45 | 0.93 | (Torres-Netto et al. 2002) |
| 3.11 | $\text{Chl} = 44.5885 + 0.7188X + 0.0933X^2$ | $\mu\text{mol m}^{-2}$ | Coffee leaves | 110 | 0 - 80 | 0 - 70 | 0.96 | (Torres-Netto et al. 2005) |

na. = Not available

Model 3.8 displayed negative values of chlorophyll content when tested on the SPAD-502 reading of this study, which include some lower SPAD-502 readings, therefore it was excluded from our analysis.

Seasonal variation of biophysical and biochemical properties of a deciduous forest (oak, beech and hornbeam) with differences between sun and shade leaves and abaxial and adaxial surfaces were considered for Model 3.9. Specific transformation models for samples of oak and beech were presented but a general relationship was found to be a better estimator of chlorophyll concentration. The results of the model showed a good relationship with chlorophyll concentration estimated by the inversion process of the radiative transfer model PROSPECT. When we applied this model to our dataset, the chlorophyll content values increased exponentially with SPAD-502 readings and reached implausibly high values of chlorophyll content ($1862 \mu\text{g cm}^{-2}$) for SPAD-502 readings >60 units. Consequently, we excluded this model from further analysis.

In 2002 two species of papaya used to assess chlorophyll content from SPAD-502 readings. The study also took into account carotenoids and foliar nitrogen content and their relationship with chlorophyll content. The model provided is described as Model 3.10. In 2005 a similar study was carried out, this time using coffee plants (Model 3.11). When applied to our data set both models estimated average chlorophyll values of $36 \mu\text{g cm}^{-2}$ and $26 \mu\text{g cm}^{-2}$, which are considered extremely low for foliar chlorophyll content in tropical rainforest. They were also excluded from further analysis.

Annex 4 Chlorophyll indices based on reflectance indices excluded from the analysis

| ID | Index | Model | Units | Tested in | Sampl es | Chl range ($\mu\text{m cm}^{-2}$) | RMSE | R^2 | Sourc e |
|-----|---|---|--------------------|---|-------------|---|-----------|-------------|--|
| 4.6 | $[(R_{750} - 800) / (R_{720} - 730)] - 1$ | Chl = 0.3418 X + 0.2075 | g m^{-2} | Maize and soybean | 82 | 3 - 43.3 | 3.2 | 0.95 | (Gitelson et al. 2005) |
| 4.7 | $[(R_{760} - 800) / (R_{690} - 720)] - 1$ | 10 linear models, one per each plant specie | mg m^{-2} | Beech, chestnut, mapple, maize, soybean, dogwood from different years | 38 | 37.5 (mean) | 0.8 - 4 | 0.91 - 0.95 | (Gitelson; Kedyan & Merzlyak 2006) |
| 4.8 | $[(R_{760} - 800) / (R_{540} - 560)] - 1$ | 8 linear models, one per each plant specie | mg m^{-2} | Beech, chestnut, mapple, maize, soybean, dogwood from different years | 38 | 37.5 (mean) | 2.5 - 7.5 | 0.91 - 0.95 | (Gitelson; Kedyan & Merzlyak 2006) |
| 4.9 | $[(R_{750} - 800) / (R_{695} - 740)] - 1$ | Chl = 118.11 * X | mg m^{-2} | European hazel, siberian dogwood, norway mapple and virginia creeper | 173 | 0.063 - 53.9 | 2.1 | 0.97 | (Gitelson; Chivkuno va & Merzlyak 2009, Gitelson 2012) |

Accurate estimation of chlorophyll content in a multi-species scenario is proposed by narrowing the red edge range (720-730 nm) and applying a model specified in Model 4.6. When this model was applied to our dataset, it estimated negative chlorophyll content values for the lower SPAD-502 readings and hence it was not considered further here.

Following the same three-band conceptual model described by Model 4.4-Table 3.5, implemented a series of models based on near infrared, red edge and visible

spectra indices. Each model was tested for specific trees and crops in a dataset of 306 leaf samples. A total of 18 different models were presented, one for each plant species. The models allowed accurate estimation of chlorophyll content when they were compared to the validation dataset by the authors of that study. The cited study also considered models for carotenoids and anthocyanins content estimation. Here, we applied the model for 'beech 1996' in the red edge (Model 4.7) and green (Model 4.8) ranges to our dataset. The results showed extremely low mean values (less than 5 $\mu\text{g cm}^{-2}$), therefore these models were not considered for tropical rainforest any further.

Anthocyanins are another important plant pigment responsible for the red colouration of the leaves. Their presence in the leaves may be caused by stress such as deficiencies in nitrogen and phosphorus, wounding, pathogen infection desiccation, low temperature and UV-irradiation. Therefore a negative relationship is assumed between anthocyanins and chlorophyll content. In 2009, Gitelson et al. [31] proposed indices for chlorophyll and anthocyanin estimation in leaves of four unrelated tree species with widely variable pigment content and composition. A two spectral band index called red edge chlorophyll index (CI_{red edge}) and its corresponding model were able to accurately estimate chlorophyll content up to 54 $\mu\text{g cm}^{-2}$. Later, using the same foliar dataset of Models 4.7 and 4.8, different indices which had previously been developed for chlorophyll were tested and their accuracy compared. The indices applied were the Simple Ratio (SR), Normalized Difference Vegetation Index (NDVI), Enhanced Vegetation Index (EVI2), Red Edge NDVI, Eucalyptus Chlorophyll Index (ECI) and Red Edge Chlorophyll index (CI_{red edge}). Results of the study showed that the best estimation was performed by CI_{red edge} (Model 4.9). When we applied this index to our dataset, mean chlorophyll content values illustrated very low values (<10 $\mu\text{g cm}^{-2}$), therefore we excluded it as well.

A possible explanation of the low range of chlorophyll estimates from the last four indices (4.6, 4.7, 4.8 and 4.9) is that they were created using a validation

dataset that represented a low chlorophyll content range (see Table of this annex), which makes them unsuitable for the tropical rainforests in our study area.

Annex 5 R code for estimate reflectance and transmittance based on Trans- flectance (double-reflectance)

```

# Estimation of Reflectance and Transmittance using Jacquemoud and Sebastien method
# SITE 3
#Read input files
L1 <-read.csv(file = "L1.csv", header=TRUE)#DN (Radiance) of white panel only (constant)
L3 <-read.csv(file = "L3_Site3_reord.csv", header=TRUE)#DN (Radiance) of black panel+leaf
(all samples)
L4 <-read.csv(file = "L4_site3.csv", header=TRUE)#DN (Radiance) of white panel+leaf (all
samples)
Reach_w <-read.csv(file = "SG_Trans_Site3_reord.csv", header=TRUE)#Transmittance (all
samples)
Reach_b <-read.csv(file = "SG_Ref_Site3.csv", header=TRUE)#Reflectance (all samples)
R_w <-read.csv(file = "Rw.csv", header=TRUE)#Reflectance [0-1] white disk (constant)
R_b <-read.csv(file = "Rb.csv", header=TRUE)#Reflectance [0-1] black disk (constant)
#
# Calculate Lamp Luminance (Linc)
Linc <- L1$L1/ R_w$Rw #vector
# Calculate L2
L2_c <- (R_b * Linc) #vector
# Calculate L3_c
L3_c <- (Reach_w * Linc)
# Calculate L4_c
L4_c <- (Reach_b * Linc)
#
#Transform L1, R_w and R_b to vector
L1_v <-as.vector(t(L1))
R_w_v <-as.vector(t(R_w))
R_b_v <-as.vector(t(R_b))
#
# Calculate Rb, Reach_w and Reach_b
Rb_c <- (L2_c * R_w_v)/L1_v
Reach_w_c <- (L3_c * R_w_v)/L1_v
Reach_b_c <- (L4_c * R_w_v)/L1_v
#
#Calculate Reflectance
R <- ((Reach_w_c*R_b_v)-(Reach_b_c*R_w_v)) / (R_b_v-
R_w_v+(R_w_v*R_b_v*(Reach_w_c-Reach_b_c)))
# Plot R
matplot(wave,R,lty=1, pch=".", ylim=c(0,0.7))
# Export R results
write.table(R, file = "R.csv", sep = ",", col.names = NA, qmethod = "double")
#
#Calculate Transmittance from Transflectance
T <- sqrt((Reach_w - R)*(1-R*R_w_v)/(R_w_v))
# Plot T
matplot(wave,T,lty=1, pch=".", ylim=c(0,0.5))
# Export T Results
write.table(T, file = "T.csv", sep = ",", col.names = NA, qmethod = "double")

```

Annex 6 MATLAB® code of the modified inversion process of PROSPECT model

The full MATLAB® version of the inversion process of PROSPECT model is available in <http://teledetection.ipgp.jussieu.fr/prosail/>. In order to apply the inversion in spectral data acquired in the range 400-1075 the following two files were modified: "invleafP5B.m" (renamed as "invleafP5B_PA.m") and "chi2P5B.m" (renamed as "chi2P5B_PA.m"). The modified versions of the MATLAB® files are presented:

```
% _____
% invleafP5B_PA.m
% version modified for the range: 400-1075 (October, 5th 2012)
% subroutines required: prospect_5B.m, tav.m, dataSpec_P5B.m
%           chi2P5B_PA.m, fminsearchbnd.m (optional)
% authors: Javier Pacheco-Labrador (javier.pacheco@cchs.csic.es) &
%         Stéphane Jacquemoud (jacquemoud@ipgp.fr)
% _____
%
% invleafP5B_PA.m inverts the PROSPECT-5B radiative transfer model by
% estimating the six input variables:
%
%   - N    = leaf structure parameter
%   - Cab  = chlorophyll a+b content in  $\mu\text{g}/\text{cm}^2$ 
%   - Car  = carotenoids content in  $\mu\text{g}/\text{cm}^2$ 
%   - Cbrown = brown pigments content in arbitrary units
%   - Cw   = equivalent water thickness in  $\text{g}/\text{cm}^2$  or cm
%   - Cm   = dry matter content in  $\text{g}/\text{cm}^2$ 
%
% using directional-hemispherical reflectance (DHR) and/or transmittance
% (DHT) spectra acquired in the domain 400-1075nm with 1nm step. Model
% inversion is performed using the Dantzig's simplex algorithm (Dantzig
% et al., 1955), a geometric method implemented in the matlab function
% fminsearch.m
%
% Remark : it is possible to use boundary values for each variable to
% avoid problems during the inversion. The routine "fminsearchbnd.m"
% developed by John D'Errico is then used:
% http://www.mathworks.com/matlabcentral/fileexchange/8277
% This routine works as the original fminsearch, but it transforms the
% constrained variables.
% _____
%
% F  ret, J.B., Fran  ois, C., Asner, G.P., Gitelson, A.A., Martin, R.E.,
% Bidel, L.P.R., Ustin, S.L., le Maire, G., & Jacquemoud, S. (2008).
% "PROSPECT-4 and 5: advances in the leaf optical properties model
% separating photosynthetic pigments". Remote Sensing of Environment,
% 112:3030-3043.
% Dantzig, G., Orden, A., & Wolfe, P. (1955). "The generalized simplex
% method for minimizing a linear form under inequality restraints".
% Pacific Journal of Mathematics. 8:183-195.
% Nelder, J.A., & Mead, R. (1965). A simplex method for function
```

```

% minimization, Computer Journal. 7:308-313.
% Lagarias, J.C., Reeds, J.A., Wright, M.H., & Wright, P.E. (1998).
% "Convergence properties of the Nelder-Mead simplex method in low
% dimensions", SIAM Journal of Optimization, 9:112-147.
% _____

clear all
clc
tic

% dir *.txt
% filename=input('file name (without extention): ','s');
% eval(['load ',filename,'.txt'])
% eval(['leaf=',filename,'])

%Reading my Reflectance and Trasmittance data
R = csvread('R.csv', 1,1);
T = csvread('T_0.csv', 1,1);
%n=length(R);
[r, c]=size(R)
R_est = zeros(r, c);
T_est = zeros(r, c);
par = zeros(c,6);
l = [400:1:1075];
for i=1:c
    % Assign R and T from the imported file to rmes and tmes variables
    rmes=R(:,i);
    tmes=T(:,i);

    % l=leaf(:,1);
    % rmes=leaf(:,2);
    % tmes=leaf(:,3);
    n=length(rmes);
    i
    % P0=[N Cab Car Cbrown Cw Cm]
    P0=[1.5 50 10 0 0 0.01];
    sol=fminsearch('chi2P5B_PA',P0,[],rmes,tmes);

    % variant: inversion using bounded variables
    % LB=[1 0 0 0 0.000063 0.0019];
    % UB=[3 100 30 1 0.04 0.0165];
    % sol=fminsearchbnd('chi2P5B',P0,LB,UB,[],rmes,tmes);

    RT=prospect_5B(sol(1),sol(2),sol(3),sol(4),sol(5),sol(6));

% Plotting
p=plot(l,rmes,l,1-tmes,l,RT(1:n,2),l,1-RT(1:n,3));
set(p(1),'LineWidth',2.5,'Color',[0.99,0.75,0.75])
set(p(2),'LineWidth',2.5,'Color',[0.75,0.75,0.99])
set(p(3),'LineWidth',1.5,'Color',[0.6,0,0],'LineStyle',':')
set(p(4),'LineWidth',1.5,'Color',[0,0,0.7],'LineStyle',':')
xlabel('Wavelength (nm)','FontSize',11,'FontWeight','Bold')
ylabel('Reflectance Transmittance','FontSize',12,'FontWeight','Bold')
title(['N=',num2str(sol(1),'%4.2f'),' Cab=',num2str(sol(2),'%4.1f'),...
' Car=',num2str(sol(3),'%4.2f'),' Cbrown=',num2str(sol(4),'%4.1f'),...

```

```

' Cw=',num2str(sol(5),'%7.5f'),' Cm=',num2str(sol(6),'%7.5f')], 'FontWeight','Bold')
axis([400 l(end) 0 1])
legend('R measured','T measured','R inverted','R inverted','Location',...
'SouthOutside','Orientation','Horizontal')
% Save estimated reflectance and Transmittance in separated files
R_est(:,i) = rmes;
T_est(:,i) = tmes;
% Save six parameters to matrix "par"
par(i,:) = sol;
end
toc
% _____
%
% chi2P5B_PA.m
% merit function
% _____

function chi2=chi2P5B_PA(x,rmes,tmes)

N=x(1);
Cab=x(2);
Car=x(3);
Cbrown=x(4);
Cw=x(5);
Cm=x(6);
RT=prospect_5B(N,Cab,Car,Cbrown,Cw,Cm);

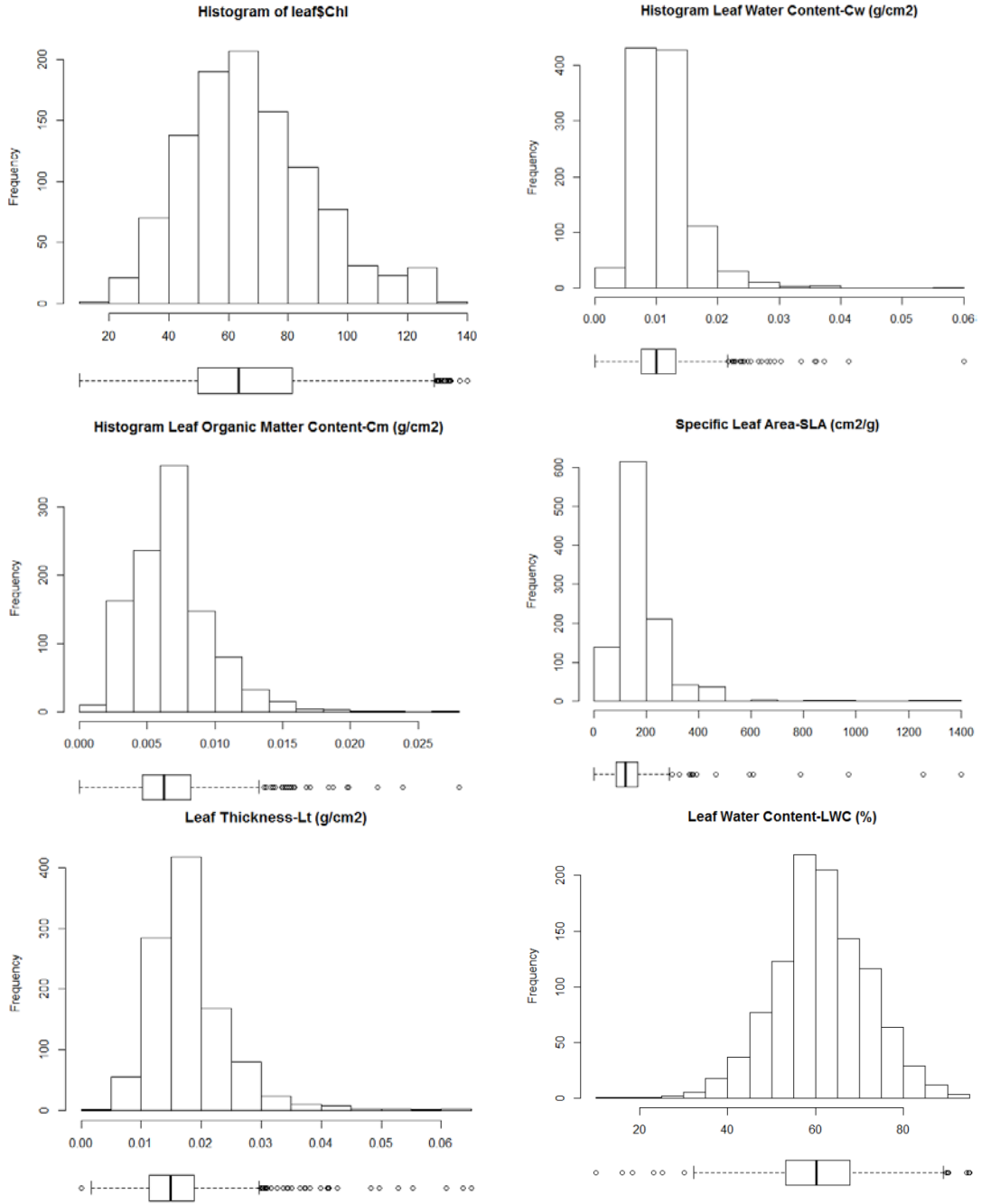
n=length(rmes);
chi2=sqrt(sum((RT(1:n,2)-rmes).^2+(RT(1:n,3)-tmes).^2));

% variant: plot of the result at each iteration

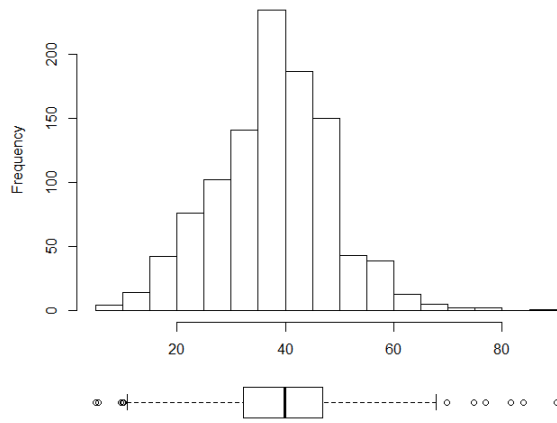
p=plot(RT(:,1),rmes,RT(:,1),1-tmes,RT(:,1),RT(:,2),RT(:,1),1-RT(:,3)));
set(p(1),'LineWidth',2.5,'Color',[0.99,0.75,0.75])
set(p(2),'LineWidth',2.5,'Color',[0.75,0.75,0.99])
set(p(3),'LineWidth',1.5,'Color',[0.6,0,0],'LineStyle',':')
set(p(4),'LineWidth',1.5,'Color',[0,0,0.7],'LineStyle',':')
xlabel('Wavelength (nm)','FontSize',11,'FontWeight','Bold')
ylabel('Reflectance Transmittance','FontSize',12,'FontWeight','Bold')
title(['N=',num2str(N,'%4.2f'),' Cab=',num2str(Cab,'%4.1f'),...
' Car=',num2str(Car,'%4.2f'),' Cbrown=',num2str(Cbrown,'%4.1f'),...
' Cw=',num2str(Cw,'%7.5f'),' Cm=',num2str(Cm,'%7.5f')], 'FontWeight','Bold')
axis([400 2500 0 1])
legend('R measured','T measured','R inverted','R inverted','Location',...
'SouthOutside','Orientation','Horizontal')
pause(0.00000001)

```

Annex 7 Histograms of leaf parameters (all sites)



Leaf Dry Matter Content-LDMC (%)



Annex 8 Descriptive statistics of foliar traits in the upper canopy for the three study sites

| | Ch_{ab} ($\mu\text{g cm}^{-2}$) | C_w (g cm^{-2}) | C_m (g cm^{-2}) | SLA ($\text{cm}^2 \text{g}^{-1}$) | L_t (g cm^{-2}) | LWC (%) | LDMC (%) |
|---|---|--|--|---|--|-------------------|--------------------|
| Oil Spill site | | | | | | | |
| Mean | 64.26 | 0.0140 | 0.0087 | 136.07 | 0.0226 | 61.04 | 38.96 |
| Maximum | 123.55 | 0.0398 | 0.0224 | 628.32 | 0.0622 | 89.47 | 73.33 |
| Minimum | 25.66 | 0.0025 | 0.0016 | 44.68 | 0.0075 | 26.67 | 10.53 |
| SD | 21.30 | 0.0058 | 0.0034 | 70.14 | 0.0082 | 9.39 | 9.39 |
| No polluted site | | | | | | | |
| Mean | 72.28 | 0.0118 | 0.0090 | 132.37 | 0.0207 | 56.70 | 43.30 |
| Maximum | 129.98 | 0.0274 | 0.0261 | 418.88 | 0.0535 | 85.00 | 80.00 |
| Minimum | 32.88 | 0.0037 | 0.0024 | 38.30 | 0.0122 | 20.00 | 15.00 |
| SD | 24.70 | 0.0042 | 0.0039 | 61.29 | 0.0065 | 12.23 | 12.23 |
| Pristine forest-Yasuni National Park | | | | | | | |
| Mean | 71.84 | 0.0111 | 0.0072 | 160.87 | 0.0183 | 60.22 | 39.78 |
| Maximum | 127.01 | 0.0233 | 0.0143 | 1,396.26 | 0.0347 | 94.38 | 61.11 |
| Minimum | 34.55 | 0.0048 | 0.0007 | 69.81 | 0.0092 | 38.89 | 5.63 |
| SD | 21.16 | 0.0036 | 0.0025 | 105.32 | 0.0047 | 9.94 | 9.94 |

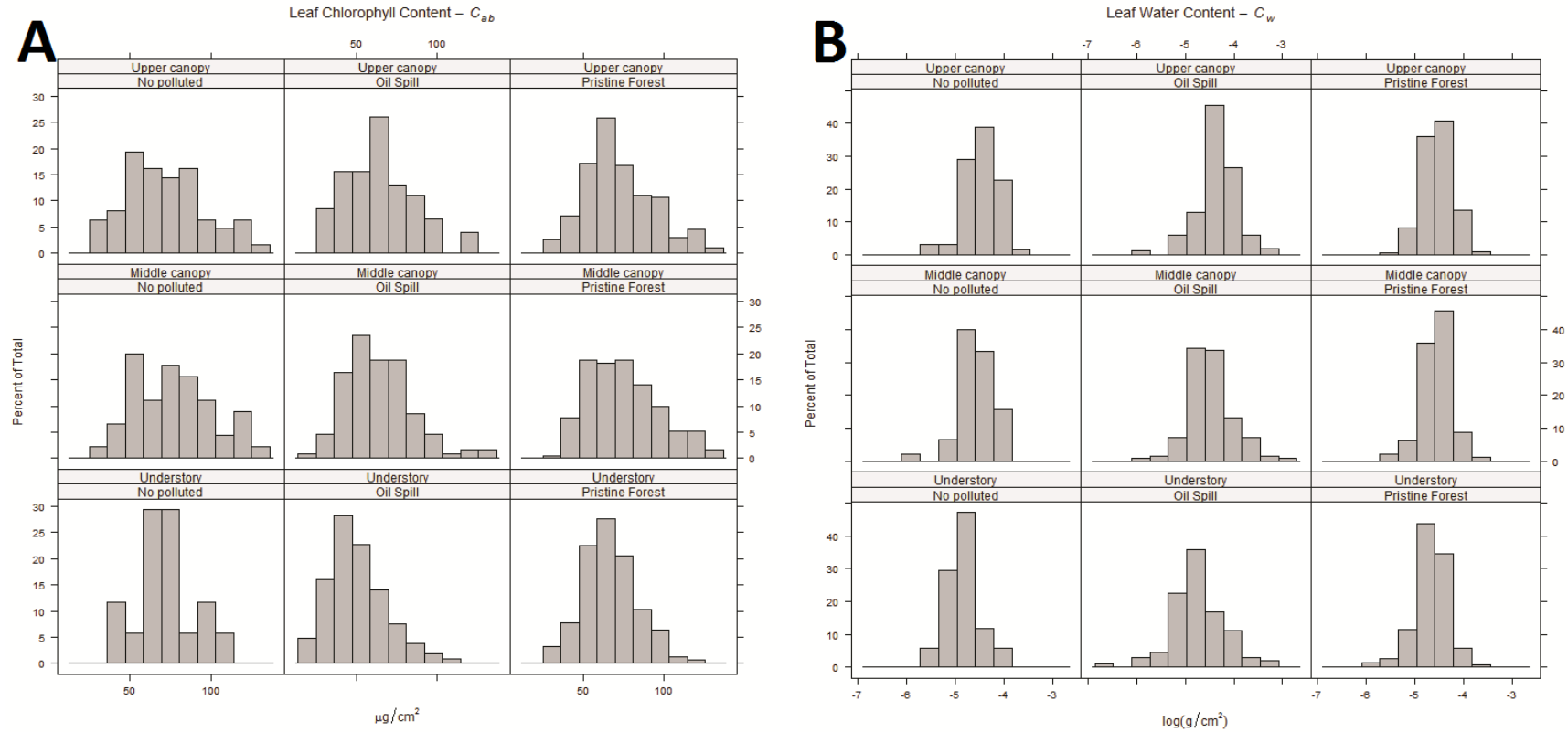
Annex 9 Descriptive statistics of foliar traits in the middle canopy for the three study sites

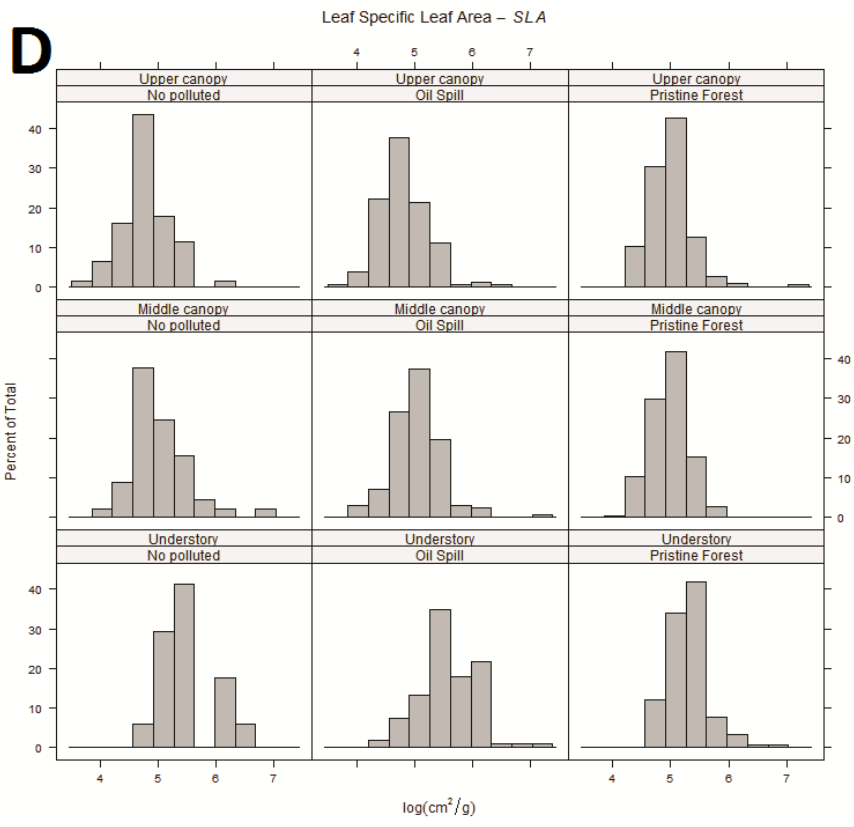
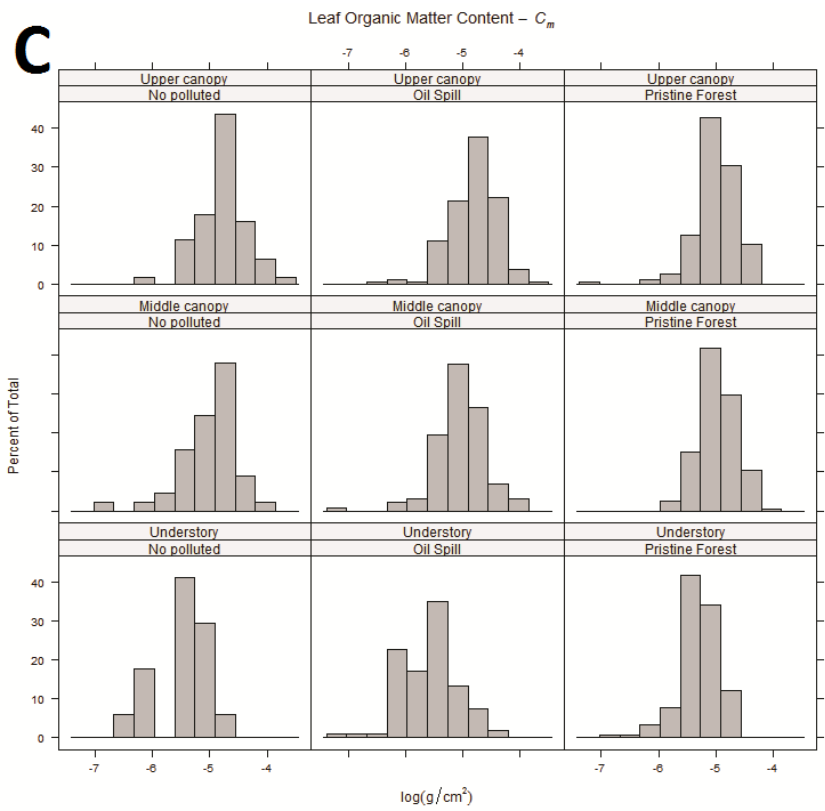
| | Ch_{ab} ($\mu\text{g cm}^{-2}$) | C_w (g cm^{-2}) | C_m (g cm^{-2}) | SLA ($\text{cm}^2 \text{g}^{-1}$) | L_t (g cm^{-2}) | LWC (%) | LDMC (%) |
|---|---|--|--|---|--|-------------------|--------------------|
| Oil Spill site | | | | | | | |
| Mean | 63.47 | 0.0125 | 0.0070 | 172.24 | 0.0195 | 62.60 | 37.40 |
| Maximum | 126.34 | 0.0572 | 0.0177 | 1,256.64 | 0.0609 | 94.44 | 64.71 |
| Minimum | 17.96 | 0.0025 | 0.0008 | 56.55 | 0.0062 | 35.29 | 5.56 |
| SD | 20.45 | 0.0070 | 0.0028 | 117.27 | 0.0084 | 10.54 | 10.54 |
| No polluted site | | | | | | | |
| Mean | 77.31 | 0.0111 | 0.0073 | 170.69 | 0.0183 | 60.30 | 39.70 |
| Maximum | 132.18 | 0.0199 | 0.0174 | 804.25 | 0.0373 | 87.50 | 77.78 |
| Minimum | 34.79 | 0.0025 | 0.0012 | 57.45 | 0.0099 | 22.22 | 12.50 |
| SD | 24.97 | 0.0037 | 0.0029 | 118.16 | 0.0054 | 12.15 | 12.15 |
| Pristine forest-Yasuni National Park | | | | | | | |
| Mean | 74.80 | 0.0110 | 0.0073 | 151.84 | 0.0183 | 59.75 | 40.25 |
| Maximum | 127.35 | 0.0226 | 0.0162 | 353.43 | 0.0354 | 81.01 | 66.67 |
| Minimum | 34.93 | 0.0040 | 0.0028 | 61.87 | 0.0088 | 33.33 | 18.99 |
| SD | 21.90 | 0.0034 | 0.0024 | 50.49 | 0.0045 | 9.63 | 9.63 |

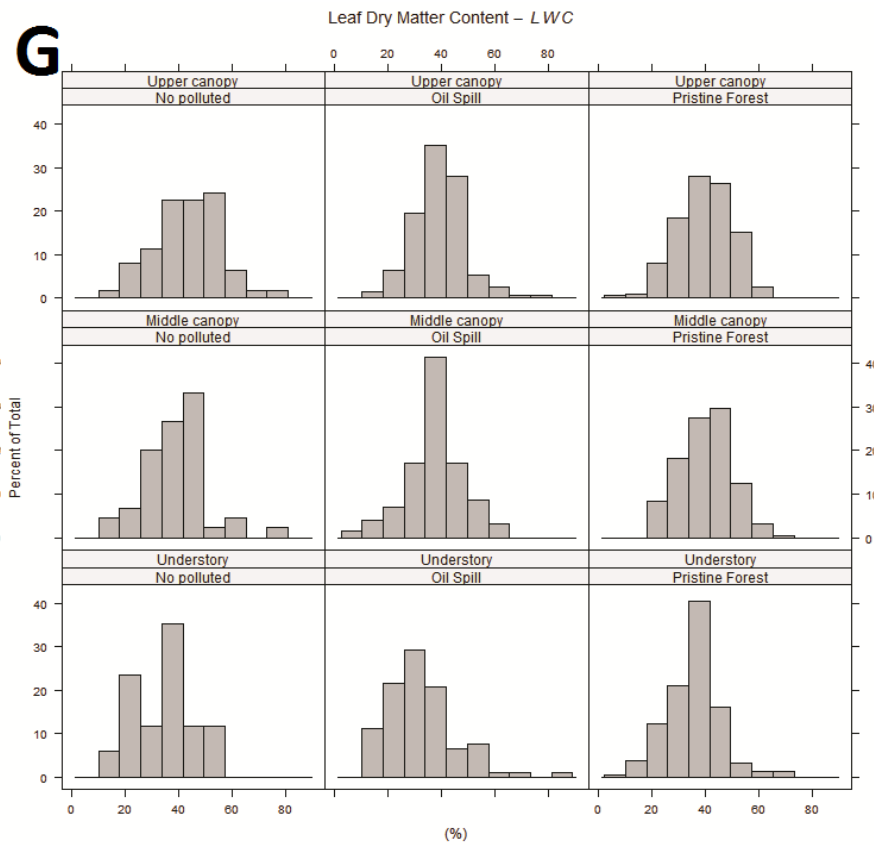
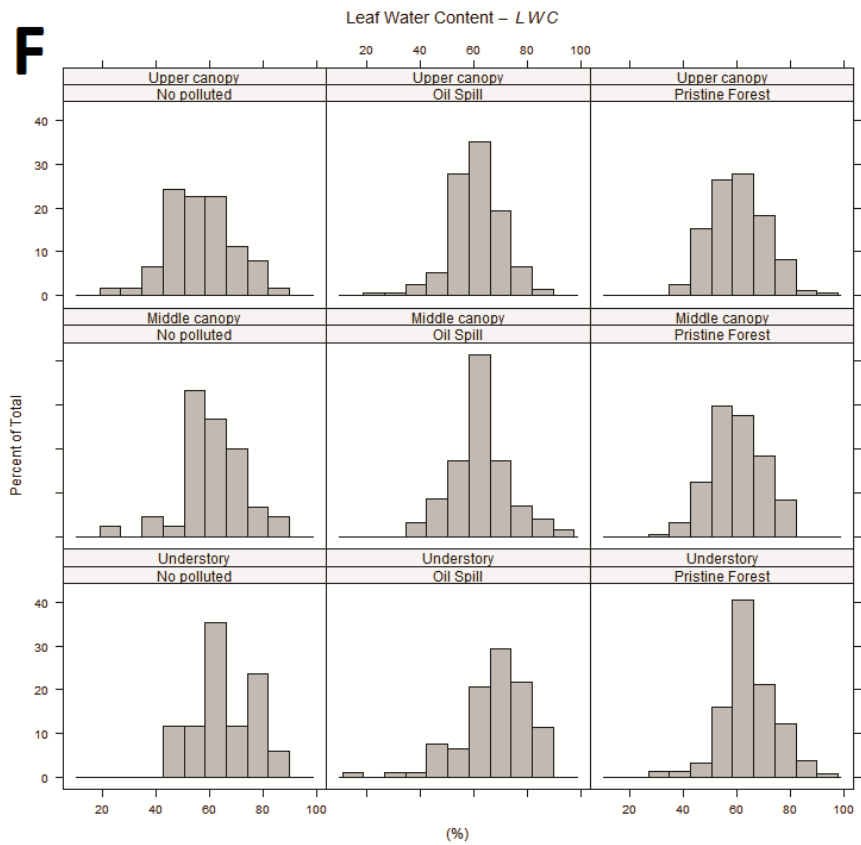
Annex 10 Descriptive statistics of foliar traits in the understory for the three study sites

| | Ch_{ab} ($\mu\text{g cm}^{-2}$) | C_w (g cm^{-2}) | C_m (g cm^{-2}) | SLA ($\text{cm}^2 \text{g}^{-1}$) | L_t (g cm^{-2}) | LWC (%) | LDMC (%) |
|---|---|--|--|---|--|-------------------|--------------------|
| Oil Spill site | | | | | | | |
| Mean | 50.16 | 0.0121 | 0.01 | 184.46 | 0.0184 | 63.55 | 36.45 |
| Maximum | 107.46 | 0.0572 | 0.01 | 1,256.64 | 0.0609 | 94.44 | 64.71 |
| Minimum | 22.84 | 0.0025 | 0.00 | 73.11 | 0.0062 | 35.29 | 5.56 |
| SD | 17.91 | 0.0072 | 0.00 | 115.52 | 0.0079 | 10.72 | 10.72 |
| No polluted site | | | | | | | |
| Mean | 71.42 | 0.0099 | 0.01 | 193.14 | 0.0162 | 60.94 | 39.06 |
| Maximum | 107.17 | 0.0212 | 0.01 | 628.32 | 0.0271 | 85.00 | 77.78 |
| Minimum | 36.84 | 0.0025 | 0.00 | 78.54 | 0.0064 | 22.22 | 15.00 |
| SD | 18.75 | 0.0035 | 0.00 | 104.66 | 0.0046 | 11.88 | 11.88 |
| Pristine forest-Yasuni National Park | | | | | | | |
| Mean | 66.39 | 0.0098 | 0.01 | 213.40 | 0.0150 | 64.28 | 35.72 |
| Maximum | 118.88 | 0.0249 | 0.01 | 981.75 | 0.0298 | 90.00 | 66.67 |
| Minimum | 32.88 | 0.0031 | 0.00 | 98.17 | 0.0041 | 33.33 | 10.00 |
| SD | 16.48 | 0.0031 | 0.00 | 96.72 | 0.0036 | 9.72 | 9.72 |

Annex 11 Histograms of leaf parameters for each study site and canopy layer







Annex 12 Pairwise comparison between sites and vertical profile of the canopy. *p-values* adjustment method of Holms

| | | Chlorophyll content (C_{ab}) | | | | | | | | |
|--------------------|----------------------|----------------------------------|---------------|------------|--------------|---------------|------------|-----------------|---------------|------------|
| | | OIL SPILL | | | No polluted | | | Pristine forest | | |
| | | Upper canopy | Middle canopy | Understory | Upper canopy | Middle canopy | Understory | Upper canopy | Middle canopy | Understory |
| A | Oil Spill | | 7.5E-01 | 8.0E-08 | 1.0E-02 | 2.1E-04 | 1.8E-01 | 6.8E-04 | 2.8E-06 | 3.7E-01 |
| | | | | 1.1E-06 | 6.0E-03 | 1.2E-04 | 1.4E-01 | 3.8E-04 | 1.8E-06 | 2.4E-01 |
| | | *** | *** | | 3.6E-11 | 3.2E-13 | 8.9E-05 | 2.0E-16 | 2.0E-16 | 6.5E-10 |
| No polluted | Upper canopy | * | ** | *** | | 2.1E-01 | 8.8E-01 | 8.8E-01 | 4.0E-01 | 5.8E-02 |
| | Middle canopy | *** | *** | *** | | | 3.2E-01 | 1.1E-01 | 4.6E-01 | 1.9E-03 |
| | Understory | | | *** | | | | 9.4E-01 | 5.2E-01 | 3.4E-01 |
| Pristine | Upper canopy | *** | *** | *** | | | | | 1.6E-01 | 1.4E-02 |
| | Middle canopy | *** | *** | *** | | | | | | 1.7E-04 |
| | Understory | | | *** | | ** | | * | *** | |

| | | Foliar Water Content (C_w) | | | | | | | | |
|--------------------|----------------------|--------------------------------|---------------|------------|--------------|---------------|------------|--------------|---------------|------------|
| | | OIL SPILL | | | No polluted | | | Pristine | | |
| | | Upper canopy | Middle canopy | Understory | Upper canopy | Middle canopy | Understory | Upper canopy | Middle canopy | Understory |
| B | Oil Spill | | 1.3E-02 | 7.5E-11 | 2.2E-03 | 4.0E-04 | 4.2E-05 | 2.1E-08 | 9.4E-09 | 1.6E-14 |
| | | * | | 5.3E-05 | 2.8E-01 | 7.7E-02 | 3.5E-03 | 6.3E-03 | 4.0E-03 | 9.6E-07 |
| | | *** | *** | | 2.3E-02 | 2.1E-01 | 4.0E-01 | 6.5E-02 | 9.2E-02 | 6.6E-01 |
| No polluted | Upper canopy | ** | | * | | 4.7E-01 | 3.3E-02 | 3.3E-01 | 2.7E-01 | 5.5E-03 |
| | Middle canopy | *** | | | | | 1.2E-01 | 1.0E+00 | 9.1E-01 | 1.0E-01 |
| | Understory | *** | ** | | * | | | 7.9E-02 | 9.3E-02 | 5.1E-01 |
| Pristine | Upper canopy | *** | ** | | | | | | 8.6E-01 | 9.8E-03 |
| | Middle canopy | *** | ** | | | | | | | 1.7E-02 |
| | Understory | *** | *** | | ** | | | ** | * | |

Organic Matter content (Cm)

| | Organic Matter content (Cm) | | | | | | | | |
|-----------------------|-----------------------------|---------------|------------|--------------|---------------|------------|--------------|---------------|------------|
| | OIL SPILL | | | No polluted | | | Pristine | | |
| | Upper canopy | Middle canopy | Understory | Upper canopy | Middle canopy | Understory | Upper canopy | Middle canopy | Understory |
| C Oil Spill | Upper canopy | 2.0E-06 | 2.0E-16 | 1.0E+00 | 1.8E-02 | 4.6E-08 | 6.4E-06 | 2.2E-05 | 2.0E-16 |
| | Middle canopy | *** | 4.2E-13 | 3.4E-05 | 1.0E+00 | 6.0E-03 | 1.0E+00 | 1.0E+00 | 1.1E-06 |
| | Understory | *** | *** | 2.0E-16 | 1.2E-08 | 1.0E+00 | 2.0E-16 | 2.0E-16 | 3.5E-02 |
| No polluted | Upper canopy | *** | *** | *** | 1.4E-02 | 5.4E-08 | 1.4E-04 | 2.8E-04 | 2.0E-16 |
| | Middle canopy | * | *** | * | 5.8E-03 | 1.0E+00 | 1.0E+00 | 1.0E+00 | 1.6E-04 |
| | Understory | *** | ** | *** | ** | 1.3E-03 | 9.4E-04 | 1.0E+00 | |
| Pristine | Upper canopy | *** | *** | *** | ** | 1.0E+00 | 1.5E-10 | | |
| | Middle canopy | *** | *** | *** | *** | 4.7E-11 | | | |
| | Understory | *** | *** | * | *** | *** | *** | *** | |

Specific Leaf Area (SLA)

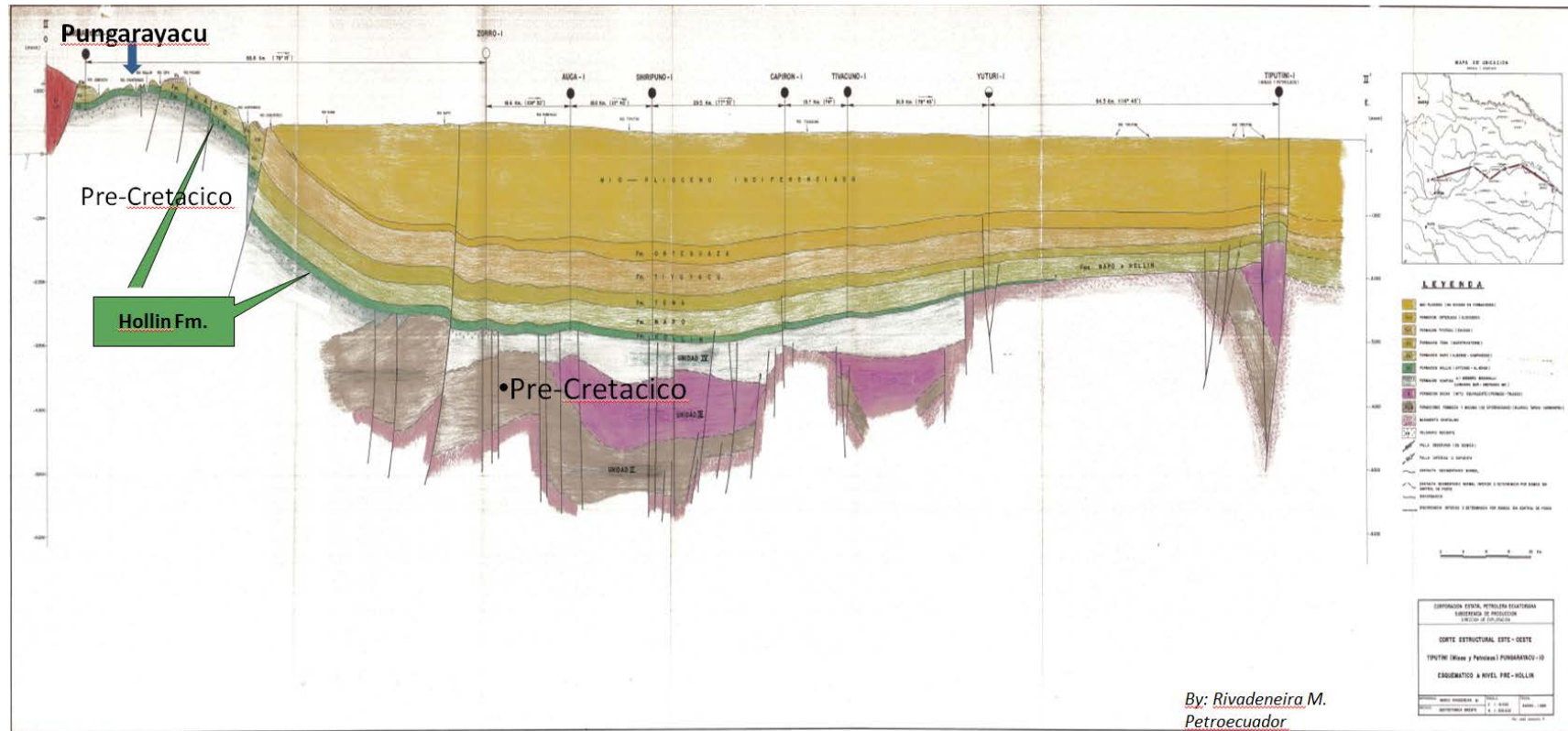
| | Specific Leaf Area (SLA) | | | | | | | | |
|-------------|--------------------------|---------------|------------|--------------|---------------|------------|--------------|---------------|------------|
| | OIL SPILL | | | No polluted | | | Pristine | | |
| | Upper canopy | Middle canopy | Understory | Upper canopy | Middle canopy | Understory | Upper canopy | Middle canopy | Understory |
| Oil Spill | Upper canopy | 3.8E-02 | 2.0E-16 | 1.0E+00 | 5.5E-01 | 1.8E-05 | 2.9E-01 | 1.0E+00 | 2.2E-10 |
| | Middle canopy | * | 4.1E-16 | 1.5E-01 | 1.0E+00 | 9.5E-03 | 1.0E+00 | 6.8E-01 | 9.4E-03 |
| | Understory | *** | *** | 2.0E-16 | 4.9E-09 | 1.0E+00 | 2.0E-16 | 2.0E-16 | 3.5E-07 |
| No polluted | Upper canopy | *** | *** | *** | 6.2E-01 | 4.8E-05 | 6.2E-01 | 1.0E+00 | 1.5E-06 |
| | Middle canopy | *** | *** | *** | 2.5E-02 | 1.0E+00 | 1.0E+00 | 1.0E+00 | 1.7E-01 |
| | Understory | *** | ** | *** | * | 1.3E-03 | 2.8E-04 | 6.4E-01 | |
| Pristine | Upper canopy | *** | *** | *** | ** | 1.0E+00 | 1.7E-05 | | |
| | Middle canopy | *** | *** | *** | *** | 2.2E-07 | | | |
| | Understory | *** | ** | *** | *** | *** | *** | *** | |

| | | Leaf Thickness | | | | | | | | |
|-----------------------|---------------|----------------|---------------|------------|--------------|---------------|------------|--------------|---------------|------------|
| | | OIL SPILL | | | No polluted | | | Pristine | | |
| | | Upper canopy | Middle canopy | Understory | Upper canopy | Middle canopy | Understory | Upper canopy | Middle canopy | Understory |
| E Oil Spill | Upper canopy | | 3.8E-02 | 2.0E-16 | 1.0E+00 | 5.5E-01 | 1.8E-05 | 2.9E-01 | 1.0E+00 | 2.2E-10 |
| | Middle canopy | * | | 4.1E-16 | 1.5E-01 | 1.0E+00 | 9.5E-03 | 1.0E+00 | 6.8E-01 | 9.4E-02 |
| | Understory | *** | *** | | 2.0E-16 | 4.9E-09 | 1.0E+00 | 2.0E-16 | 2.0E-16 | 3.5E-07 |
| No polluted | Upper canopy | | | *** | | 6.2E-01 | 4.8E-05 | 6.2E-01 | 1.0E+00 | 1.5E-06 |
| | Middle canopy | | | *** | | | 2.5E-02 | 1.0E+00 | 1.0E+00 | 1.7E-01 |
| | Understory | *** | ** | | *** | * | | 1.3E-03 | 2.8E-04 | 6.4E-01 |
| Pristine | Upper canopy | | | *** | | | ** | | 1.0E+00 | 1.7E-05 |
| | Middle canopy | | | *** | | | *** | | | 2.2E-07 |
| | Understory | *** | | *** | *** | | | *** | *** | |

| | | Leaf Water Content (%) | | | | | | | | |
|-----------------------|---------------|------------------------|---------------|------------|--------------|---------------|------------|--------------|---------------|------------|
| | | OIL SPILL | | | No polluted | | | Pristine | | |
| | | Upper canopy | Middle canopy | Understory | Upper canopy | Middle canopy | Understory | Upper canopy | Middle canopy | Understory |
| F Oil Spill | Upper canopy | | 1.0E+00 | 1.1E-05 | 1.5E-01 | 1.0E+00 | 1.0E+00 | 1.0E+00 | 1.0E+00 | 1.6E-01 |
| | Middle canopy | | | 4.4E-03 | 7.8E-03 | 1.0E+00 | 1.0E+00 | 8.2E-01 | 3.8E-01 | 1.0E+00 |
| | Understory | *** | ** | | 1.7E-09 | 1.7E-03 | 1.0E+00 | 7.6E-08 | 9.4E-09 | 1.6E-01 |
| No polluted | Upper canopy | | ** | *** | | 1.0E+00 | 6.2E-02 | 4.4E-01 | 8.2E-01 | 5.1E-05 |
| | Middle canopy | | | ** | | | 1.0E+00 | 1.0E+00 | 1.0E+00 | 4.9E-01 |
| | Understory | | | | | | | 8.2E-01 | 6.2E-01 | 1.0E+00 |
| Pristine | Upper canopy | | | *** | | | | | 1.0E+00 | 8.6E-03 |
| | Middle canopy | | | *** | | | | | | 1.9E-03 |
| | Understory | | | | *** | | | ** | ** | |

| Leaf Dry Matter Content (%) | | | | | | | | | | |
|-----------------------------|---------------|---------------|------------|--------------|---------------|------------|--------------|---------------|------------|---------|
| | OIL SPILL | | | No polluted | | | Pristine | | | |
| | Upper canopy | Middle canopy | Understory | Upper canopy | Middle canopy | Understory | Upper canopy | Middle canopy | Understory | |
| G Oil Spill | Upper canopy | | 1.0E+00 | 1.1E-05 | 6.2E-02 | 1.0E+00 | 1.1E+01 | 1.0E+00 | 1.0E+00 | 1.6E-01 |
| | Middle canopy | | | 4.4E-03 | 1.5E-01 | 1.0E+00 | 1.0E+00 | 8.2E-01 | 3.8E-01 | 1.0E+00 |
| | Understory | *** | ** | | 7.8E-03 | 1.7E-03 | 1.0E+00 | 7.6E-08 | 9.4E-09 | 1.6E-01 |
| No polluted | Upper canopy | | | ** | | 1.0E+00 | 6.2E-02 | 4.4E-01 | 8.2E-01 | 5.1E-05 |
| | Middle canopy | | | ** | | | 1.0E+00 | 1.0E+00 | 1.0E+00 | 4.9E-01 |
| | Understory | | | | | | | 8.2E-01 | 6.2E-01 | 1.0E+00 |
| Pristine | Upper canopy | | | *** | | | | | 1.0E+00 | 8.6E-03 |
| | Middle canopy | | | *** | | | | | | 1.9E-03 |
| | Understory | | | | *** | | | ** | ** | |

Annex 13 Structural profile of the Oriente sedimentary Basin where Pungarayacu oil field is located at the left side



Source: National Agency of Regulation and Control of Hydrocarbons. Non-Renewable Resources Ministry of Ecuador.

Annex 14 De-stripping algorithm for Hyperion images generated in MATLAB based on Datt et al. 2003 and modified to exclude cloud/shadow pixels

```

% Des-tripping algorithm of Hyperion image (242 bands) excluding the pixels affected by clouds
and shadows.
% Author: Paul Arellano
% MATLAB code
X = multibandread('KW_EO1_BC',[226 256 242], 'int16',0, 'bsq','ieee-le'); %Read the stripped
image
Clouds = multibandread('Mask_clouds_shadows', [226 256 1], 'int8',0, 'bsq','ieee-le'); % Read the
mask of clouds (1=clouds, 0=data)
[r,c,b] = size(X); % Dimensions of the image (r=row, c=col, b=bands)
B = 0.*X;
p = 0;
pp = 0;
s = 0;
st = 0;
pp1 = 0;
MeanCol(1,256)=0;
SD(1,256)=0;
for k = 1:b % loop for each band (242 bands)
    AA=X(:, :,k);
    BB = 0.*AA;
    %MEAN VALUES PER COLUMN
    for x=1:256 % Columns
        for z=1:226 % Rows
            if Clouds(z,x)== 0; % Exclude the cloud-pixels
                p = p+AA(z,x);
                pp = pp+1;
            end;
        end
        Mean = p/pp; %Mean per column
        MeanCol(x) = Mean;
        p = 0;
        pp = 0;
    end

    %STANDARD DEVIATION PER COLUMN
    for x=1:256
        for z=1:226
            if Clouds(z,x)== 0;
                s = s +((AA(z,x) - MeanCol(x)) * (AA(z,x) - MeanCol(x))); %SD of columns
                st = st + ((AA(z,x) - MeanCol(x)) * (AA(z,x) - MeanCol(x))); %SD of Band
                pp1 = pp1 + 1;
                pp = pp + 1;
            end;
        end
        %Standard Deviation per Column

```

```

    SD(x) = (s/pp)^(1/2);
    pp = 0;
    s = 0;
end
% Standard deviation all Band
SdBand = (st/pp1)^(1/2);
st = 0;
pp1 = 0;
% Mean all Band
MeanBand = mean(MeanCol);
% GAIN and OFFSET per column
GAIN = SdBand./SD;
OFFSET = MeanBand-(GAIN.*MeanCol);

% Apply GAINS and OFFSETs to every pixel
for j=1:256
    BB(:,j) = GAIN(j) * AA(:,j) + OFFSET(j);
end

% Add each band to the final matrix
B(:,k) = BB(:,k);

end
% Export MatLab matrix to ENVI format
multibandwrite(int16(B),'data.bsq','bsq');
% multibandwrite(B,'data.bsq','bsq',[1 1 k],[r, c, b]);
% enviwrite(BB, 'd.dat');

```

Annex 15 Descriptive statistics of Broad band vegetation indices for the three study sites

| | BROAD-BAND INDICES | | | | |
|-------------------------|--|-------------|--------------|------------|-------------|
| | SR | NDVI | GNDVI | EVI | ARVI |
| | <i>SITE 1. OIL SPILL</i> | | | | |
| Mean | 15.2416 | 0.8720 | 0.7830 | 0.3873 | 0.6024 |
| Standard Error | 0.6696 | 0.0064 | 0.0074 | 0.0076 | 0.0111 |
| Median | 16.3065 | 0.8844 | 0.7987 | 0.3929 | 0.6125 |
| Mode | nd | 0.8568 | 0.8099 | nd | 0.6122 |
| Standard Deviation | 2.9947 | 0.0284 | 0.0329 | 0.0338 | 0.0494 |
| Sample Variance | 8.9682 | 0.0008 | 0.0011 | 0.0011 | 0.0024 |
| Kurtosis | - 0.4174 | 2.1710 | - 0.1547 | - 0.9930 | 0.2481 |
| Skewness | - 0.6969 | - 1.4770 | - 0.9048 | - 0.4276 | - 0.9743 |
| Range | 10.9274 | 0.1113 | 0.1079 | 0.1109 | 0.1772 |
| Minimum | 8.5502 | 0.7906 | 0.7096 | 0.3216 | 0.4850 |
| Maximum | 19.4776 | 0.9019 | 0.8175 | 0.4324 | 0.6622 |
| Sum | 304.8 | 17.4 | 15.7 | 7.7 | 12.0 |
| Confidence Level(95.0%) | 1.4016 | 0.0133 | 0.0154 | 0.0158 | 0.0231 |
| | SR | NDVI | GNDVI | EVI | ARVI |
| | <i>SITE 2. SECUNDARY FOREST</i> | | | | |
| Mean | 17.6047 | 0.8921 | 0.8120 | 0.3447 | 0.5864 |
| Standard Error | 0.3095 | 0.0018 | 0.0027 | 0.0048 | 0.0045 |
| Median | 17.4542 | 0.8916 | 0.8131 | 0.3452 | 0.5849 |
| Mode | nd | nd | 0.8146 | 0.3513 | 0.5805 |
| Standard Deviation | 1.2381 | 0.0071 | 0.0106 | 0.0193 | 0.0180 |
| Sample Variance | 1.5330 | 0.0001 | 0.0001 | 0.0004 | 0.0003 |
| Kurtosis | 0.0340 | 0.0992 | 0.6518 | 0.8379 | 1.3364 |
| Skewness | 0.3205 | - 0.0305 | 0.3173 | 0.4139 | 0.8482 |
| Range | 4.8335 | 0.0281 | 0.0428 | 0.0802 | 0.0699 |
| Minimum | 15.3028 | 0.8773 | 0.7926 | 0.3096 | 0.5616 |
| Maximum | 20.1364 | 0.9054 | 0.8354 | 0.3898 | 0.6315 |
| Sum | 281.7 | 14.3 | 13.0 | 5.5 | 9.4 |
| Confidence Level(95.0%) | 0.6598 | 0.0038 | 0.0057 | 0.0103 | 0.0096 |
| | SR | NDVI | GNDVI | EVI | ARVI |
| | <i>SITE 3. PRISTINE FOREST (YASUNI NATIONAL PARK)</i> | | | | |
| Mean | 19.8991 | 0.9037 | 0.8251 | 0.3144 | 0.5212 |
| Standard Error | 0.2016 | 0.0009 | 0.0014 | 0.0056 | 0.0083 |
| Median | 19.5647 | 0.9028 | 0.8237 | 0.3137 | 0.5313 |
| Mode | 19.3566 | 0.9011 | 0.8185 | 0.3637 | 0.3924 |
| Standard Deviation | 1.7109 | 0.0076 | 0.0118 | 0.0473 | 0.0703 |
| Sample Variance | 2.9270 | 0.0001 | 0.0001 | 0.0022 | 0.0049 |
| Kurtosis | 1.0143 | 0.6054 | 0.0288 | - 1.0065 | - 0.8020 |
| Skewness | 0.8085 | 0.2506 | 0.4641 | - 0.0011 | - 0.4164 |
| Range | 8.8460 | 0.0402 | 0.0550 | 0.1993 | 0.2845 |
| Minimum | 16.0263 | 0.8825 | 0.8023 | 0.2144 | 0.3679 |
| Maximum | 24.8723 | 0.9227 | 0.8573 | 0.4137 | 0.6524 |
| Sum | 1,432.7 | 65.1 | 59.4 | 22.6 | 37.5 |
| Confidence Level(95.0%) | 0.4020 | 0.0018 | 0.0028 | 0.0111 | 0.0165 |

Annex 16 Descriptive statistics of Narrow-band vegetation indices for the three study sites

| NARROW-BAND VEGETATION INDICES | | | | | | | | | | | | | | |
|---|---------|---------|---------------------|--------------------|----------------------|------------------|-------------|---------|----------|------------------------|---------|---------|-------------------|---------|
| | SG | PSSRa | NDVI ₇₀₅ | mSR ₇₀₅ | mMDVI ₇₀₅ | CRT ₂ | LIC1 /PSNda | OSAVI | MCARI | Der ₇₂₅₋₇₀₂ | REP | VOGI | CI ₅₉₀ | MTCI |
| <i>SITE 1. OIL SPILL</i> | | | | | | | | | | | | | | |
| Mean | 0.0201 | 14.9883 | 0.7478 | 4.2158 | 0.6129 | 0.0965 | 0.8720 | 1.0187 | 264.8 | 2.3913 | 0.7277 | 2.4938 | 17.8813 | 4.3116 |
| Standard Error | 0.0007 | 0.6586 | 0.0096 | 0.1127 | 0.0089 | 0.0051 | 0.0064 | 0.0076 | 20.0 | 0.1152 | 0.0026 | 0.0462 | 0.7357 | 0.1190 |
| Median | 0.0193 | 16.0014 | 0.7620 | 4.2970 | 0.6223 | 0.0867 | 0.8844 | 1.0291 | 300.0 | 2.4713 | 0.7277 | 2.5724 | 18.8420 | 4.4889 |
| Mode | 0.0166 | nd | 0.7228 | 4.2251 | 0.6172 | 0.0786 | 0.8568 | 1.0220 | nd | nd | 0.7277 | 2.5724 | nd | 4.3617 |
| Standard Deviation | 0.0030 | 2.9454 | 0.0427 | 0.5038 | 0.0396 | 0.0228 | 0.0284 | 0.0341 | 89.3 | 0.5154 | 0.0114 | 0.2067 | 3.2901 | 0.5324 |
| Sample Variance | 0.0000 | 8.6755 | 0.0018 | 0.2538 | 0.0016 | 0.0005 | 0.0008 | 0.0012 | 7,980.1 | 0.2656 | 0.0001 | 0.0427 | 10.8249 | 0.2834 |
| Kurtosis | 0.7445 | -0.3467 | 1.3226 | -0.4222 | 0.1483 | 2.1179 | 2.1710 | 1.1719 | -1.4 | -1.0919 | 9.5002 | 0.0056 | -0.3443 | 0.0511 |
| Skewness | 0.9437 | -0.6900 | -1.3065 | -0.4587 | -0.8426 | 1.5478 | -1.4770 | -1.2031 | -0.1 | -0.2217 | 1.9773 | -0.9456 | -0.6663 | -0.8773 |
| Range | 0.0118 | 10.8549 | 0.1563 | 1.8326 | 0.1440 | 0.0843 | 0.1113 | 0.1304 | 271.6 | 1.6849 | 0.0611 | 0.6955 | 11.5017 | 1.9652 |
| Minimum | 0.0160 | 8.3391 | 0.6351 | 3.2118 | 0.5251 | 0.0759 | 0.7906 | 0.9284 | 142.4 | 1.5000 | 0.7073 | 2.0433 | 10.7908 | 3.0824 |
| Maximum | 0.0278 | 19.1940 | 0.7914 | 5.0444 | 0.6691 | 0.1603 | 0.9019 | 1.0588 | 414.0 | 3.1849 | 0.7684 | 2.7388 | 22.2926 | 5.0476 |
| Sum | 0.4 | 299.8 | 15.0 | 84.3 | 12.3 | 1.9306 | 17.4392 | 20.3741 | 5,296.7 | 47.8 | 14.6 | 49.9 | 357.6 | 86.2 |
| Confidence Level(95.0%) | 0.0014 | 1.3785 | 0.0200 | 0.2358 | 0.0185 | 0.0107 | 0.0133 | 0.0159 | 41.8 | 0.2412 | 0.0054 | 0.0968 | 1.5398 | 0.2492 |
| | SG | PSSRa | NDVI ₇₀₅ | mSR ₇₀₅ | mMDVI ₇₀₅ | CRT ₂ | LIC1 /PSNda | OSAVI | MCARI | Der ₇₂₅₋₇₀₂ | REP | VOGI | CI ₅₉₀ | MTCI |
| <i>SITE 2. SECONDARY FOREST</i> | | | | | | | | | | | | | | |
| Mean | 0.0140 | 17.3058 | 0.7795 | 4.0113 | 0.6002 | 0.0825 | 0.8921 | 1.0414 | 243.2 | 2.7249 | 0.7353 | 2.7036 | 19.6664 | 4.9205 |
| Standard Error | 0.0004 | 0.3211 | 0.0041 | 0.0560 | 0.0043 | 0.0012 | 0.0018 | 0.0027 | 9.9 | 0.1507 | 0.0041 | 0.0222 | 0.3585 | 0.0700 |
| Median | 0.0141 | 17.1341 | 0.7773 | 3.9600 | 0.5968 | 0.0820 | 0.8916 | 1.0427 | 242.7 | 2.5124 | 0.7277 | 2.7020 | 19.5377 | 4.8737 |
| Mode | 0.0124 | nd | nd | nd | nd | nd | nd | nd | 242.7 | nd | 0.7277 | nd | nd | 4.8531 |
| Standard Deviation | 0.0014 | 1.2844 | 0.0164 | 0.2242 | 0.0172 | 0.0049 | 0.0071 | 0.0106 | 39.4 | 0.6029 | 0.0164 | 0.0888 | 1.4340 | 0.2799 |
| Sample Variance | 0.0000 | 1.6497 | 0.0003 | 0.0502 | 0.0003 | 0.0000 | 0.0001 | 0.0001 | 1,553.8 | 0.3635 | 0.0003 | 0.0079 | 2.0565 | 0.0783 |
| Kurtosis | -0.7234 | -0.0319 | -0.7767 | 1.3481 | 0.7880 | -1.2318 | 0.0992 | -0.7784 | 5.8 | -0.4041 | 1.2849 | -0.8555 | 1.3619 | 3.4296 |
| Skewness | -0.1770 | 0.3097 | 0.2824 | 1.1672 | 0.9521 | 0.0834 | -0.0305 | 0.0672 | -1.8 | 0.7577 | 1.7719 | -0.0317 | 0.5803 | 1.5037 |
| Range | 0.0048 | 5.0021 | 0.0517 | 0.8346 | 0.0632 | 0.0162 | 0.0281 | 0.0333 | 182.7 | 1.9660 | 0.0407 | 0.3033 | 6.1816 | 1.1643 |
| Minimum | 0.0116 | 14.8979 | 0.7557 | 3.7391 | 0.5780 | 0.0742 | 0.8773 | 1.0248 | 122.6 | 2.0652 | 0.7277 | 2.5462 | 16.9559 | 4.5335 |
| Maximum | 0.0164 | 19.9000 | 0.8074 | 4.5737 | 0.6412 | 0.0904 | 0.9054 | 1.0581 | 305.3 | 4.0313 | 0.7684 | 2.8495 | 23.1375 | 5.6978 |
| Sum | 0.2 | 276.9 | 12.5 | 64.2 | 9.6 | 1.3206 | 14.2730 | 16.6619 | 3,892.0 | 43.6 | 11.8 | 43.3 | 314.7 | 78.7 |
| Confidence Level(95.0%) | 0.0008 | 0.6844 | 0.0087 | 0.1194 | 0.0092 | 0.0026 | 0.0038 | 0.0057 | 21.0 | 0.3213 | 0.0087 | 0.0473 | 0.7641 | 0.1491 |
| | SG | PSSRa | NDVI ₇₀₅ | mSR ₇₀₅ | mMDVI ₇₀₅ | CRT ₂ | LIC1 /PSNda | OSAVI | MCARI | Der ₇₂₅₋₇₀₂ | REP | VOGI | CI ₅₉₀ | MTCI |
| <i>SITE 3. PRISTINE FOREST (YASUNI NATIONAL PARK)</i> | | | | | | | | | | | | | | |
| Mean | 0.0136 | 20.1001 | 0.8177 | 5.4032 | 0.6842 | 0.0616 | 0.9037 | 1.0508 | 234.3 | 5.3793 | 0.7284 | 3.1861 | 22.4486 | 5.7596 |
| Standard Error | 0.0003 | 0.2022 | 0.0010 | 0.0812 | 0.0039 | 0.0004 | 0.0009 | 0.0011 | 7.9 | 0.0975 | 0.0000 | 0.0145 | 0.2472 | 0.0496 |
| Median | 0.0137 | 19.7453 | 0.8184 | 5.3148 | 0.6835 | 0.0613 | 0.9028 | 1.0521 | 245.4 | 5.1977 | 0.7284 | 3.1723 | 22.1984 | 5.6986 |
| Mode | 0.0104 | 19.2990 | 0.8224 | 5.1954 | 0.6772 | 0.0602 | 0.9011 | 1.0579 | 112.4 | 5.0074 | 0.7284 | 3.1369 | 21.7121 | 5.4921 |
| Standard Deviation | 0.0029 | 1.7154 | 0.0087 | 0.6888 | 0.0329 | 0.0036 | 0.0076 | 0.0093 | 67.1 | 0.8271 | 0.0000 | 0.1229 | 2.0975 | 0.4206 |
| Sample Variance | 0.0000 | 2.9427 | 0.0001 | 0.4745 | 0.0011 | 0.0000 | 0.0001 | 0.0001 | 4,496.8 | 0.6841 | 0.0000 | 0.0151 | 4.3996 | 0.1769 |
| Kurtosis | -0.5138 | 0.9018 | -0.3994 | 2.4917 | 1.3967 | 0.3586 | 0.6054 | 0.2476 | -0.1 | 0.1394 | -2.0580 | 2.9965 | 0.9798 | 4.0223 |
| Skewness | -0.2666 | 0.8166 | -0.2725 | 0.8428 | -0.1870 | 0.6232 | 0.2506 | -0.4549 | -0.8 | 0.8134 | -1.0214 | 1.2038 | 0.5004 | 1.3616 |
| Range | 0.0120 | 8.7546 | 0.0371 | 4.3340 | 0.2027 | 0.0153 | 0.0402 | 0.0477 | 281.6 | 3.3477 | 0.0000 | 0.6675 | 11.8101 | 2.3942 |
| Minimum | 0.0070 | 16.3465 | 0.7978 | 3.7280 | 0.5770 | 0.0552 | 0.8825 | 1.0225 | 70.4 | 4.1409 | 0.7284 | 2.9720 | 16.9880 | 5.0789 |
| Maximum | 0.0191 | 25.1011 | 0.8349 | 8.0620 | 0.7797 | 0.0706 | 0.9227 | 1.0703 | 352.0 | 7.4886 | 0.7284 | 3.6395 | 28.7982 | 7.4731 |
| Sum | 1.0 | 1,447.2 | 58.9 | 389.0 | 49.3 | 4.4363 | 65.0666 | 75.6566 | 16,871.7 | 387.3 | 52.4 | 229.4 | 1,616.3 | 414.7 |
| Confidence Level(95.0%) | 0.0007 | 0.4031 | 0.0020 | 0.1619 | 0.0077 | 0.0008 | 0.0018 | 0.0022 | 15.8 | 0.1944 | 0.0000 | 0.0289 | 0.4929 | 0.0988 |

Annex 17 Descriptive statistics of Leaf Pigment and Water vegetation indices for the three study sites

| | OTHER PIGMENTS | | | | WATER INDICES | | | | |
|---|----------------|---------|---------|---------|---------------|---------|---------|---------|---------|
| | SIPI | RG | ARI1 | ARI2 | WBI | NDWI | MSI | NDII_1 | NHI |
| SITE 1. OIL SPILL | | | | | | | | | |
| Mean | 1.1940 | 1.0180 | 5.4795 | -3.9557 | 0.6082 | 0.0139 | 0.4879 | 0.3423 | -0.2294 |
| Standard Error | 0.0067 | 0.0113 | 0.4384 | 0.2940 | 0.0066 | 0.0049 | 0.0111 | 0.0103 | 0.0074 |
| Median | 1.1846 | 1.0002 | 5.3961 | -4.3693 | 0.6036 | 0.0180 | 0.4716 | 0.3537 | -0.2255 |
| Mode | 1.1766 | 0.9802 | 6.4305 | -5.3083 | 0.6021 | nd | nd | 0.3868 | -0.2548 |
| Standard Deviation | 0.0301 | 0.0505 | 1.9608 | 1.3148 | 0.0297 | 0.0221 | 0.0499 | 0.0462 | 0.0332 |
| Sample Variance | 0.0009 | 0.0025 | 3.8446 | 1.7286 | 0.0009 | 0.0005 | 0.0025 | 0.0021 | 0.0011 |
| Kurtosis | -0.1029 | -1.0678 | 1.0943 | -0.5875 | 0.7599 | -0.3389 | 1.9462 | 1.0752 | 0.5063 |
| Skewness | 0.8724 | 0.3866 | 0.8789 | 0.5827 | -0.1088 | -0.4124 | 1.4682 | -1.2952 | -0.7837 |
| Range | 0.1047 | 0.1727 | 7.8737 | 4.6048 | 0.1290 | 0.0855 | 0.1902 | 0.1616 | 0.1245 |
| Minimum | 1.1556 | 0.9416 | 2.7870 | -5.7959 | 0.5389 | -0.0336 | 0.4365 | 0.2252 | -0.3091 |
| Maximum | 1.2603 | 1.1143 | 10.6607 | -1.1910 | 0.6679 | 0.0519 | 0.6268 | 0.3868 | -0.1845 |
| Sum | 23.9 | 20.4 | 109.6 | -79.1 | 12.2 | 0.3 | 9.8 | 6.8 | -4.6 |
| Confidence Level(95.0%) | 0.0141 | 0.0236 | 0.9177 | 0.6153 | 0.0139 | 0.0103 | 0.0233 | 0.0216 | 0.0156 |
| | SIPI | RG | ARI1 | ARI2 | WBI | NDWI | MSI | NDII_1 | NHI |
| SITE 2. SECONDARY FOREST | | | | | | | | | |
| Mean | 1.2159 | 1.0620 | 7.8794 | -4.1339 | 0.6183 | 0.0251 | 0.4584 | 0.3486 | -0.2174 |
| Standard Error | 0.0034 | 0.0106 | 0.6023 | 0.2350 | 0.0074 | 0.0059 | 0.0050 | 0.0048 | 0.0191 |
| Median | 1.2175 | 1.0725 | 7.3946 | -4.0489 | 0.6160 | 0.0246 | 0.4584 | 0.3457 | -0.2101 |
| Mode | nd | 1.0792 | nd | -5.1362 | nd | nd | nd | 0.3401 | -0.2214 |
| Standard Deviation | 0.0136 | 0.0424 | 2.4090 | 0.9400 | 0.0295 | 0.0213 | 0.0202 | 0.0172 | 0.0764 |
| Sample Variance | 0.0002 | 0.0018 | 5.8034 | 0.8836 | 0.0009 | 0.0005 | 0.0004 | 0.0003 | 0.0058 |
| Kurtosis | 0.6527 | 0.5050 | -0.5238 | -1.3153 | 1.1870 | 0.4360 | -0.2293 | 1.6180 | 0.6927 |
| Skewness | -0.7647 | -0.8576 | 0.1918 | -0.1720 | 0.8500 | 0.0070 | 0.1312 | -0.2839 | -0.3835 |
| Range | 0.0521 | 0.1483 | 8.5257 | 3.0136 | 0.1153 | 0.0822 | 0.0734 | 0.0711 | 0.3031 |
| Minimum | 1.1838 | 0.9705 | 3.4494 | -5.7389 | 0.5771 | -0.0161 | 0.4257 | 0.3100 | -0.3913 |
| Maximum | 1.2359 | 1.1187 | 11.9751 | -2.7253 | 0.6924 | 0.0662 | 0.4992 | 0.3811 | -0.0882 |
| Sum | 19.5 | 17.0 | 126.1 | -66.1 | 9.9 | 0.3 | 7.3 | 4.5 | -3.5 |
| Confidence Level(95.0%) | 0.0072 | 0.0226 | 1.2837 | 0.5009 | 0.0157 | 0.0128 | 0.0107 | 0.0104 | 0.0407 |
| | SIPI | RG | ARI1 | ARI2 | WBI | NDWI | MSI | NDII_1 | NHI |
| SITE 3. PRISTINE FOREST (YASUNI NATIONAL PARK) | | | | | | | | | |
| Mean | 1.1659 | 0.9965 | 2.6079 | -5.4606 | 0.6597 | 0.0382 | 0.4484 | 0.3826 | -0.2339 |
| Standard Error | 0.0038 | 0.0092 | 0.4343 | 0.1300 | 0.0035 | 0.0021 | 0.0031 | 0.0024 | 0.0062 |
| Median | 1.1630 | 0.9818 | 2.3004 | -5.4741 | 0.6611 | 0.0381 | 0.4432 | 0.3835 | -0.2256 |
| Mode | 1.1630 | 0.9445 | 2.1428 | -5.8481 | 0.6583 | 0.0226 | 0.4211 | 0.3837 | -0.3127 |
| Standard Deviation | 0.0324 | 0.0781 | 3.6849 | 1.1034 | 0.0298 | 0.0165 | 0.0266 | 0.0185 | 0.0529 |
| Sample Variance | 0.0011 | 0.0061 | 13.5781 | 1.2175 | 0.0009 | 0.0003 | 0.0007 | 0.0003 | 0.0028 |
| Kurtosis | 1.8926 | 1.9066 | 1.7433 | 0.0977 | 0.4751 | -0.3940 | 0.0201 | -0.0717 | 0.0389 |
| Skewness | 0.6011 | 1.3026 | 0.9024 | 0.3268 | -0.3900 | -0.0601 | 0.4186 | 0.1837 | -0.5605 |
| Range | 0.1937 | 0.3964 | 20.0904 | 5.1547 | 0.1454 | 0.0731 | 0.1324 | 0.0840 | 0.2539 |
| Minimum | 1.0840 | 0.8839 | -3.5298 | -7.7280 | 0.5767 | -0.0018 | 0.3884 | 0.3467 | -0.3754 |
| Maximum | 1.2777 | 1.2802 | 16.5607 | -2.5733 | 0.7222 | 0.0713 | 0.5208 | 0.4307 | -0.1215 |
| Sum | 83.9 | 71.7 | 187.8 | -393.2 | 47.5 | 2.3 | 32.3 | 23.0 | -16.8 |
| Confidence Level(95.0%) | 0.0076 | 0.0184 | 0.8659 | 0.2593 | 0.0070 | 0.0043 | 0.0063 | 0.0048 | 0.0124 |

Bibliography

- Abrams, M.A. 1996, "Distribution of subsurface hydrocarbon seepage in near-surface marine sediments" in *Hydrocarbon migration and its near-surface expression*, eds. D. Schumacher & M.A. Abrams, AAPG Memoir 66 edn, American Association of Petroleum Geologists, , pp. 1-14.
- Alloway, B.J. 2000, "Soil pollution and land contamination" in *Understanding our environment pollution, causes, effects and control*, ed. R.M. Harrison, Fourth edn, University of Birmingham, Birmingham-UK.
- Alonso, L. & Moreno, J. 2005, "Advances and limitations in a parametric geometric correction of CHRIS/proba data", , pp. 7.
- Alonso, L. & Moreno, J. 2004, "Quasi-automatic geometric correction and related geometric issues in the exploitation of CHRIS/PROBA data", , pp. 16.
- Alton, P.B., North, P., Kaduk, L. & Los, S. 2005, "Radiative transfer modeling of direct and diffuse sunlight in a Siberian pine forest", *Journal of Geophysical Research*, vol. 110.
- Apan, A., Held, A., Phinn, S. & Markley, J. 2004, "Detecting sugarcane 'orange rust' disease using EO-1 Hyperion hyperspectral imagery", *International Journal of Remote Sensing*, vol. 25, no. 2, pp. 489-498.
- Arnon, D.I. 1949, "Copper enzymes in isolated chloroplasts. Polyphenoloxidase in *Beta Vulgaris*", *Plant Physiology. American Society of Plant Biologists*, vol. 24, no. 1, pp. 1-15.
- Asner, G.P. 1998, "Biophysical and biochemical sources of variability in canopy reflectance", *Remote Sensing of Environment*, vol. 64, pp. 234-253.
- Asner, G.P., Nepstad, D., Cardinot, G. & Ray, D. 2004, "Drought stress and carbon uptake in an Amazon forest measured with spaceborne imaging spectroscopy", *Proceedings of the National Academy of Sciences of the United States of America*, vol. 101, no. 16, pp. 6039-6044.
- ATSDR & EPA 1999, *Toxicological profile for Total Petroleum Hydrocarbons (TPH)*, U.S.Department of Health and Human Services, Atlanta, Georgia, USA.
- Baker, J.M. 1970, "The effects of oil on plants", *Environmental Pollution*, vol. 1, pp. 27-44.

- Barnsley, M.J., Settle, J.J., Cutter, M.A., Lobb, D.R. & Teston, F. 2004, "The PROBA/CHRIS mission: A low-cost smallsat for hyperspectral multiangle observations of the earth surface and atmosphere", *IEEE Transactions on Geoscience and Remote Sensing*, vol. 42, no. 7, pp. 1512-1520.
- Barry, P. 2001, *EO-1 / Hyperion Science Data User's Guide. Level 1_B*, TRW Space, Defense & Information Systems, Redondo Beach, CA.
- Bass, M.S., Finer, M., Jenkins, C.N., Kreft, H., Cisneros-Heredia, D.F., McCracken, S.F., Pitman, N.C.A., English, P.H., Swing, K., Villa, G., Di Fiore, A., Voigt, C.C. & Kunz, T.H. 2010, "Global conservation significance of Ecuador's Yasuní National Park", *PLoS ONE*, vol. 5, no. 1.
- Beck, R. 2003, *EO-1 User Guide v. 2.3*, University of Cincinnati, Cincinnati, Ohio.
- Bernal, A.M. 2011, "Power, powerlessness and petroleum: Indigenous environmental claims and the limits of transnational law", *New Political Science*, vol. 33, no. 2, pp. 143-167.
- Blackburn, G.A. 2007, "Hyperspectral remote sensing of plant pigments", *Journal of Experimental Botany*, vol. 58, no. 4, pp. 855-867.
- Blackburn, G.A. 1998a, "Spectral indices for estimating photosynthetic pigment concentrations: A test using senescent tree leaves", *International Journal of Remote Sensing*, vol. 19, no. 4, pp. 657-675.
- Blackburn, G.A. 1998b, "Quantifying Chlorophylls and Carotenoids at Leaf and Canopy Scales: An Evaluation of Some Hyperspectral Approaches", *Remote Sensing of Environment*, vol. 66, no. 3, pp. 273-285.
- Bonan, G. 2008, *Ecological Climatology*, Second edn, Cambridge University Press, United Kingdom.
- Boudet, H., Clarke, C., Bugden, D., Maibach, E., Roser-Renouf, C. & Leiserowitz, A. 2014, "'Fracking' controversy and communication: Using national survey data to understand public perceptions of hydraulic fracturing", *Energy Policy*, vol. 65, pp. 57-67.
- Boyd, D.S., Almond, S., Dash, J., Curran, P.J., Hill, R.A. & Foody, G.M. 2012, "Evaluation of envisat MERIS terrestrial chlorophyll index-based models for the estimation of terrestrial gross primary productivity", *IEEE Geoscience and Remote Sensing Letters*, vol. 9, no. 3, pp. 457-461.
- Cao, K.F. & Booth, E.W. 2001, "Leaf anatomical structure and photosynthetic induction for seedlings of five dipterocarp species under contrasting light

- conditions in a Bornean heath forest", *Journal of Tropical Ecology*, vol. 17, no. 2, pp. 163-175.
- Carswell, F.E., Meir, P., Wandelli, E.V., Bonates, L.C.M., Kruijt, B., Barbosa, E.M., Nobre, A.D., Grace, J. & Jarvis, P.G. 2000a, "Photosynthetic capacity in a central Amazonian rain forest", *Tree physiology*, vol. 20, no. 3, pp. 179-186.
- Carswell, F.E., Meir, P., Wandelli, E.V., Bonates, L.C.M., Kruijt, B., Barbosa, E.M., Nobre, A.D., Grace, J. & Jarvis, P.G. 2000b, "Photosynthetic capacity in a central Amazonian rain forest", *Tree physiology*, vol. 20, no. 3, pp. 179-186.
- Carter, G.A. 1994, "Ratios of leaf reflectances in narrow wavebands as indicators of plant stress", *International Journal of Remote Sensing*, vol. 15, no. 3, pp. 697-703.
- Casa, R. & Jones, H.G. 2004, "Retrieval of crop canopy properties: a comparison between model inversion from hyperspectral data and image classification", *International Journal of Remote Sensing*, vol. 25, no. 6, pp. 1119-1130.
- Castro-Esau, K.L., Sánchez-Azofeifa, G.A., Rivard, B., Wright, S.J. & Quesada, M. 2006, "Variability in leaf optical properties of mesoamerican trees and the potential for species classification", *American Journal of Botany*, vol. 93, no. 4, pp. 517-530.
- Cerovic, Z.G., Masdoumier, G., Ghazlen, N.B. & Latouche, G. 2012, "A new optical leaf-clip meter for simultaneous non-destructive assessment of leaf chlorophyll and epidermal flavonoids", *Physiologia Plantarum*, vol. 146, no. 3, pp. 251-260.
- Chandrasekhar, S. 1950, *Radiative Transfer*, Clarendon Press, Oxford-UK.
- Chazdon, R.L. & Fetcher, N. 1984, "Photosynthetic Light Environments in a Lowland Tropical Rain Forest in Costa Rica", *Journal of Ecology*, vol. 72, no. 2, pp. 553-564.
- Ciganda, V., Gitelson, A. & Schepers, J. 2009, "Non-destructive determination of maize leaf and canopy chlorophyll content", *Journal of Plant Physiology*, vol. 166, no. 2, pp. 157-167.
- Clevers, J.P.G.W. & Jongschaap, R. 2006, "Imaging Spectrometry for Agricultural Applications" in *Imaging Spectrometry*, eds. F. van der Meer & S.M. de Jong, Springer, The Netherlands, pp. 157-199.

- Clevers, J.G.P.W., De Jong, S.M., Epema, G.F., Van der Meer, F.D., Bakker, W.H., Skidmore, A.K. & Scholte, K.H. 2002, "Derivation of the red edge index using the MERIS standard band setting", *International Journal of Remote Sensing*, vol. 23, no. 16, pp. 3169-3184.
- Colombo, R., Meroni, M., Marchesi, A., Busetto, L., Rossini, M., Giardino, C. & Panigada, C. 2008, "Estimation of leaf and canopy water content in polar plantations by means of hyperspectral indices and inverse modeling", *Remote Sensing of Environment*, vol. 112, pp. 1820-1834.
- Coste, S., Baraloto, C., Leroy, C., Marcon, É., Renaud, A., Richardson, A.D., Roggy, J.-., Schimann, H., Uddling, J. & Hérault, B. 2010, "Assessing foliar chlorophyll contents with the SPAD-502 chlorophyll meter: A calibration test with thirteen tree species of tropical rainforest in French Guiana", *Annals of Forest Science*, vol. 67, no. 6, pp. 607p1-607p5.
- Curran, P.J. & Dash, J. 2005, *Algorithm theoretical basis document ATBD 2.2: chlorophyll index*, University of Southampton, Southampton-UK.
- Dadon, A., Ben-Dor, E. & Karnieli, A. 2010, "Use of Derivative Calculations and Minimum Noise Fraction Transform for Detecting and Correcting the Spectral Curvature Effect (Smile) in Hyperion Images", *Geoscience and Remote Sensing, IEEE Transactions on*, vol. 48, no. 6, pp. 2603-2612.
- Dash, J. & Curran, P.J. 2004, "The MERIS terrestrial chlorophyll index", *International Journal of Remote Sensing*, vol. 25, no. 23, pp. 5403-5413.
- Dash, J., Curran, P.J., Tallis, M.J., Llewellyn, G.M., Taylor, G. & Snoeij, P. 2010, "Validating the MERIS Terrestrial Chlorophyll Index (MTCI) with ground chlorophyll content data at MERIS spatial resolution", *International Journal of Remote Sensing*, vol. 31, no. 20, pp. 5513-5532.
- Datt, B. 1999, "Remote sensing of water content in Eucalyptus leaves", *Australian Journal of Botany*, vol. 47, no. 6, pp. 909-923.
- Datt, B., McVicar, T.R., Van Niel, T.G., Jupp, D.L.B. & Pearlman, J.S. 2003, "Preprocessing EO-1 Hyperion hyperspectral data to support the application of agricultural indexes", *IEEE Transactions on Geoscience and Remote Sensing*, vol. 41, no. 6 PART I, pp. 1246-1259.
- Daughtry, C.S.T., Walthall, C.L., Kim, M.S., de Colstoun, E.B. & McMurtrey III, J.E. 2000, "Estimating Corn Leaf Chlorophyll Concentration from Leaf and Canopy Reflectance", *Remote Sensing of Environment*, vol. 74, no. 2, pp. 229-239.

- Davids, C. & Tyler, A.N. 2003, "Detecting contamination-induced tree stress within the Chernobyl exclusion zone", *Remote Sensing of Environment*, vol. 85, no. 1, pp. 30-38.
- Davidson, E.A., De Araújo, A.C., Artaxo, P., Balch, J.K., Brown, I.F., C. Bustamante, M.M., Coe, M.T., Defries, R.S., Keller, M., Longo, M., Munger, J.W., Schroeder, W., Soares-Filho, B.S., Souza Jr., C.M. & Wofsy, S.C. 2012, "The Amazon basin in transition", *Nature*, vol. 481, no. 7381, pp. 321-328.
- Dawson, T.P. & Curran, P.J. 1998, "A new technique for interpolating the reflectance red edge position", *International Journal of Remote Sensing*, vol. 19, no. 11, pp. 2133-2139.
- Dawson, T.P., Curran, P.J., North, P.R.J. & Plummer, S.E. 1999, "The propagation of foliar biochemical absorption features in forest canopy reflectance: A theoretical analysis", *Remote Sensing of Environment*, vol. 67, no. 2, pp. 147-159.
- Dawson, T.P., Curran, P.J. & Plummer, S.E. 1998, "LIBERTY - Modeling the effects of Leaf Biochemical Concentration on Reflectance Spectra", *Remote Sensing of Environment*, vol. 65, no. 1, pp. 50-60.
- Dawson, T.P., North, P.R.J., Plummer, S.E. & Curran, P.J. 2003, "Forest ecosystem chlorophyll content: Implications for remotely sensed estimates of net primary productivity", *International Journal of Remote Sensing*, vol. 24, no. 3, pp. 611-617.
- Demarez, V. & Gastellu-Etchegorry, J.P. 2000, "A modelling approach for studying forest chlorophyll content", *Remote Sensing of Environment*, vol. 71, pp. 226-238.
- Demarez, V., Gastellu-Etchegorry, J.P., Mougin, E., Marty, G., Proisy, C., Dufrêne, E. & Dantec, V.L. 1999, "Seasonal variation of leaf chlorophyll content of a temperate forest. Inversion of the PROSPECT model", *International Journal of Remote Sensing*, vol. 20, no. 5, pp. 879-894.
- Doble, M. & Kumar, A. 2005, *Biotreatment of Industrial Effluents*, Elsevier Inc., USA.
- Dolman, A.J., Gash, J.H.C., Roberts, J. & Shuttleworth, W.J. 1991, "Stomatal and surface conductance of tropical rainforest", *Agricultural and Forest Meteorology*, vol. 54, no. 2-4, pp. 303-318.
- España-Boquera, M.L., Cárdenas-Navarro, R., López-Pérez, L., Castellanos-Morales, V. & Lobit, P. 2006, "Estimating the nitrogen concentration of

- strawberry plants from its spectral response", *Communications in Soil Science and Plant Analysis*, vol. 37, no. 15-20, pp. 2447-2459.
- Etiopie, G. 2004, "New Directions: GEM—Geologic Emissions of Methane, the missing source in the atmospheric methane budget", *Atmospheric Environment*, vol. 38, no. 19, pp. 3099-3100.
- Etiopie, G. & Klusman, R.W. 2002, "Geologic emissions of methane to the atmosphere", *Chemosphere*, vol. 49, no. 8, pp. 777-789.
- FAO 2000, *Global ecofloristic zones mapped by the United Nations Food and Agricultural Organization*, adapted by Ruesch, Aaron, and Holly K. Gibbs. 2008.
- Feret, J. 2008, "PROSPECT-4 and 5: Advances in the leaf optical properties model separating photosynthetic pigments", *Remote Sensing of Environment*, vol. 112, no. 6, pp. 3030-3043.
- Féret, J., François, C., Gitelson, A., Asner, G.P., Barry, K.M., Panigada, C., Richardson, A.D. & Jacquemoud, S. 2011, "Optimizing spectral indices and chemometric analysis of leaf chemical properties using radiative transfer modeling", *Remote Sensing of Environment*, vol. 115, no. 10, pp. 2742-2750.
- Finer, M., Jenkins, C.N., Pimm, S.L., Keane, B. & Ross, C. 2008, "Oil and gas projects in the Western Amazon: Threats to wilderness, biodiversity, and indigenous peoples", *PLoS ONE*, vol. 3, no. 8.
- Fitton, L.J. 2000, "Helminthiasis and culture change among the cofán of Ecuador", *American Journal of Human Biology*, vol. 12, no. 4, pp. 465-477.
- Fortunel, C., Fine, P.V.A. & Baraloto, C. 2012, "Leaf, stem and root tissue strategies across 758 Neotropical tree species", *Functional Ecology*, vol. 26, no. 5, pp. 1153-1161.
- France, G. 1990, *Remote sensing of tropical Forest*, PhD edn, University of Leicester, Leicester-UK.
- Gamon, J.A. & Surfus, J.S. 1999, "Assessing leaf pigment content and activity with a reflectometer", *New Phytologist*, vol. 143, no. 1, pp. 105-117.
- Gao, B.-. 1996, "NDWI - A normalized difference water index for remote sensing of vegetation liquid water from space", *Remote Sensing of Environment*, vol. 58, no. 3, pp. 257-266.
- Gastellu-Etchegorry, J.P., Guillevic, P., Zagolski, F., Demarez, V., Trichon, V., Deering, D. & Leroy, M. 1999, "Modeling BRDF and radiation regime of

- boreal and tropical forests: I.BRF", *Remote Sensing of Environment*, vol. 68, pp. 281-316.
- Gastellu-Etchegorry, J.P., Demarez, V., Pinel, V. & Zagolski, F. 1996, "Modeling Radiative Transfer in Heterogeneous 3-D Vegetation Canopies", *Remote Sensing of Environment*, vol. 58, pp. 131-156.
- Gerber, F., Marion, R., Olioso, A., Jacquemoud, S., Ribeiro da Luz, B. & Fabre, S. 2011, "Modeling directional-hemispherical reflectance and transmittance of fresh and dry leaves from 0.4 μm to 5.7 μm with the PROSPECT-VISIR model", *Remote Sensing of Environment*, vol. 115, no. 2, pp. 404-414.
- Gitelson, A. 2012, "Nondestructive estimation of foliar pigment (Chlorophylls, Carotenoids, and Anthocyanins) contents: Evaluating a semianalytical tree-band model" in *Hyperspectral Remote Sensing of Vegetation*, eds. P. Thenkabail, J. Lyon & A. Huete, CRC Press, Boca Raton, FL, USA, pp. 141-165.
- Gitelson, A., Chivkunova, O. & Merzlyak, M.N. 2009, "Nondestructive estimation of Anthocyanins and Chlorophylls in Anthocyanic leaves", *American Journal of Botany*, vol. 96, no. 10, pp. 1861-1868.
- Gitelson, A. & Merzlyak, N. 1994, "Spectral reflectance changes associated with autumn senescence of *Aesculus hippocastanum* L. and *Acer platanoides* L. leaves. Spectral features and relation to chlorophyll estimation.", *Journal of Plant Physiology*, vol. 143, pp. 286-292.
- Gitelson, A.A., Gritz, Y. & Merzlyak, M.N. 2003, "Relationships between leaf chlorophyll content and spectral reflectance and algorithms for non-destructive chlorophyll assessment in higher plant leaves", *Journal of Plant Physiology*, vol. 160, no. 3, pp. 271-282.
- Gitelson, A.A., Kaufman, Y.J. & Merzlyak, M.N. 1996, "Use of a green channel in remote sensing of global vegetation from EOS- MODIS", *Remote Sensing of Environment*, vol. 58, no. 3, pp. 289-298.
- Gitelson, A.A., Keydan, G.P. & Merzlyak, M.N. 2006, "Three-band model for noninvasive estimation of chlorophyll, carotenoids, and anthocyanin contents in higher plant leaves", *Geophysical Research Letters*, vol. 33, no. 11, pp. L11402.
- Gitelson, A.A. & Merzlyak, M.N. 1997, "Remote estimation of chlorophyll content in higher plant leaves", *International Journal of Remote Sensing*, vol. 18, no. 12, pp. 2691-2697.

- Gitelson, A.A., Merzlyak, M.N. & Chivkunova, O.B. 2001, "Optical properties and nondestructive estimation of anthocyanin content in plant leaves", *Photochemistry and photobiology*, vol. 74, no. 1, pp. 38-45.
- Gitelson, A.A., Viña, A., Ciganda, V., Rundquist, D.C. & Arkebauer, T.J. 2005, "Remote estimation of canopy chlorophyll content in crops", *Geophysical Research Letters*, vol. 32, no. 8, pp. 1-4.
- Goel, N.S. 1988, "Models of vegetation canopy reflectance and their use in estimation of biophysical parameters from reflectance data", *Remote Sensing Reviews*, vol. 4, pp. 1-212.
- Gomez-Chova, L., Alonso, L., Guanter, L., Calpe, J. & Moreno, J. 2008, *CHRIS/PROBA Noise Reduction Module. Algorithm theoretical basis document*, ESA ESRIN.
- Goodenough, D.G., Dyk, A., Niemann, K.O., Pearlman, J.S., Chen, H., Han, T., Murdoch, M. & West, C. 2003, "Processing Hyperion and ALI for forest classification", *IEEE Transactions on Geoscience and Remote Sensing*, vol. 41, no. 6 PART I, pp. 1321-1331.
- Goodenough, D.G., Quinn, G.S., Gordon, P.L., Niemann, K.O. & Chen, H. 2011, "Linear and nonlinear imaging spectrometer denoising algorithms assessed through chemistry estimation", , pp. 4320.
- Grace, J. 1999, "Environmental controls of gas exchange in tropical rain forests" in *Physiological Plant Ecology*, eds. M.C. Press, J.D. Scholes & M.G. Barker, British Ecological Society, , pp. 367-389.
- Guanter, L., Alonso, L., Gomez-Chova, L. & Moreno, J. 2008, *CHRIS/PROBA Atmospheric Correction Module: Algorithm theoretical basis document*, ESA ESRIN.
- Gustafson, F. 1950, "Is the American Elm (*Ulmus americana*) injured by natural gas?", *Plant Physiology*, vol. 25, no. 422, pp. 440.
- Gustafson, F. 1944, "Is natural gas injurious to flowering plants?", *Plant Physiology*, vol. 19, pp. 551-558.
- Guyot, G., Baret, F. & Major, D.J. 1988, "High spectral resolution: Determination of spectral shifts between the red and the near infrared", *International Archives of Photogrammetry and Remote Sensing*, vol. 11, pp. 740-760.
- Hall, G. 2013, *Fugro Tellus Sedimentary Basins of the World Map*, U.S. Department of Energy.

- Hardisky, M.A., Klemas, V. & Smart, R.M. 1983, "The influence of soil salinity, growth form, and leaf moisture on the spectral radiance of *Spartina alterniflora* canopies.", *Photogrammetric Engineering & Remote Sensing*, vol. 49, no. 1, pp. 77-83.
- Hawkins, T.S., Gardiner, E.S. & Comer, G.S. 2009, "Modeling the relationship between extractable chlorophyll and SPAD-502 readings for endangered plant species research", *Journal for Nature Conservation*, vol. 17, no. 2, pp. 125-129.
- Hiscox, J.D. & Israelstam, G.F. 1979, "A method for the extraction of chlorophyll from leaf tissue without maceration.", *Canadian Journal of Botany*, vol. 57, pp. 1332-1334.
- Hoel, B.O. 1998, "Use of a hand-held chlorophyll meter in winter wheat: Evaluation of different measuring positions on the leaves", *Acta Agriculturae Scandinavica - Section B Soil and Plant Science*, vol. 48, no. 4, pp. 222-228.
- Horvitz, L. 1982, "Near-surface evidence of hydrocarbon movement from depth" in *Problems of petroleum migration*, eds. W.H. Roberts & R.J. Cordell, AAPG Studies in Geology 10 edn, American Association of Petroleum Geologists, Tulsa, Oklahoma, USA, pp. 241-263.
- Horvitz, L. 1972, "Vegetation and geochemical prospecting for petroleum", *American Association of Petroleum Geologists Bulletin*, vol. 56, no. 5, pp. 925-940.
- Hoscilo, A. 2009, *Fire regime, vegetation dynamics and land cover change in tropical peatland, Indonesia*, PhD edn, University of Leicester, Leicester-UK.
- Houghton, J.T., Meira, L.G., Callander, B.A., Harris, N., Kattenberg, A. & Maskell, K. 1996, *Climate Change 1995. The Science of Climate Change. Contribution of the Working Group I to the Second Assessment Report of the Intergovernmental Panel on Climate Change*, IPCC, Cambridge-England.
- Houghton, R.A. 2012, "Carbon emissions and the drivers of deforestation and forest degradation in the tropics", *Current Opinion in Environmental Sustainability*, vol. 4, no. 6, pp. 597-603.
- Howard, J.A., Watson, R.D. & Hessin, T.D. 1971, "Spectral reflectance properties of *Pinus ponderosa* in relation to copper content of the soil - Malachite Mine, Jefferson Country, Colorado", *Proceedings of the 7th International Symposium on Remote Sensing of Environment*, May 1971, pp. 285.

- Huete, A.R., Liu, H.Q., Batchily, K. & Van Leeuwen, W. 1997, "A comparison of vegetation indices over a global set of TM images for EOS-MODIS", *Remote Sensing of Environment*, vol. 59, no. 3, pp. 440-451.
- Hunt Jr, E.R. & Rock, B.N. 1989a, "Detection of changes in leaf water content using Near- and Middle-Infrared reflectances", *Remote Sensing of Environment*, vol. 30, no. 1, pp. 43-54.
- Hunt Jr, E.R. & Rock, B.N. 1989b, "Detection of changes in leaf water content using Near- and Middle-Infrared reflectances", *Remote Sensing of Environment*, vol. 30, no. 1, pp. 43-54.
- Hunt, J.M. 1996, *Petroleum Geochemistry and Geology*, Second edn, W.H. Freeman and Company, New York.
- Hurtig, A.K. & San-Sebastián, M. 2005, "Epidemiology vs epidemiology: The case of oil exploitation in the Amazon basin of Ecuador [5]", *International journal of epidemiology*, vol. 34, no. 5, pp. 1170-1172.
- Inoue, Y., Sakaiya, E., Zhu, Y. & Takahashi, W. 2012, "Diagnostic mapping of canopy nitrogen content in rice based on hyperspectral measurements", *Remote Sensing of Environment*, vol. 126, pp. 210-221.
- ISO 2012, *Determination of transmittance by diffuse reflectance measurement. ISO 22891:2012(E)*, International Standard Organization.
- Jacquemoud, S. & Marcq, S. 2012, *Personal communication*, Institut de Physique du Globe de Paris & Université Paris Diderot.
- Jacquemoud, S., 2009, "PROSPECT SAIL models: A review of use for vegetation characterization", *Remote Sensing of Environment*, vol. 113, no. 1, pp. S56-S66.
- Jago, R.A., Cutler, M.E.J. & Curran, P.J. 1999, "Estimating canopy chlorophyll concentration from field and airborne spectra", *Remote Sensing of Environment*, vol. 68, no. 3, pp. 217-224.
- Jaspal, R. & Nerlich, B. 2014, "Fracking in the UK press: Threat dynamics in an unfolding debate", *Public Understanding of Science*, vol. 23, no. 3, pp. 348-363.
- Jensen, J.R. 2007, *Remote sensing of the environment : an earth resource perspective*, Second edn, Pearson Education, Inc., USA.
- Jones, H.G. & Vaughan, R.A. (eds) 2010, *Remote Sensing of Vegetation. Principles, techniques and applications*, Oxford University Press, New York.

- Kamaluddin, M. & Grace, J. 1993, "Growth and photosynthesis of tropical forest tree seedlings (*Bischofia javanica* Blume) as influenced by a change in light availability", *Tree Physiology*, vol. 13, no. 2, pp. 189-201.
- Kamaluddin, M. & Grace, J. 1992, "Photoinhibition and light acclimation in seedlings of *Bischofia javanica*, a tropical forest tree from Asia", *Annals of Botany*, vol. 69, no. 1, pp. 47-52.
- Kaufman, Y.J. & Tanre, D. 1992, "Atmospherically resistant vegetation index (ARVI) for EOS-MODIS", *IEEE Transactions on Geoscience and Remote Sensing*, vol. 30, no. 2, pp. 261-270.
- Kempeneers, P., Zarco-Tejada, P.J., North, P.R.J., de Backer, S., Delalieux, S., Sepulcre-Canto, G., Morales, F., van Aardt, J.A.N., Sagardoy, R., Coppin, P. & Scheunders, P. 2008, "Model inversion for chlorophyll estimation in open canopies from hyperspectral imagery", *International Journal of Remote Sensing*, vol. 29, no. 17-18, pp. 5093-5111.
- Konica Minolta 2009, *Chlorophyll meter SPAD-502Plus. Instruction manual*, Konica Minolta Sensing, Inc, Japan.
- Kruse, F.A., Boardman, J.W. & Huntington, J.F. 2003, "Comparison of airborne hyperspectral data and EO-1 Hyperion for mineral mapping", *IEEE Transactions on Geoscience and Remote Sensing*, vol. 41, no. 6 PART I, pp. 1388-1400.
- Kumar, L., Schmidt, K. & Dury, S. 2006, "Imaging spectrometry and vegetation science" in *Imaging Spectrometry. Basic Principles and Prospective Applications*, eds. F. van del Meer & S. de Jong, Fourth edn, Springer, Dordrecht, The Netherlands, pp. 111-155.
- Kvenvolden, K.A. & Rogers, B.W. 2005, "Gaia's breath—global methane exhalations", *Marine and Petroleum Geology*, vol. 22, no. 4, pp. 579-590.
- Lambers, H.F., Chapin III, F.S. & Pons, T.L. 2008, *Plant physiological ecology*, Second edn, Springer New York, Springer-Verlag New York.
- Lang, H.R., Aldman, W.H. & Sabins, F.F. 1985, *Patrick Draw, Wyoming-Petroleum Test Case Report.*, American Association of Petroleum Geologists-AAPG.
- Lang, H.R., Curtis, J.B. & Kavacs, J.C. 1985, *Lost River, West Virginia petroleum test site report*, American Association of Petroleum Geologists, AAPG.
- Larcher, W. 2003, *Physiological Plant Ecology*, Fourth edn, Spinger, Germany.

- Lichtenthaler, H.K. 1987, [34] *Chlorophylls and carotenoids: Pigments of photosynthetic biomembranes*.
- Lichtenthaler, H.K., Lang, M., Sowinska, M., Heisel, F. & Miehe, J.A. 1996, "Detection of vegetation stress via a new high resolution fluorescence imaging system", *Journal of Plant Physiology*, vol. 148, no. 5, pp. 599-612.
- Lichtenthaler, H.K. 1996, "Vegetation Stress: an Introduction to the Stress Concept in Plants", *Journal of Plant Physiology*, vol. 148, no. 1-2, pp. 4-14.
- Lloyd, J., Grace, J. & Miranda, A.C. 1995, "A simple calibrated model of Amazon rainforest productivity based on leaf biochemical properties.", *Plant, Cell and Environment*, , no. 18, pp. 1129-1145.
- Longman, K.A. 1987, *Tropical forest and its environment*, 2nd edn, , London, UK.
- Lyons, W.C. & Plisga, G.J. 2005, *Standard handbook of petroleum and natural gas engineering*, 2nd edn, Gulf Professionals-Elsevier Inc., Oxford, UK.
- Malhi, Y., Roberts, J.T., Betts, R.A., Killeen, T.J., Li, W. & Nobre, C.A. 2008, "Climate change, deforestation, and the fate of the Amazon", *Science*, vol. 319, no. 5860, pp. 169-172.
- Malhi, Y., Wood, D., Baker, T.R., Wright, J., Phillips, O.L., Cochrane, T., Meir, P., Chave, J., Almeida, S., Arroyo, L., Higuchi, N., Killeen, T.J., Laurance, S.G., Laurance, W.F., Lewis, S.L., Monteagudo, A., Neill, D.A., Vargas, P.N., Pitman, N.C.A., Quesada, C.A., Salomão, R., Silva, J.N.M., Lezama, A.T., Terborgh, J., Martínez, R.V. & Vinceti, B. 2006, "The regional variation of aboveground live biomass in old-growth Amazonian forests", *Global Change Biology*, vol. 12, no. 7, pp. 1107-1138.
- Marenco, R.A., Antezana-Vera, S.A. & Nascimento, H.C.S. 2009, "Relationship between specific leaf area, leaf thickness, leaf water content and SPAD-502 readings in six Amazonian tree species", *Photosynthetica*, vol. 47, no. 2, pp. 184-190.
- Marquez-Riquelme, E.F., van der Steen, J., Baltzer, C. & Maas, W. 2010, "Accurate correlations to estimate refinery fuel gas, natural gas, and fuel oil CO2 emission factors and its uncertainty", *American Institute of Chemical Engineers Journal*, vol. 56, no. 9, pp. 2478-2487.
- Martin, P.L. 2011, "Global governance from the amazon: Leaving oil underground in Yasuní National park, Ecuador", *Global Environmental Politics*, vol. 11, no. 4, pp. 22-42.

- Marwell, J., Osterman, J. & Mitchell, J. 1995, "Calibration of the Minolta SPAD-502 leaf chlorophyll meter", *Photosynthesis Research*, vol. 46, pp. 467-472.
- Marx, E. 2010, "The fight for Yasuni", *Science*, vol. 330, no. 6008, pp. 1170-1171.
- McAuliffe, C.D. 1982, "Oil and Gas Migration: Chemical and Physical Constraints" in *Problems of Petroleum Migration*, eds. W.H. Roberts & R.J. Cordell, American Association of Petroleum Geologists - AAPG, Tulsa, Oklahoma, USA, pp. 89-107.
- Melo, M.R., Concalves, F.T., Babinski, N.A. & Miranda, F.P. 1996, "Hydrocarbon prospecting in the Amazon rainforest: application of surface geochemical, microbiological, and remote sensing methods" in *Hydrocarbon migration and its near-surface expressions*, eds. D. Schumecher & M.A. Abrams, American Association of Petroleum Geologists, AAPG, , pp. 401-411.
- Ministerio de Energia y Minas 2002, *Archivo historico exploracion bloque Pungarayacu*, Drilling reports edn, Ministerio de Energia y Minas del Ecuador, Quito-Ecuador.
- Monje, O.A. & Bugbee, B. 1992, "Inherent limitations of nondestructive chlorophyll meters: a comparison of two types of meters.", *HortScience*, vol. 27, no. 1, pp. 69-71.
- Munden, R., Curran, P.J. & Catt, J.A. 1994, "The relationship between red edge and chlorophyll concentration in the Broadbalk winter wheat experiment at Rothamsted", *International Journal of Remote Sensing*, vol. 15, no. 3, pp. 705-709.
- Noomen, M.F. 2007, *Hyperspectral Reflectance of vegetation affected by underground hydrocarbon gas seepage*, PhD edn, International Institute for Geo-Information Science & Earth Observation-ITC, Enschede-The Netherlands.
- Noomen, M.F. & Skidmore, A.K. 2009, "The effects of high soil CO₂ concentrations on leaf reflectance of maize plants", *International Journal of Remote Sensing*, vol. 30, no. 2, pp. 481-497.
- Noomen, M.F., Smith, K.L., Colls, J.J., Steven, M.D., Skidmore, A.K. & Van Der Meer, F.D. 2008, "Hyperspectral indices for detecting changes in canopy reflectance as a result of underground natural gas leakage", *International Journal of Remote Sensing*, vol. 29, no. 20, pp. 5987-6008.

- Noomen, M.F., van der Werff, H.M.A. & van der Meer, F.D. 2012, "Spectral and spatial indicators of botanical changes caused by long-term hydrocarbon seepage", *Ecological Informatics*, vol. 8, pp. 55-64.
- North, P. 1996, "Three-dimensional forest light interaction model using a Monte Carlo method", *IEEE Transactions on Geoscience and Remote Sensing*, vol. 34, no. 4, pp. 946-956.
- Panigada, C., Rossini, M., Busetto, L., Meroni, M., Fava, F. & Colombo, R. 2010, "Chlorophyll concentration mapping with MIVIS data to assess crown discoloration in the Ticino Park oak forest", *International Journal of Remote Sensing*, vol. 31, no. 12, pp. 3307.
- Penuelas, J., Filella, I., Lloret, P., Munoz, F. & Vilajeliu, M. 1995, "Reflectance assessment of mite effects on apple trees", *International Journal of Remote Sensing*, vol. 16, no. 14, pp. 2727-2733.
- Peñuelas, J., Piñol, J., Ogaya, R. & Filella, I. 1997, "Estimation of plant water concentration by the reflectance Water Index WI (R900/R970)", *International Journal of Remote Sensing*, vol. 18, no. 13, pp. 2869-2875.
- Percival, G.C., Keary, I.P. & Noviss, K. 2008, "The potential of a chlorophyll content SPAD meter to quantify nutrient stress in foliar tissue of Sycamore (*Acer pseudoplatanus*), English Oak (*Quercus robur*), and European beech (*Fagus sylvatica*)", *Arboriculture & Urban Forestry*, vol. 34, no. 2, pp. 89-100.
- Peters, K.E., Walters, C.C. & Moldowan, J.M. 2005, *The Biomarkers Guide. Biomarkers and Isotopes in Petroleum Exploration and Earth History*, Second edn, Cambridge University Press, UK.
- Phillips, O.L., Aragão, L.E.O.C., Lewis, S.L., Fisher, J.B., Lloyd, J., López-González, G., Malhi, Y., Monteagudo, A., Peacock, J., Quesada, C.A., Van Der Heijden, G., Almeida, S., Amaral, I., Arroyo, L., Aymard, G., Baker, T.R., Bánki, O., Blanc, L., Bonal, D., Brando, P., Chave, J., De Oliveira, Á.C.A., Cardozo, N.D., Czimczik, C.I., Feldpausch, T.R., Freitas, M.A., Gloor, E., Higuchi, N., Jiménez, E., Lloyd, G., Meir, P., Mendoza, C., Morel, A., Neill, D.A., Nepstad, D., Patiño, S., Peñuela, M.C., Prieto, A., Ramírez, F., Schwarz, M., Silva, J., Silveira, M., Thomas, A.S., Steege, H.T., Stropp, J., Vásquez, R., Zelazowski, P., Dávila, E.A., Andelman, S., Andrade, A., Chao, K.-., Erwin, T., Di Fiore, A., Honorio, E.C., Keeling, H., Killeen, T.J., Laurance, W.F., Cruz, A.P., Pitman, N.C.A., Vargas, P.N., Ramírez-Angulo, H., Rudas, A., Salamão, R., Silva, N., Terborgh, J. & Torres-Lezama, A. 2009, "Drought sensitivity of the amazon rainforest", *Science*, vol. 323, no. 5919, pp. 1344-1347.

- Pimstein, A., Eitel, J.U.H., Long, D.S., Mufradi, I., Karnieli, A. & Bonfil, D.J. 2009, "A spectral index to monitor the head-emergence of wheat in semi-arid conditions", *Field Crops Research*, vol. 111, no. 3, pp. 218-225.
- Poorter, L., Kwant, R., Hernández, R., Medina, E. & Werger, M.J.A. 2000, "Leaf optical properties in Venezuelan cloud forest trees", *Tree physiology*, vol. 20, no. 8, pp. 519-526.
- Porra, R.J., Thompson, W.A. & Kriedemann, P.E. 1989, "Determination of accurate extinction coefficients and simultaneous equations for assaying chlorophylls a and b extracted with four different solvents: verification of the concentration of chlorophyll standards by atomic absorption spectroscopy", *BBA - Bioenergetics*, vol. 975, no. 3, pp. 384-394.
- Press, N.P. 1974, "Remote sensing for detect the toxic effects of metals on vegetation of mineral exploration", *Proceesings of the 9th International Symposium on Remote Sensing of Environment* Michigan, 15-19 April, pp. 2027.
- Prieto-Blanco, A., North, P.R.J., Barnsley, M.J. & Fox, N. 2009, "Satellite-driven modelling of Net Primary Productivity (NPP): Theoretical analysis", *Remote Sensing of Environment*, vol. 113, no. 1, pp. 137-147.
- Reich, P.B., Kloeppel, B.D., Ellsworth, D.S. & Walters, M.B. 1995, "Different photosynthesis-nitrogen relations in deciduous hardwood and evergreen coniferous tree species", *Oecologia*, vol. 104, no. 1, pp. 24-30.
- Reich, P.B., Walters, M.B., Ellsworth, D.S. & Uhl, C. 1994, "Photosynthesis-nitrogen relations in Amazonian tree species", *Oecologia*, vol. 97, pp. 62-72.
- Richardson, A.D., 2002, "Changes in foliar spectral reflectance and chlorophyll fluorescence of four temperate species following branch cutting", *Tree physiology*, vol. 22, no. 7, pp. 499-506.
- Richardson, A.D., Duigan, S.P. & Berlyn, G.P. 2002, "An evaluation of noninvasive methods to estimate foliar chlorophyll content", *New Phytologist*, vol. 153, no. 1, pp. 185-194.
- Roberts, J., Cabral, O.M.R. & Ferreira De Aguiar, L. 1990, "Stomatal and boundary-layer conductances in an Amazonian terra firme rain forest", *Journal of Applied Ecology*, vol. 27, no. 1, pp. 336-353.
- Rondeaux, G., Steven, M. & Baret, F. 1996, "Optimization of soil-adjusted vegetation indices", *Remote Sensing of Environment*, vol. 55, no. 2, pp. 95-107.

- Ross, J. 1975, "Radiative Transfer in Plant Communities" in *Vegetation and the Atmosphere*, ed. J.L. Monteith, Academic Press Limited, London-UK, pp. 13-55.
- Rosso, P.H., Pushnik, J.C., Lay, M. & Ustin, S.L. 2005, "Reflectance properties and physiological responses of *Salicornia virginica* to heavy metal and petroleum contamination", *Environmental Pollution*, vol. 137, no. 2, pp. 241-252.
- Rouse, J.W., Haas, R.H. & Schell, J.A. 1974, "Monitoring the Vernal Advancement of Retrogradation of Natural Vegetation", .
- Ruiz-Espinoza, F.H., Murillo-Amador, B., Garcia-Hernandez, J.L., Fenech-Larios, L., Rueda-Puente, E.O., Troyo-Diequez, E., Kaya, C. & Beltran-Morales, A. 2010a, "Field evaluation of the relationship between chlorophyll content in basil leaves and a portable chlorophyll meter (spad-502) readings", *Journal of Plant Nutrition*, vol. 33, no. 3, pp. 423-438.
- Ruiz-Espinoza, F.H., Murillo-Amador, B., Garcia-Hernandez, J.L., Fenech-Larios, L., Rueda-Puente, E.O., Troyo-Diequez, E., Kaya, C. & Beltran-Morales, A. 2010b, "Field evaluation of the relationship between chlorophyll content in basil leaves and a portable chlorophyll meter (spad-502) readings", *Journal of Plant Nutrition*, vol. 33, no. 3, pp. 423-438.
- Sánchez-Azofeifa, G.A., Castro, K., Wright, S.J., Gamon, J., Kalacska, M., Rivard, B., Schnitzer, S.A. & Feng, J.L. 2009, "Differences in leaf traits, leaf internal structure, and spectral reflectance between two communities of lianas and trees: Implications for remote sensing in tropical environments", *Remote Sensing of Environment*, vol. 113, no. 10, pp. 2076-2088.
- Shumacher, D. 1996, "Hydrocarbon-induced alteration of soils and sediments" in *Hydrocarbon migration and its near-surface expression: APPG Memoir 66*, eds. D. Shumacher & M.A. Abrams, pp. 71-89.
- Sims, D.A. & Gamon, J.A. 2002, *Relationships between leaf pigment content and spectral reflectance across a wide range of species, leaf structures and developmental stages*.
- Smith, K.L., Steven, M.D. & Colls, J.J. 2004, "Remote sensing techniques for monitoring plant stress responses to gas leaks", *International Gas Research Conference Proceedings*, .
- Smith, K.L., Colls, J.J. & Steven, M.D. 2005, *A Facility to Investigate Effects of Elevated Soil Gas Concentration on Vegetation*, Springer Netherlands.

- Smith, K.L., Steven, M.D. & Colls, J.J. 2005, "Plant spectral responses to gas leaks and other stresses", *International Journal of Remote Sensing*, vol. 26, no. 18, pp. 4067.
- Smith, K.L., Steven, M.D. & Colls, J.J. 2004, "Use of hyperspectral derivative ratios in the red-edge region to identify plant stress responses to gas leaks", *Remote Sensing of Environment*, vol. 92, no. 2, pp. 207-217.
- Solomon, S., Qin, D., Manning, M., Chen, Z., Marquis, M., Averyt, K.B., Tignor, M. & Miller, H.L. 2007, *Contribution of Working Group I to the Fourth Assessment Report of the Intergovernmental Panel on Climate Change*, 2007, NY-USA.
- Stratoulas, D., Balzter, H., Zlinszky, A. & Tóth, V.R. in press, "Identification of physiological changes in reed vegetation from hyperspectral imagery in a lakeshore environment", *Remote Sensing of Environment*, .
- Tedersoo, L., Sadam, A., Zambrano, M., Valencia, R. & Bahram, M. 2010, "Low diversity and high host preference of ectomycorrhizal fungi in Western Amazonia, a neotropical biodiversity hotspot", *ISME Journal*, vol. 4, no. 4, pp. 465-471.
- Tempfli, K., Huurneman, G.C., Bakker, W.H. & Janssen, L.L.F. (eds) 2009, *Principles of Remote Sensing: An Introductory Textbook*, Fourth edn, International Institute of Geoinformation and Earth Observation-ITC, Enschede, The Netherlands.
- Terashima, I. & Saeki, T. 1983, "Light environment within a leaf I. Optical properties of paradermal sections of camellia leaves with special reference to differences in the optical properties of palisade and spongy tissues", *Plant and Cell Physiology*, vol. 24, no. 8, pp. 1493-1501.
- Torres-Netto, A., Campostrini, E., Gonçalves de Oliveira, J. & Bressan-Smith, R. 2005, "Photosynthetic pigments, nitrogen, chlorophyll *a* fluorescence and SPAD-502 readings in coffee leaves", vol. 104, pp. 199-209.
- Torres-Netto, A., Campostrini, E., Gonçalves de Oliveira, J. & Yamanishi, O. 2002, "Portable chlorophyll meter for the quantification of photosynthetic pigments, nitrogen and the possible use for assessment of the photochemical process in *Carica papaya L.*", *Brazilian Journal of Plant Physiology*, vol. 14, no. 3, pp. 203-210.
- UNFCCC 2007, *Reducing emissions from deforestation in developing countries approaches to stimulate actions. Decision 2/CP.13.* .

- Ustin, S.L., Gitelson, A.A., Jacquemoud, S., Schaepman, M., Asner, G.P., Gamon, J.A. & Zarco-Tejada, P. 2009, "Retrieval of foliar information about plant pigment systems from high resolution spectroscopy", *Remote Sensing of Environment*, vol. 113, no. SUPPL. 1, pp. S67-S77.
- Valencia, R. 2004, "Yasuni forest dynamic plot, Ecuador" in *Tropical Forest Diversity and Dynamism: Findings from a Large-Scale Plot Network.*, eds. E. Losos, J. Leigh & E. Giles, University of Chicago Press, Chicago, pp. 609-628.
- Valencia, R., Foster, R.B., Richard-Conditt, G.V., Svenning, J.C., Hernández, C., Romoleroux, K., Losos, E., Magards, E. & Balslev, H. 2004, "Tree species distributions and local habitat variation in the Amazon: large forest plot in eastern Ecuador", *Journal of Ecology*, vol. 92, pp. 214-229.
- van der Meer, F., de Jong, S. & Bakker, W. 2006, "Imaging Spectrometry: Basic Analytical Techniques" in *Imaging Spectrometry. Basic Principles and Prospective Applications*, eds. F. van der Meer & S. de Jong, Third edn, Springer, , pp. 35.
- van der Meer, F., Yang, H. & Kroonenberg, S. 2006, "Imaging spectrometry and petroleum geology" in *Imaging Spectrometry*, eds. F. van der Meer & S.M. de Jong, Springer, Dordrecht, The Netherlands, pp. 219-241.
- Verhoef, W. 1984, "Light scattering by leaf layers with applications to canopy reflectance model: the SAIL model", *Remote Sensing of Environment*, vol. 16, pp. 125-141.
- Verhoef, W., 2007, "Coupled soil-leaf-canopy and atmosphere radiative transfer modeling to simulate hyperspectral multi-angular surface reflectance and TOA radiance data", *Remote Sensing of Environment*, vol. 109, no. 2, pp. 166-182.
- Vile, D., Garnier, É., Shipley, B., Laurent, G., Navas, M.-., Roumet, C., Lavorel, S., Díaz, S., Hodgson, J.G., Lloret, F., Midgley, G.F., Poorter, H., Rutherford, M.C., Wilson, P.J. & Wright, I.J. 2005, "Specific leaf area and dry matter content estimate thickness in laminar leaves", *Annals of Botany*, vol. 96, no. 6, pp. 1129-1136.
- Vogelmann, J.E., Rock, B.N. & Moss, D.M. 1993, "Red edge spectral measurements from sugar maple leaves", *International Journal of Remote Sensing*, vol. 14, no. 8, pp. 1563-1575.
- Walsh Environment Scientists and Engineers 2005, *Auditoria ambiental externa de las actividades hidrocarburiiferas en el Bloque Tarapoa y el campo compartido Fanny 18B*, AEC, Ecuador Ltd, Quito-Ecuador.

- White, J.W. & Montes-R, C. 2005, "Variation in parameters related to leaf thickness in common bean (*Phaseolus vulgaris* L.)", *Field Crops Research*, vol. 91, no. 1, pp. 7-21.
- Witkowski, E.T.F. & Lamont, B.B. 1991, "Leaf specific mass confounds leaf density and thickness", *Oecologia*, vol. 88, no. 4, pp. 486-493.
- Wright, I.J., Reich, P.B., Westoby, M., Ackerly, D.D., Baruch, Z., Bongers, F., Cavender-Bares, J., Chapin, T., Cornellissen, J.H.C., Diemer, M., Flexas, J., Garnier, E., Groom, P.K., Gulias, J., Hikosaka, K., Lamont, B.B., Lee, T., Lee, W., Lusk, C., Midgley, J.J., Navas, M.-., Niinemets, Ü., Oleksyn, J., Osada, H., Poorter, H., Pool, P., Prior, L., Pyankov, V.I., Roumet, C., Thomas, S.C., Tjoelker, M.G., Veneklaas, E.J. & Villar, R. 2004, "The worldwide leaf economics spectrum", *Nature*, vol. 428, no. 6985, pp. 821-827.
- Yang, H. 1999, *Imaging Spectrometry for Hydrocarbon Microseepage*, Delf University of Technology.
- Yang, B. 1997, "Natural gas prospecting by using satellite MT data in Chishui Area, Guizhou", *Chinese Journal of Geochemistry*, vol. 16, no. 1, pp. X7-74.
- Yang, H., Zhang, J., Van Der Meer, F. & Kroonenberg, S.B. 2000, "Imaging spectrometry data correlated to hydrocarbon microseepage", *International Journal of Remote Sensing*, vol. 21, no. 1, pp. 197-202.
- Yang, H., Zhang, J., Van Der Meer, F. & Kroonenberg, S.B. 1999, "Spectral characteristics of wheat associated with hydrocarbon microseepages", *International Journal of Remote Sensing*, vol. 20, no. 2-4, pp. 807-813.
- Zhu, L., Zhao, X., Lai, L., Wang, J., Jiang, L., Ding, J., Liu, N., Yu, Y., Li, J., Xiao, N., Zheng, Y. & Rimmington, G.M. 2013, "Soil TPH Concentration Estimation Using Vegetation Indices in an Oil Polluted Area of Eastern China", *PLoS ONE*, vol. 8, no. 1.